Damage Localization of Mechanical Structures by Subspace Identification and Krein Space Based $\mathcal{H}^\infty$ Estimation

Dissertation

zur Erlangung des akademischen Grades

Doktor-Ingenieur (Dr.-Ing.)

an der Fakultät Bauingenieurwesen

der

Bauhaus-Universität Weimar

vorgelegt von

Max Vollmering

aus Leipzig

Gutachter: 1. Prof. Dr.-Ing. habil. Carsten Könke (Mentor)
2. Prof. Dr. techn. Christian Bucher
3. Prof. Dr.-Ing. Armin Lenzen

Tag der Disputation: 18. Mai 2018

ABSTRACT

This dissertation is devoted to the theoretical development and experimental laboratory verification of a new damage localization method: The state projection estimation error (SP2E). This method is based on the subspace identification of mechanical structures, Krein space based $\mathcal{H}^{\infty}$ estimation and oblique projections. To explain method SP2E, several theories are discussed and laboratory experiments have been conducted and analysed.

A fundamental approach of structural dynamics is outlined first by explaining mechanical systems based on first principles. Following that, a fundamentally different approach, subspace identification, is comprehensively explained. While both theories, first principle and subspace identification based mechanical systems, may be seen as widespread methods, barely known and new techniques follow up. Therefore, the indefinite quadratic estimation theory is explained. Based on a Popov function approach, this leads to the Krein space based $\mathcal{H}^{\infty}$ theory. Subsequently, a new method for damage identification, namely SP2E, is proposed. Here, the introduction of a difference process, the analysis by its average process power and the application of oblique projections is discussed in depth.

Finally, the new method is verified in laboratory experiments. Therefore, the identification of a laboratory structure at Leipzig University of Applied Sciences is elaborated. Then structural alterations are experimentally applied, which were localized by SP2E afterwards. In the end four experimental sensitivity studies are shown and discussed. For each measurement series the structural alteration was increased, which was successfully tracked by SP2E. The experimental results are plausible and in accordance with the developed theories. By repeating these experiments, the applicability of SP2E for damage localization is experimentally proven.

ZUSAMMENFASSUNG

In dieser Dissertation wird eine neue Methode der Schadenslokalisation theoretisch hergeleitet und im Labor experimentell verifiziert: Sie trägt den Namen 'State Projection Estimation Error' (SP2E) und basiert auf der Subspace Identifikation mechanischer Strukturen, der Kreinraum basierten $\mathcal{H}^\infty$ Schätztheorie und schiefen Projektionen. Um die Methode SP2E zu erklären, werden in dieser Arbeit verschiedene Theorien diskutiert und Laborversuche ausgewertet.

Die Arbeit beginnt mit einigen Ausführungen der analytischen Mechanik, welche zur Modellierung mechanischer System in der Strukturdynamik Anwendung finden. Darauf aufbauend wird die Subspace Identifikation umfassend erklärt. Während beide erstgenannten theoretischen Teile als weitverbreitet angesehen werden können, folgen daraufhin wenig bekannte bis unbekannte Ansätze: Dafür wird zuerst die Theorie der indefiniten quadratischen Schätzung behandelt. Auf Basis einer popov Funktion führt dies zur Kreinraum basierten $\mathcal{H}^\infty$ Schätztheorie. Im Anschluss daran wird die neue Methodik SP2E eingeführt. Dabei sind vorrangig die Definition eines Differenzprozesses, dessen Auswertung mit der mittleren Prozessleistung und die Anwendung schiefer Projektionen wichtig.

Abschließend wird die neu entwickelte Methodik in Laborversuchen verifiziert. Dafür wird zunächst die Identifikation einer Laborstruktur an der Leipzig University of Applied Sciences umfassend erklärt. An dieser Laborstruktur wurden experimentell strukturelle Veränderungen eingebracht, welche mit SP2E erfolgreich lokalisiert werden konnten. Zum Schluss werden vier durchgeführte experimentelle Sensitivitätsstudien aufgezeigt und diskutiert. In diesen vier Versuchsreihen wurde die strukturelle Veränderung sukzessive erhöht. Diese Veränderungen konnten mit SP2E verfolgt werden und die Ergebnisse waren plausibel. Da die Versuche jeweils wiederholt wurden, konnte so die Anwendbarkeit von SP2E zur Schadenslokalisation experimentell nachgewiesen werden.

CONTENTS

LIST OF FIGURES

LIST OF TABLES

INTRODUCTION

1.1 Monitoring of Large-Scale Structures

The environmental life-cycle assessment of buildings is an important research issue to improve sustainability and economic efficiency. Hereby, central states (design, construction, operation, demolition and waste treatment) of technical structures (infrastructure, buildings, plants, etc.) must be considered altogether.[1-3]

To design buildings, infrastructure and so on, finite element modelling (FEM) is a generally accepted and common engineering oriented tool.[4] Thereby, complex models are usually applied to accurately estimate mechanical quantities, like displacements, strains and so forth. However, in maintenance existing structures may be constantly observed to measure mechanical quantities (e.g. accelerations, velocities, strains), which can be used to validate those models. Based on that, it is advantageous to implement a model-based operation and maintenance. This may save natural resources and invested capital. Unfortunately, adjustments of complex models in consequence of new measurements are unsuitable, because from a theoretical perspective, the process might be ambiguous, inconsistent and is in general real-time incapable.[5] Because maintenance can be the most cost-intensive part (compared to the total costs of buildings), an alternative is necessary here.

Research of degradation evaluation of mechanical structures during maintenance phase is referred to as structural health monitoring (SHM). For that, a vast variety of techniques have been proposed.[6,7] Although it is beyond the scope of this thesis to give a complete overview of this topic, the most common approaches are summarized in the following. Based on this overview of scientific fields, the central dissertation research issue is then derived.

1.2 Modelling during Operational Phase

During the operational phase of buildings it is fundamentally important to reduce the complex physical behaviour of large-scale mechanical structures to an analysable model.[8] To validate these models, mechanical vibration measurements can be usefully applied, which is discussed below.

According to the system-theoretic and cybernetic approach, modelling techniques can be classified as i) white-box, ii) black-box and iii) grey-box.[9] The grey-box model is a combination of both first named approaches and is not discussed here.

WHITE-BOX MODELS of mechanical structures are based on analytical-physical first principles.[4] Here, conservation laws (mass, momentum, energy), geometrical kinematic properties and constitutive equations (for the particular material) are applied to mathematically determine a model. Then this model describes the analysed mechanical system. Often these defined fundamental equations are analytically derivable for special cases only. Thus, these equations are solved by numerical approximation techniques based on discrete elements, like the finite element method, boundary element method, finite differences and modal techniques.[5, 10]

The derived equations of white-box models can be directly interpreted in a physical sense, which is advantageous.[11] On the other hand, complex problems require an enormous methodical and numerical effort during the lifespan of a mechanical structure. Important examples for that are the influence of environmental and operational conditions (temperatures, humidities, etc.), non-linearities (geometrical and material-dependent), variable operational states and so on.

Because of the issues outlined above, finite element models are usually adjusted by an updating process according to measured mechanical quantities in structural dynamics.[12–14] Here, modal data is predominantly determined from measurements and used for the updating process. As it may be seen as an optimization, it is difficult to expediently choose a low number of mechanical parameters to be adjusted out of a large number of defined ones in accordance with the conducted experiment.[5] Furthermore, a problem is the choice of updating approach and the physical interpretation of its result afterwards. In addition to that, the model order of defined finite element models usually is very high. Hence, real-time applications are typically impossible in the maintenance phase.

BLACK-BOX MODELS are fundamentally different to the previously described approach, because those models are at first usually derived from a mathematical-general perspective only. As they are based on measurements of physical quantities, black-box models characterize the transfer function of a system input to its output in a general way. Very importantly, these models may be categorized as follows: i) parametric – non-parametric, ii) linear – non-linear, iii) continuous-time – discrete-time, iv) single degree of freedom – multi degree of freedom, v) recursive estimate – identification in blocks, vi) deterministic – stochastic, vii) time-domain – frequency-domain, viii) explicit – implicit, ix) output-only – input-output, x) time-invariant – time-variant.[4, 15]

Following the given classifications, there are numerous black-box system identification techniques and model structures, like the autoregressive moving average model, the state space models and so forth.[16] Most commonly, multi degree of freedom parametrized models are linearized at an operation point. Thus, frequently used state space models are presupposed in the following.

1.3 BLACK BOX SYSTEM IDENTIFICATION

Black-box systems may be parametrized following numerical methods, which are based on measured (or theoretically presumed) excitations and measured structural responses.[17–19] The direct application of measured physical-structural behaviour allows an appropriate system realization. Here, the parametrization of systems based on measured signals, so called system identification techniques, usually is classified according to applied test loads in deterministic and stochastic approaches.[9] Deterministic identification techniques are based on measurable test loads like impulses, sweep function and so forth.

On the other hand, stochastic identification techniques are based on ambient excitations, for example wind, traffic and waves. Another important categorization distinguishes between output-only and input-output identification. Especially completely parametrized input-output models describe the causal transfer behaviour from excitations to structural responses of mechanical systems.[20] For this reason, subspace techniques can be advantageously applied.[17,19]

DETERMINISTIC IDENTIFICATION   typically is devoted to parametrize a chosen model structure in a certain theoretical frame. Commonly, subspace methods in connection with a least-squares approach are used to determine (and eventually parametrize) a transfer system on the basis of structural measurements. To name widespread methods, one may revisit the method of Ho-Kalman,[21] the numerical algorithms for state subspace system identification (N4SID)[22] and the multivariable output error state space algorithm (MOESP).[23,24]

It usually is hard to apply deterministic test loads during operation at large-scale structures, like bridges, wind energy plants and airplanes. Nevertheless, those structures are characteristic in civil and mechanical engineering. In addition to that, deterministic test loads are elaborate and thus expensive to apply at large-scale structures.[25] In opposite to that, ambient vibrations are already present during operation. Because active test load applications may be omitted, stochastic identification techniques are generally preferable, and thus are primarily considered in this dissertation.

STOCHASTIC IDENTIFICATION   is premised on measured stochastic structural responses or derived correlation functions. Important techniques are, among others, the stochastic realization,[26] the canonical variate analysis (CVA)[27] and the canonical correlation analysis (CCA).[28,29] Most recently, mixed stochastic-deterministic identification techniques have been developed, for example the past-output MOESP (Po-MOESP),[30] the orthogonal decomposition technique (ORT)[19] and the input-output CCA.[19] Furthermore, closed-loop identification techniques recently got more attention by researchers.[31,32]

To identify completely parametrized state space models based on stochastic excitations, Kalman filtering theory may be applied, as van Overschee and de Moor[22] point

out. One approach for that is the canonical factorization of the power spectral density, which itself is estimated based on measured structural responses. In result an innovation model is parametrized, which describes the transfer behaviour of a causal, theoretical input (innovation process) to measured structural responses.[20]

If one wants to numerically compute an innovation model, an optimization problem must be analysed. Therefore, a Riccati equation is commonly solved, for which several numerical approaches have been developed, like the direct iteration, the doubling algorithm and the application of an extended symplectic pencil.[33,34] Unfortunately, there might be no solution at all to the Riccati equation due to numerical inaccuracies of identified system parameters. The background and compensation methods for that have been constantly analysed, formerly from a system-theoretic viewpoint.[35–37]

1.4 Output-Only and Operational Modal Analysis

Output-only methods may be seen as a special case of black-box system identification and are usually used to determine modal data, like natural frequencies, dampings and unscaled mode shapes.[38] These parameters solely describe the dynamics of a mechanical structure in opposite to completely parametrized state space models. According to Cunha et al.,[15] the application of output-only identification for modal analyses have originally been developed in mechanical engineering in frequency domain. At that time the adjustment of theoretical frequency response functions has been a central research object.

Being commonly applied for decades, single degree of freedom systems were analysed by several methods, for instance peak amplitude, curve fit and inverse methods.[15] Later on the analysis of multiple degree of freedom systems required more elaborate approaches, which were found for example by the rational fractional polynomial, the complex exponential frequency domain and the polyreference frequency domain.[39] Unfortunately, those frequency-domain methods are limited by the applicable frequency resolutions, influenced for example by spectral leakage. This can lead to inaccurate frequency estimates.[15]

In addition to that, the number of measured natural frequencies is fundamental.[15] Consequently, time domain methods have been developed, which are based on adjustments of measured and estimated time series. To classify here, indirect (e.g. least squares, Ibrahim time domain (ITD), eigensystem realization) and direct techniques (e.g. based on the autoregressive-moving average (ARMA) model) may be named.[15]

Operational modal analysis is an active research field, especially in structural dynamics and structural health monitoring. Based on ambient vibration excitations (typically presupposed as white noise), modal data is primarily identified rather than general system parameters. In view of the historical development, operational modal analysis (OMA) techniques have originally been derived based on non-

parametric descriptions in the frequency domain, as can be seen by peak picking,[39] the frequency-domain decomposition (FDD)[40] and the enhanced frequency domain decomposition (EFDD).[41]

Although these methods are very useful, more accurate techniques are generally based on parametrized, mathematical systems in time-domain, especially ARMA-models and state space systems. Here, several methods can be named, like the Ibrahim time domain (ITD) method, the multiple reference ITD, the covariance based stochastic subspace identification (SSI-Cov) and the Data-Driven stochastic subspace identification.[42–45] More recently, modal analysis methods have been developed on the premise of parametric descriptions in the frequency-domain, as can be seen by operational PolyMAX, polyreference least-squares complex frequency-domain (pLSCF) and polyreference maximum likelihood estimator (pMLE).[46–49] Additionally, a hybrid identification technique on the basis of partially measured structural excitations was introduced, which is called OMA with exogenous inputs (OMAX).[50]

1.5 DAMAGE IDENTIFICATION

An important application of system identification is structural health monitoring (SHM). Typically, damage sensitive parameters, also known as features,[51] are applied here according to various different damage identification techniques. The technique capabilities can be hierarchically categorized following Rytter:[52] (1) damage detection, (2) damage localization (3) damage assessment and (4) prediction of remaining lifetime. Furthermore, vibration-based structural health monitoring has been described as a four-step statistical pattern recognition paradigm by Farrar et al.[51] and fundamental axioms for the same topic were proposed by Worden et al.[53]

A very rudimentary damage analysis technique is based on defined maximal vibration magnitudes. Here, german standardizations for civil engineering (DIN 4150) and mechanical engineering (DIN ISO 10816) give exemplary guideline values. In contrary to symptom based damage identification, model based damage identification is more significant[54] and will be elaborated in the following. However, a complete overview of damage identification techniques is beyond the scope of this summary.

MODAL DATA are, by the author's knowledge, the most common applied damage identification feature. Modal data of two systems states are compared to each other according to defined approaches. For example natural frequency shifts and mode shape alterations are analysed, for instance based on the modal assurance criterion (MAC) and the coordinate modal assurance criterion (CoMAC).[55,56] Furthermore, frequency response functions,[57,58] modal curvatures,[59,60] modal strain energy[61] and experimental flexibility parameters[62–64] are applied for damage identification. Usually damage detection is possible only. Even that can be questionable, especially when environ-

mental and operational conditions (e.g. temperature, traffic density) at large-scale structures need to be additionally considered.[15, 16]

Besides a direct comparison of modal data, these parameters are also typically used for finite element model updating.[5] By adjusting a model, structural damage may be found with the help of optimized (updated) mechanical parameters.[14]

Being an active research community, several other damage identification techniques have been defined for structural health monitoring. Although less used, they might be worth our attention. Examples are polynomial coefficient alterations of ARMA-models,[65] wavelet transformation coefficients of structural responses,[66] modal filters,[67] transmissibilities[68] and correlation functions.[69] A fundamentally different damage identification approach is the application of wave propagation theory.[70] In addition to the named alternative damage identification techniques, estimation theory gives a different viewpoint on that topic.

Applied estimation theory is here an umbrella term for damage identification based on Kalman filters, $\mathcal{H}^\infty$ estimators and so on. Especially Kalman filtering theory has been used for system identification,[71–73] to recursively compute mechanical parameters[74–76] and to define a novelty index based on estimation errors.[77] Although system theoretic approaches are constantly used to determine modal data, analyses beyond that seem to be rarely applied in structural health monitoring. That can hardly be explained, but one could argue that system theory and structural health monitoring simply are different research communities, which are not often considered as a whole.

Kalman filtering can be referred to as $\mathcal{H}^2$ estimation.[78] Furthermore, it can be seen as a special case of $\mathcal{H}^\infty$ estimation. Although $\mathcal{H}^\infty$ theory has been very comprehensively studied and practically used in control,[79–81] it is, to the best of the author's knowledge, less used in estimation[82] and almost unknown in system and damage identification. Nevertheless, few studies exist, like the identification of modal mass,[83] frequency and damping tracking[84] and design of a fault detection filter.[85] Because further research in $\mathcal{H}^\infty$ theory based damage identification may lead to huge improvements in the field of structural health monitoring, a new method should be developed. This will enter the dissertation research issue in section 1.7.

1.6 Industrial Need for Damage Localization

Structural health monitoring may prevent ecological and economical catastrophes. To show possible areas of practical application, structural monitoring of bridges and wind energy plants are discussed in the following. Nevertheless, this thesis covers a theoretical discourse and experimental verification only and these industry-practical examples are not revived again.

BRIDGES are typical technical objects to monitor, because undetected structural damage may lead to enormous catastrophes. Monitoring examples of bridges can be found all over the world.[86–89] Nevertheless, automatic bridge monitoring still is uncommon in Germany, in opposite to periodic inspections. Although German bridges are manually monitored following standardization DIN 1076, there are several problems in Germany: i) Most bridges are partially damaged, ii) the owner (federal administration, etc.) has few economic possibilities for maintenance, iii) state identification according to DIN 1076 depends on the engineer's experience, iv) occuring structural damage can be detected only according to the maintenance interval (main analysis repeats every 6 years), v) structural damage can be seen at accessible construction parts only and vi) non-destructive testing (e.g. eddy-current testing, ultrasonic testing, etc.) is locally confined and is mostly useful, if the damage position is already known.

These arguments emphasize the requirement for reliable automated damage localization techniques. The German directive 'Richtlinie zur Nachrechnung von Straßenbrücken im Bestand' explicitly allows monitoring methods in level 4 of recalculation, which are called here compensating supervision measures (German: 'kompensierende Überwachungsmaßnahmen'). Possibly monitored objects might be: i) Global structural state (e.g. detection of anomalies during operation, erosion), ii) fatigue, iii) local structural state (e.g. suspensions, cables), iv) local forces (e.g. in prestressed concrete, cables), v) loads (e.g. traffic).

WIND ENERGY PLANTS are another important application field for monitoring.[90] Here, a possible classification distinguishes between the (more mechanical engineering oriented) monitoring of nacelle and blades[91–93] and the long-term tower analysis.[94,95] The later one is mostly covered in civil engineering, as this discipline also deals with historical, residential and office towers.[96,97]

Energy plants in offshore fields are cost-intensive, and thus are worth to analyse. In Germany those plants must be developed in all phases (design, construction, operation and demolition) according to the directive 'Konstruktive Ausführung von Offshore Windenergieanlagen' of the Federal Maritime and Hydrographic Agency of Germany (German: Bundesamt für Seeschifffahrt und Hydrographie (BSH)). Therein periodic inspections (25% of all constructions per year) are legally demanded, which is economically expansive (e.g. examination of submarine transition joints, rotor blades). Here, a problem are inaccessible construction parts. To give building permissions, the named agency expects at least 10% of offshore wind energy plants to be equipped with a monitoring system.

Nevertheless, the capability and extend of this monitoring system has not been defined so far. Hence, its usefulness might be questionable. Here, the advantages of monitoring should be explained to the operators, which might exemplarily be: i) State identification and early damage detection, ii) coordination of optimized inspection operations, iii) reduction of economical costs due to predictive maintenance, iv) damage growth prediction and determination of the remaining life-time, v) metrological recording of real loadings, vi) optimized structural design for new plants and vii) op-

erational management based on low vibration levels (e.g. control of rotor blade pitch angles).

Both given examples emphasize the need for robust damage localization methodologies for industrial applications. Unfortunately, most existing damage identification techniques are only able to detect (level 1 damage identification). Localization of structural damage has not been utilized in industrial applications so far and it is thus useful to develop a new approach.

1.7 THE DERIVED DISSERTATION RESEARCH ISSUE

Technical constructions are described by models in all life-time phases (design, construction, operation and demolition). Maintenance is the most cost-intensive phase, in which white-box models (e.g. FE models) are disadvantageous due to, among other things, large model orders and real-time capability. Instead, black-box models are preferable, because low model order systems may be implemented in real-time applications.

Black-box models are directly based on structural measurements. For that, subspace identification techniques based on ambient vibrations are advantageous. Furthermore, uncertainty-tolerant $\mathcal{H}^\infty$ estimators may achieve great progress for damage localization due to unknown excitations. Hence, stochastic excitation presumptions are not necessary, as ambient excitations are presumed. Reliable damage localization methods are needed by the industry, which might be applied for early damage detection, inspection optimization and analysis of inaccessible structural parts.

Concluding the above statements, a new damage localization method based on black-box (subspace) identification and $\mathcal{H}^\infty$ theory shall be theoretically developed. Here, it is important to consider unknown structural excitations (ambient vibrations). To verify this new method, experimental sensitivity studies in laboratory must be conducted. Although this method should be practically applicable in the end, theoretical considerations are discussed first and it is beyond the scope of this dissertation to develop an industrial implementation. Hence, the consideration of environmental and operational conditions is excluded at first, as the former issues are elaborate enough.

2

DISSERTATION STRUCTURE

2.1 OUTLINE

Based on the derived dissertation research issue of section 1.7, several important scientific areas are subsequentially covered to derive and verify a new damage localization technique. The line of arguments is structured in three parts, which is illustrated in figure 2.1.

```
┌──────────────────┐   ┌──────────────────┐   ┌──────────────────┐
│     PART I       │   │     PART II      │   │     PART III     │
│ Widespread       │   │ New Methods:     │   │ Experimental     │
│ Methods:         │   │ H∞ Estimation    │   │ Verificiation    │
│ Models of        │   │ SP2E             │   │ in Laboratory    │
│ Mechanical       │   │                  │   │                  │
│ Structures       │   │                  │   │                  │
└──────────────────┘   └──────────────────┘   └──────────────────┘

┌──────────────────┐
│   CHAPTER 3      │
│ Models Based on  │
│ First Principles │
└──────────────────┘

┌──────────────────┐   ┌──────────────────┐   ┌──────────────────┐
│   CHAPTER 4      │   │   CHAPTER 5      │   │   CHAPTER 7      │
│ Subspace         │   │ Krein Space      │   │ Identification of│
│ Identification   │   │ H∞ Estimation    │   │ Laboratory Struct.│
└──────────────────┘   └──────────────────┘   └──────────────────┘

                       ┌──────────────────┐   ┌──────────────────┐
                       │   CHAPTER 6      │   │   CHAPTER 8      │
                       │ New Method       │   │ SP2E Verification│
                       │ SP2E             │   │ Sensitivity Studies│
                       └──────────────────┘   └──────────────────┘
```

Figure 2.1: Dissertation Outline

PART I is devoted to a review of widespread modelling techniques for mechanical structures. Here, chapter 3 describes the derivation of white-box models following first principles. The focus lies in state space representations and frequency-domain (modal) analysis. Finally, two models of the later used laboratory structure are numerically constructed and analysed.

In opposite to the given white-box approach, the subspace identification of black-box models is described in chapter 4. The most important deterministic and stochastic approaches are discussed. After that, a direct damage identification application of these techniques is given by briefly discussing the identification of experimental mechanical parameters by corresponding matrices. For that, the application at a real bridge near Hünxe (Germany) is briefly shown afterwards. These deterministic experiments are then compared to ambient excitation experiments, which is applied in the end to numerically identify the multi degree of freedom mechanical system of chapter 3.

PART II introduces barely known and new methods to the field of structural dynamics. At first Krein space based $\mathcal{H}^\infty$ theory is engineering oriented explained in chapter 5. This comprehensive elaboration covers time-variant systems in finite horizon, which mostly leads to time-domain expressions. Based on that time-invariant problems are discussed. Formerly described in the frequency domain, this case is commonly referred to as the infinite horizon. In the end of that chapter the 'filtering signals in additive noise' approach is exemplified at the former mechanical system.

Chapter 6 then introduces a new damage identification technique. Based on stochastic subspace identification and $\mathcal{H}^\infty$ estimation, the method state projection estimation error (SP2E) is derived. It starts by defining a general difference process. Applied with estimation errors, an approach for synchronization and normalization is shown, which leads to an advantageous state space representation. Afterwards state projections are discussed and used for damage identification. The chapter closes with the introduced mechanical system example.

PART III covers the experimental verification of SP2E in laboratory. For that, the identification of a laboratory structure is described in chapter 7. Here, several numerical-practical issues are addressed, like the model order determination, model reduction and so forth.

Hereafter, experimental damage localization by SP2E is shown in chapter 8. Plausibility and applicability have been analysed for that with the help of experimental sensitivity studies, especially the identification of successive, experimental damage growth. This then leads to the dissertation conclusions and a discussion of possible future research in chapter 9.

2.2 SCIENTIFIC INNOVATIONS AND PUBLISHED WORK

This dissertation offers several scientific highlights and innovations. While the most important ones are named in the following, a list of publications is given afterwards:

i) SUBSPACE IDENTIFICATION is comprehensively described with a focus on its application in chapter 4. This overview may give engineers a solid basis for their own structural analyses.

ii) THE $\mathcal{H}^\infty$ ESTIMATION THEORY following the indefinite-quadratic estimation approach is comprehensively worked through in chapter 5. Very importantly, somewhat contradictory scientific work of $\mathcal{H}^\infty$ estimation is unified and presented in step-by-step explanations. By focussing on engineering oriented statements, it is introduced to structural dynamics and health monitoring.

iii) THE DAMAGE LOCALIZATION METHOD SP2E is proposed and analysed in chapter 6. The application of both stochastic subspace identification and $\mathcal{H}^\infty$ theory to define a damage-sensitive difference process is new. The analysis by synchronization and normalization in a state space system allows vast theoretical developments. Furthermore, state projections enhance the damage identification result.

iv) EXPERIMENTAL SENSITIVITY STUDIES were conducted to verify method SP2E. Therein, structural alterations have been applied to the laboratory structure of chapter 7. By experimentally increasing the structural alteration, plausibility and applicability of SP2E were studied. Based on that, chapter 8 confirms the practicability of the new method.

PUBLISHED ARTICLES

[Art1] A. Lenzen and M. Vollmering. An output only damage identification method based on $\mathcal{H}_\infty$ theory and state projection estimation error (SP2E). *Structural Control and Health Monitoring*, 24(11), 2017.

[Art2] A. Lenzen and M. Vollmering. On experimental damage localization by SP2E: Application of $\mathcal{H}^\infty$ estimation and oblique projections. *Mechanical Systems and Signal Processing*, 104:648–662, 2018.

PRESENTATIONS AND PUBLISHED PROCEEDINGS

[Proc1] A. Lenzen and M.Vollmering. A new technique for damage localisation using estimates in krein spaces. *6th International Operational Modal Analysis Conference*, Proceedings:239–248, 2015.

[Proc2] A. Lenzen and M.Vollmering. Eine neue Methodik zur schwingungsbasierten Schadensidentifikation. *5.VDI-Fachtagung Baudynamik 2015*, VDI-Berichte 2244:171–185, 2015.

[Proc3] A. Lenzen and M.Vollmering. Vergleich verschiedener Ansätze zur Identifikation instationärer Eigenfrequenzen. *4.VDI-Fachtagung Schwingungsanalyse & Identifikation 2016*, VDI-Berichte 2259:179–196, 2016.

2.3 NOMENCLATURE

This dissertation follows the common nomenclature of structural dynamics, system theory and linear algebra in general. Because of this interdisciplinary approach, multiple notation usage sometimes is unavoidable. In the following, repeatedly used, important acronyms and notations are listed.

ACRONYMS

DARE	Discrete-time Algebraic Riccati Equation
EOC	Environmental and Operational Conditions
FEM	Finite Element Model
MAC	Modal Assurance Criterion
MIMO	Multiple Input Multiple Output
OMA	Operational Modal Analysis
SHM	Structural Health Monitoring
SISO	Single Input Single Output
SP2E	State Projection Estimation Error
SSI	Stochastic Subspace Identification

SYSTEMS

Δ	System: $y \to d$
$\mathcal{H}, H$	System: $w, v \to y$
$\mathcal{K}$	System: $y \to \hat{s}$
$\mathcal{L}$	System: $w \to s$
$\mathcal{T}_K$	System: $w, v \to \tilde{s}$
Ω	System: $w, v \to d$
Π	System: $e \to y$
G	System: $f \to x, \dot{x}, \ddot{x}$

MATRICES

Π	Lyapunov solution
H	Impulse response matrix
$I, 0$	Identity and zero matrix
K_p	Gain matrix
L	Weighting matrix
M	Input Gramian
M, K, D	Mass, stiffness, damping matrix
N	Control matrix
P, Σ	Solution of Riccati equations

P_x, Π_x	Projectors onto x
Q, R, S	Gramians of w and v
R_x	Gramian/covariance of x
S_x	Spectral density of x
S_y, Σ	Popov function
U, V	Basis of spaces $\mathcal{U}$ and $\mathcal{V}$
Y, Z	Coupling matrices
A	System matrix
B	Control matrix
C	Observer matrix
D	Feed-through matrix

OPERATIONS

$\langle \times \rangle$	Gramian matrix
$\|\times\|_2$	Matrix 2-norm, Euclidian distance
$\|\times\|_F$	Frobenius norm
$\|\times\|_{\mathcal{H}^2}$	$\mathcal{H}^2$-norm
$\|\times\|_{\mathcal{H}^\infty}$	$\mathcal{H}^\infty$-norm
$E\{\times\}$	Expected value
$\times^T$	Transpose
$\times^*$	Conjugate transpose
$\times^{-1}$	Inverse
$\times^{-*}$	Inverse of conjugate transpose
$\times^\dagger$	Moore-Penrose pseudoinverse

SPACES

$\mathcal{H}, \mathcal{K}$	Hilbert and Krein space
$\mathcal{U}, \mathcal{V}$	Complementary subspaces
$\mathcal{W}$	Vector space
$\mathbb{N}$	Non-negative natural numbers
$\mathbb{R}$	Real numbers
$\mathbb{C}$	Complex numbers

SCALAR QUANTITIES

δ_{kl}	Kronecker delta
γ	Upper bound
k, l	Discrete time-step
m	Number of block rows/columns
M_x	Measurement Position
N	Number of samples
n	Number of states
p	Number of meas. positions
z	Complex number
ω, θ	Angular frequency
f	Natural frequency
ζ	Modal damping

VECTORS

$\bar{P}$	Average process power
Δt	Time difference
λ, σ	Eigenvalue, singular value
ϕ, ψ	Mode shapes
d	Difference process
e	Estimation error
f	Force vector
s	Desired signal
u, y	Input and output vector
v	Measurement noise
w	Process noise
x, z	State vector
$x, \dot{x}, \ddot{x}$	Displacement and derivates

2.4 ACKNOWLEDGEMENTS

Part I

MECHANICAL SYSTEMS BY FIRST PRINCIPLES AND SUBSPACE IDENTIFICATION

MODELS BASED ON FIRST PRINCIPLES IN STRUCTURAL DYNAMICS

CHAPTER OUTLINE

This chapter covers important solutions of structural dynamics. For that, the main concern can be seen as the determination of structural responses of an analytically derived mechanical system due to known load excitations. To explain that, a fundamental classification between time and Laplace-domain solutions can be given, which has been kept by sections 1 and 2. These models are derived following physical first principles, especially Newton's mechanics and the thereof derived analytical mechanics. The term 'first principle based' has been chosen on purpose to highlight that empirical data is not primarily used here.
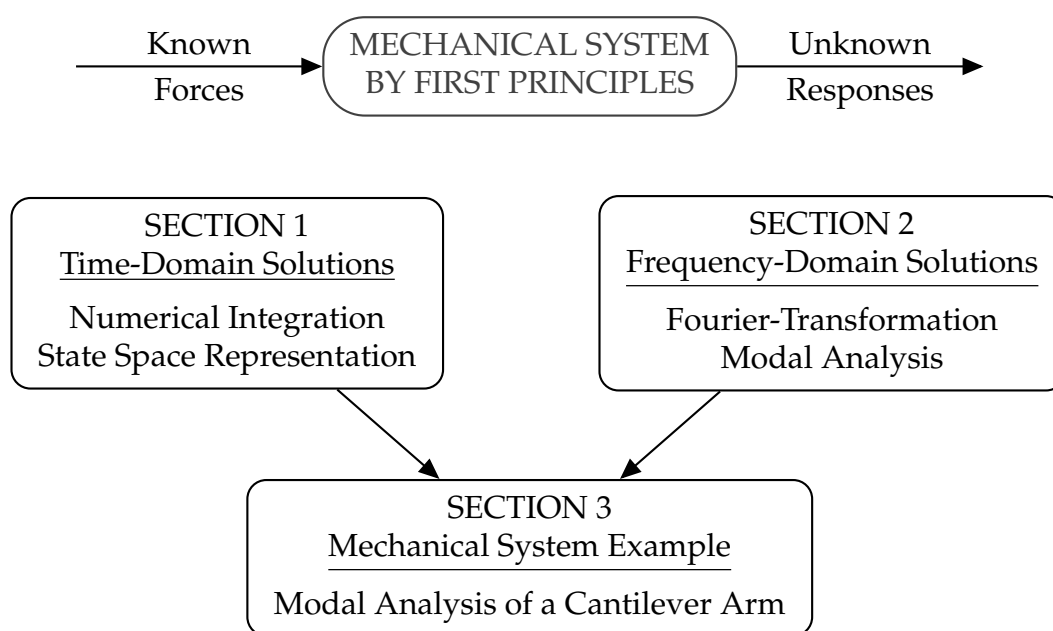
Figure 3.1: Chapter Outline

Most importantly, derivations following analytical mechanics are continuous-time solutions, which then are implemented numerically in discrete-time. In the end an illustrative mechanical system example is given to clarify the given results.

3.1 Time-Domain Solution

3.1.1 Equation of Motion in Structural Dynamics

An engineering oriented analysis of a mechanical structure requires a usable model. In the design phase of buildings, infrastructures and so forth the load capacity and serviceability are typically studied. Here, first principles of mechanics are usually applied. Because of the high relevance of first principle based models, they are discussed in the following. Although they are important in the design phase, an application during operation for structural health monitoring is rather elaborate and cost-intensive. Thus, just a brief overview of most important aspects is given.

A structural analysis also covers mechanical systems due to loads. These forces may vary over time, which typically is considered in structural dynamics. To describe the dynamic behaviour of a system, an equation of motion

$$\mathcal{M}\Big(x(t), \dot{x}(t), \ddot{x}(t), f(t), t\Big) = 0 \tag{3.1}$$

typically is set up. At this point, the vector of external forces $f \in \mathbb{R}^N$, the displacement vector $x \in \mathbb{R}^N$ and its time derivations, velocity $\dot{x} \in \mathbb{R}^N$ and acceleration $\ddot{x} \in \mathbb{R}^N$, are utilized. Very importantly, the degree of freedom N has been used here.

Most commonly, Newton's second law of motion is used to derive analytical models in structural dynamics. Based on Newton's classical mechanics, analytical mechanics arose to extend the theory. To name but a few approaches: i) Principle of virtual work, ii) Hamilton's principle, iii) principle of least action and so forth. Following analytical mechanics, the well known equation of motion in structural dynamics

$$M\ddot{x}(t) + D\dot{x}(t) + Kx(t) = f(t) \tag{3.2}$$

can be defined, which is a widespread approximation (linearization) at an operating point.[4] As it is common-practice in structural dynamics, viscous damping and linear-elastic system behaviour are presupposed approximately. The mechanical structure itself is described by the physically derived stiffness matrix $K \in \mathbb{R}^{N \times N}$, mass matrix $M \in \mathbb{R}^{N \times N}$ and damping matrix $D \in \mathbb{R}^{N \times N}$.

Due to Betti's theorem, the Lagrangian formalism and the Rayleigh damping approach, all three matrices (K, M, D) are presumed here as positive definite and symmetric.[4] Besides that, gyroscopic and circulatory forces have been explicitly omitted above.

The equation of motion (3.2) is primarily known as a fundamental equation in finite element modelling and multi-body simulations. Besides their significance, both methods are not described in this thesis.

As was explained before, a structural response $x(t)$ shall be numerically determined based on known system parameters (K, M, D), defined forces f and initial displacements, velocities and accelerations $(t = 0)$. To do so, the convolution

$$x(t) = G(t) * f(t) = \int_0^t G(t - \tau)f(\tau) \; d\tau \tag{3.3}$$

must be solved in general, which is elaborate. Here, matrix function $G \in \mathbb{R}^{N \times N}$ refers to the structural response of the mechanical system due to a successive Dirac impulse $\delta(t)$ excitation at each measurement position. As can be seen in equation (3.3), the mechanical structure is comprehensively described by its impulse response function.

Unfortunately, based on the equation of motion (3.2), this approach is elaborate, as it needs numerical integration. In opposite to that, a discrete-time process

$$x_k = \sum_{l=0}^{k} H_{k-l} f_l \quad \text{with} \quad M\ddot{x}_k + D\dot{x}_k + Kx_k = f_k \tag{3.4}$$

may be used instead, following the discrete-time impulse response H_k with $t = k\Delta t$ and $k, l \in \mathbb{N}$. The numerical determination of these sequences is explained below based on the general state space approach.

3.1.2 MECHANICAL STRUCTURES IN STATE SPACE FORM

State space systems allow the development of more comprehensive system analysis techniques and lead to a general solution. Very importantly, mechanical structures can be seen as a special case of state space systems with distinctive properties, in opposite, for instance, to certain electrical components.

In the following, mechanical structures are discussed only. For that, the core concept is the introduction of a state vector

$$z(t) = \begin{bmatrix} x(t) \\ \dot{x}(t) \end{bmatrix} \quad \text{with} \quad z \in \mathbb{R}^{2N} . \tag{3.5}$$

This state vector is used as an intermediate result, when analysing the mapping from an excitation to the structural response. Following that approach, the equation of motion (3.2) is equivalently rewritten to formulate a state space representation[98,99]

$$\begin{bmatrix} D & M \\ M & 0 \end{bmatrix} \begin{bmatrix} \dot{x}(t) \\ \ddot{x}(t) \end{bmatrix} + \begin{bmatrix} K & 0 \\ 0 & -M \end{bmatrix} \begin{bmatrix} x(t) \\ \dot{x}(t) \end{bmatrix} = P\dot{z}(t) + Qz(t) = \begin{bmatrix} I \\ 0 \end{bmatrix} f(t) . \tag{3.6}$$

This approach allows to analyse the second order differential equation (3.2) as a first order one. By reordering the above expression, a state space system in controllable canonical form

$$\dot{z}(t) = \begin{bmatrix} 0 & I \\ -M^{-1}K & -M^{-1}D \end{bmatrix} \begin{bmatrix} x(t) \\ \dot{x}(t) \end{bmatrix} + \begin{bmatrix} 0 \\ M^{-1} \end{bmatrix} f(t) \qquad = \bar{A}z(t) + \bar{B}f(t) \qquad (3.7a)$$

$$x(t) = \begin{bmatrix} I & 0 \end{bmatrix} \begin{bmatrix} x(t) \\ \dot{x}(t) \end{bmatrix} \qquad = \bar{C}_d z(t) \qquad (3.7b)$$

with continuous-time parameters $\bar{A} \in \mathbb{R}^{2N \times 2N}$, $\bar{B} \in \mathbb{R}^{2N \times N}$ and $\bar{C}_d \in \mathbb{R}^{N \times 2N}$ arises. Thus, continuous-time state space system $G(\bar{A}, \bar{B}, \bar{C}_d)$ maps loads $f(t)$ to measurable displacements $x(t)$ here, as is depicted in figure 3.2.
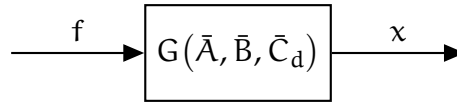
Figure 3.2: Continuous-Time State Space System G

In practice (e.g. at a bridge) displacements x are elaborate to measure, because an independent measuring base is necessary. Instead velocities and accelerations are much easier to determine experimentally. Hence, the observer equation (3.7b) can be replaced to measure velocities or accelerations by

$$\dot{x}(t) = \begin{bmatrix} 0 & I \end{bmatrix} \begin{bmatrix} x(t) \\ \dot{x}(t) \end{bmatrix} \qquad = \bar{C}_v z(t) \quad \text{or} \qquad (3.8)$$

$$\ddot{x}(t) = \begin{bmatrix} -M^{-1}K & -M^{-1}D \end{bmatrix} \begin{bmatrix} x(t) \\ \dot{x}(t) \end{bmatrix} + M^{-1}f(t) \qquad = \bar{C}_a z(t) + \bar{D}_a f(t) . \qquad (3.9)$$

According to Ebert,[25] these observer equations are based on

$$\bar{C}_v = \bar{C}_d \bar{A}, \quad \bar{C}_a = \bar{C}_d \bar{A}^2, \quad \bar{D}_v = \bar{C}_d \bar{B} = 0 \quad \text{and} \quad \bar{D}_a = \bar{C}_d \bar{A}\bar{B} . \qquad (3.10)$$

Following that, displacements, velocities and accelerations can easily be determined, if states $z(t)$ have already been computed. In the following, the index of $\bar{C}$ and $\bar{D}$ is conveniently dropped and should be thought in context of the respective requirement. Very importantly, a similarity transform with

$$\tilde{z}(t) = Tz(t), \quad \tilde{A} = T\bar{A}T^{-1}, \quad \tilde{B} = T\bar{B}, \quad \tilde{C} = \bar{C}T^{-1} \quad \text{and} \quad \tilde{D} = \bar{D} \qquad (3.11)$$

alters the state z, while the structural response persists. Thus, the controllable canonical form in equation (3.7) is a special case of an infinite number of possible state space structures according to a positive definite transformation matrix $T > 0$.

THE NUMERICAL SOLUTION of equation (3.7a) can now be given. For that, the analytical approach follows the convolution

$$z(t) = e^{\bar{A}t}z_0 + \int_0^t e^{\bar{A}(t-\tau)}\bar{B}f(\tau)\,d\tau\,. \tag{3.12}$$

Therein matrix function $e^{\bar{A}t}$ is important, which can be determined differently, for instance by the Cayley Hamilton theorem, series expansion or Taylor series.[100] Most importantly, it can be used to get the response of the mechanical system due to a Dirac impulse excitation at each measurement point

$$G(t) = \bar{C}e^{\bar{A}t}\bar{B} \quad \text{if} \quad \bar{D} = 0\,, \tag{3.13}$$

which was used in equation (3.3).

In accordance with the equation of motion (3.4), discrete-time sequences with $t = k\Delta t$ must be applied. By assuming a constant input f during a time step Δt, the discrete-time state space observer equation

$$z_{k+1} = e^{\bar{A}t}z_k + \bar{A}^{-1}\left(e^{\bar{A}t} - I\right)\bar{B}f_k = Az_k + Bf_k \tag{3.14}$$

emerges. This method is also known as zero-order-hold, because it holds each sample value for one sample interval, which leads to

$$A = e^{\bar{A}\Delta t}, \qquad B = \bar{A}^{-1}\left(e^{\bar{A}\Delta t} - I\right)\bar{B}, \qquad C = \bar{C} \quad \text{and} \quad D = \bar{D}\,. \tag{3.15}$$

The shown discretization may be numerically disadvantageous due to high matrix exponential, among others. Thus, approximation solutions can be applied, for instance the Tustin transform.[25]

Finally, an impulse response function H_k can be defined based on the discrete-time parameters (A, B, C, D):

$$H_k = \begin{cases} D, & k = 0 \\ CA^{k-1}B, & k > 0 \end{cases}\,. \tag{3.16}$$

This impulse response solution H_k is important, because it comprehensively describes a mechanical system, as was explained for equation (3.4).

3.2 FREQUENCY-DOMAIN SOLUTION

3.2.1 LAPLACE AND Z-TRANSFORM

The determination of continuous-time structural responses are based on the convolution of equation (3.3). Based on that, elaborate numerical integration methods are necessary, as was explained before. At this point, a Laplace transform

$$x(t) = G(t) * f(t) \qquad \circ\!\!-\!\!\bullet \qquad x(s) = G(s)f(s) \quad \text{with} \quad s = \sigma + j\omega \tag{3.17}$$

allows much easier derivations.[4] Hence, the elaborate convolution has been replaced by a matrix multiplication. It is based on the two-sided Laplace transform $\mathcal{L}(\times)$ and its inverse $\mathcal{L}^{-1}(\times)$, for instance

$$\bar{x}(s) = \mathcal{L}\big(x(t)\big) = \int\limits_{-\infty}^{\infty} x(t)e^{-st}\,dt\,. \tag{3.18}$$

Although the central signal information is analysed differently, it is preserved, because the Laplace transform is also referred to as a unitary linear operator.[4] Furthermore, the transfer matrix function

$$G(s) = \big(Ms^2 + Ds + K\big)^{-1} \tag{3.19}$$

directly follows the Laplace transform of the equation of motion (3.2).

Here, a very important special case with $\sigma = 0$ is called the continuous-time Fourier transform $\mathcal{F}$, which is widely applied with $s = j\omega$: By computing the structural response in frequency domain with $x(j\omega)$, a time-domain solution can easily be given by the inverse continuous-time Fourier transform $x(t) = \mathcal{F}^{-1}\big(x(j\omega)\big)$.

STATE SPACE SYSTEMS are advantageous, because their transfer matrix function is generally known regardless of its application. Based on that, the transfer matrix function for mechanical structures

$$G(s) = \int\limits_{-\infty}^{\infty} G(t)e^{-st}\,dt = \bar{C}\big(sI - \bar{A}\big)^{-1}\bar{B} + \bar{D} \quad \text{with} \quad \big(sI - \bar{A}\big)^{-1} = \mathcal{L}\big(e^{\bar{A}t}\big) \tag{3.20}$$

directly follows the impulse response matrix function in equation (3.13).

Besides the given continuous-time solution, a discrete-time approach is especially necessary, when a measurement sequence is present. This is the typical case due to digital technologies. For that, the two-sided z-transform

$$x(z) = \sum\limits_{k=-\infty}^{\infty} x_k z^{-k} \quad \text{with} \quad z = e^{s\Delta t} \tag{3.21}$$

can be used. The z-transform converges to the Laplace transform with $\Delta t \to 0$, as can be seen by comparing equations (3.18) and (3.21).

However, the discrete-time state space representation is well known in z-domain by

$$H(z) = \sum\limits_{k=0}^{\infty} H_k z^{-k} = C(zI - A)^{-1}B + D, \quad \text{for example} \quad x(z) = H(z)f(z)\,. \tag{3.22}$$

In the above equation the unilateral z-transform of the discrete-time impulse matrix function H_k in equation (3.16) has been used. By using discretization methods, an

error is unavoidable. This error is minimized for $\Delta t \to 0$, for example in frequency domain by

$$G(j\omega) = \lim_{\Delta t \to 0} H(e^{j\theta}) \quad \text{with} \quad \theta = \omega \Delta t, \quad \theta \in [-\pi, \pi] . \tag{3.23}$$

Summarizing the given Laplace and z-transform applications, the frequency domain results avoid elaborate numerical integration. Thus, advantageous solutions to determine structural responses can be used instead.

3.2.2 Modal Analysis of Mechanical Systems

Based on the results above, the vibrational properties of a mechanical structure can be studied. This leads to an important mechanical system description. For that, consider the search for zeros in

$$\left(Ms^2 + Ds + K\right)x = 0 , \tag{3.24}$$

which follows transfer matrix function $G(s)$ in equation (3.19).

To find solutions $\lambda_i = s_i$ to the above problem, the state space description is an excellent approach. Thus, an eigenvalue analysis

$$\left(\bar{A} - \lambda_i I\right)\psi_i = 0 \quad \text{or} \quad \left(Q + P\lambda_i\right)\psi_i = 0 \quad \text{with} \quad \bar{A} = -P^{-1}Q \tag{3.25}$$

must be solved.[101] While the first approach follows system matrix $\bar{A}$ in equation (3.7a), the second one is a generalization according to equation (3.6). Therefore, the analytical solution is known by

$$\lambda_{i,i+1} = -\delta_i \pm j\,\omega_{d,i} = -\zeta_i\omega_{0,i} \pm j\,\omega_{0,i}\sqrt{1 - \zeta_i^2} \quad \text{and} \quad \psi_i = \begin{bmatrix} \phi_i \\ \phi_i\lambda_i \end{bmatrix} . \tag{3.26}$$

Here, an index $i = 1, 3, \ldots, 2N - 1$ has been introduced, which marks complex conjugated mode pairs.

Furthermore, the undamped and damped angular frequencies ω_0 and ω_d, the decay constant δ and the modal damping ζ has been used. Thus, the damped frequency and the modal damping can be easily determined based on eigenvalues with

$$f_i = \frac{\Im(\lambda_i)}{2\pi} = \frac{\omega_{d,i}}{2\pi} \quad \text{and} \quad \zeta_i = -\frac{\Re(\lambda_i)}{|\lambda_i|} = \frac{\zeta_i\omega_{0,i}}{\sqrt{\zeta_i^2\omega_{0,i}^2 + \omega_{0,i}^2(1 - \zeta_i^2)}} = \frac{\zeta_i\omega_{0,i}}{\omega_{0,i}} . \tag{3.27}$$

Additionally, the generalized mode shapes ϕ_{i+1} are the complex conjugate of ϕ_i.[101] For further analysis all modal results are reordered in compact matrices as

$$\Psi = \begin{bmatrix} \psi_1 & \psi_2 & \ldots & \psi_{2N} \end{bmatrix} = \begin{bmatrix} \Phi \\ \Phi\Lambda \end{bmatrix} = \begin{bmatrix} \phi_1 & \phi_2 & \ldots & \phi_{2N} \\ \phi_1\lambda_1 & \phi_2\lambda_2 & \ldots & \phi_{2N}\lambda_{2N} \end{bmatrix} . \tag{3.28}$$

THE JORDAN FORM of state space systems refers to a special representation in diagonal canonical form. From a system theoretic view, poles of the mechanical structure, which numerically can be determined by eigenvalues λ_i, are diagonally placed in the system matrix. This is achieved by applying the similarity transformation of equation (3.11) with a chosen transformation matrix $T = \Psi^{-1}$, which leads to

$$q(t) = \Psi^{-1} z(t), \qquad \Lambda = \Psi^{-1} \bar{A} \Psi, \qquad \hat{B} = \Psi^{-1} \bar{B} \quad \text{and} \quad \Phi = \bar{C}_d \Psi. \tag{3.29}$$

Here, subelements are introduced for further analysis:

$$q^*(t) = \begin{bmatrix} q_1^*(t) & q_2^*(t) & \dots & q_{2N}^*(t) \end{bmatrix} \quad \text{and} \quad \hat{B}^* = \begin{bmatrix} \hat{b}_1^* & \hat{b}_2^* & \dots & \hat{b}_{2N}^* \end{bmatrix}. \tag{3.30}$$

This transform has very important implications: In accordance with the state evolution in equation (3.12), the time-domain result is a sum of independent generalized mode shapes following

$$x(t) = \Phi q(t) = \sum_{i=1}^{2N} \phi_i q_i(t) \quad \text{with} \quad q_i(t) = e^{\lambda_i t} q_{i,0} + \int_0^t e^{\lambda_i(t-\tau)} \hat{b}_i f(\tau) \, d\tau. \tag{3.31}$$

If velocities or accelerations shall be measured instead, the approach keeps very similar, in general by $\hat{C} = \bar{C}\psi$ with column vectors $\hat{c}_i$. This leads to a rewritten form of the transfer matrix function of equation (3.20)

$$G(s) = \bar{D} + \hat{C}(sI - \Lambda)\hat{B} = \bar{D} + \sum_{i=1}^{2N} \frac{\hat{c}_i \hat{b}_i}{s - \lambda_i}. \tag{3.32}$$

Centrally, the above statements define a mechanical structure as the sum of its vibrational properties, especially mode shapes, natural frequencies and dampings.

3.2.3 MODEL REDUCTION OF MECHANICAL STRUCTURES

From an application-oriented viewpoint, system norms can be seen as a response measure of a system due to a standard excitation, especially the unit impulse (deterministic) or white noise with standard deviation (stochastic).[102] In this thesis system norms are repeatedly used i) to apply model reduction and ii) as a basis for $\mathcal{H}^\infty$ estimation theory. While the second issue is treated in chapter 5, model reduction is subsequently explained following Gawronski[102] and Wirnitzer:[103]

Consider a continuous-time state space system, for instance G in equation (3.20), then the $\mathcal{H}^2$ and the $\mathcal{H}^\infty$ norm are

$$\|G\|_{\mathcal{H}^2}^2 = \frac{1}{2\pi} \int_{-\infty}^{\infty} \left\| G(j\omega)G^*(j\omega) \right\|_F d\omega, \quad \|G\|_{\mathcal{H}^\infty}^2 = \max_\omega \sigma_{max}\left(G(j\omega)G^*(j\omega)\right). \tag{3.33}$$

A feed-through matrix $\bar{D}$ should be ignored here, because a transfer matrix function with $G(j\omega) = \bar{D}$ for all ω leads to an infinitely large $\mathcal{H}^2$ norm. However, for discrete-time systems, like H in equation (3.22), slight changes are necessary:

$$\|H\|_{\mathcal{H}^2}^2 = \frac{1}{2\pi} \int_{-\pi}^{\pi} \left\| H(e^{j\theta})H^*(e^{j\theta}) \right\|_F d\theta, \qquad \|H\|_{\mathcal{H}^\infty}^2 = \max_\theta \sigma_{\max}\left(H(e^{j\theta})H^*(e^{j\theta})\right). \quad (3.34)$$

Following Gawronski,[102] both cases, the continuous and the discrete-time system norms, are related by

$$\|G\|_{\mathcal{H}^2}^2 = \frac{\|H\|_{\mathcal{H}^2}^2}{\Delta t} \quad \text{and} \quad \|G\|_{\mathcal{H}^\infty}^2 = \lim_{\Delta t \to 0} \|H\|_{\mathcal{H}^\infty}^2 . \quad (3.35)$$

THE NORM OF A VIBRATIONAL MODE can be determined based on the modal description of equation (3.32). Modes arise complex conjugated for mechanical systems, thus mode pairs should be analysed by

$$\left\|G_i + G_{i+1}\right\|_{\mathcal{H}^2}^2 \approx \frac{\|\hat{c}_i\|_2^2 \|\hat{b}_i\|_2^2}{\zeta_i \omega_{0,i}} \quad \text{and} \quad \left\|G_i + G_{i+1}\right\|_{\mathcal{H}^\infty}^2 = \frac{\|\hat{c}_i\|_2^2 \|\hat{b}_i\|_2^2}{\zeta_i^2 \omega_{0,i}^2} . \quad (3.36)$$

The complete mechanical structure then is the sum of its mode pairs in the case of $\mathcal{H}^2$ or the maximum in the case of $\mathcal{H}^\infty$:

$$\|G\|_{\mathcal{H}^2}^2 = \sum_{i=1}^{2N} \|G_i\|_{\mathcal{H}^2}^2 \quad \text{and} \quad \|G\|_{\mathcal{H}^\infty}^2 = \max_i \|G_i\|_{\mathcal{H}^\infty}^2 . \quad (3.37)$$

Here, a feed-through matrix $\bar{D}$ has been neglected again, as it is unusable for the $\mathcal{H}^2$ case and it is presumed to have a small impact on the entire $\mathcal{H}^\infty$ norm.

Based on the above definitions, model reduction directly follows. Because a mechanical structure is the sum of its vibrational modes, a straightforward model reduction technique neglects modes, which are unnecessary. Formally, a state space system is ordered as 'reduced' G_r and 'truncated' G_t by

$$G\left(\begin{bmatrix} \Lambda_r & 0 \\ 0 & \Lambda_t \end{bmatrix}, \begin{bmatrix} \hat{B}_r \\ \hat{B}_t \end{bmatrix}, \begin{bmatrix} \hat{C}_r & \hat{C}_t \end{bmatrix} \right) \quad \longrightarrow \quad G_r\left(\Lambda_r, \hat{B}_r, \hat{C}_r\right) \quad \text{with } G = G_r + G_t . \quad (3.38)$$

The truncated system G_t is then analysed with the help of truncated modes, especially equation (3.37). Hence, a possible model reduction error can be quantified by

$$e_{\mathcal{H}^2} = \|G_t\|_{\mathcal{H}^2}^2 \quad \text{or} \quad e_{\mathcal{H}^\infty} = \|G_t\|_{\mathcal{H}^\infty}^2 . \quad (3.39)$$

3.3 STRUCTURAL DYNAMICS EXAMPLE

3.3.1 SINGLE DEGREE OF FREEDOM SYSTEM

In the following, the former derivations are applied at two mechanical systems of a bending beam. These are in accordance with the laboratory structure, which is used in chapter 7: A steel rectangular hollow section $80 \times 40 \times 2.9$mm, which is depicted in figure 7.2. At first a single input single output (SISO) system is analysed: Consider the cantilever beam in figure 3.3 with Young's modulus $E = 2.1 \cdot 10^{11} \mathrm{N/m^2}$ and a second moment of area $I = 17.7 \cdot 10^{-8} \mathrm{m^4}$. Thus, flexibility δ and stiffness k follow with

$$\delta = \frac{1}{3}\frac{l^3}{EI} \approx 1.24 \times 10^{-4}\,\frac{m}{N} \quad \text{and} \quad k = \frac{1}{\delta} \approx 8.1 \times 10^3\,\frac{N}{m} = 8.1\,\frac{N}{mm}\,. \tag{3.40}$$

$$x(t) \qquad \text{constant } EI$$

$$l = 240\text{cm}$$
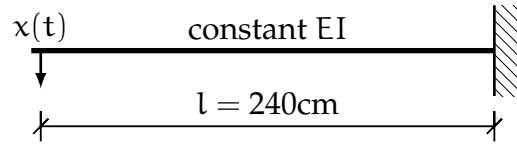
Figure 3.3: Mechanical SISO System

Mass m and damping factor d are reasonably chosen as

$$m = 7.25\,\text{kg} = 7.25\,\frac{Ns^2}{m} = 7.25 \times 10^{-3}\,\frac{Ns^2}{mm} \quad \text{and} \quad d = 10\,\frac{Ns}{m} = 10^{-2}\,\frac{Ns}{mm}\,. \tag{3.41}$$

The mass followed the specific weight of structural steel $\gamma = 78,5\text{kN/m}^3$ and an area of $A = 6,55\text{cm}^2$. In addition to that a sensor mass of $m_S \approx 0,95\text{kg}$ was presumed. This illustrative structural dynamics example leads to modal data

$$f = \frac{1}{2\pi}\sqrt{\frac{k}{m}}\left(1 - \zeta^2\right) \approx 5.31\text{Hz} \quad \text{and} \quad \zeta = \frac{d}{d_{crit}} = \frac{d}{2\sqrt{km}} \approx 2.1\%\,. \tag{3.42}$$

To measure displacements, a state space system G is defined, in accordance with equation (3.7), with

$$\dot{z}(t) = \begin{bmatrix} \dot{x}(t) \\ \ddot{x}(t) \end{bmatrix} = \begin{bmatrix} 0 & 1 \\ -m^{-1}k & -m^{-1}d \end{bmatrix} \begin{bmatrix} x(t) \\ \dot{x}(t) \end{bmatrix} + \begin{bmatrix} 0 \\ m^{-1} \end{bmatrix} f(t) \quad = \bar{A}z(t) + \bar{B}f(t) \tag{3.43a}$$

$$x(t) = \begin{bmatrix} 1 & 0 \end{bmatrix} \begin{bmatrix} x(t) \\ \dot{x}(t) \end{bmatrix} \qquad\qquad\qquad = \bar{C}_d z(t)\,. \tag{3.43b}$$

This leads to the system norms of equation (3.33). Because a SISO system is analysed, only one mode pair is present, whose norms are

$$\|G\|_{\mathcal{H}^2}^2 \approx 6.2 \quad \text{and} \quad \|G\|_{\mathcal{H}^\infty}^2 \approx 9.0 \,. \tag{3.44}$$

These results can be interpreted best, when considering a standardized input,[102] for instance a unit impulse or a white noise excitation with standard deviation (deterministic or stochastic). Thus, a white noise excitation process with covariance $R_f(0) = 1N^2$ leads to an average structural response process power of $R_y(0) = 6.2mm^2$, which can be derived following the $\mathcal{H}^2$ norm. Furthermore, the power spectrum $S_y = \mathcal{F}(R_y)$ at the natural frequency is known by $9.0mm^2$. Here, the peak (maximum) was found by the $\mathcal{H}^\infty$ norm.

3.3.2 MULTI DEGREE OF FREEDOM SYSTEM

The former example shall now be extended. Thus, eight degrees of freedom are used instead, which are depicted in figure 3.4.
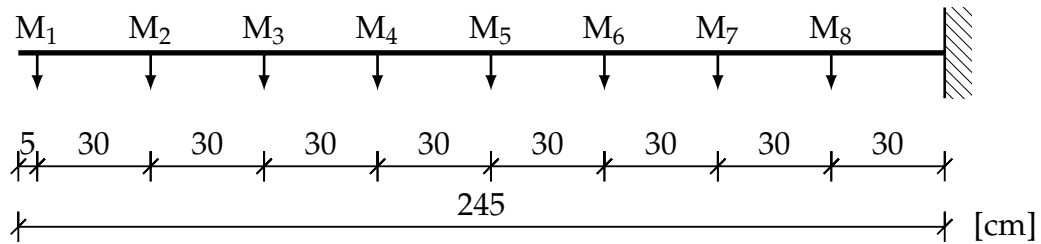
Figure 3.4: Mechanical MIMO System

At this point, a state space representation based on equations (3.7a) and (3.9) is used to define a system G with

$$\dot{z}(t) = \begin{bmatrix} 0 & I \\ -M^{-1}K & -M^{-1}D \end{bmatrix} \begin{bmatrix} x(t) \\ \dot{x}(t) \end{bmatrix} + \begin{bmatrix} 0 \\ M^{-1} \end{bmatrix} f(t) \qquad = \bar{A}z(t) + \bar{B}f(t) \tag{3.45a}$$

$$\ddot{x}(t) = \begin{bmatrix} -M^{-1}K & -M^{-1}D \end{bmatrix} \begin{bmatrix} x(t) \\ \dot{x}(t) \end{bmatrix} + M^{-1}f(t) \qquad = \bar{C}_a z(t) + \bar{D}_a f(t) \,, \tag{3.45b}$$

which maps forces to accelerations. Again, the Youngs's modulus $E = 2.1 \cdot 10^{11} N/m$ of structural steel and a second moment of area with $I = 17.7 \cdot 10^{-8} m^4$ has been used.

To derive the flexibility matrix Δ, the principle of virtual forces has been applied. Thus, displacements δ_{ij} at measurement position i with regard to a virtual force excitation at j have been determined. Afterwards δ_{ij} are rearranged in the flexibility matrix $F \in \mathbb{R}^{8 \times 8}$, which then led to the stiffness matrix by inversion $K = F^{-1}$.
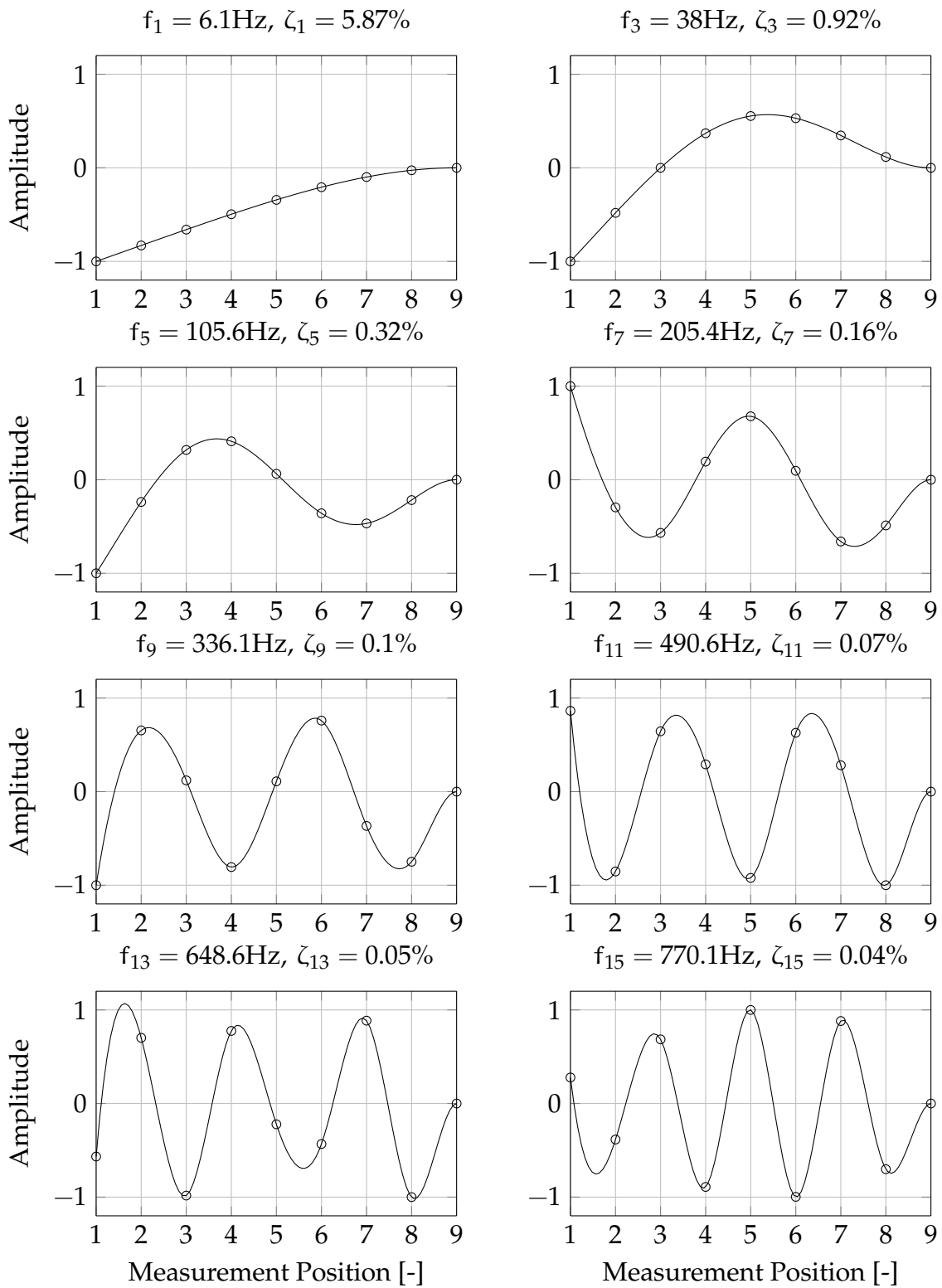
Figure 3.5: Analytical Modal Analysis: Normalized Mode Shapes (Circles) and Cubic Spline Interpolation (Continuous Line)
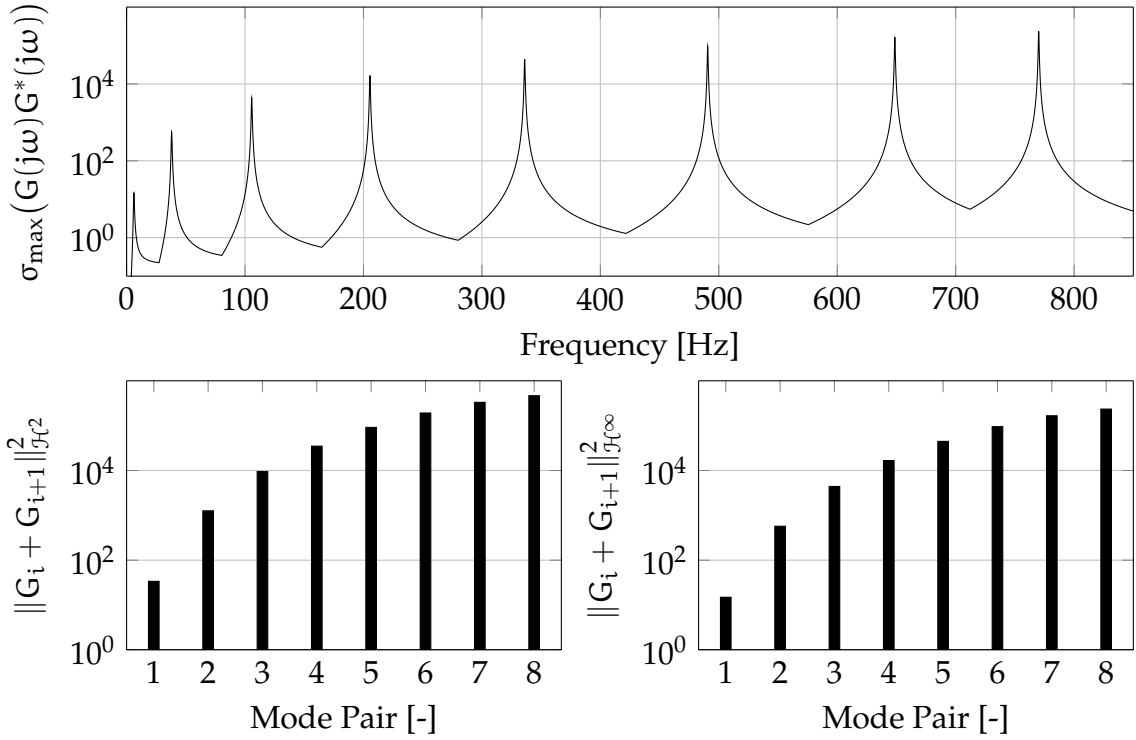
Figure 3.6: Norms of Mode Pairs

The mass and damping matrices have been reasonably chosen following the specific weight $\gamma = 78,5\text{kN/m}^3$, $A = 6,55\text{cm}^2$ and a sensor mass of $m_S \approx 0,95\text{kg}$. A diagonal matrix M then emerges with

$$m_1 \approx 1.7\frac{\text{Ns}^2}{\text{m}}, \quad m_2 = m_3 = \ldots = m_8 \approx 2.5\frac{\text{Ns}^2}{\text{m}}, \quad d_1 = d_2 = \ldots = d_8 = 10\frac{\text{Ns}}{\text{m}} . \quad (3.46)$$

Based on above definitions a modal analysis has been conducted following equations (3.25) and (3.27). The results are shown in figure 3.5. To get a clear representation, the complex mode shapes have been normalized to be real valued and comparable. Furthermore, a cubic spline interpolation has been conducted to enhance the representation in between measurement positions. Nevertheless, this interpolation is arbitrary, and thus is for illustration purposes only. As can be concluded here, the computed natural frequencies, mode shapes and modal dampings are plausible.

Finally, transfer matrix function $G(j\omega)$ of equation (3.32) has been numerically computed and was used to determine norms of mode pairs. The results are in accordance to equation (3.36) and are shown in figure 3.6. As can be seen in this figure, the maximum singular value of $G(j\omega)G^*(j\omega)$ shows eight natural frequencies in vertical direction. Then all eight complex conjugated mode pairs have been analysed by systems norms as a whole with

$$\|G\|_{\mathcal{H}^2}^2 \approx 1.1 \cdot 10^6 \quad \text{and} \quad \|G\|_{\mathcal{H}^\infty}^2 \approx 2.3 \cdot 10^5 . \quad (3.47)$$

The $\mathcal{H}^2$ norm of each mode pair determines the average structural response of the appropriate natural frequency. Because the structural response is the sum of all eight frequencies, the norm $\|G\|^2_{\mathcal{H}^2}$ can be determined as the sum of squared $\mathcal{H}^2$ norms of all mode pairs.

Furthermore, the $\mathcal{H}^\infty$ norm of all mode pairs has been shown in figure 3.6, which essentially gives the peak value due to a standardized input. Then the $\mathcal{H}^\infty$ norm $\|G\|^2_{\mathcal{H}^\infty}$ is the largest value, which here follows the eight mode.

SUBSPACE IDENTIFICATION OF MECHANICAL STRUCTURES

CHAPTER OUTLINE

While chapter 3 mainly dealt with the structural response determination based on known excitations and an analytically derived mechanical system, here the inverse approach is undertaken: Based on measured structural responses and presumed (or measured) excitations, a mechanical system is numerically determined by subspace identification methods. Henceforth, discrete-time signals and systems are analysed due to the necessary measurement digitization. Very importantly, these parametrization techniques have been defined for general processes and multiple-applicable state space systems.
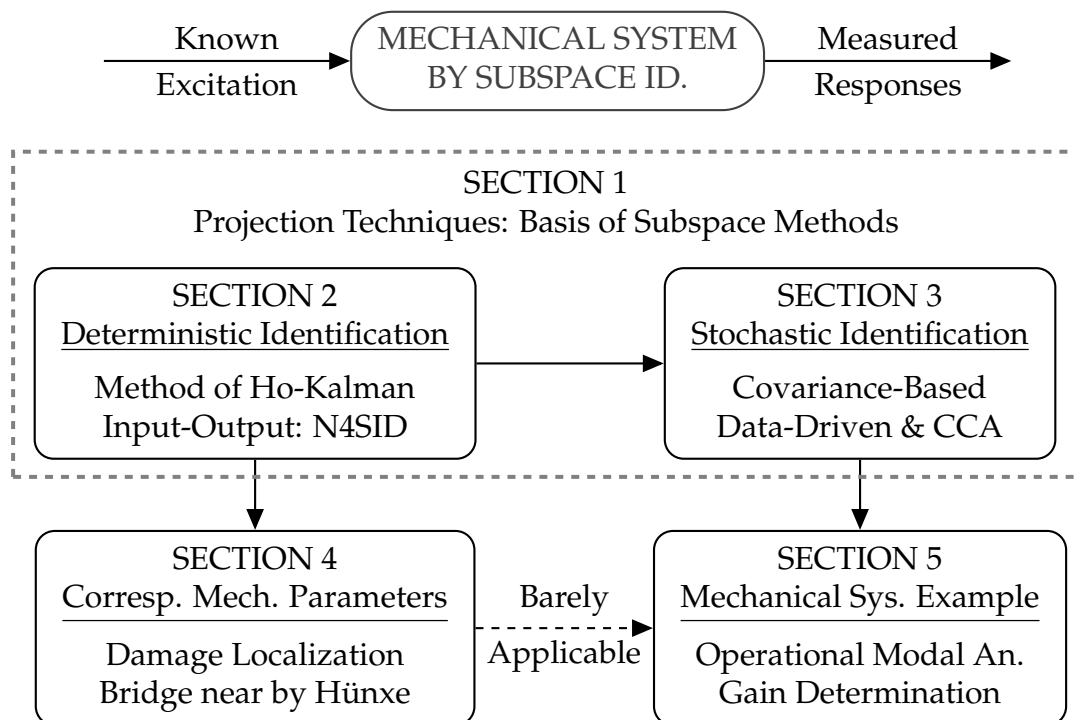
Figure 4.1: Chapter Outline

In this chapter the focus relies on the identification of mechanical structures. Based on projection techniques (section 1), deterministic subspace identification is explained first in section 2, leading the way for further analyses. Afterwards, stochastic subspace

identification is discussed comprehensively in section 3. Additionally, method variations are also given.

Although corresponding mechanical parameters can be determined (e.g. for damage localization) based on known or measured excitations (section 4), it is barely useful when input processes are unknown. This will be explained in the end at the operational modal analysis example of the last section.

4.1 Projections in Linear Algebra

4.1.1 Selected Matrix Decompositions

Projection techniques are essential elements of subspace methods and rely on numerical methods. To understand numerical methods for projections, several matrix decompositions must be revisited. For that, the eigenvalue analysis is shown first.

Consider an invertible matrix $A \in \mathbb{C}^{n \times n}$. Then n eigenvalues λ and eigenvectors $x \in \mathbb{C}^n$, $x \neq 0$ exist, which characterize matrix A. Most importantly, by multiplying A and x the direction remains, thus $Ax_i = \lambda_i x_i$. Eigenvalue λ_i then serves as a scaling factor for x_i. Furthermore, a matrix is called positive definite, positive semi-definite, negative definite, negative semi-definite or indefinite according to its eigenvalues. However, all eigenvalue analysis results are typically condensed in block form with $\Lambda, X \in \mathbb{C}^{n \times n}$ as

$$AX = X\Lambda \quad \text{with} \quad X = \begin{bmatrix} x_1 & x_2 & \cdots & x_n \end{bmatrix}, \, \Lambda = \mathrm{diag}(\lambda_1, \lambda_2, \cdots, \lambda_n) \, . \qquad (4.1)$$

By reordering, the eigendecomposition $A = X\Lambda X^{-1}$ emerges. Only if matrix A is symmetric, the inverse $X^{-1} = X^*$. Furthermore, the shown eigenvalue analysis can be generalized on the basis of invertible matrices $C, B \in \mathbb{C}^{n \times n}$ to

$$Bx_i = C\lambda_i x_i \quad \text{with} \quad A = C^{-1}B \, . \qquad (4.2)$$

THE QR DECOMPOSITION   is another important matrix decomposition, because it allows to determine a recursive eigenvalue algorithm. The idea is to introduce a unitary matrix $Q \in \mathbb{C}^{n \times n}$ ($QQ^* = I$) and an upper triangular matrix $R \in \mathbb{C}^{n \times n}$ to define a decomposition

$$A = QR \quad \text{or} \quad A^* = LQ^* \quad \text{with} \quad L = R^* \, . \qquad (4.3)$$

Several methods have been defined to determine the QR factorization, like the Gram-Schmidt procedure.[20] The actual eigenvalue determination based on the QR decomposition follows

$$A_k = Q_k R_k \quad \text{and} \quad A_{k+1} = R_k Q_k \quad \text{for} \quad k \in \mathbb{N} \, . \qquad (4.4)$$

By complying certain conditions, A_{k+1} converges to the so called Schur form, which has eigenvalues on its principal diagonal.[104]

THE SINGULAR VALUE DECOMPOSITION (SVD) is a generalization of the eigen-decomposition to arbitrary matrices $A \in \mathbb{C}^{m \times n}$. The central idea is to determine the eigendecomposition of

$$AA^* = U\Sigma\Sigma^*U^* \quad \text{and} \quad A^*A = V\Sigma^*\Sigma V^* . \tag{4.5}$$

Thus, singular values $\sigma(A) = \sqrt{\lambda(AA^*)} = \sqrt{\lambda(A^*A)}$ can be determined. Here, the left and right singular vectors $U \in \mathbb{C}^{m \times m}$ and $V \in \mathbb{C}^{n \times n}$ have been used, which are orthonormal eigenvectors of AA^* and A^*A respectively. Those unitary matrices are important because $U^{-1} = U^*$ and $V^{-1} = V^*$.

A central element of this technique are singular values σ_i, which are condensed to

$$\Sigma = \begin{bmatrix} \mathrm{diag}(\sigma_1, \sigma_2, \cdots, \sigma_r) & 0 \end{bmatrix} \quad \text{if} \quad n > m . \tag{4.6}$$

These singular values are crucial characteristics, as they give the rank r of a matrix, among others. Very importantly, the singular value decomposition

$$A = \begin{bmatrix} U_1 & U_2 \end{bmatrix} \begin{bmatrix} \Sigma_1 & 0 \\ 0 & \Sigma_2 \end{bmatrix} \begin{bmatrix} V_1^* \\ V_2^* \end{bmatrix} \approx U_1 \Sigma_1 V_1^* \quad \text{with} \quad \Sigma_2 \to 0 \tag{4.7}$$

allows to distinguish between $U_1 \in \mathbb{C}^{m \times r}$ and $U_2 \in \mathbb{C}^{m \times (m-r)}$ according to singular values, which also is applicable for $V_1 \in \mathbb{C}^{n \times r}$ and $V_2 \in \mathbb{C}^{n \times (n-r)}$. This allows to efficiently determine fundamental subspaces of matrix A, especially

i) the column space $\mathcal{C}(A) = \mathrm{span}\,(U_1)$,

ii) the row space $\mathcal{R}(A) = \mathrm{span}\,(V_1)$,

iii) the null space (kernel) $\mathcal{N}(A) = \mathrm{span}\,(V_2)$ and

iv) the left null space (cokernel) $\mathcal{N}(A^*) = \mathrm{span}\,(U_2)$.

One important application of singular values is the determination of matrix norms, which constantly will be reused in this thesis:

$$\|A\|_2 = \sigma_{\max}, \qquad \|A\|_F^2 = \sum_{i=1}^r \sigma_i^2 . \tag{4.8}$$

4.1.2 ORTHOGONAL PROJECTIONS

The projection technique allows to conduct linear transformations onto certain vector spaces. For that, the column space projector P and the row space projector Π are introduced. As it follows central presumptions, projectors must be idempotent, thus $P^2 = P$ and $\Pi^2 = \Pi$. To define matrix projections, the row space projector

$$\Pi_B = B^\dagger B = B^* (BB^*)^{-1} B \tag{4.9}$$

is defined. By applying Π_B to an appropriate matrix A, the orthogonal projection of A onto B

$$A\Pi_B = AB^* (BB^*)^\dagger B \quad \text{with} \quad \Pi_{B\perp} = I - \Pi_B \tag{4.10}$$

is conducted. A geometrical illustration is given in figure 4.2. The orthogonal complement of row space B is easily determined based on $\Pi_{B\perp}$.
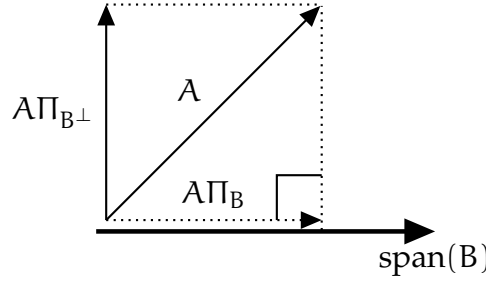
Figure 4.2: Orthogonal Projection of A onto B

Besides that, the projection operator onto the column space of B is given by

$$P_B = B^\dagger B = (B^* B)^{-1} B^* \quad \text{with} \quad P_{B\perp} = I - P_B \ . \tag{4.11}$$

NUMERICAL METHODS for the computation of orthogonal projection operators can now be given following de Cock.[105] By considering a singular value decomposition

$$B = \begin{bmatrix} U_1 & U_2 \end{bmatrix} \begin{bmatrix} \Sigma_1 & 0 \\ 0 & 0 \end{bmatrix} \begin{bmatrix} V_1^* \\ V_2^* \end{bmatrix} \ , \tag{4.12}$$

row and column space projection operators are numerically advantageous derivable by

$$P_B = U_1 U_1^*, \qquad P_{B\perp} = U_2 U_2^*, \qquad \Pi_B = V_1 V_1^* \quad \text{and} \quad \Pi_{B\perp} = V_2 V_2^* \ . \tag{4.13}$$

Another useful numerical method is the application of LQ-factorization

$$\begin{bmatrix} B \\ A \end{bmatrix} = \begin{bmatrix} L_{11} & 0 \\ L_{21} & L_{22} \end{bmatrix} \begin{bmatrix} Q_1^* \\ Q_2^* \end{bmatrix} \quad \text{with} \quad I = QQ^* = \begin{bmatrix} Q_1 & Q_2 \end{bmatrix} \begin{bmatrix} Q_1^* \\ Q_2^* \end{bmatrix} \ . \tag{4.14}$$

By applying L and Q, row space projection operator

$$\Pi_B = Q_1 Q_1^*, \qquad \Pi_{B\perp} = Q_2 Q_2^* = I - Q_1 Q_1^* \tag{4.15}$$

and projection results are easy determinable[105] by

$$A\Pi_B = (L_{21} Q_1^* + L_{22} Q_2^*)(Q_1 Q_1^*) = L_{21} Q_1^* \quad \text{and} \quad A\Pi_{B\perp} = L_{22} Q_2^* \ . \tag{4.16}$$

4.1.3 OBLIQUE PROJECTIONS

Orthogonal projections are a special case of oblique projections.[17] This more general linear algebra method can be explained easily by defining sub blocks in equation (4.9), which leads to

$$\Pi_{\begin{bmatrix} B \\ C \end{bmatrix}} = \begin{bmatrix} B^* & C^* \end{bmatrix} \begin{bmatrix} BB^* & BC^* \\ CB^* & CC^* \end{bmatrix}^{-1} \begin{bmatrix} B \\ C \end{bmatrix} . \tag{4.17}$$

The orthogonal projection operator can be split up in two oblique projection operators[17] with the help of

$$\Pi_{\begin{bmatrix} B \\ C \end{bmatrix}} = \Pi_{B,\|C} + \Pi_{C,\|B} . \tag{4.18}$$
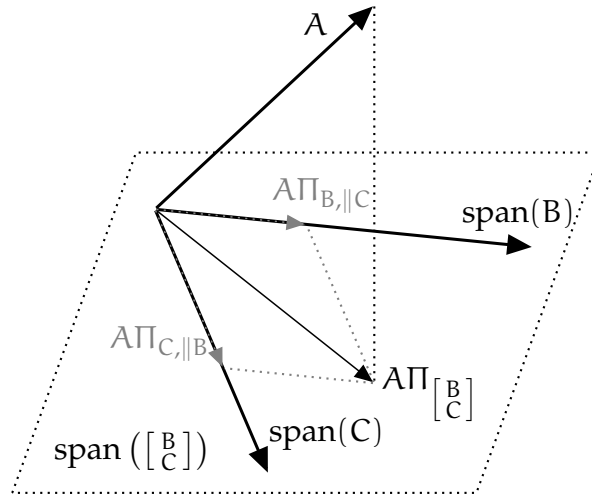
Figure 4.3: Oblique Projection of A

While $\Pi_{B,\|C}$ is the projector onto B along C, matrix $\Pi_{C,\|B}$ allows the converse projection. Both oblique projectors

$$\Pi_{B,\|C} = \begin{bmatrix} B^* & C^* \end{bmatrix} \begin{bmatrix} BB^* & BC^* \\ CB^* & CC^* \end{bmatrix}^{-1} \begin{bmatrix} B \\ 0 \end{bmatrix} , \quad \Pi_{C,\|B} = \begin{bmatrix} B^* & C^* \end{bmatrix} \begin{bmatrix} BB^* & BC^* \\ CB^* & CC^* \end{bmatrix}^{-1} \begin{bmatrix} 0 \\ C \end{bmatrix} \tag{4.19}$$

are illustrated at an example in figure 4.3. A numerical solution can be given on the basis of a LQ*-factorization

$$A\Pi_{C,\|B} = L_{32}L_{22}^\dagger C, \quad A\Pi_{\begin{bmatrix} B \\ C \end{bmatrix}} = L_{31}Q_1^* + L_{32}Q_2^* \quad \text{with} \quad \begin{bmatrix} B \\ C \\ A \end{bmatrix} = \begin{bmatrix} L_{11} & 0 & 0 \\ L_{21} & L_{22} & 0 \\ L_{31} & L_{32} & L_{33} \end{bmatrix} \begin{bmatrix} Q_1^* \\ Q_2^* \\ Q_3^* \end{bmatrix} . \tag{4.20}$$

4.2   DETERMINISTIC SUBSPACE IDENTIFICATION

4.2.1   INTRODUCTION TO SYSTEM IDENTIFICATION

Mathematical systems are applied in many scientific fields, like physics, economy, biology and so forth.[17]   Especially in structural dynamics, mechanical systems are analysed, for example bridges and towers. To determine a system, basically two fundamentally different approaches can be taken: At one hand there is the analytical white-box approach based on first principles, which has been explained in chapter 3. In contrast to that, the system identification black-box approach allows the determination of far less complex models. Most importantly, the identification of a mechanical structure during its operational phase allows a comprehensive system analysis, for instance to automatically localize structural damage.

To identify a system, the first important question is the choice of model. For that, at least some a priori engineering based knowledge of the structure must be known. Here, the discrete-time linear time-invariant system is state-of-the-art . Although this probably is a simple choice, it is the most common approach for mechanical systems. Thus, non-linear behaviour usually is linearized at a certain working-point.

Secondly, model validation is a key element to evaluate whether the identification process has been successful or not. A comprehensive overview of the system identification workflow is given by Katayama and van Overschee.[17,19]   As can be seen there, the model choice and its validation based on the chosen identification technique is a trade-off, usually of numerical accuracy, time-consumption and so on. At this point it is important to understand that identification techniques always lead to an approximation of real systems, and a 'true' system does not exist.[19]

The classical approaches for system identification are prediction error methods (PEM), which have been developed to parametrize single input single output (SISO) autoregressive moving average (ARMA) models.[106]   Since then multi input multi output (MIMO) systems can be parametrized too and are convertible to more advantageous state space systems. Nevertheless, MIMO identification remains with numerical difficulties due to local minima in contrast to global solutions.[19]

Besides prediction error methods, subspace identification techniques are more appropriate approaches. Its name follows a common technique of linear algebra, namely the orthogonal and oblique projection in certain (sub-)spaces, which have been described before. The core of subspace identification is the determination of system states by projection techniques. Then a least-squares problem, defined on the basis of estimated states, leads to the parametrization of the searched state space system with the help of numerical methods.[19]

Hence, subspace identification methods generally are more appropriate to parametrize MIMO systems, which thus are discussed in this chapter. These techniques are

based on numerical methods, especially the QR and the singular value decomposition (SVD), which allow to avoid non-linear optimization techniques.

A LINEAR, DISCRETE-TIME STATE SPACE SYSTEM   follows the above statements and shall be parametrized. It is denoted by H:

$$x_{k+1} = Ax_k + Bu_k + w_k \qquad (4.21a)$$
$$y_k = Cx_k + Du_k + v_k \, . \qquad (4.21b)$$

The above state space equation (4.21) is a generalization of the mechanical system state evolution equation (3.14). Here, the general input and output processes $u \in \mathbb{R}^q$ and $y \in \mathbb{R}^p$ have been used. In the case of a mechanical system, forces, displacements, velocities, accelerations and so forth can be used. The number of excitation and measurement points q and p can be different. In opposite to the first principle based mechanical system in equation (3.7), the degree of freedom N is unused here.

Besides the deterministic (known) input u, disturbance processes w and v are introduced, which in general are unknown. Process noise $w \in \mathbb{C}^n$ disturbs state vector x and has in general no physical pendant, because of a possibly non-physical definition of state vector x. For mechanical systems, w might be, in a broader sense, in consequence of non-measurable ambient excitations, like wind, traffic, waves and so on. In opposite to that, measurement noise $v \in \mathbb{R}^p$ refers to static noise, quantizing noise, numerical inaccuracies and so forth.

Most importantly, state vector $x \in \mathbb{C}^n$ is used, which may be without physical meaning, in contrary to z in equation (3.14). At this point the number of states n directly follows system identification techniques and not necessarily is $2N$, which can be in contrast to the analytically derived mechanical system.

The system itself is described by matrices $A \in \mathbb{C}^{n \times n}$, $B \in \mathbb{C}^{n \times q}$, $C \in \mathbb{C}^{p \times n}$ and $D \in \mathbb{R}^{p \times q}$. Based on that, a similarity transformation with

$$x \longrightarrow Tx \quad \text{and} \quad H(A, B, C, D) \longrightarrow H(TAT^{-1}, TB, CT^{-1}, D) \qquad (4.22)$$

can be conducted. Because a mechanical structure is represented in a state space form, the system properties are advantageously analysable, for instance by controlability, observability and stability. Furthermore, the transfer matrix function and the discrete-time impulse function

$$H(z) = C(zI - A)^{-1}B + D \quad \text{and} \quad H_k = \begin{cases} D, & k = 0 \\ CA^{k-1}B, & k > 0 \end{cases} \qquad (4.23)$$

easily follow defined state space parameters, which is in accordance with equations (3.16) and (3.22) .

IDENTIFICATION THEORIES   may cover the parametrization of state space parameter A, B, C and D based on measured quantities, for example impulse response

matrices H_k, a transfer matrix function $H(e^{j\theta})$, input-output data or system responses only (output-only). To do so, various identification techniques have been developed, which give a solution for the named realization problems, namely the method of Ho-Kalman,[21] stochastic realization,[26] canonical variate analysis,[27] numerical algorithms for subspace state space identification (N4SID),[22] multivariable output error state space (MOESP),[17] canonical correlation analysis,[29] orthogonal decomposition technique[19] and so forth.

In the following, the method of Ho-Kalman and the numerical algorithms for subspace state space identification (N4SID) are presented. These deterministic approaches serve as an ideal theoretical foundation for the subsequent stochastic subspace identification derivations.

4.2.2 THE METHOD OF HO-KALMAN

As has been explained for equation (3.4), a mechanical system is comprehensively described by its impulse response sequence H_k. Following that an appropriate technique is shown below, namely the method of Ho-Kalman.[21] It can be seen as the theoretical basis for subsequently explained subspace identification techniques. Nevertheless, instrumentation conditions for impulse experiments at large-scale structures, for instance bridges, are very disadvantageous, as will be pointed out in section 4.4.4.

The method of Ho-Kalman[21] utilizes measured impulse response matrices H_k with $k \in \mathbb{N}$ to determine A, B, C and D. Essentially, this technique is the inverse approach to equation (4.23). Thus, $D = H_0$ can be determined very easily. To derive triplet (A, B, C), further assumptions are necessary, especially

$$
\underbrace{\begin{bmatrix} y_0 \\ y_1 \\ \vdots \end{bmatrix}}_{y_+} = \underbrace{\begin{bmatrix} H_1 & H_2 & \cdots \\ H_2 & H_3 & \\ \vdots & & \ddots \end{bmatrix}}_{\bar{\mathcal{H}}_\infty} \underbrace{\begin{bmatrix} u_{-1} \\ u_{-2} \\ \vdots \end{bmatrix}}_{u_-} \quad \text{and} \quad u_k \begin{cases} \neq 0, & k < 0 \\ = 0, & k \geqslant 0 \end{cases}. \tag{4.24}
$$

Basically, past inputs can be arbitrary and must stop at $k = 0$. Thus, a discrete-time pulse-function with $u(-1) = 1/\Delta t$ and $u(k) = 0$ for $k \neq -1$ can be used in theory above. Then future measurements $y_+ = [y_k]_{k=0}^{\infty}$ only depend on past inputs $u_- = [u_k]_{k=-\infty}^{-1}$, which are related by a Hankel matrix $\bar{\mathcal{H}}_\infty$.

The infinite dimensional Hankel matrix $\bar{\mathcal{H}}_\infty$ is the key element for the identification, because it has a finite rank n. Hence, a truncated block Hankel matrix $\bar{\mathcal{H}}_m \in \mathbb{R}^{pm \times qm}$ can be defined which has the identical rank n. Here, index m refers to the number of block rows and columns. Afterwards, a factorization in extended observability and controllability matrices

$$
\bar{\mathcal{H}}_m = \mathcal{O}_m \bar{\mathcal{C}}_m \quad \text{with} \quad \text{rank}(\bar{\mathcal{H}}_m) = \text{rank}(\mathcal{O}_m) = \text{rank}(\bar{\mathcal{C}}_m) = n \tag{4.25}
$$

is introduced. A detailed description of this factorization follows equation (4.23) and is defined by

$$
\begin{bmatrix}
CA^0B & CA^1B & \cdots & CA^{m-1}B \\
CA^1B & CA^2B & & \vdots \\
\vdots & & \ddots & \\
CA^{m-1}B & & & CA^{2m-1}B
\end{bmatrix}
=
\begin{bmatrix}
C \\
CA \\
\vdots \\
CA^{m-1}
\end{bmatrix}
\begin{bmatrix}
B & AB & \cdots & A^{m-1}B
\end{bmatrix} .
\tag{4.26}
$$

AN EFFICIENT NUMERICAL SOLUTION   has been found a decade after the original proposition of Ho and Kalman by Zeiger and McEwen.[107] It follows a singular value decomposition (SVD)

$$
\bar{\mathcal{H}}_m = \begin{bmatrix} U_1 & U_2 \end{bmatrix} \begin{bmatrix} \Sigma_1 & 0 \\ 0 & \Sigma_2 \end{bmatrix} \begin{bmatrix} V_1^\mathsf{T} \\ V_2^\mathsf{T} \end{bmatrix} \approx U_1 \Sigma_1 V_1^\mathsf{T}
\tag{4.27a}
$$

$$
\text{with} \quad \mathcal{O}_m = U_1 \Sigma_1^{1/2}, \quad \bar{\mathcal{C}}_m = \Sigma_1^{1/2} V_1^\mathsf{T} .
\tag{4.27b}
$$

This can be seen as the determination of subspaces of $\mathcal{H}_m$, namely the column and row spaces by U_1 and V_1. The number of relevant singular values σ_i and left/right singular vectors is defined by n. This choice typically is determined by $\sigma_1 \geqslant \sigma_2 \geqslant \ldots \sigma_n \gg \sigma_{n+1}$. Hence, by neglecting σ_i with $i > n$, additional measurement noise can be rejected.[29]

Finally, the minimal triplet (A, B, C) can be determined on the basis of extended observability and controllability matrices. For that, C and B can be taken as the first block elements of $\mathcal{O}_m$ and $\bar{\mathcal{C}}_m$. To determine system matrix A, the Moore-Penrose pseudoinverse of the observability matrix can be computed by

$$
A = \mathcal{O}_{m-1}^\dagger \mathcal{O}_m^\uparrow \quad \text{with} \quad \underbrace{\begin{bmatrix} C \\ CA \\ \vdots \\ CA^{m-2} \end{bmatrix}}_{\mathcal{O}_{m-1}} A = \underbrace{\begin{bmatrix} CA \\ CA^2 \\ \vdots \\ CA^{m-1} \end{bmatrix}}_{\mathcal{O}_m^\uparrow} .
\tag{4.28}
$$

In summary, the method of Ho and Kalman is perfect to parametrize a mechanical system based on impulse response experiments. Practical issues for that are discussed in section 4.4.2.

4.2.3 NUMERICAL ALGORITHMS FOR SUBSPACE STATE SPACE IDENTIFICATION (N4SID)

A very powerful input-output subspace identification technique, namely numerical algorithms for subspace state space identification (N4SID), has been developed by van Overschee and de Moor.[22] This method is based on measured input-output data with $[u_k]_{k=0}^N$ and $[y_k]_{k=0}^N$. For instance exciting forces u and accelerations of a mechanical structure y can be measured.

To derive the identification technique, several notations must be explained first. For that, measurement data is reordered in block form as

$$Y_k(m|i) = \begin{bmatrix} y_k & y_{k+1} & \cdots & y_{k+i-1} \\ y_{k+1} & y_{k+2} & & \vdots \\ \vdots & & \ddots & \\ y_{k+m-1} & \cdots & & y_{k+m+i-2} \end{bmatrix}. \tag{4.29}$$

Equivalently to $Y_k(m|i) \in \mathbb{R}^{mp \times i}$, the input block matrix $U_k(m|i)$ is identically constructed based on u. The notation has been chosen to instantly see the number of block rows m and columns i. This allows to comprehensively rewrite the state space system of equation (4.21) without noise disturbances in block form as

$$Y_k(m|i) = \mathcal{O}_m X_k(i) + \Psi_m U_k(m|i) \quad \text{with} \quad X_k(i) = \begin{bmatrix} x_k & x_{k+1} & \cdots & x_{k+i-1} \end{bmatrix}. \tag{4.30}$$

At this point, an extended observability matrix and a Toeplitz matrix have been defined by

$$\mathcal{O}_m = \begin{bmatrix} C \\ CA \\ \vdots \\ CA^{m-1} \end{bmatrix} \quad \text{and} \quad \Psi_m = \begin{bmatrix} D & 0 & 0 & 0 \\ CA^0B & D & 0 & 0 \\ \vdots & & \ddots & 0 \\ CA^{m-2}B & \ldots & CA^0B & D \end{bmatrix}. \tag{4.31}$$

OBLIQUE PROJECTIONS are used in the following to estimate system states based on above definitions. This is a central idea of subspace identification, in contrary to prediction error methods (PEM). For that, a past and a future data space is defined, which essentially is the basic approach for several subspace identification techniques:

$$W_p = \begin{bmatrix} U_p \\ Y_p \end{bmatrix} = \begin{bmatrix} U_0(m|i) \\ Y_0(m|i) \end{bmatrix}, \ W_f = \begin{bmatrix} U_f \\ Y_f \end{bmatrix} = \begin{bmatrix} U_m(m|i) \\ Y_m(m|i) \end{bmatrix} \quad \text{and} \quad \begin{bmatrix} X_p \\ X_f \end{bmatrix} = \begin{bmatrix} X_0(i) \\ X_m(i) \end{bmatrix}. \tag{4.32}$$

Following that approach, the available amount of data must be taken into account, thus $N \geqslant 2m + i - 2$. To estimate states, the oblique projection of Y_f onto W_p along U_f

$$Y_f \Pi_{W_p, \| U_f} = \mathcal{O}_m X_f \quad \text{with} \quad \text{span}(X_f) \subset \left(\text{span}(W_p) \cap \text{span}(W_f) \right) \tag{4.33}$$
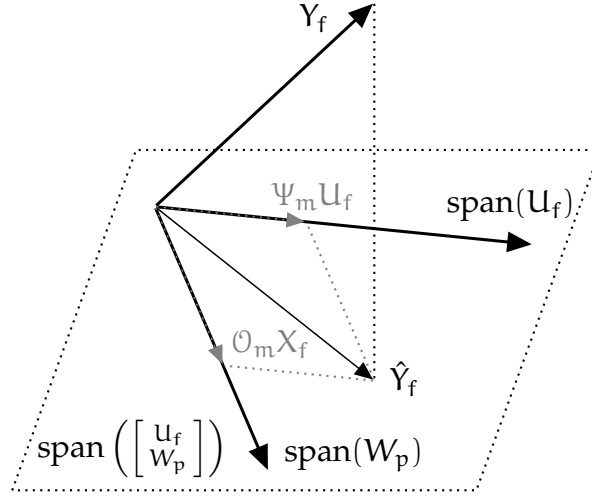
Figure 4.4: Oblique Projection of Y_f

leads to the desired result. This follows a geometrical approach of central system equations and its theoretical core is depicted in figure 4.4.

There are several numerical methods to determine projections. Here, the oblique projection is efficiently conducted with the help of a LQ^T decomposition

$$Y_f \Pi_{W_p, \| U_f} = L_{32} L_{22}^\dagger W_p = \mathcal{O}_m X_f \quad \text{with} \quad \begin{bmatrix} U_f \\ W_p \\ Y_f \end{bmatrix} = \begin{bmatrix} L_{11} & 0 & 0 \\ L_{21} & L_{22} & 0 \\ L_{31} & L_{32} & L_{33} \end{bmatrix} \begin{bmatrix} Q_1^\mathsf{T} \\ Q_2^\mathsf{T} \\ Q_3^\mathsf{T} \end{bmatrix} . \quad (4.34)$$

To understand this oblique projection, revisit equation (4.20). According to Katyama,[19] L_{33} should be a zero matrix, which allows certain theoretical simplifications.

THE PARAMETER IDENTIFICATION   follows the block matrix of future states X_f. To determine this matrix, a singular value decomposition (SVD) is used analogue to equation (4.27) by

$$\mathcal{O}_m X_f = \begin{bmatrix} U_1 & U_2 \end{bmatrix} \begin{bmatrix} \Sigma_1 & 0 \\ 0 & \Sigma_2 \end{bmatrix} \begin{bmatrix} V_1^\mathsf{T} \\ V_2^\mathsf{T} \end{bmatrix} \approx U_1 \Sigma_1 V_1^\mathsf{T} \quad (4.35a)$$

$$\text{with} \quad \mathcal{O}_m = U_1 \Sigma_1^{1/2}, \quad \hat{X}_f = \Sigma_1^{1/2} V_1^\mathsf{T} . \quad (4.35b)$$

Henceforth, estimates are noted by $\hat{\times}$. Again, the rank n must be chosen, which determines the system order. Based on estimated states in block form $\hat{X}_f = \hat{X}_m(i)$ with $\hat{X}_m(i) \in \mathbb{C}^{n \times i}$, the state space system of equation (4.30) can be rewritten. This leads to a least-squares approach

$$\begin{bmatrix} X_{m+1}(j) \\ Y_m(1|j) \end{bmatrix} = \begin{bmatrix} A & B \\ C & D \end{bmatrix} \begin{bmatrix} X_m(j) \\ U_m(1|j) \end{bmatrix} \longrightarrow \begin{bmatrix} A & B \\ C & D \end{bmatrix} = \begin{bmatrix} \hat{X}_{m+1}(j) \\ Y_m(1|j) \end{bmatrix} \begin{bmatrix} \hat{X}_m(j) \\ U_m(1|j) \end{bmatrix}^\dagger \quad (4.36)$$

with $j = i - 1$. That finally allows to determine all state space parameters A, B, C and D. To verify this result, the system output is estimated by

$$\hat{Y}_m(1|j) = \begin{bmatrix} C & D \end{bmatrix} \begin{bmatrix} \hat{X}_m(j) \\ U_m(1|j) \end{bmatrix} \quad \text{with} \quad \hat{Y}_m(1|j) = \begin{bmatrix} \hat{y}_m & \hat{y}_{m+1} & \cdots & \hat{y}_{m+i-2} \end{bmatrix} . \quad (4.37)$$

These estimates are based on deterministic inputs, and thus are denoted by y_d. A comparison to initially measured signals y allows to verify the result based on $y_s = y - y_d$.[19] However, there are several variations of this method, for instance the Po-MOESP method[30] and the orthogonal decomposition technique.[19] Usually, the identification of a stochastic subsystem according to w and v follows y_s. In the following, the identification of y_s is explained, which also is possible for $y_d = 0$. This is the case when deterministic inputs u are unknown.

4.3 STOCHASTIC SUBSPACE IDENTIFICATION

4.3.1 COVARIANCE BASED STOCHASTIC SUBSPACE IDENTIFICATION

The identification based on known deterministic input data, which has been formerly developed in mechanical engineering,[15] is the theoretical foundation for stochastic approaches. Although deterministic methods are powerful, an experiment with impulse or sweep excitations is very elaborate for large-scale structures.[25] Because active test loads can be omitted, ambient vibrations, for example wind, traffic, waves, are more preferable. Thus, stochastic subspace identification can be used instead.

Stochastic subspace identification, traditionally also referred to as stochastic realization, has been comprehensively developed several decades ago by Faurre, Akaike, van Overschee and so forth.[17,26,28] Nevertheless, it has been recently popularized for operational modal analysis (OMA). Especially Peeters, de Roeck, and Reynders[108,109] applied stochastic identification methods for modal analysis. An overview of operational modal analysis can be found in Magalhães et al.[15,110]

THE PRESUMPTIONS of stochastic subspace identification are very important to understand the method's capability: An ergodic (strongly stationary) measurement process $y \in \mathbb{R}^p$ is presumed, which in general could be market prices, weather data, cell growth rates and so on. Typically, accelerations are measured in structural health monitoring. In the named research field velocities, displacements, strains and inclinations are also sometimes considered.

The measurement data is gathered by $[y_k]_{k=0}^N$ in discrete-time and $k \in \mathbb{N}$ with $t = k\Delta t$. All statistical moments of y are time-independent, which leads to an auto-covariance function

$$R_y(l) = E\{y_{k+l}y_k^T\} \quad \text{with} \quad R_y \in \mathbb{R}^{p \times p} . \quad (4.38)$$

Here, a sufficient long measurement duration is necessary, which should be used to determine the covariance function $R_y(l)$ of equation (4.38) by averaging. This will be explained at an example in section 7.1 of chapter 7, devoted to the laboratory experiments. However, the spectral density function

$$S_y(z) = \mathcal{Z}\big(R_y(l)\big) = \sum_{l=-\infty}^{\infty} R_y(l)z^{-l} \quad \text{with} \quad S_y \in \mathbb{C}^{p \times p} \tag{4.39}$$

follows by applying the well-known Wiener-Khinchine theorem, which is applied here based on the z-transform of R_y.

Most commonly, the Fourier transform $\mathcal{F}\big(R_y(l)\big)$ with $z = e^{j\theta}$ is applied here.[4] However, a deterministic input u is explicitly unknown, thus state space parameters B and D in equation (4.21) are non-determinable. Hence, a state space model $H(A, C)$ shall be parametrized by stochastic subspace identification:

$$x_{k+1} = Ax_k + \begin{bmatrix} I & 0 \end{bmatrix} \begin{bmatrix} w_k \\ v_k \end{bmatrix} = Ax_k + w_k \tag{4.40a}$$

$$y_k = Cx_k + \begin{bmatrix} 0 & I \end{bmatrix} \begin{bmatrix} w_k \\ v_k \end{bmatrix} = Cx_k + v_k . \tag{4.40b}$$
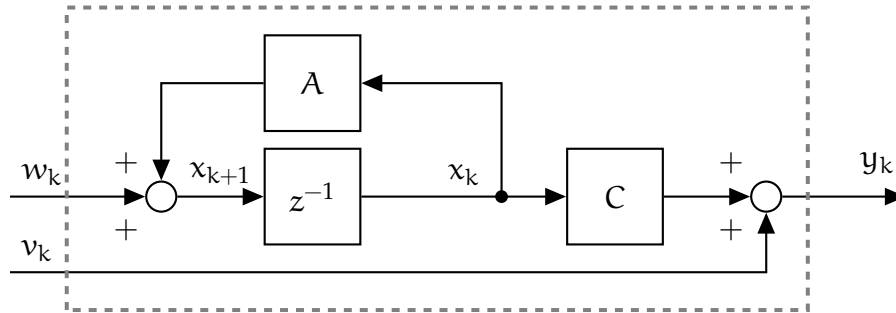
Figure 4.5: Time-Invariant System H

State space model H, is depicted in figure 4.5 and is defined by its time-invariant parameters $A \in \mathbb{C}^{n \times n}$ and $C \in \mathbb{C}^{p \times n}$. Time-invariant system H maps disturbance processes w and v to measured quantities y. Central element of the state space system are states $x \in \mathbb{C}^n$, which are disturbed by process noise $w \in \mathbb{C}^n$.

In large-scale structures ambient vibrations induce mechanical oscillations, for instance wind excitations, earthquakes, waves at offshore structures, traffic at bridges, and so on. Besides w, measurement noise $v \in \mathbb{R}^p$ alters process y, for example noise in electrical wires, quantizing noise and so forth. Both signals w and v are typically unmeasurable and unknown. Although both disturbance processes may be arbitrary in real-life applications, they are conveniently modelled as mean-free, white noise

processes with defined second-order statistical parameters,[19] which is a theoretical presumption only:

$$\mathsf{E}\left\{ \begin{bmatrix} w_k \\ v_k \end{bmatrix} \begin{bmatrix} w_l \\ v_l \end{bmatrix}^* \right\} = \begin{bmatrix} Q & S \\ S^* & R_v \end{bmatrix} \delta_{kl} = M\delta_{kl}\,. \tag{4.41}$$

SPECTRAL FACTORIZATION   is a very powerful approach to understand stochastic subspace identification, which follows the above definitions. It focuses on the factorization of spectrum S_y in equation (4.39)

$$S_y(z) = H(z)MH^*(z^{-*}) \quad \text{based on} \quad H(z) = \begin{bmatrix} H_w(z) & I \end{bmatrix} = \begin{bmatrix} C(zI - A)^{-1} & I \end{bmatrix}\,. \tag{4.42}$$

The spectral factorization and its general form, the Popov function, are concepts of system theory, and thus will be excessively discussed at its appropriate position in section 5.2.

Very importantly, the factorization of S_y is not unique. Although $S_y(z)$ remains, an infinite number of matrices M are possible due to different state definitions.[19,20] Because w and v are non-measurable, matrix M can be altered by

$$M(\Pi) = \mathsf{E}\left\{ \begin{bmatrix} w_k \\ v_k \end{bmatrix} \begin{bmatrix} w_k \\ v_k \end{bmatrix}^* \right\} = \begin{bmatrix} Q & S \\ S^* & R_v \end{bmatrix} = \begin{bmatrix} \Pi - A\Pi A^* & N - A\Pi C^* \\ N^* - C\Pi A^* & R_y(0) - C\Pi C^* \end{bmatrix} \geqslant 0\,. \tag{4.43}$$

This approach is based on the covariance matrix of states $\Pi \in \mathbb{C}^{n \times n}$, which follows the unique solution of Lyapunov equation

$$\Pi = A\Pi A^* + Q \quad \text{with} \quad \mathsf{E}\left\{ \begin{bmatrix} w_k \\ v_k \\ x_k \end{bmatrix} \begin{bmatrix} w_k^* & v_k^* & x_k^* & 1 \end{bmatrix} \right\} = \begin{bmatrix} Q & S & 0 & 0 \\ S^* & R_v & 0 & 0 \\ 0 & 0 & \Pi & 0 \end{bmatrix}\,. \tag{4.44}$$

These definitions lead to a matrix $N \in \mathbb{C}^{n \times p}$, which is a key element for covariance based stochastic subspace identification. It is derived by

$$N = \mathsf{E}\{x_{k+1}y_k^\mathsf{T}\} = \mathsf{E}\left\{ (Ax_k + w_k)(Cx_k + v_k)^\mathsf{T} \right\} = A\Pi C^* + S\,. \tag{4.45}$$

COVARIANCE BASED STOCHASTIC SUBSPACE IDENTIFICATION   is a common technique to parametrize state space model $H(A, C)$ of equation (4.40) based on system responses only (output-only). Its core element are factorized covariance matrices

$$R_y(l) = \begin{cases} CA^{l-1}N, & l > 0 \\ R_v + C\Pi C^*, & l = 0 \\ R_y^\mathsf{T}(-l), & l < 0 \end{cases}\,. \tag{4.46}$$

Here, it is more engineering oriented to discuss spectra, because structural dynamics typically analyses modal data. At this point compare to the discussion of chapter 3,

especially section 3.2.2. Thus, an equivalence in z-domain directly follows equation (4.43) with $\Pi = 0$:

$$S_y(z) = H(z)M(0)H^*(z^{-*}) = \begin{bmatrix} C(zI-A)^{-1} & I \end{bmatrix} \begin{bmatrix} 0 & N \\ N^* & R_y(0) \end{bmatrix} \begin{bmatrix} C(zI-A)^{-1} & I \end{bmatrix}^* . \quad (4.47)$$

The stochastic realization problem, which was addressed first by Faurre,[26] follows: Based on a measured process y, and thus a known covariance function $R_y(l)$, determine reasonable state space parameters (A, C) and covariance matrices (Q, R, S). As can be seen in equation (4.47), the quadrupel $(A, N, C, R_y(0))$ is a solution to that. Therefore, the central idea is the adaptation of deterministic realization method of Ho and Kalman[21] (section 4.2.2) to covariance matrices, as Aoki[111] points out. Thus, consider the arrangement of known covariance matrices $R_y(l)$ in an infinite dimensional and a truncated block Hankel matrix

$$\mathcal{H}_\infty = \begin{bmatrix} R_y(1) & R_y(2) & R_y(3) & \cdots \\ R_y(2) & R_y(3) & R_y(4) & \\ R_y(3) & R_y(4) & R_y(5) & \\ \vdots & & & \ddots \end{bmatrix} \quad \text{and} \quad \mathcal{H}_m = \begin{bmatrix} R_y(1) & R_y(2) & \cdots & R_y(m) \\ R_y(2) & R_y(3) & \cdots & \vdots \\ \vdots & \vdots & \ddots & \\ R_y(m) & \cdots & & R_y(2m-1) \end{bmatrix} . \quad (4.48)$$

Although block Hankel matrix $\mathcal{H}_\infty$ is infinite dimensional, it has a finite rank n.[19] Hence, it is appropriate to consider the finite dimensional block Hankel matrix $\mathcal{H}_m \in \mathbb{R}^{pm \times pm}$, because $\text{rank}(\mathcal{H}_\infty) = \text{rank}(\mathcal{H}_m)$.[112] Again, m is the number of block rows and columns.

Following theoretical descriptions of R_y in equation (4.46), extended observability and controllability matrices $\mathcal{O}_m$ and $\mathcal{C}_m$ are applied to factorize the block Hankel matrix

$$\mathcal{H}_m = \mathcal{O}_m \mathcal{C}_m \quad \text{with} \quad \text{rank}(\mathcal{H}_m) = \text{rank}(\mathcal{O}_m) = \text{rank}(\mathcal{C}_m) = n . \quad (4.49)$$

Equivalently to $\bar{\mathcal{H}}_m$ in equation (4.26), block Hankel matrix $\mathcal{H}_m$ is factorized here by

$$\begin{bmatrix} CA^0N & CA^1N & \cdots & CA^{m-1}N \\ CA^1N & CA^2N & & \vdots \\ \vdots & & \ddots & \\ CA^{m-1}N & & & CA^{2m-1}N \end{bmatrix} = \begin{bmatrix} C \\ CA \\ \vdots \\ CA^{m-1} \end{bmatrix} \begin{bmatrix} N & AN & \cdots & A^{m-1}N \end{bmatrix} . \quad (4.50)$$

Henceforth, the approach for both Hankel matrices $\bar{\mathcal{H}}_m$ and $\mathcal{H}_m$ nearly are identical. Thus, a singular value decomposition

$$\mathcal{H}_m = \begin{bmatrix} U_1 & U_2 \end{bmatrix} \begin{bmatrix} \Sigma_1 & 0 \\ 0 & \Sigma_2 \end{bmatrix} \begin{bmatrix} V_1^T \\ V_2^T \end{bmatrix} \approx U_1 \Sigma_1 V_1^T \quad (4.51a)$$

$$\text{with} \quad \mathcal{O}_m = U_1 \Sigma_1^{1/2} \quad \text{and} \quad \mathcal{C}_m = \Sigma_1^{1/2} V_1^T \quad (4.51b)$$

must be applied to determine rank n. Based on that, the extended observability and controllability matrices $\mathcal{O}_m$ and $\mathcal{C}_m$ are determinable. This leads to the determination of the triplet (A, N, C) based on equation (4.28), which nearly is identical to the method of Ho-Kalman. In summary, state space system $H(A, C)$ of equation (4.40) and figure 4.5 is fully parametrized. This can be applied to determine modal data.

OPERATIONAL MODAL ANALYSIS comprises the utilization of stochastic system identification techniques for modal analysis. Its core are ambient excitations (see above). Thus, the stochastic realization method of Faurre[26] has been restated as covariance based stochastic subspace identification (SSI-Cov) by Peeters et al.[108] The focus therein is set on modal identification, which is realized by comparing a mechanical system in state space form, especially equation (3.7) in chapter 3, to the identified general system of equation (4.40). Based on that, the modal identification of section 3.2.2 can be partially applied. Although this approach leads to useful results, the fundamental different system derivations (first principles and system identification) must be kept in mind. For example the non-conform definitions of the degree of freedom N and the number of measurement position p illustrates radical differences.

The central idea of modal analysis is to treat the identified discrete-time parameter A like it was derived by analytical mechanics. Of course the analytically derived and the numerically identified system matrix A may be different, thus physical parameters (e.g. stiffness and mass) are non-determinable at this point. If this is kept in mind, the numerically identified state space parameters must be transformed to continuous-time based on the zero order hold method of equation (3.15) to conduct an eigendecomposition

$$\bar{A} = X \Lambda X^{-1} \quad \text{with} \quad \bar{A} = \frac{\text{Ln}(A)}{\Delta t} \quad \text{and} \quad \bar{C} = C . \tag{4.52}$$

Here, the difference of eigenvectors X in comparison to Ψ of equation (3.28) are evident. The subsequent modal analysis follows section 3.2.2: According to Brincker et al.[113] the eigenvalues of system matrix A

$$\lambda_{i,i+1} = -\delta_i \pm j\omega_{d,i} = -\zeta_i \omega_{0,i} \pm j\omega_{0,i}\sqrt{1 - \zeta_i^2}, \qquad i = 1, 2, \ldots, n \tag{4.53}$$

are directly applied to compute natural frequencies f, modal dampings ζ and unscaled mode shapes ϕ by

$$f_i = \frac{\mathfrak{I}(\lambda_i)}{2\pi} = \frac{\omega_{d,i}}{2\pi}, \qquad \zeta_i = -\frac{\mathfrak{R}(\lambda_i)}{|\lambda_i|} \quad \text{and} \quad \Phi = \begin{bmatrix} \phi_1 & \phi_2 & \cdots & \phi_n \end{bmatrix} = \bar{C}X . \tag{4.54}$$

Only if complex conjugated eigenvalues $\lambda_{i,i+1}$ occur, a mechanical relevant property may be found. Otherwise, certain states surely describe noise terms. Nevertheless, these modal results are very powerful, because they are based on structural measurements only. Hence, imprecise a priori presumptions can not be present in the above results. However, a possibly lower mode shape resolution and an arbitrary mode shape scaling (due to unknown excitations) are commonly accepted disadvantages.

SUMMARY: COVARIANCE BASED STOCHASTIC SUBSPACE IDENTIFICATION

i) Measure system responses y, for example accelerations due to an ambient excitation. Based on that, determine the covariance function $R_y(l)$ of equation (4.38) by averaging a sufficient amount of measurement data.

ii) The block Hankel matrix of equation (4.48) must be constructed and analysed by singular value decomposition. Therefore, the number of block rows and columns m has to be reasonably chosen.

iii) Based on (U, Σ, V), determine model order n in equation (4.51), which leads to triplet (A, N, C) from (U_1, Σ_1, V_1), for instance by equation (4.28).

iv) To verify the identification results, estimated and measured spectra S_y can be compared.

v) Finally, take the transformation from discrete to continuous-time into account and compute modal parameters according to equation (4.54). If non-plausible modal data occur, model reduction techniques of chapter 3, especially section 3.2.3, should be applied.

4.3.2 DATA-DRIVEN STOCHASTIC SUBSPACE IDENTIFICATION

While the formerly described stochastic identification technique has been based on covariance data R_y, here an approach based on projections of data y is presented following van Overschee and de Moor.[17] Although stochastic identification is known for at least two decades, it usually is referred today to as the data-driven stochastic subspace identification technique (data-driven SSI), which has been popularized for modal identification by Reynders.[109] Because this approach can be seen as a square-root technique, it may have numerical benefits.

Furthermore, it has resemblance to the numerical algorithms for subspace state space identification (N4SID) technique of section 4.2.3. Hence, consider past and future block matrices in accordance with equation (4.29) with

$$Y_f = Y_0(m|i), \qquad Y_p = Y_m(m|i) \quad \text{and} \quad X_f = X_m(i). \tag{4.55}$$

Again the future measurement block matrix Y_f shall be projected onto the past data space in accordance with equation (4.34). But in opposite to the N4SID method, input data is unknown here. Thus, a projection of Y_f onto Y_p

$$\mathcal{P}_m = Y_f \Pi_{Y_p} = L_{21} Q_1^T = \mathcal{O}_m X_f \quad \text{with} \quad \begin{bmatrix} Y_p \\ Y_f \end{bmatrix} = \begin{bmatrix} L_{11} & 0 \\ L_{21} & L_{22} \end{bmatrix} \begin{bmatrix} Q_1^T \\ Q_2^T \end{bmatrix} \tag{4.56}$$

is conducted. At this point other numerical approaches to determine the projection are possible, which were pointed out in section 4.1.

THE PARAMETER IDENTIFICATION   is very similar to N4SID, except it is based on projection $\mathcal{P}_m$ instead. Therefore, consider a singular value decomposition

$$W_1 \mathcal{P}_m W_2 = W_1 \mathcal{O}_m X_f W_2 = \begin{bmatrix} U_1 & U_2 \end{bmatrix} \begin{bmatrix} \Sigma_1 & 0 \\ 0 & \Sigma_2 \end{bmatrix} \begin{bmatrix} V_1^\mathsf{T} \\ V_2^\mathsf{T} \end{bmatrix} \approx U_1 \Sigma_1 V_1^\mathsf{T} \tag{4.57a}$$

$$\text{with} \quad \hat{X}_f = \Sigma_1^{1/2} V_1^\mathsf{T} W_2^{-1} \quad \text{and} \quad \mathcal{O}_m = W_1^{-1} U_1 \Sigma_1^{1/2}, \tag{4.57b}$$

which essentially revisits equation (4.35). However, weighting matrices W_1 and W_2 have been additionally used here, which allow more precise estimations. Their choice should be defined application-oriented, as van Overschee et al.[17] point out. To define weighting matrices, consider covariance matrices

$$\Phi_{ff} = E\{Y_p Y_f^\mathsf{T}\}, \qquad \Phi_{fp} = E\{Y_f Y_p^\mathsf{T}\} \quad \text{and} \quad \Phi_{pp} = E\{Y_p Y_p^\mathsf{T}\}. \tag{4.58}$$

By comparing the above definitions to equation (4.50), one realizes that Φ_{fp} just is a reordered block Hankel matrix $\mathcal{H}_m$, thus

$$\Phi_{fp} = \mathcal{O}_m \tilde{\mathcal{C}}_m \quad \text{with} \quad \tilde{\mathcal{C}}_m = \begin{bmatrix} A^{m-1}N & A^{m-2}N & \cdots & N \end{bmatrix}. \tag{4.59}$$

The most important weighting approaches are the following:

i) The principal component (PC) method of Aoki[111] is based on the analysis of principle components of Φ_{fp}. Because of central definitions

$$W_1 = I, \qquad W_2 = Y_p^\mathsf{T} \Phi_{pp}^{-1/2} Y_p \quad \longrightarrow \quad W_1 \mathcal{P}_m W_2 = \Phi_{fp} \Phi_{pp}^{-1/2} Y_p \tag{4.60}$$

the left singular vectors of $W_1 \mathcal{P}_k W_2$ and Φ_{fp} are equal.

ii) A rather simple choice follows the unweighted principal component (UPC) approach with

$$W_1 = I, \qquad W_2 = I \quad \longrightarrow \quad W_1 \mathcal{P}_m W_2 = \mathcal{P}_m. \tag{4.61}$$

iii) Finally, a method based on principle angles and directions between Y_f and Y_p is taken in the canonical variate algorithm (CVA) of Akaike[28] by

$$W_1 = \Phi_{ff}^{-1/2}, \qquad W_2 = I, \quad \longrightarrow \quad W_1 \mathcal{P}_m W_2 = \Phi_{ff}^{-1/2} \Phi_{fp} \Phi_{pp}^{-1} Y_p. \tag{4.62}$$

Based on the singular value decomposition results (U, Σ, V), states X_f are estimated by $\hat{X}_f$. These states are used to determine state space parameters A and C by a least-squares approach

$$\begin{bmatrix} X_{m+1}(j) \\ Y_m(1|j) \end{bmatrix} = \begin{bmatrix} A \\ C \end{bmatrix} X_m(j) \quad \longrightarrow \quad \begin{bmatrix} A \\ C \end{bmatrix} = \begin{bmatrix} \hat{X}_{m+1}(j) \\ Y_m(1|j) \end{bmatrix} \hat{X}_m(j)^\dagger \tag{4.63}$$

with $j = i - 1$, which is a simplification of equation (4.36). To evaluate the identified parameters, estimation residua can be analysed:

$$\begin{bmatrix} \rho_w \\ \rho_v \end{bmatrix} = \begin{bmatrix} \hat{X}_{m+1}(j) \\ Y_m(1|j) \end{bmatrix} - \begin{bmatrix} A \\ C \end{bmatrix} \hat{X}_m(j) \quad \text{with} \quad \begin{bmatrix} \hat{Q} & \hat{S} \\ \hat{S}^* & \hat{R} \end{bmatrix} = E\left\{ \begin{bmatrix} \rho_w \\ \rho_v \end{bmatrix} \begin{bmatrix} \rho_w \\ \rho_v \end{bmatrix}^\mathsf{T} \right\}. \tag{4.64}$$

CLASSICAL AND SUBSPACE IDENTIFICATION methods can be perfectly opposed at this point in connection with former statements on main differences. As was explained in section 4.2.1, classical techniques utilize a transfer function model to get a state space realization. Based on that, system states can be determined with the help of a Kalman filter. In opposite to that, system states $\hat{x}$ have been estimated directly by projection techniques in equation (4.56) in connection with a singular value decomposition in equation (4.57).

Although system states are already available, a Kalman filter can be determined as a comparison. For that, covariance matrices of residua ρ_w and ρ_v in equation (4.64) can be applied to solve a discrete-time algebraic Riccati equation

$$P = APA^* - \left(APC^* + \hat{S}\right)\left(CPC^* + \hat{R}_v\right)^{-1}\left(APC^* + \hat{S}\right)^* + \hat{Q} \, . \tag{4.65}$$

This is a common approach to determine a Kalman filter. Alternatively, a covariance based Kalman filter can be determined by solving a Lyapunov equation

$$\Sigma = A\Sigma A^* + \hat{Q} \quad \text{and compute} \quad N = A\Sigma C^* + \hat{S}, \quad R_y(0) = C\Sigma C^* + \hat{R} \, . \tag{4.66}$$

These results are then used to solve a second Riccati equation

$$\Sigma = A\Sigma A^* + \left(N - A\Sigma C^*\right)\left(R_y(0) - C\Sigma C^*\right)^{-1}\left(N - A\Sigma C^*\right)^* \, . \tag{4.67}$$

Either way, central Kalman filter parameters

$$K_p = \left(APC^* + \hat{S}\right)R_e^{-1} = \left(N - A\Sigma C^*\right)R_e^{-1}, \qquad R_e = CPC^* + \hat{R}_v = R_y(0) - C\Sigma C^* \tag{4.68}$$

are used to estimate states by classical methods following

$$\hat{x}_{k+1} = (A - K_p C)\hat{x}_k + K_p y_k = A_p \hat{x}_k + K_p y_k \, . \tag{4.69}$$

Because the determination of a Kalman filter is not a crucial element of stochastic subspace identification, it is not explained in detail here. Nevertheless, covariance based Kalman filtering theory is comprehensively explained in the context of Wiener-Kalman filtering in section (5.2.1) of chapter 5, especially equation (5.137). Furthermore, numerical approaches to solve the named Riccati equations and occurring numerical issues are also discussed in section 5.2.1.

There are several possible method variations, as can be seen in van Overschee et al.[17] For example state space parameters A and C can be determined based on the extended observability matrix $\mathcal{O}_m$ in accordance with equation (4.28). Furthermore, a possible operational modal analysis is identical to the shown approach of equation (4.54) in section 4.3.1.

Summary: Data-Driven Stochastic Subspace Identification

1. Determine the projection of Y_f onto Y_p, which is denoted as $\mathcal{P}_m$ in equation (4.56). For that, the number of block rows m must be chosen.

2. Choose weighting matrices (W_1, W_2) and apply the singular value decomposition according to equation (4.57).

3. Determine model order n based on (U, Σ, V), which leads to estimated states $\hat{X}$.

4. By using block matrix $\hat{X}$, the Least-Squares approach of equation (4.63) must be solved to determine A and C.

5. Evaluate the solution by analysing residua in equation (4.64). Again, modal data can be gathered on the basis of equation (4.54). Eventually, model reduction techniques are necessary.

4.3.3 Balanced Stochastic Realization

As a last example of stochastic identification, a balanced stochastic realization approach shall be shown based on the canonical correlation analysis (CCA) following Katayama.[19] It is similar to the canonical variate analysis (CVA) approach, which has been named above. It is discussed because its clarity is very advantageous.

Central idea of balanced stochastic realization is to determine a Riccati solution Σ of equation (4.67) with distinctive properties. In view of the more general Riccati equation (4.68), various solutions according to $\Sigma \leqslant \Pi \leqslant \bar{\Sigma}^{-1}$ are possible. Here, solution $\bar{\Sigma}$ follows the backward Riccati equation

$$\bar{\Sigma} = E\{\hat{x}_{b,k}\hat{x}_{b,k}^*\} = A^*\bar{\Sigma}A + \left(C^* - A^*\bar{\Sigma}N\right)\left(R_y(0) - N^*\bar{\Sigma}N\right)^{-1}\left(C^* - A^*\bar{\Sigma}N\right)^*. \quad (4.70)$$

This equation can be derived from the backward state space system

$$x_{b,k-1} = A^*x_{b,k} + w_{b,k} \quad (4.71a)$$

$$y_k = N^*x_{b,k} + v_{b,k} \,. \quad (4.71b)$$

Now, according to van Overschee et al.[17] a balanced stochastic realization is present, when both solutions Σ and $\bar{\Sigma}$ are equal and diagonal:

$$\Pi \to E\{x_k x_k^\mathsf{T}\} = E\{x_{b,k-1}x_{b,k-1}^\mathsf{T}\} = \hat{\Sigma} \,, \quad (4.72)$$

which is accomplished in the following by applying CCA.

Canonical correlation analysis for stochastic system identification is based on canonical vectors α_k and β_k, which have distinctive covariance matrices

$$E\{\alpha_k\alpha_k^\mathsf{T}\} = E\{\beta_k\beta_k^\mathsf{T}\} = I \quad \text{and} \quad E\{\beta_k\alpha_k^\mathsf{T}\} = \hat{\Sigma} = \mathrm{diag}(\sigma_1, \sigma_2, \ldots, \sigma_n) \,. \quad (4.73)$$

The canonical correlations $\sigma \in [0, 1]$ shall be used here with $\Sigma = \bar{\Sigma} = \hat{\Sigma}$. The singular values of matrix product $\Sigma\bar{\Sigma}$ essentially are the named canonical correlations.[19] Based on that, the idea is to introduce past and future data spaces

$$\mathcal{Y}_{p,k} = \text{span}(y_{k-1}, y_{k-2}, \ldots, y_{k-m}) \quad \text{and} \quad \mathcal{Y}_{f,k} = \text{span}(y_k, y_{k+1}, \ldots, y_{k+m-1}), \tag{4.74}$$

which lead to the named canonical correlations: Essentially, the canonical correlations σ may be geometrically interpreted as angles between principal directions of past and future spaces $\mathcal{Y}_p$ and $\mathcal{Y}_f$.[17,105] Following that, an inverse approach is taken: In computing canonical correlations between past and future data

$$y_{p,k}^\mathsf{T} = \begin{bmatrix} y_{k-1}^\mathsf{T} & y_{k-2}^\mathsf{T} & \cdots & y_{k-m}^\mathsf{T} \end{bmatrix}, \qquad y_{f,k}^\mathsf{T} = \begin{bmatrix} y_k^\mathsf{T} & y_{k+1}^\mathsf{T} & \cdots & y_{k+m-1}^\mathsf{T} \end{bmatrix}, \tag{4.75}$$

a solution to the forward and backward Riccati equations with $\Sigma = \bar{\Sigma}$ is found.

At first consider covariance matrices

$$\mathcal{H}_m = E\{y_{f,k} y_{p,k}^\mathsf{T}\}, \quad T_f = E\{y_{f,k} y_{f,k}^\mathsf{T}\} \quad \text{and} \quad T_p = E\{y_{p,k} y_{p,k}^\mathsf{T}\}. \tag{4.76}$$

Here, Hankel matrix $\mathcal{H}_m$ of equation (4.48) has been reconstituted. Furthermore, two Toeplitz matrices

$$T_f = \begin{bmatrix} R_y(0) & R_y^\mathsf{T}(1) & \ldots & R_y^\mathsf{T}(m-1) \\ R_y(1) & R_y(0) & \ldots & \vdots \\ \vdots & \vdots & \ddots & \\ R_y(m-1) & \ldots & & R_y(0) \end{bmatrix}, \quad T_p = \begin{bmatrix} R_y(0) & R_y(1) & \ldots & R_y(m-1) \\ R_y^\mathsf{T}(1) & R_y(0) & \ldots & \vdots \\ \vdots & \vdots & \ddots & \\ R_y^\mathsf{T}(m-1) & \ldots & & R_y(0) \end{bmatrix} \tag{4.77}$$

are defined. A numerical efficient way to determine these matrices is the application of a LQ^T decomposition and data matrices:

$$\begin{bmatrix} T_p & \mathcal{H}_m^\mathsf{T} \\ \mathcal{H}_m & T_f \end{bmatrix} = \begin{bmatrix} L_{11} & 0 \\ L_{21} & L_{22} \end{bmatrix} \begin{bmatrix} L_{11}^\mathsf{T} & L_{21}^\mathsf{T} \\ 0 & L_{22}^\mathsf{T} \end{bmatrix} \quad \text{with} \quad \frac{1}{\sqrt{i}} \begin{bmatrix} Y_p \\ Y_f \end{bmatrix} = \begin{bmatrix} L_{11} & 0 \\ L_{21} & L_{22} \end{bmatrix} \begin{bmatrix} Q_1^\mathsf{T} \\ Q_2^\mathsf{T} \end{bmatrix}, \tag{4.78}$$

$$Y_p = \begin{bmatrix} y_{m-1} & y_m & \cdots & y_{m+i-2} \\ y_{m-2} & y_{m-1} & \cdots & y_{m+i-3} \\ \cdots & \cdots & \cdots & \cdots \\ y_0 & y_1 & \cdots & y_{i-1} \end{bmatrix}, \quad Y_f = \begin{bmatrix} y_m & y_{m+1} & \cdots & y_{m+i-1} \\ y_{m+1} & y_{m+2} & \cdots & y_{m+i} \\ \cdots & \cdots & \cdots & \cdots \\ y_{2m-1} & y_{2m} & \cdots & y_{2m+i-2} \end{bmatrix}. \tag{4.79}$$

While $Y_f = Y_m(m|i)$ of equation (4.29), the past data block matrix Y_p essentially is $Y_0(m|i)$, but block row reversed.

THE NUMERICAL SOLUTION is in principal based on Cholesky factorizations of both Toeplitz matrices T_p and T_f and a singular value decomposition. Thus, lower triangular matrices L and M are introduced. Similar to equation (4.51), a singular value decomposition

$$L^{-1}\mathcal{H}_m M^{-T} = \begin{bmatrix} U_1 & U_2 \end{bmatrix} \begin{bmatrix} \Sigma_1 & 0 \\ 0 & \Sigma_2 \end{bmatrix} \begin{bmatrix} V_1^T \\ V_2^T \end{bmatrix} \approx U_1\Sigma_1 V_1^T, \qquad T_p = MM^T, \; T_f = LL^T \quad (4.80)$$

is applied. This can be seen as a normalization of block Hankel matrix $\mathcal{H}_m$. Most importantly, canonical correlations and the extended observability and controllability matrices can be determined here by

$$\hat{\Sigma} = \Sigma_1, \quad \mathcal{O}_m = LU\hat{\Sigma}^{1/2} \quad \text{and} \quad \mathcal{C}_m = \hat{\Sigma}^{1/2}V^TM^T. \qquad (4.81)$$

This leads to the numerical solution of the central element of the method: Canonical vectors

$$\alpha_k = V^TM^{-1}y_{p,k} \quad \text{and} \quad \beta_k = U^TL^{-1}y_{f,k} \qquad (4.82)$$

can be determined based on singular value results.[19] Furthermore, states of the forward and backward state space model are determinable following canonical variables by

$$x_k = \hat{\Sigma}^{1/2}\alpha_k = \mathcal{C}_m T_p^{-1}y_{p,k} \quad \text{and} \quad x_{b,k-1} = \hat{\Sigma}^{1/2}\beta_k = \mathcal{O}_m^T T_f^{-1}y_{f,k}, \qquad (4.83)$$

which emphasizes the core concept of balanced realization theory: Both solutions of forward and backward Riccati equations are equal and diagonal in accordance with equation (4.72). Then slight modifications of equation (4.83) lead to the block state estimate

$$\hat{X}_m(i) = \hat{\Sigma}^{1/2}V^TM^{-1}Y_p. \qquad (4.84)$$

Finally, the output estimate is interesting. Again it is derived by projection techniques, which is observable with the help of projections of y_f onto $\mathcal{Y}_p$ and y_p onto $\mathcal{Y}_f$:[19]

$$y_{f,k}\Pi_{\mathcal{Y}_{p,k}} = LU\hat{\Sigma}\alpha_k = \mathcal{O}_m x_k, \qquad y_{p,k}\Pi_{\mathcal{Y}_{f,k}} = MV\hat{\Sigma}\beta_k = \mathcal{C}_m^T x_{b,k-1}. \qquad (4.85)$$

Both projection results can be determined based on results of the singular value decomposition and derived canonical vectors. However, the parameter identification of A and C can be conducted following two formerly described methods: i) The classical method based on the Moore-Penrose-inverse of the extended observability matrix $\mathcal{O}_m$ in equation (4.28), and ii) following the least-squares solution of equation (4.63) in connection with estimated states $\hat{X}_m(i)$ of equation (4.84).

Furthermore, a Kalman filter can be derived analogue to the statements of section 4.3.2. Due to redundancy, these statements are omitted here. Finally, a summary of balanced stochastic realization can be given, which essentially is a slight modification of covariance based stochastic subspace identification with a singular value decomposition of a normalized Hankel matrix in equation (4.80).

4.4 EXAMPLE: DETERMINISTIC IDENTIFICATION FOR DAMAGE LOCALIZATION

4.4.1 MECHANICAL SYSTEMS BASED ON FIRST PRINCIPLES AND SUBSPACE IDENTIFICATION

As has been pointed out in the introduction in section 1.5, system identification is a typical basis for damage assessment in structural health monitoring. To show the complexity and difficulties to do so, a brief summary of research on deterministic identification for damage localization on the basis of corresponding mechanical parameters by Ebert[25] is summarized below. This example has been chosen here, because it shows the experimental problems with deterministic excitations, in this case with an impulse hammer. This directly leads to the usage of ambient excitations, which will be discussed afterwards.

In both chapters, 3 and 4, mechanical systems have been derived from fundamentally different viewpoints: The first principle based (analytical) approach with a priori model uncertainties seems to be incompatible on a deeper level in comparison to the a posteriori measurement based subspace identification. Nevertheless, this also allows to define an applicable damage localization technique: The idea is to think of analytical, mechanical systems not just as models, but as an inherent structure of nature itself. Then a theoretically perfect measurement based system identification technique should lead to mechanical parameters like mass, stiffness and damping. This, of course, is questionable and reveals a philosophical discourse, which is explicitly not pursued in this dissertation.

Instead the following question is discussed: If we treat subspace identification based mechanical systems like they have been derived from first principles, can we extract physical parameters and use them for damage identification? This is discussed in the context of corresponding mechanical parameters of Ebert.[25] Furthermore, it depends on the work of many more.[98, 114–116]

At first one may rethink operational modal analysis of section 4.3.1, which must be seen in the context of output-only identification. Therein, the numerically identified discrete-time state space parameters A and C are treated with methods of the first principle based systems, especially modal analysis techniques, which have been discussed in section 3.2.2. In the following, this is expanded to use whole identified state space systems $H(A, B, C, D)$ in accordance with equation (4.21), because more information of a mechanical system should, in principle, lead to better damage identification results.

CONTINUOUS-TIME MARKOV PARAMETERS are usable for damage identification.[25] Given a first principle based mechanical system like equation (3.7), mass and stiffness matrices can be determined by matrix multiplications:

$$\bar{C}_d \bar{A} \bar{B} = \begin{bmatrix} I & 0 \end{bmatrix} \begin{bmatrix} 0 & I \\ -M^{-1}K & -M^{-1}D \end{bmatrix} \begin{bmatrix} 0 \\ M^{-1} \end{bmatrix} = M^{-1} \qquad (4.86)$$

$$\bar{C}_d \bar{A}^{-1} \bar{B} = \begin{bmatrix} I & 0 \end{bmatrix} \begin{bmatrix} -K^{-1}D & -K^{-1}M \\ I & 0 \end{bmatrix} \begin{bmatrix} 0 \\ M^{-1} \end{bmatrix} = K^{-1} . \qquad (4.87)$$

These parameters have a very important advantage: The above results are invariant to a similarity transformation with

$$\bar{C}_d \bar{A}^i \bar{B} = \bar{C}_d (T^{-1}T) \bar{A}^i (T^{-1}T) \bar{B} \quad \text{with} \quad T > 0 , \qquad (4.88)$$

which is in accordance with equation (3.11). Hence, the parameters of a numerically identified state space system with non-physical states can be used too. Furthermore, it can be adapted to velocity measurements by

$$\bar{C}_v \bar{A}^0 \bar{B} = M^{-1} \quad \text{and} \quad \bar{C}_v \bar{A}^{-2} \bar{B} = K^{-1} . \qquad (4.89)$$

While above $\bar{C}_d = \bar{C}_v A^{-1}$ has been used, acceleration measurements can be treated with $\bar{C}_d = \bar{C}_a A^{-2}$, which leads to

$$\bar{C}_a \bar{A}^{-1} \bar{B} = M^{-1} \quad \text{and} \quad \bar{C}_a \bar{A}^{-3} \bar{B} = K^{-1} . \qquad (4.90)$$

As good as this sounds, a comparison of both fundamental different modelling approaches is necessary to point out theoretical issues.

A COMPARISON OF IDENTIFIED AND ANALYTICAL SYSTEMS reveals fundamental differences, which must be dealt with to apply the named Markov parameters:

i) System identification theory is built on *a posteriori* known input/output data, impulse response matrices or a transfer matrix function. In opposite to that, analytical derivations assume *a priori* mechanical parameters.

ii) While input/output data types of analytical models are defined physically, for instance displacement measurements in equation (3.7), those signals can in general be arbitrary in the identification process.[17]

iii) The equation of motion (3.2) is deterministic and noise-free in this dissertation. Realization theory can be seen from a stochastic and/or deterministic point of view, depending on the chosen identification method.[19]

iv) Measurement and excitation points are defined differently compared to the degree of freedom. On the one hand, the number of excitation and measurement points q and p are restricted by experimental technology. On the other hand, the degree of freedom N must be chosen in analytical derivations for a proper approximation of the mechanical system.

v) Excitations are empirically presumed in analytical derivations, while in realization theory excitations are presumed or measured, depending on the chosen algorithm.

vi) States x of realized systems (equation (4.21)) may be non-physical in contrast to the mechanically defined state vector z of analytical models (equation (3.14)).

vii) Analytically derived models are continuous-time, in contrast to numerically identified discrete-time systems.

viii) Parameter matrices of analytically derived state space systems have, in contrast to identified models, a predefined structure. Therefore, the feed-through matrix $\bar{D}$ is a zero matrix in the case of displacement and velocity measurements. Furthermore, the stiffness, mass and damping matrices are symmetric for particular conditions. Furthermore, the matrix multiplication $\bar{C}_d \bar{B} = 0$ is defined in analytical derivations, in contrast to the general case of realization theory.

ix) Measurement data is crucial for system identification, as non-measured properties, for example certain natural vibrations, get lost otherwise. In contrary, important mechanical characteristics must be known a priori in the modelling process of analytical systems.

Although the shown discrepancies seem insuperable, there is an outstanding similarity: Both theories allow the parametrization of a state space system, which maps a load function to accelerations (displacements, velocities, etc.). Based on that, the introduced Markov parameters can be applied, if certain ideal conditions and model modifications are taken into account.

4.4.2 IDEAL CONDITIONS AND MODEL MODIFICATIONS

To apply Markov parameters, several ideal conditions and model modifications are necessary, which is in accordance with the elaborations of Ebert.[25] A key element of identified systems are measurements, which should represent the mechanical structure. Thus, a broadband excitation is necessary, which clearly is an ideal condition. Otherwise, important structural information is non-detectable.

Furthermore, the mechanical parameter matrices in the equation of motion (3.2) usually are symmetric and positive definite, which constitutes reciprocal system behaviour. Therefore, mechanical models based on realization theory shall behave reciprocally too, which defines a second ideal condition. Unfortunately, due to experimental circumstances, among others, the reciprocity requirement may be violated.[25] Additionally, reciprocity requires linearity, which only is an approximation at certain operating points. Finally, the excitation and measurement positions should be taken into account. Especially the number of excitation and measurement positions (p, q) and the degree of freedom N should be harmonized engineering oriented.

If the described ideal conditions are taken into account, identified systems are more likely to be physically interpretable. Nevertheless, model modifications are neces-

sary: Numerically identified discrete-time systems $H(A, B, C, D)$ must be redefined as continuous-time systems $G(\bar{A}, \bar{B}, \bar{C}, \bar{D})$. Although the zero order hold method of equation (3.15) is an excellent approach for that, other methods are possible too, like first order hold, Tustin approximation and so forth.

Secondly, the identified model must be enforced to have a certain structure, for example like equation (3.7), because the parameter structure of identified systems nearly is arbitrary in the first place. For example $\bar{C}_d \bar{B} = 0$ should be enforced.

This can be explained by analysing analytical impulse response matrices $G(t) = \bar{C}_d e^{\bar{A}t} \bar{B}$ of equation (3.13). Here, displacements are measured and the initial state $z(0) = 0$. Then the impulse response matrix at $t = 0$ is $G(0) = \bar{C}_d I \bar{B} = 0$. This essentially defines causality, because we observe the mechanical system to respond after an impulse excitation.

IMPULSE RESPONSE EXPERIMENTS are common deterministic test scenarios. Model modifications must be chosen in accordance with the conducted experiments, which has crucial consequences for impulse response measurements. The theoretical presumption of a pulse function excitation (in discrete-time) with $f(-1) = 1/\Delta t$ and $f(k) = 0$ for $k \neq -1$ is non-applicable in real life experiments. In practice the structure responds before the excitation finished, because the excitation lasts longer than a fraction of time, especially Δt. To overcome this issue, Ebert[25] defines a correction method to normalize identified state space parameters. Here, the idea is to replace the identified triplet (A, B, C) with a corrected one $(A, \tilde{B}, \tilde{C})$ following

$$H_k = \left(CA^{-(c-1)/2}\right) A^{k-1} \left(A^{-(c-1)/2}B\right) = \tilde{C}A^{k-1}\tilde{B} \quad \text{with} \quad k \in \mathbb{N}, c \in \mathbb{Z}. \quad (4.91)$$

In computing the correction value c, a virtual starting time is determined. Based on analytical derivations, this point in time must be in accordance with the measured data type.

Considering $\Delta t \to 0$, we need to correct the impulse response matrix H_k for $k = 1$. Hence, one must find the minimum in the case of displacement and acceleration measurements and the maximum in the case of velocity measurements:

$$\text{Disp./Acc.} \quad \min_c \left\|CA^{-c+1}B\right\|_F \qquad \text{Veloc.} \quad \max_c \left\|CA^{-c+1}B\right\|_F. \quad (4.92)$$

Here, the Frobenius norm has conveniently be chosen. From the viewpoint of application an accurate bandwidth for c must be chosen to compute the optimized impulse response matrix as a local minimum/maximum.

4.4.3 Corresponding Mechanical Parameters

The physical interpretation of Markov parameters is facilitated by satisfying the ideal conditions at its best and by carrying out the described model modifications. Based

on that, an identified state space model $H(A, B, C, D)$, which maps a load function to structural accelerations, can be physically analysed by its corresponding mass and stiffness parameters

$$M_c = \left(\bar{C}_{Id,a} \bar{A}_{Id}^{-1} \bar{B}_{Id} \right)^{-1} \quad \text{and} \quad K_c = \left(\bar{C}_{Id,a} \bar{A}_{Id}^{-3} \bar{B}_{Id} \right)^{-1} . \tag{4.93}$$

Though acceleration measurements are presumed here, other data types are also possible, like velocities. Most importantly, the size of corresponding matrices is set to $M_c, K_c \in \mathbb{R}^{p \times p}$, which presupposes $N = p = q$. For this approximation excitation and measurement positions must be taken into account. It is very important to notice here that in computing corresponding matrices, the parameters of a finite element model or a multi-body simulation are not estimated. The described method is thought to interpret identified mechanical state space systems in a physical sense. Finally, numerical accuracy can be a problem here, because of the inversion. Thus, it can be reasonable to analyse the corresponding flexibility matrix $F_c = K_c^{-1}$ instead.

The application for damage identification follows straightforward the defined corresponding parameters by analysing a difference of two system states. For example the difference corresponding flexibility matrix $\Delta F_c = F_{c,1} - F_{c,2}$ can be utilized for damage detection and localization.

4.4.4 LARGE-SCALE EXPERIMENT EXAMPLE: BRIDGE NEAR BY HÜNXE

To show the capability of the corresponding parameters, the damage localization results of Lenzen and Ebert[25, 117, 118] are briefly summarized below. Furthermore, this is a good basis to pursue stochastic experiments afterwards and discuss essential differences.

Figure 4.6: Tied Arch Bridge near by Hünxe (North Rhine-Westphalia, Germany)

A tied arch bridge near the city Hünxe (North Rhine-Westphalia, Germany) was used for large-scale damage identification experiments. The bridge, which had a length of 62.5m (between the abutments), a width of 13.9m and a maximum arch rise of 8.6m, is shown in figure 4.6. Because of a planned demolition, the opportunity of evaluating

the corresponding parameters was used. Therefore, a reference-state measurement and a measurement in damaged-state was conducted. The structural damage was experimentally induced by severing a concrete hanger between measurement points 10 and 11, which is shown in figure 4.7b. Unfortunately, a successive artificial damage growth was not possible, because the bridge's demolition was scheduled shortly after the experiments.

(a) Impulse-hammer

(b) Severed Hanger

Figure 4.7: Experimental Conditions

The large-scale experiments have been planed with deterministic excitations. For that, the impulse-hammer of figure 4.7a was used. The sensing system had 16 channels for simultaneous analogue-digital-converting. While one channel was used for tracking the acceleration of the exciting mass (150kg), the remaining channels were used to measure structural responses with accelerators. Because an impulse response test at each measurement positions has been conducted, the number of excitation and measurement points was uniformly $p = q = 15$.

Due to sensing technology, the excitation positions have been 2m besides the measurement locations. In addition to the spacial difference of measurement and excitation points, several other bounding conditions, like non-linear material behaviour, geometric non-linearities and so forth, had been present. Nevertheless, reciprocity was approximately measured, which has been verified in comparing y_{ij} to y_{ji} (exchange of response i and excitation j).

In the large-scale experiments numerous effects beside the important structural behaviour have been tracked. To compensate these effects, a finite impulse response Parks-McClellan band-pass filter was used. Here, several filter adjustments have been applied. Finally the bandpass $2\text{Hz} \ldots 25\text{Hz}$ and $13\text{Hz} \ldots 23\text{Hz}$ have been chosen.

The system identification primarily followed the method Ho and Kalman of section 4.2.2. Based on that, the causality condition had to be enforced following equation (4.92). This led to the damage identification by a comparison of two system states.

THE DAMAGE IDENTIFICATION has been in accordance with the analysis of difference corresponding matrices following equation (4.93). Thus, two identified systems were compared: The reference and the damaged state, especially with the severed hanger. In preparation of the damage analysis, finite element models have been generated to predict the system behaviour. Therein, the simulated difference corresponding flexibility matrix showed a single peak at induced structural damage.

The large-scale experiment results are shown in figure 4.8, which is reformulated data from Ebert.[25] As can be seen here, the position of the severed hanger can clearly be seen at measurement position 11. For more details on that matter see Lenzen and Ebert.[25, 117, 118]
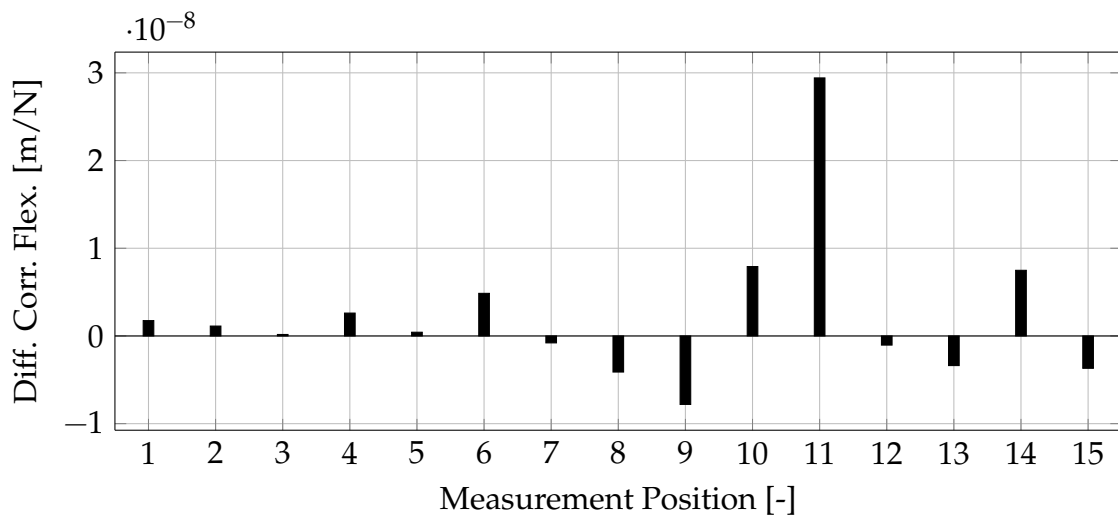
Figure 4.8: Diagonal of Difference Corresponding Flexibility Matrix

In this section the physical interpretation of a numerically identified mechanical state space system has been discussed. Especially the large-scale experiment example showed its clear applicability for damage localization. Nevertheless, these results are based on deterministic excitations, which are very elaborate: The transportation and operation of the impulse-hammer is very cost and time intensive. Thus, an automation clearly is not possible. Henceforth, an ambient excitation is necessary instead. The theoretical consequences of that are discussed below.

4.5 EXAMPLE: OPERATIONAL MODAL ANALYSIS

The stochastic system identification, for example following the techniques of section 4.3, is advantageous, because an elaborate test load induction can be omitted. Although an output-only identification of $H(A, C)$ and derived operational modal analysis is quite possible based on these techniques, the identification of all state space parameters $H(A, B, C, D)$ leads to central issues. Because of that, the application of

corresponding mechanical parameters is not useful based on stochastic identification, as will be discussed in the end.

To exemplify stochastic system identification, the multi-degree-of-freedom example of chapter 3, especially section 3.3.2, is analysed. Therein, a mechanical structure with force inputs and acceleration outputs was simulated by continuous-time state space parameters $\bar{A}$, $\bar{B}$, $\bar{C}_a$ and $\bar{D}_a$. Based on that, the zero-order-hold method of equation (3.15) is applied with $\Delta t = 2 \cdot 10^{-4}$s, which leads to a discrete-time state space model $H(A, B, C, D)$. Because basic details shall be shown only, a simple excitation is chosen. Therefore, stationary white noise processes w and v are used:

$$E \left\{ \begin{bmatrix} w_k \\ v_k \end{bmatrix} \begin{bmatrix} w_k \\ v_k \end{bmatrix}^* \right\} = \begin{bmatrix} Q & S \\ S^* & R_v \end{bmatrix} = \begin{bmatrix} I\, N^2 & 0 \\ 0 & I\, m^2/s^4 \end{bmatrix} . \tag{4.94}$$
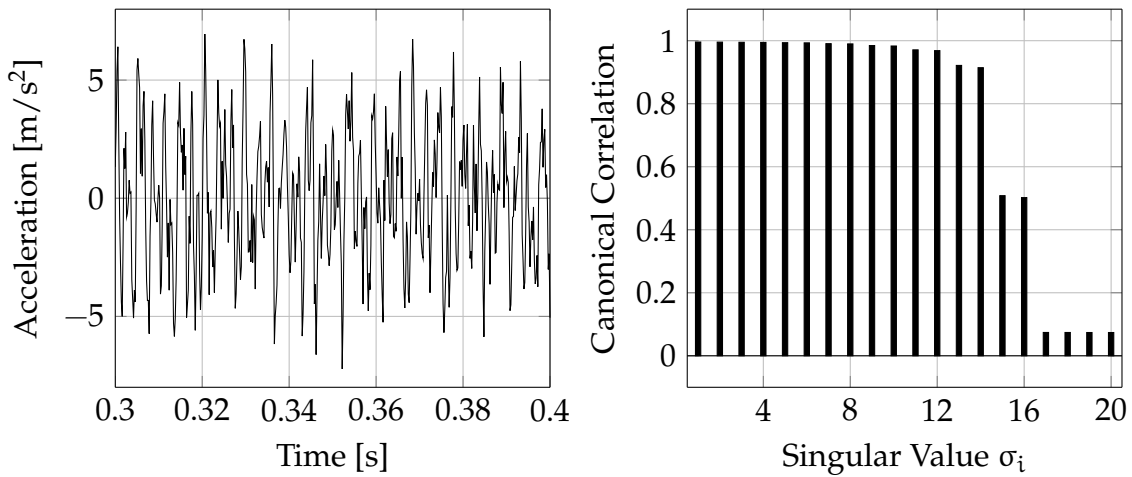
Figure 4.9: Exemplary Measurement at M_1 and Singular Values

Here, a total measurement time of about 11min has been sufficient for further analyses. An exemplary measurement at the free end of the cantilever arm (M_1) is shown in figure 4.9. As can be seen, the measured signal is in fact stochastic, which demands suitable system identification techniques.

The measurement y had an appropriate magnitude, which can be seen by comparing the output to ambient vibration test results at Vasco da Gama Bridge of Cunha et al.[15] Based on acceleration measurements, the balanced stochastic realization technique is subsequently applied, because of its clarity. However, other identification methods are possible too.

THE BALANCED STOCHASTIC REALIZATION   technique of section 4.3.3 has been used in connection with the Moore-Penrose pseudo-inverse of the extended observability matrix following equation (4.28). To do so, a covariance function $R_y(l)$ has been estimated by inverse Fourier transform of a power spectral density (PSD) estimate of

y. To determine the PSD, Welch's method[119] has been used with a Hanning window ($N = 2^{15}$) and 50% overlap, which follows the efficient numerical covariance determination of Cunha et al.[120] Further explanations for that will follow in section 7.1.2. An exemplary covariance function at M_1 is given in figure 4.10a.
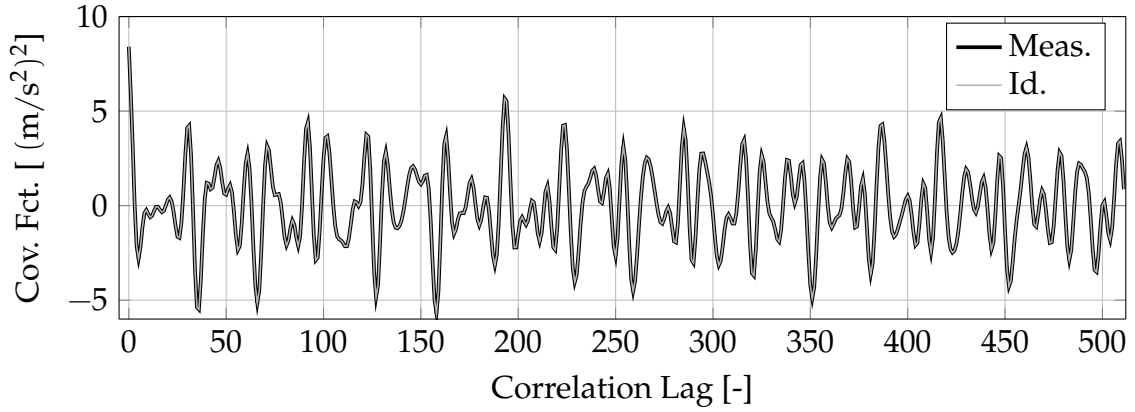
(a) Comparison of Measured and Identified Covariance Functions at M_1
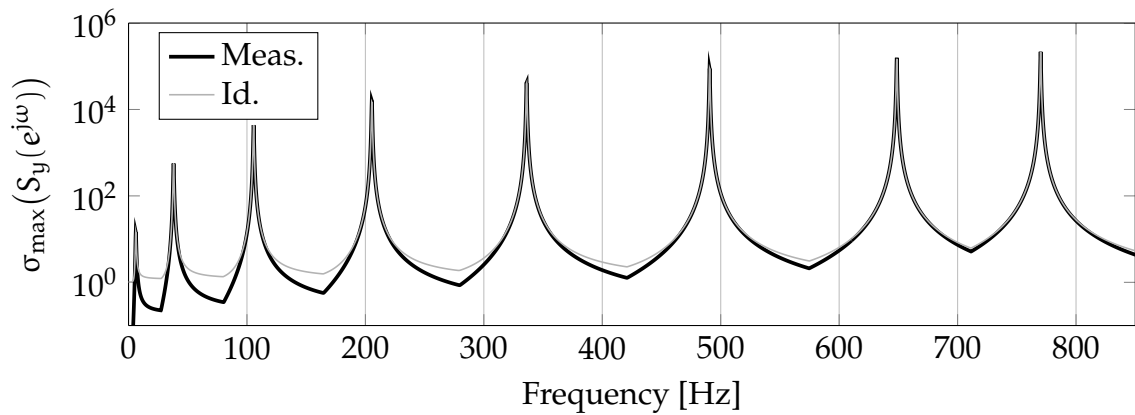
(b) Comparison of Measured and Identified Spectra

Figure 4.10: Evaluation of System Identification Results

Based on the covariance function $R_y(l)$, Hankel matrix $\mathcal{H}_m$ and both Toeplitz matrices (T_f, T_p) have been constructed in accordance with equations (4.48) and (4.77). Then the singular value decomposition in equation (4.80) with $m = 2^9$ was conducted. The first 20 singular values are also shown in figure 4.9. As can be seen here, the first 16 canonical correlations are relevant, thus $n = 16$ was chosen. This led to extended observability and controllability matrices $\mathcal{O}_k$ and $\mathcal{C}_k$, which allowed to determine the system identification result: The computation of triplet (A, N, C) according to equation (4.28). Very importantly, the identification quality must be analysed. Because a covariance based method has been used, it is reasonable to compare measured and identified covariance functions. Here, $R_y(l)$ is compared to its identification result

$CA^{l-1}N$ for $l > 0$. An example at M_1 is shown in figure 4.10a. Because of an appropriate identification, both functions nearly are identical.

The analysis of covariance matrix function R_y is limited. In our case matrix R_y has 64 elements, which are difficult to analyse at once. Engineering-oriented analyses are more appropriate in the frequency domain, because modal data can be seen in principal there. Thus, the first dominant singular value of S_y, both measured and identified, is presented in figure 4.10b. Central advantage of this type of presentation is that it is an integral quantity of all measurement positions.

At this point it is important to note the similarity to figure 3.6 in chapter 3. Here, measurement noise v marks the only difference, which is negligible. The accurate parametrization of the identified spectrum S_y is observable here, which essentially retrieves the results of covariance function $R_y(l)$ in figure 4.10a. While the measured spectrum is the Fourier transform result of R_y, the identified one follows $H(z)$ in equation (4.47).

Operational modal analysis (OMA) is a central element for applied structural dynamics. It allows to give another viewpoint on spectrum S_y by applying modal analysis techniques of section 4.3.1. Thus, system parameters A and C are used to determine natural frequencies, modal dampings and normalized mode shapes following equation (4.54). The modal identification results are shown in figure 4.11. Therein measurement position 9 refers to the clamped end of the beam. Most interestingly, a comparison to the analytical results in chapter 3, especially figure 3.5, shows a resemblance. Here, the operational modal identification results are plausible and fit very well to the originally modelled mechanical system.

Because only fundamental knowledge has been shown in this example, very important topics on numerical issues have been omitted here. Nevertheless, a more practical laboratory example will be given in chapter 7.

IMPORTANT CONCLUSIONS follow the above statements: Summarizing above, the question arises, which damage identification technique is reasonable to use based on stochastic identification. Most commonly, damage identification based on modal data is applied only, as was discussed in the introduction in chapter 1. However, damage identification based on modal data sometimes is questionable. Thus, the application of complete state space systems $H(A, B, C, D)$ may have advantages in comparison to output-only identifications $H(A, C)$.

Unfortunately, the corresponding parameters of section 4.4 are non-applicable here, because gain matrix B is non-determinable. Here, the Kalman filter gain could be used instead. Nevertheless, it is connected to several numerical issues, which will be discussed for the laboratory example in section 7.3. Because of that, it is very useful to discuss the generalization of Kalman filter, so called $\mathcal{H}^{\infty}$ estimation, in the following. This allows to cope with noise uncertainties, which is advantageous, as ambient excitations are non-measurable. Based on $\mathcal{H}^{\infty}$ estimators, a new damage localization technique will be defined in chapter 6.
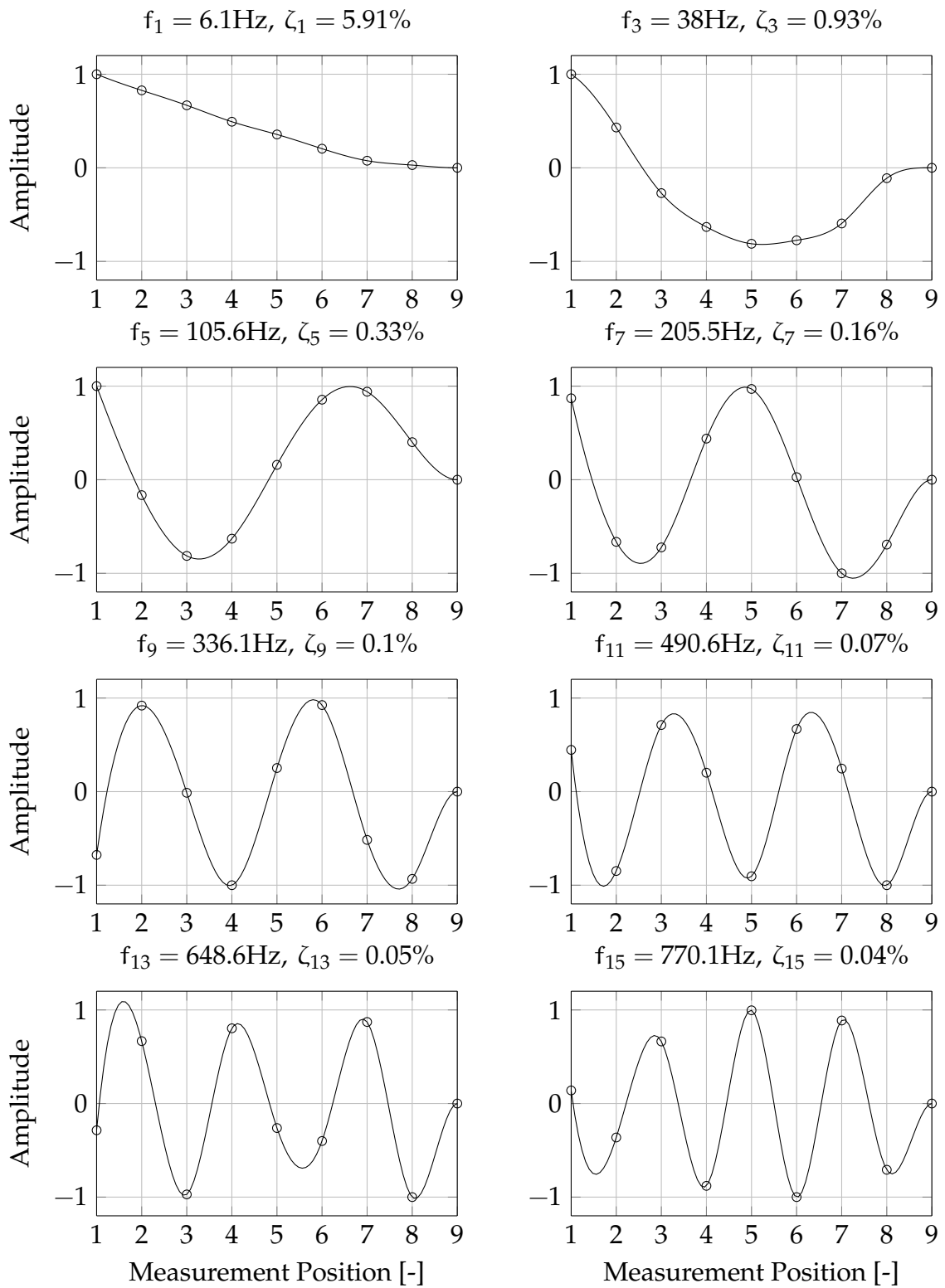
Figure 4.11: Operational Modal Analysis: Normalized Mode Shapes (Circles) and Cubic Spline Interpolation (Continuous Line)

Part II

STATE PROJECTION ESTIMATION ERROR:

A SYNTHESIS OF $\mathcal{H}^{\infty}$ ESTIMATION THEORY AND OBLIQUE PROJECTIONS FOR DAMAGE LOCALIZATION

5

AN OVERVIEW OF $\mathcal{H}^\infty$ ESTIMATION ON THE BASIS OF KALMAN FILTERING

CHAPTER OUTLINE

In this chapter $\mathcal{H}^\infty$ theory is explained on the basis of commonly known Kalman filtering. For that, it is typical to describe two fundamental different estimation theory approaches, which are explained here: While the 1st section covers finite horizon $\mathcal{H}^\infty$ theory, which leads to a so called Krein space Kalman filter, the 2nd section is devoted to the canonical factorization of a so-called Popov function in infinite horizon. In fact, the name originates from the presupposed data, like $y = \left[y_k\right]_{k=0}^N$ (finite) and $y = \left[y_k\right]_{k=-\infty}^\infty$ (doubly infinite). This leads to the analysis of time-variant systems in time-domain on one hand, and time-invariant systems in z-domain on the other hand.

```
        ┌─────────────────────────┐
        │   KREIN SPACE BASED     │
        │ ℋ∞ ESTIMATION THEORY    │
        └─────────────────────────┘
```
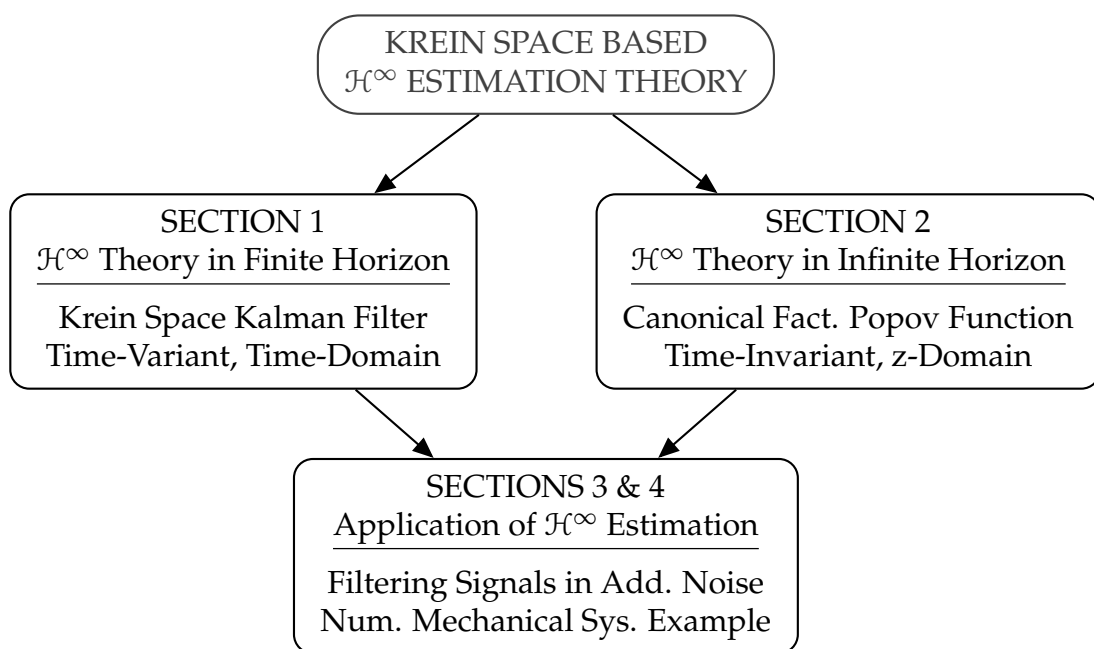
Figure 5.1: Chapter Outline

In both final sections the application of $\mathcal{H}^\infty$ theory is discussed, which then enters the mechanical system example of chapter 3, namely section 3.3.1. Here, the filtering of displacements in a noise disturbed environment is discussed.

5.1 Finite Horizon: Krein Space Kalman Filter

5.1.1 Introduction to Estimation Theory

Estimation problems must be faced in many industrial fields like communications, control, econometrics and signal processing.[20] At first, central concepts of estimation theory are summarized, which then is the basis for Kalman filter and $\mathcal{H}^\infty$ estimator derivations.

To begin with, the measurement process $y \in \mathbb{R}^p$ is introduced, which is the observable output of an analysed system. Numerous possible measurement examples can be given (e.g. voltage, current, forces, flow rates, etc.). As was pointed out in chapter 3, accelerations of a mechanical structure are typically measured in structural health monitoring.[15] Furthermore, displacements, velocities, strains, inclinations and so forth may be analysed too.

Based on the measurement signal y, a desired one, denoted by $s \in \mathbb{R}^m$, shall be estimated,[78] for instance corrected price developments, temperatures, pressures or noise free accelerations. Nevertheless, the desired signal s is unmeasurable in general, thus, it must be estimated by $\hat{s}$. Estimation approaches, referred below as $\mathcal{E}(\times)$, have been analysed by researchers for decades and a huge variety of approaches has been developed for that.

PREDICTION, FILTERING AND SMOOTHING are important concepts of estimation theory.[19,121,122] To understand these concepts, consider the estimation of the desired signal s_{k+M} based on measurements $y_1, y_2, \ldots, y_k$ as follows:

$$\hat{s}_{k+M|k} = \mathcal{E}\left(s_{k+M} \,|\, y_1, y_2, \ldots, y_k\right) \quad \text{for} \quad M \begin{cases} > 0 : & \text{Prediction} \\ = 0 : & \text{Filtering} \\ < 0 : & \text{Smoothing} \end{cases} . \quad (5.1)$$
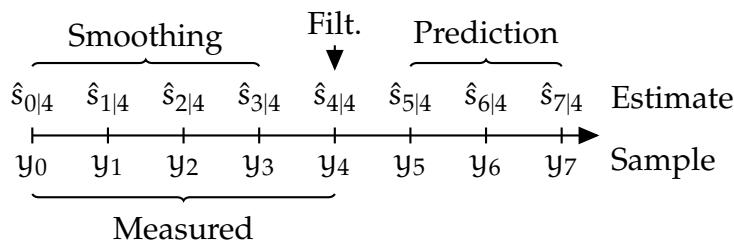
Figure 5.2: Visualization of Notion at an Example

The estimate $\hat{s}_{k+M|k}$ with $M > 0$ is assigned as prediction, because it is beyond the current measurement sample y_k. The opposite case is called smoothing, namely the

estimation of a past value. Using measurements y to estimate s of the same time instant is called filtering. The last statement also refers to an a posteriori estimate, which is denoted by $\hat{s}_{k|k}$. In opposite to that, a priori estimates $\hat{s}_{k+1|k}$ essentially are one-step predictions.[121] A notation visualization at an example is given in figure 5.2. Conveniently, the notation of a priori estimates is simplified below, for example by $\hat{s}_{k+1} = \hat{s}_{k+1|k}$.

Because of the profound mathematical background of estimation theory, norms are often used to derive estimators. Thus, important mathematical norms are briefly summarized below.

MATHEMATICAL NORMS are functions that assign a strictly positive number to mathematical objects (e.g. sequences, vectors, matrices, functions, etc.). For example the p-norm of a n-dimensional vector x

$$\|x\|_p = \left(\sum_{i=0}^{n} |x_i|^p \right)^{1/p} \tag{5.2}$$

can be seen as a generalized distance measure for $1 \leqslant p < \infty$. Note that i refers to the element in x. As it is often used, the 2-norm ($p = 2$), namely the Euclidian norm, is a special case of equation (5.2).

By using matrix $A \in \mathbb{C}^{m \times n}$ instead of vector x, this can be extended to determine matrix norms, for instance the spectral norm and the Frobenius norm:

$$\|A\|_2 = \max_{x \neq 0} \frac{\|Ax\|_2}{\|x\|_2} = \sigma_{max}, \qquad \|A\|_F^2 = \sum_{i=1}^{m} \sum_{j=1}^{n} |a_{ij}|^2 = \sum_{i=1}^{r} \sigma_i^2 . \tag{5.3}$$

Here, the connection between the singular values of a matrix and its norm has already been given. For details on the singular value decomposition see section 4.1.1.

Furthermore, the matrix 2-norm is a special case of the operator norm. Thus, consider the more general case of $y = \mathcal{T}x$ in operator notation with finite vectors x and y, then the induced 2-norm of operator $\mathcal{T}$ follows accordingly as

$$\|\mathcal{T}\|_{i2} = \sup_{x \neq 0} \frac{\|\mathcal{T}x\|_2}{\|x\|_2} . \tag{5.4}$$

A generalization of the p-norm in equation (5.2) to infinite processes x and integrable functions f lead to the introduction of the l^p-norm and $\mathcal{L}^p$-norm:

$$\|x\|_{l^p} = \left(\sum_{i=0}^{\infty} |x_i|^p \right)^{1/p}, \qquad \|x\|_{l^\infty} = \sup_i |x_i|, \qquad \|f\|_{\mathcal{L}^p} = \left(\int_{-\infty}^{\infty} |f(z)|^p \, dz \right)^{1/p} . \tag{5.5}$$

Based on that, l^p-sequences are defined by $\|x\|_{l^p} < \infty$. Furthermore, the $\mathcal{L}^p$-space is introduced. The $\mathcal{L}^p$-spaces, also known as the Lebesgue spaces, are the set of all

Lebesgue p-integrable functions, for which $\|\times\|_{\mathcal{L}^p} < \infty$. Especially the case $p = 2$ is technically relevant: l^2-sequences are square-summable and $\mathcal{L}^2$-functions are square-integrable.

The Hardy spaces $\mathcal{H}^p$ are subsets of $\mathcal{L}^p$ (for $1 \leqslant p \leqslant \infty$), defined by $\|\times\|_{\mathcal{H}^p} < \infty$. Frequently used in estimation and control theory, the cases of $p = 2$ and $p = \infty$ for matrix valued functions $T(z)$ are important, which are defined here on the unit disc:

$$\|\mathcal{T}\|_{\mathcal{H}^2}^2 = \frac{1}{2\pi} \int_0^{2\pi} \left\| T(e^{j\theta}) T^*(e^{j\theta}) \right\|_F d\theta, \quad \|\mathcal{T}\|_{\mathcal{H}^\infty}^2 = \sup_\theta \sigma_{\max}\left(T(e^{j\theta}) T^*(e^{j\theta}) \right). \quad (5.6)$$

Of course one might discuss the above topic in more detail, but in the frame of this dissertation that is omitted. Based on the given norm definitions, this now allows us to analyse systems in more detail.

CAUSALITY, INVERTIBILITY AND STABILITY are analysable system properties.[78] In order to define causality, consider a system in an operator description $\mathcal{A}$ with $y = \mathcal{A}u$ and processes $y \in \mathbb{R}^p$, $u \in \mathbb{R}^q$. Both processes are defined in this section as finite processes u_k and y_k with $k = 0, 1, \ldots, N$, thus $u = [u_k]_{k=0}^N$ and $y = [y_k]_{k=0}^N$. Furthermore, the operator $\mathcal{A}$ is represented in finite horizon with the help of matrices A_{kl}. Based on that, causality is defined by the subsequent statements:

$$\mathcal{A} = \left[A_{kl} \right]_{k,l=0}^N, \quad y_k = \sum_{l=0}^N A_{kl} u_l, \quad A_{kl} = 0, \quad \begin{cases} k < l: & \text{Causal} \\ k \leqslant l: & \text{Strictly Causal} \\ k > l: & \text{Anti-Causal} \\ k \geqslant l: & \text{Strictly Anti-Causal} \end{cases} . \quad (5.7)$$

Thus, a system is strictly causal, if future inputs have no influence on the current output. On the other side, if a system is not causal, for example when $A_{kl} \neq 0$ for $l > k$, then system $\mathcal{A}$ is referred to as non-causal.[78] To understand this, consider a mechanical structure (e.g. a tower), which is excited by an impulse. A non-causal system would respond before an impulse hammer actually hits the structure, which obviously seems unnatural. This fact is observable in chapter 3, especially equation (3.13). However, in addition to causality, invertibility of a system can be analysed. An inverse system $\mathcal{A}^{-1}$ may be used to determine the input

$$u = \mathcal{A}^{-1} y \quad \text{with} \quad \mathcal{A}\mathcal{A}^{-1} = \mathcal{A}^{-1}\mathcal{A} = I. \quad (5.8)$$

Furthermore, a system is stable if it maps bounded inputs to bounded outputs. Processes are referred to as bounded l^2-sequences, if their energy is finite. Finite energy of processes are defined by infinite processes with

$$\|y\|_{l^2} = \sum_{k=0}^\infty y_k y_k^T < \infty \quad \text{and} \quad \|u\|_{l^2} = \sum_{k=0}^\infty u_k u_k^T < \infty \quad (5.9)$$

and these processes lead to a so called l^2-induced stability of $\mathcal{A}$. To visualize the above statement, consider an impulse excitation at a damped mechanical structure, for instance a real bridge: Both, the impulse (force) input and the measurable acceleration decay function, have finite energy. Here, a practical impulse has been considered, not the Dirac impulse. Thus, the system of this damped mechanical structure must be l^2-induced stable.

Besides l^2-induced stability, other definitions are possible, for example the l^∞-induced stability (or boundness), which considers bounded amplitude inputs and outputs by

$$\|u\|_{l^\infty} = \sup_k \max_l |u_{kl}| < \infty \quad \text{and} \quad \|y\|_{l^\infty} = \sup_k \max_l |y_{kl}| < \infty . \tag{5.10}$$

Again consider a damped mechanical structure, but with an ambient excitation, namely wind and vehicle traffic. This excitation is typically modelled as white noise, which has infinite energy, thus l^2-induced stability is non-applicable here. Nevertheless, the l^∞-norm of the ambient excitation and the structural response is finite. Otherwise, the damped mechanical structure would collapse. Thus, the mechanical system must be l^∞-induced stable, which is a more demanding property than l^2-induced stability.[78]

Finally, the above discussion leads to the introduction of a very important estimation approach:

THE LINEAR LEAST-MEAN-SQUARES ESTIMATOR

is based on complex zero-mean, vector-valued random variables. Thus, given a set $\{y_0, y_1, \ldots, y_N\}$ with $y \in \mathbb{C}^p$, we would like to estimate variable $s \in \mathbb{C}^m$ by $\hat{s}$ with a linear combination

$$\hat{s} = Ky, \qquad K \in \mathbb{C}^{m \times p(N+1)} . \tag{5.11}$$

By defining some covariance matrices $R_y = E\{yy^*\} > 0$ and $R_{ys} = E\{ys^*\} = R_{sy}^*$, this leads to the error covariance matrix

$$R_{\tilde{s}} = E\{\tilde{s}\tilde{s}^*\} = R_s - KR_{ys} - R_{sy}K^* + KR_yK^* \quad \text{with} \quad \tilde{s} = s - Ky . \tag{5.12}$$

Here, the question arises: What is the optimal solution for an estimator K? To see that, a joint covariance matrix is introduced and analysed by LDU decomposition:

$$E\left\{ \begin{bmatrix} s \\ y \end{bmatrix} \begin{bmatrix} s \\ y \end{bmatrix}^* \right\} = \begin{bmatrix} R_s & R_{sy} \\ R_{ys} & R_y \end{bmatrix} = \begin{bmatrix} I & R_{sy}R_y^{-1} \\ 0 & I \end{bmatrix} \begin{bmatrix} R_s - R_{sy}R_y^{-1}R_{ys} & 0 \\ 0 & R_y \end{bmatrix} \begin{bmatrix} I & 0 \\ R_y^{-1}R_{ys} & 0 \end{bmatrix} . \tag{5.13}$$

This then is applied to rewrite the error covariance matrix

$$R_{\tilde{s}} = R_s - KR_{ys} - R_{sy}K^* + KR_yK^* = \begin{bmatrix} I & -K \end{bmatrix} \begin{bmatrix} R_s & R_{sy} \\ R_{ys} & R_y \end{bmatrix} \begin{bmatrix} I \\ -K^* \end{bmatrix} \tag{5.14a}$$

$$= R_s - R_{sy}R_y^{-1}R_{ys} + \underbrace{\left(R_{sy}R_y^{-1} - K\right) R_y \left(R_{sy}R_y^{-1} - K\right)^*}_{K_0 = R_{sy}R_y^{-1} \,\to\, 0} . \tag{5.14b}$$

71

As can clearly be seen above, the minimum-mean-square-error matrix $R_{\tilde{s}}$ arises, as $K_0 = R_{sy}R_y^{-1}$ is chosen, which is the optimal solution.[20]

A GEOMETRICAL REFORMULATION   is a repeatedly applied theme of estimation theory, as it allows a more graphical interpretation. For that, rewrite the linear least-mean-squares solution $K_0 = R_{sy}R_y^{-1}$ as

$$K_0 E\{yy^*\} = E\{sy^*\} \quad \longrightarrow \quad E\left\{(s - K_0 y)y^*\right\} = 0 . \tag{5.15}$$

To analyse above, the idea is to treat random variables, like y and s, as vectors,[20] which suggests that

$$E\left\{(s - K_0 y)y^*\right\} = 0 \quad \longrightarrow \quad \langle s - K_0 y, y \rangle = 0 \quad \longrightarrow \quad s - K_0 y \perp y . \tag{5.16}$$
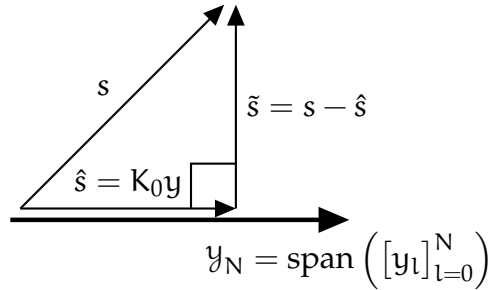
Figure 5.3: Orthogonal Projection of s

As is shown in figure 5.3, the found orthogonality $s - K_0 y \perp y$ considerably improves the interpretability of results. This technique is constantly reused in the finite horizon section 5.1.

THE EQUIVALENCE OF DETERMINISTIC AND STOCHASTIC PROBLEMS   is another important theme of estimation theory. The idea is to come up with a solution, which essentially is the same for the deterministic and the stochastic case. For instance consider the minimization of a scalar quadratic form (deterministic problem)

$$J(s, y) = \begin{bmatrix} s^* & y^* \end{bmatrix} \begin{bmatrix} R_s & R_{sy} \\ R_{ys} & R_y \end{bmatrix}^{-1} \begin{bmatrix} s \\ y \end{bmatrix} \quad \text{with} \quad \begin{bmatrix} R_s & R_{sy} \\ R_{ys} & R_y \end{bmatrix} = \left\langle \begin{bmatrix} s \\ y \end{bmatrix}, \begin{bmatrix} s \\ y \end{bmatrix} \right\rangle_{\mathcal{H}} > 0 . \tag{5.17}$$

By reusing the LDU factorization of equation (5.13), one can find a minimum:[78]

$$J(s, y) = \begin{bmatrix} (s^* - y^* R_y^{-1} R_{sy}) & y^* \end{bmatrix} \begin{bmatrix} (R_s - R_{sy}R_y^{-1}R_{ys})^{-1} & 0 \\ 0 & R_y^{-1} \end{bmatrix} \begin{bmatrix} s - R_{sy}R_y^{-1}y \\ y \end{bmatrix} \tag{5.18a}$$

$$\min J(s_0, y) = \begin{bmatrix} 0 & y^* \end{bmatrix} \begin{bmatrix} \times & 0 \\ 0 & R_y^{-1} \end{bmatrix} \begin{bmatrix} 0 \\ y \end{bmatrix} = y^* R_y^{-1} y . \tag{5.18b}$$

Again, the optimal solution (maximum likelihood estimate) is $s_0 = R_{sy} R_y^{-1} y$, which is equivalent to the stochastic solution of the linear least-mean-squares estimate. This suggests to treat deterministic and stochastic problems equivalently.

5.1.2 TIME-VARIANT KALMAN FILTER

In this chapter $\mathcal{H}^\infty$ estimation theory is explained comprehensively on the basis of widespread estimation techniques, especially the Wiener and the Kalman filter.[123,124] For that, the indefinite-quadratic estimation theory[78] is an outstanding approach, because within this theory Wiener and Kalman filters are directly applied. To derive finite horizon $\mathcal{H}^\infty$ estimators, Kalman filtering is explained below, which leads to a solution based on a so called Krein space Kalman filter. The discussed theoretical development of the finite horizon section is summarized in table 5.1.

STATE SPACE MODELS are commonly used approaches to parametrize a system. These models are very advantageous to parametrize a multi input multi output (MIMO) system in both time-domain and z-domain. Its central concept is the introduction of a possibly non-measurable auxiliary vector, the so called state $x \in \mathbb{C}^n$. Because ambient excitations are primarily considered in this thesis, a state space model H is introduced here, which maps disturbance processes w and v to the measurement y (see figure 5.4). This time-variant system is a generalization of equation (4.40) and written in time-domain as follows:

$$x_{k+1} = A_k x_k + \begin{bmatrix} I & 0 \end{bmatrix} \begin{bmatrix} w_k \\ v_k \end{bmatrix} = A_k x_k + w_k \tag{5.19a}$$

$$y_k = C_k x_k + \begin{bmatrix} 0 & I \end{bmatrix} \begin{bmatrix} w_k \\ v_k \end{bmatrix} = C_k x_k + v_k \, . \tag{5.19b}$$
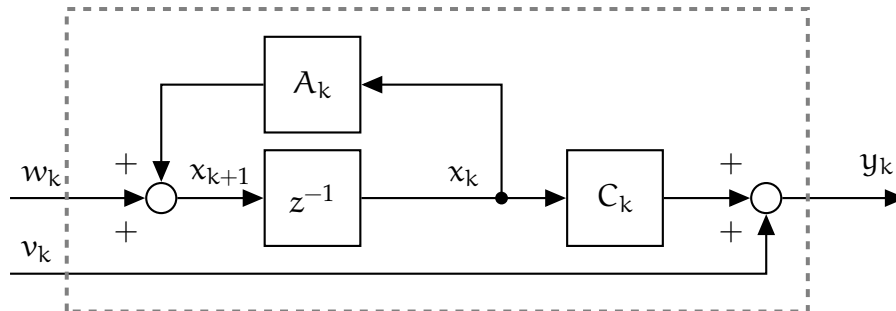
Figure 5.4: Time-Variant State Space Model H

	KALMAN FILTER	$\mathcal{H}^\infty$ ESTIMATOR
1.	Optimal State Estimate (eq.(5.23)) Estim. Error $\tilde{x}_k = x_k - \hat{x}_k$ $$\min_{\hat{x}_k} \|\tilde{x}_k\|_2^2, \quad E\{\tilde{x}_k \tilde{x}_k^*\} = P_k$$ Stochastic Processes	Worst-Case Analysis (eq. (5.57)) Estim. Error $\tilde{s}_k = s_k - \hat{s}_k$, $s_k = L_k x_k$ $$\|\mathcal{T}_K\|_{\mathcal{H}^\infty}^2 = \sup_{w,v\neq 0} \frac{\|\tilde{s}\|_2^2}{\|w\|_2^2 + \|v\|_2^2} < \gamma^2$$ Det. and Stochastic Processes
2.	State Space System (eq. (5.19)) $$x_{k+1} = A_k x_k + w_k$$ $$y_k = C_k x_k + v_k$$ $$E\left\{ \begin{bmatrix} w_k \\ v_k \end{bmatrix} \begin{bmatrix} w_l \\ v_l \end{bmatrix}^* \right\} = \begin{bmatrix} Q_k & S_k \\ S_k^* & R_{v,k} \end{bmatrix} \delta_{kl}$$	Krein Space State Space (eq. (5.63)) $$x_{k+1} = A_k x_k + w_k$$ $$\begin{bmatrix} y_k \\ \check{s}_{k|k} \end{bmatrix} = C_k x_k + \bar{v}_k$$ $$\left\langle \begin{bmatrix} w_k \\ \bar{v}_k \end{bmatrix}, \begin{bmatrix} w_l \\ \bar{v}_l \end{bmatrix} \right\rangle_{\mathcal{K}} = \begin{bmatrix} Q_k & 0 \\ 0 & \begin{bmatrix} I & 0 \\ 0 & -\gamma^2 I \end{bmatrix} \end{bmatrix} \delta_{kl}$$
3.	Innovation Form of Kalman Filter (eq. (5.37)), Innovations e_k $$\hat{x}_{k+1} = A_k \hat{x}_k + K_{p,k} e_k$$ $$y_k = C_k \hat{x}_k + e_k$$ $P_k = \text{Ric. Eq.}(A_k, C_k, Q_k, R_k, S_k)$ (5.33) $K_{p,k} = (A_k P_k C_k^* + S_k) R_{e,k}^{-1}$ $R_{e,k} = E\{e_k e_k^T\} = C_k P_k C_k^* + R_{v,k}$	A posteriori $\mathcal{H}^\infty$ Estimator (eq. (5.93)), Estimation error $e_{y,k}$ $$\hat{x}_{k+1} = A_k \hat{x}_k + K_{py,k} e_{y,k}$$ $$y_k = C_k \hat{x}_k + e_{y,k}$$ Presumption $\check{s}_{k|k} = \hat{s}_{k|k}$ $P_k = \text{Ric. Eq.}(A_k, C_k, L_k, Q_k, \gamma)$ (5.75) $K_{py,k} = A_k P_k C_k^* R_{ey,k}^{-1}$ $R_{ey,k} = \langle e_{y,k}, e_{y,k} \rangle = C_k P_k C_k^* + I$

Table 5.1: Summary of Discussed Theories in Finite Horizon

The introduced state space system is defined by both matrices $A \in \mathbb{C}^{n \times n}$ and $C \in \mathbb{C}^{p \times n}$, thus $H(A, C)$ follows. In addition, a matrix $L \in \mathbb{C}^{m \times n}$ is introduced to define the desired signal as a linear combination of states by

$$s_k = L_k x_k . \tag{5.20}$$

Matrix L is an additional design parameter, which can be used to put emphasis on some states. Furthermore, it might be used to define an application (e.g. equalization, filtering signals), as states x might be non-physical. Some possible applications are discussed by Hassibi et al.[78]

With regard to the subsequently explained Kalman filter, disturbance processes w and v are presupposed, at this point, as white noise processes with known second order statistical parameters

$$\mathsf{E}\left\{ \begin{bmatrix} w_k \\ v_k \end{bmatrix} \begin{bmatrix} w_l \\ v_l \end{bmatrix}^* \right\} = \begin{bmatrix} Q_k & S_k \\ S_k^* & R_{v,k} \end{bmatrix} \delta_{kl} . \tag{5.21}$$

KALMAN FILTERING   is a widespread state estimation technique based on known covariance matrices (Q, R_v, S) and a presupposed state space system, for example $H(A, C)$ of equation (5.19).[124] Thus, it is based on stochastic processes. The estimated state vector, noted by $\hat{x}$, is determined based on noise disturbed measurements y. Thus, a state estimation error

$$\tilde{x}_k = x_k - \hat{x}_k \tag{5.22}$$

is unavoidable. Very importantly, the state estimation error $\tilde{x}$ is minimized in Kalman filtering,[19] and the estimation error minimization considers the average energy of $\tilde{x}$ by the 2-norm with

$$\min_{\hat{x}_k} \|\tilde{x}_k\|_2^2 \quad \text{with} \quad \mathsf{E}\{\tilde{x}_k \tilde{x}_k^*\} = P_k . \tag{5.23}$$

As it is very similar to the linear least-mean-squares solution in figure 5.3, a geometrical approach has been shown in figure 5.5. Therein the orthogonal projection of states x_k onto a data space $\mathcal{Y}_k$, a linear combination of measurements $[y_l]_{l=0}^k$, leads to the estimate $\hat{x}_k$. The geometrical approach directly applies orthogonality with $\tilde{x}_k \perp \mathcal{Y}_k$.[19]
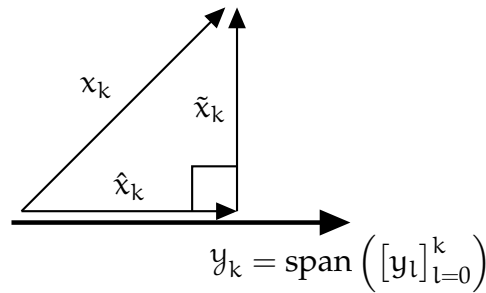
Figure 5.5: Orthogonal Projection of x

The innovation process, noted by e, is implied in the above statements. This process was introduced by Kailath[125,126] and has distinctive properties: Based on the orthogonality to the previous data space $e_k \perp \mathcal{Y}_{k-1}$, innovations are determined by a difference of actual measurements y and predicted ones with

$$e_k = y_k - \hat{y}_k = (Cx_k + v_k) - C_k \hat{x}_k = C\tilde{x}_k + v_k . \tag{5.24}$$

Furthermore, $e_k \perp \mathcal{E}_{k-1}$ must be considered based on the linear space of past innovations $\mathcal{E}_{k-1} = \mathrm{span}([e]_{l=0}^{k-1})$. Because new information is constantly introduced by e_k, it must be a white noise process and furthermore the name innovation was derived.[20] As can be seen in equation (5.24), the innovation determination can be reduced to compute the one-step state prediction $\hat{x}$. Thus, the basic estimation formulae

$$\hat{x}_{k+1} = \sum_{l=0}^{k} E\{x_{k+1}e_k^T\}R_{e,l}^{-1}e_l = \left(\sum_{l=0}^{k-1} E\{x_{k+1}e_k^T\}R_{e,l}^{-1}e_l\right) + E\{x_{k+1}e_k^T\}R_{e,k}^{-1}e_k \qquad (5.25)$$

can be used here.[20] This estimation approach is based on the covariance matrix of innovations, which directly follows equation (5.24) with

$$R_{e,k} = E\{e_k e_k^T\} = C_k P_k C_k^* + R_{v,k} . \qquad (5.26)$$

In the following, the state estimation of equation (5.25) shall be derived to allow a numerical-practical application. At first past inputs, especially innovations $[e]_{l=0}^{k-1}$, are rewritten to

$$\sum_{l=0}^{k-1} E\{x_{k+1}e_k^T\}R_{e,l}^{-1}e_l = \hat{x}_{k+1|k-1} = A_k\hat{x}_k , \qquad (5.27)$$

because they can be seen as an influence on former states. Secondly, the gain matrix

$$K_{p,k} = E\{x_{k+1}e_k^T\}R_{e,k}^{-1} \qquad (5.28)$$

is introduced. By using straightforward reflections on

$$E\{x_{k+1}e_k^T\} = A_k E\left\{x_k\left(C_k\tilde{x}_k + v_k\right)^*\right\} + E\left\{w_k\left(C_k\tilde{x}_k + v_k\right)^*\right\} = A_k P_k C_k^* + S_k , \qquad (5.29)$$

the gain matrix has been determined:

$$K_{p,k} = \left(A_k P_k C_k^* + S_k\right)\left(C_k P_k C_k^* + R_{v,k}\right)^{-1} . \qquad (5.30)$$

AN OPTIMAL STATE ESTIMATION   based on innovations now can be given by reconsidering equation (5.25) and the defined gain matrix K_p. Collecting above, the central state estimate

$$\hat{x}_{k+1} = A_k\hat{x}_k + K_{p,k}e_k \qquad (5.31)$$

depends on a continuously computed gain $K_{p,k}$, and thus a covariance matrix P_k. Here, a straightforward derivation can be found by analysing the state estimation error

$$\tilde{x}_{k+1} = x_{k+1} - \hat{x}_{k+1} = \left(A_k x_k + w_k\right) - \left(A_k\hat{x}_k + K_{p,k}e_k\right) \qquad (5.32a)$$

$$= \left(A_k - K_{p,k}C_k\right)\left(x_k - \hat{x}_k\right) + w_k - K_{p,k}v_k \qquad (5.32b)$$

$$= A_{p,k}\tilde{x}_k + \begin{bmatrix} I & -K_{p,k} \end{bmatrix}\begin{bmatrix} w_k \\ v_k \end{bmatrix} , \qquad (5.32c)$$

defining the closed-loop matrix $A_{p,k} = A_k - K_{p,k}C_k$ and then forming the covariance matrix of $\tilde{x}_{k+1}$:

$$P_{k+1} = E\{\tilde{x}_{k+1}\tilde{x}_{k+1}^*\} = A_{p,k}P_kA_{p,k}^* + \begin{bmatrix} I & -K_{p,k} \end{bmatrix} \begin{bmatrix} Q_k & S_k \\ S_k^* & R_{v,k} \end{bmatrix} \begin{bmatrix} I \\ -K_{p,k}^* \end{bmatrix} \tag{5.33a}$$

$$= A_kP_kA_k^* - (A_kP_kC_k^* + S_k)(C_kP_kC_k^* + R_{v,k})^{-1}(A_kP_kC_k^* + S_k)^* + Q_k \tag{5.33b}$$

$$= A_kP_kA_k^* - K_{p,k}R_{e,k}K_{p,k}^* + Q_k . \tag{5.33c}$$

This equation is referred to as a discrete-time Riccati recursion, whose name comes from Count Riccati (ca. 1700). While A.M. Legrende (ca. 1786) used it for the calculus of variations, it was reused by Bellmann (1957) in control theory. Afterwards Kalman applied it to numerically solve his famous Kalman filter.[124]

To apply the Riccati recursion and compute the state estimation of equation (5.31), state space parameters (A_k, C_k) and noise parameters $(Q_k, R_{v,k}, S_k)$ have to be known for all k. Furthermore, initial conditions $\hat{x}_0$ and P_0 must be defined.

Nevertheless, the iterative solution of the discrete-time Riccati recursion is far from being easy to apply. A comprehensive overview for that is given by Sima.[33] Because it is beyond the scope of this thesis to discuss them all, selected methods are given below only.

THE NUMERICAL COMPUTATION of Riccati recursion (5.33) might be problematic, as it might not converge or give inaccurate results.[33] Of course one may directly apply equation (5.33), but its convergence rate and the numerical accuracy may lack enormously.[33,127] For further analysis Riccati equation (5.33) is rewritten to

$$P_k = \tilde{A}_kP_k\left(I - C_k^*(R_{v,k} + C_kP_kC_k^*)^{-1}C_kP_k\right)\tilde{A}_k^* + \tilde{Q}_k \tag{5.34a}$$

$$\text{with} \quad \tilde{A}_k = A_k - S_kR_{v,k}^{-1}S_k^* \quad \text{and} \quad \tilde{Q}_k = Q_k - S_kR_{v,k}^{-1}C_k^* . \tag{5.34b}$$

This reformulated recursion allows to apply easier methods,[19] because S has been suppressed. Then the direct iteration can be split up in three steps:

(i) Gain computation $K_{p,k} = \tilde{A}_kP_kC_k^*(R_{v,k} + C_kP_kC_k^*)^{-1}$,

(ii) Determination of closed-loop state matrix $\tilde{A}_{p,k} = \tilde{A}_k - K_{p,k}C_k$ and

(iii) Solution of equation $P_{k+1} = \tilde{A}_{p,k}P_k\tilde{A}_{p,k}^* + K_{p,k}R_{v,k}K_{p,k}^* + \tilde{Q}_k$.

Very importantly, Sima explicitly discourages the reader to apply the direct iteration.[33] Rather than that, one can apply the Doubling algorithm,[127] which is based on the reformulated Riccati recursion

$$P_{k+1} = (\bar{G}_{21,k} + \bar{G}_{22,k}P_k)(\bar{G}_{11,k} + \bar{G}_{12,k}P_k)^{-1} \tag{5.35a}$$

$$\text{with} \quad \bar{G}_k = \begin{bmatrix} \bar{G}_{11,k} & \bar{G}_{12,k} \\ \bar{G}_{21,k} & \bar{G}_{22,k} \end{bmatrix} = \begin{bmatrix} \tilde{A}_k^{-*} & \tilde{A}_k^{-*}C_k^*R_{v,k}^{-1}C_k \\ \tilde{Q}_k\tilde{A}_k^{-*} & \tilde{A}_k + \tilde{Q}_k\tilde{A}_k^{-*}C_k^*R_{v,k}^{-1}C_k \end{bmatrix} . \tag{5.35b}$$

The central advantage is the increase of convergence. To determine result P_k one must solve

$$P_k = V_k U_k^{-1} \quad \text{following} \quad \begin{bmatrix} U_{k+1} \\ V_{k+1} \end{bmatrix} = \begin{bmatrix} \bar{G}_{11,k} & \bar{G}_{12,k} \\ \bar{G}_{21,k} & \bar{G}_{22,k} \end{bmatrix} \begin{bmatrix} U_k \\ V_k \end{bmatrix}. \tag{5.36}$$

Then result P_k can be used to determine $K_{p,k}$ of equation (5.30).

A CAUSAL AND A CAUSALLY INVERTIBLE SYSTEM   directly follow from the above analyses. These systems are important for further $\mathcal{H}^\infty$ derivations and are thus shown here. At first, a so-called innovation model, noted as Π,

$$\hat{x}_{k+1} = A_k \hat{x}_k + K_{p,k} e_k \tag{5.37a}$$

$$y_k = C_k \hat{x}_k + e_k \tag{5.37b}$$

can be defined following equation (5.31). Furthermore, the recursive desired signal estimate

$$\hat{s}_k = L_k \hat{x}_k \tag{5.38}$$

is defined. To understand their importance, an exemplary estimation of $(\hat{y}, \hat{s})$ based on y is shown in figure 5.6.
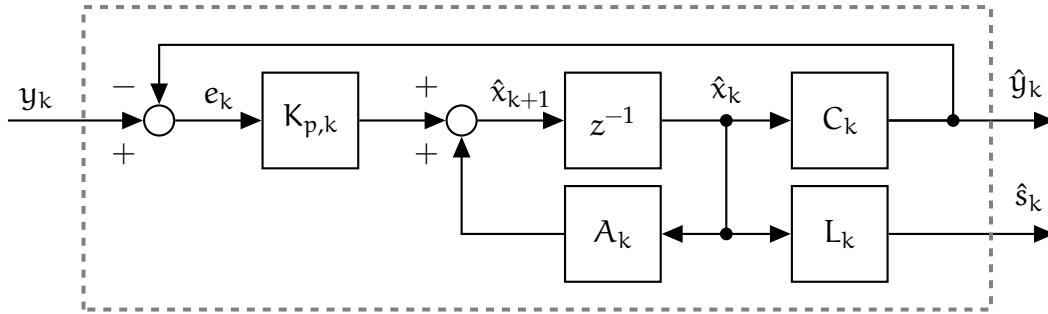
Figure 5.6: A Kalman Filter Application to Determine $\hat{y}$ and $\hat{s}$

Most interestingly, the central difference between the state space model $H(A_k, C_k)$ and the innovation model $\Pi(A_k, K_{p,k}, C_k)$ of equations (5.19) and (5.37) is the replacement of state x by its estimate $\hat{x}$ due to altered disturbance input processes

$$\begin{bmatrix} w_k \\ v_k \end{bmatrix} \longrightarrow \begin{bmatrix} K_p e_k \\ e_k \end{bmatrix}. \tag{5.39}$$

Causality is an important mathematical property of (mechanical) systems. To analyse causality of Π, the recursive computation of y on the basis of innovations e must be understood. Thus, consider an alternative approach of the innovation model with

$$\Pi = [\Pi_{kl}]_{k,l=0}^N, \qquad y_k = \sum_{l=0}^N \Pi_{kl} e_l, \qquad \Pi_{kl} = \begin{cases} C_k \Phi(k,l) K_{p,l}, & k > l \\ I, & k = l \\ 0, & k < l \end{cases} \tag{5.40}$$

based on state transition matrices Φ:

$$\Phi(k,l) = \begin{cases} A_{k-1}A_{k-2}\dots A_{l+1}, & k > l+1 \\ I, & k = l+1 \end{cases} . \tag{5.41}$$

In view of equation (5.7), model Π clearly is causal. The next important issue is invertibility of Π, hence the input determination based on measurements y. Fortunately, the inverse Π^{-1}

$$\hat{x}_{k+1} = A_{p,k}\hat{x}_k + K_{p,k}y_k \tag{5.42a}$$

$$e_k = -C_k\hat{x}_k + y_k \tag{5.42b}$$

follows straightforward from the rearranged equations (5.24) and (5.31):

$$\hat{x}_{k+1} = A_k\hat{x}_k + K_{p,k}(y_k - C_k\hat{x}_k) = (A_k - K_{p,k}C_k)\hat{x}_k + K_{p,k}y_k = A_{p,k}\hat{x}_k + K_{p,k}y_k . \tag{5.43}$$

Again causality must be analysed to determine if physically reasonable systems are present. To analyse causality of the inverse model Π^{-1} of equation (5.42), closed-loop state transition matrices

$$\Phi_p(k,l) = \begin{cases} A_{p,k-1}A_{p,k-2}\dots A_{p,l+1}, & k > l+1 \\ I, & k = l+1 \end{cases} \tag{5.44}$$

are directly applied to determine the subsequent innovations e based on measurements y:

$$\Pi^{-1} = \left[\bar{\Pi}_{kl}\right]_{k,l=0}^N, \qquad e_k = \sum_{l=0}^N \bar{\Pi}_{kl}y_l, \qquad \bar{\Pi}_{kl} = \begin{cases} -C_k\Phi_p(k,l)K_{p,l}, & k > l \\ I, & k = l \\ 0, & k < l \end{cases} . \tag{5.45}$$

As can be seen here, the inverse model $\Pi^{-1}(A_{p,k}, K_{p,k}, C_k)$ is causal too. Furthermore, e and y are bounded l^∞-sequences, which proofs stable systems. Because both systems Π and Π^{-1} are causal and stable, they are referred to as minimum phase.[78]

5.1.3 FROM KALMAN FILTER TO $\mathcal{H}^\infty$ ESTIMATOR

The given estimation theory so far is based on Kalman filtering with a focus on the innovation process. This technique is very powerful, and is thus applied in many industrial and research fields. However, Kalman filtering has theoretical flaws, which must be considered when applying it. For example perfectly known noise parameters (Q, R_v, S) are considered. If these presumptions differ from real noise disturbances, Kalman filters are unable to deal with those noise uncertainties. In opposite to that, a generalization of Kalman filters, especially $\mathcal{H}^\infty$ estimators, are designed to deal with these uncertainties. Therefore, the necessity of generalization is explained in the following.

THE GENERALIZATION OF KALMAN FILTERING is focussed, among others, on a unified approach for deterministic and stochastic problems. For that, Gramian matrices $\langle \times \rangle$ are used in the following. For example possibly deterministic or stochastic disturbance processes are analysed by

$$\begin{bmatrix} Q_k & S_k \\ S_k^* & R_{v,k} \end{bmatrix} = \left\langle \begin{bmatrix} w_k \\ v_k \end{bmatrix}, \begin{bmatrix} w_l \\ v_l \end{bmatrix} \right\rangle \delta_{kl} \,. \tag{5.46}$$

If stochastic processes are analysed, expected values $\langle \times \rangle \to E\{\times\}$ can be used instead. Besides that, the central criterion of Kalman filtering, shown in equation (5.23), shall be further developed. Thus, consider a weighted estimation error

$$\tilde{s}_k = s_k - \hat{s}_k = L_k(x_k - \hat{x}_k) = L_k \tilde{x}_k \,, \tag{5.47}$$

which clearly is a generalization of the state estimation error in equation (5.22). Process $\tilde{s}$ depends on $\tilde{x}$ and thus on w and v according to equation (5.32).

In order to study the influence of disturbance uncertainties on estimation errors, a system is introduced here, which maps w and v to $\tilde{s}$. This operator is referred to as $\mathcal{T}_K$. To give an impression how this system may look like, the equations for Kalman filtering (5.32) and (5.47) are combined. The resulting system

$$\tilde{x}_{k+1} = A_{p,k}\tilde{x}_k + \begin{bmatrix} I & -K_{p,k} \end{bmatrix} \begin{bmatrix} w_k \\ v_k \end{bmatrix} \tag{5.48a}$$

$$\tilde{s}_k = L_k \tilde{x}_k \tag{5.48b}$$

is depicted in figure 5.7. This is a special case, based on a state space representation. Other model forms are possible.
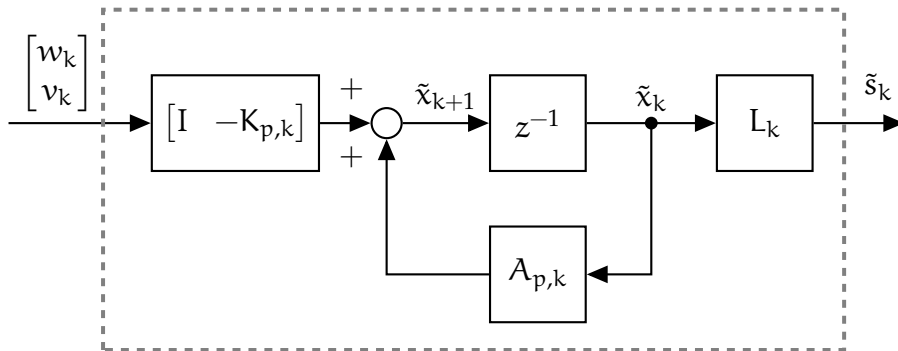
Figure 5.7: Exemplary State Space System for Operator $\mathcal{T}_K$

The operator of weighted estimation error is defined in finite horizon by

$$\mathcal{T}_K = \begin{bmatrix} T_{K,kl} \end{bmatrix}_{k,l=0}^N \quad \text{and} \quad \tilde{s}_k = \sum_{l=0}^N T_{K,kl} \begin{bmatrix} w_l \\ v_l \end{bmatrix} \,. \tag{5.49}$$

Estimation theory must apply a minimization comparable to the Kalman filtering case of equation (5.23). Therein, the 2-norm has been applied to the finite dimensional vector $\tilde{x}$. Thus, the length of $\tilde{x}$ has been minimized, which was depicted in figure 5.5. However, in the following operator $\mathcal{T}_K$ shall be minimized instead of the finite vector $\tilde{x}$, because $\mathcal{T}_K$ itself is independent of disturbance processes w and v. Because matrix T_K of equation (5.49) can be seen as an application of operator $\mathcal{T}_k$, which maps inputs w and v to $\tilde{s}$, it thus is reasonable to quantify it by mathematical norms.

IN $\mathcal{H}^2$ ESTIMATION all vectors are presumed as a set of the Hilbert space $\mathcal{H}$, which will be revisited in section 5.1.4. The minimization is applied here with the help of the $\mathcal{H}^2$ norm.[78] By presuming finite processes with $k, l < \infty$, this leads to a solution based on the Frobenius norm with

$$\min \, \|\mathcal{T}_K\|_{\mathcal{H}^2}^2 \quad \text{and} \quad \|\mathcal{T}_K\|_{\mathcal{H}^2}^2 = \sum_{k,l}^{N} \|T_{K,kl}\|_F^2 \, . \tag{5.50}$$

To illustrate the statements above, consider the following mean-free, uncorrelated, white noise processes:

$$\text{Example:} \quad \left\langle \begin{bmatrix} w_k \\ v_k \end{bmatrix}, \begin{bmatrix} w_l \\ v_l \end{bmatrix} \right\rangle = E \left\{ \begin{bmatrix} w_k \\ v_k \end{bmatrix} \begin{bmatrix} w_l^* & v_l^* \end{bmatrix} \right\} = \begin{bmatrix} I & 0 \\ 0 & I \end{bmatrix} \delta_{kl} \, . \tag{5.51}$$

Furthermore, time-invariant parameters, especially $L = I$, are presupposed. This leads to $\tilde{s} = \tilde{x}$. Now, by analysing the criterion of equation (5.50) the Kalman filtering criterion of equation (5.23) is reconstituted:

$$\text{Example:} \quad \min \|\mathcal{T}_K\|_{\mathcal{H}^2}^2 \, , \quad E\{\tilde{s}_k \tilde{s}_k^*\} = E\{\tilde{x}_k \tilde{x}_k^*\} = P_k \, . \tag{5.52}$$

The minimization of expected state estimation error energy emerges. If in addition w and v are Gaussian, a least-mean-squares estimator arises. This leads to a maximum-likelihood estimate of states x. In summary, Kalman filtering is a special case of $\mathcal{H}^2$ estimation.

Unfortunately, input Gramians (Q, R_v, S) must be known perfectly here. If presupposed disturbance parameters differ from real world processes, noise uncertainties are present.

UNCERTAINTIES IN $\mathcal{H}^2$ ESTIMATION have an important influence on estimation results. While Kalman filtering is the optimal solution for (least-squares) state estimation, if model $H(A, C)$ and second order noise parameters (Q, R_v, S) are known exactly, it is non-robust to noise uncertainties. Hence, if model or noise uncertainties occur, large estimation errors may emerge.[121] Here, an estimator capable to cope with uncertainties is called robust.[78]

An example is given by Simon:[121] The state estimation by Kalman and a robust $\mathcal{H}^\infty$ filter are compared according to uncertainties. In result, the Kalman filter performs

better than the robust estimator, if modelling and disturbance presumptions are exact. Nevertheless, the robust estimator outperforms the Kalman filter, when uncertainties are present.

Another example is described by Mangoubi:[128] Again the applicability of Kalman and robust filters are compared, but here according to the maximum singular value response. As expected, $\mathcal{H}^\infty$ estimators outperform Kalman filters in the presence of noise uncertainties.

$\mathcal{H}^\infty$ THEORY   allows the derivation of estimators, which are less susceptible to uncertainties, and are thus referred to as robust. The central approach for that is to develop estimators, which minimize (or bound) the weighted estimation error over all possible disturbances.[78] This is advantageously derived with the help of the infinity-norm, which is the origin of the name.[79] The infinity-norm

$$\|\mathcal{T}\|_{\mathcal{H}^\infty} = \|\mathcal{T}\|_{i2} = \sup_{x \neq 0} \frac{\|\mathcal{T}x\|_2}{\|x\|_2} \tag{5.53}$$

can be derived as the induced 2-norm.[128] Only if time-invariant parameters are used, this is correct in a mathematical sense. However, the induced 2-norm has been historically referred to as the infinity-norm in general,[78] which is used in this thesis too.

Nevertheless, the induced 2-norm takes the relation of Euclidean norms (for finite processes) from input x to output $\mathcal{T}x$ into account. Here, x is a square-summable sequence, thus $x \in l^2$. This approach is now used for the operator of weighted estimation error $\mathcal{T}_K$, which maps w and v to $\tilde{s}$:

$$\inf \|\mathcal{T}_K\|_{\mathcal{H}^\infty}^2 = \inf \sup_{w,v \neq 0} \frac{\|\tilde{s}\|_2^2}{\|w\|_2^2 + \|v\|_2^2} \ . \tag{5.54}$$

Finally, the infinity-norm in finite horizon is the maximum singular value of the finite block matrix $\mathcal{T}_{\text{finite}}$:[78]

$$\|\mathcal{T}_K\|_{\mathcal{H}^\infty} = \sigma_{\max}\left(\mathcal{T}_{K,\text{finite}}\right) \quad \text{of} \quad \begin{bmatrix} \tilde{s}_0 \\ \vdots \\ \tilde{s}_N \end{bmatrix} = \underbrace{\begin{bmatrix} T_{K,00} & \cdots & T_{K,0N} \\ \vdots & \ddots & \vdots \\ T_{K,N0} & \cdots & T_{K,NN} \end{bmatrix}}_{\mathcal{T}_{K,\text{finite}}} \begin{bmatrix} \begin{bmatrix} w_0 \\ v_0 \end{bmatrix} \\ \vdots \\ \begin{bmatrix} w_N \\ v_N \end{bmatrix} \end{bmatrix} . \tag{5.55}$$

Very interestingly, $\mathcal{H}^\infty$ estimators can be seen as a robust version of the Kalman filter. This argument is based on practical considerations for robust Kalman filter: Simon[121] describes a simple technique to improve the robustness of Kalman filters by increasing parameter Q_k, which then leads to a larger P_k in equation (5.33). If P_k rises, then the estimate is thought to be less trustworthy and thus a more conservative solution must be found.

THE GAME THEORY APPROACH, described by Banavar,[129] certainly is the most understandable explanation of $\mathcal{H}^\infty$ estimation. Consider the following cost function, which is a direct application of equation (5.54):

$$J_k = \min_{\hat{s}} \max_{w,v} \frac{\sum_{l=0}^{k} \|s_l - \hat{s}_l\|_2^2}{\sum_{l=0}^{k} \|w_l\|_2^2 + \sum_{l=0}^{k} \|v_l\|_2^2} \, . \tag{5.56}$$

Cost function J describes the energy gain from disturbances w and v (denominator) to weighted estimation errors $\tilde{s}$ (numerator). Now, an imaginary game is structured as follows: We, the estimator designer, begin the game and our goal is the minimization of J by a reasonable choice of $\hat{s}$ in the estimation error $\tilde{s} = s - \hat{s}$. After that nature, the second player, maximizes the cost function J through its choice of noise processes w and v. The initial state has been omitted here for clarity. This problem is also known as the minimax problem.

The described game is fundamentally different to Kalman filtering, as it presumes nature to actively degrade the estimation result.[121] Because in $\mathcal{H}^\infty$ estimation no assumptions about the disturbances are made, the resulting estimators may be over-conservative.[78]

A SUBOPTIMAL SOLUTION is necessary in $\mathcal{H}^\infty$ estimation, because the criterion in equation (5.54) is unsolvable for most theoretical cases.[78,121] Thus, a suboptimal solution is found instead by introducing an upper bound γ:

$$\|\mathcal{T}_K\|_{\mathcal{H}^\infty}^2 = \sup_{w,v\neq 0} \frac{\|\tilde{s}\|_2^2}{\|w\|_2^2 + \|v\|_2^2} \qquad < \gamma^2 \, . \tag{5.57}$$

Rather than determining an infimum (minimum), an optimal value γ_{opt} is searched. At this point, additional differences between Kalman filtering and $\mathcal{H}^\infty$ estimation are apparent: While Kalman filtering focuses on the minimization of expected estimation error energy of $\tilde{x}$, $\mathcal{H}^\infty$ theory allows to bound the weighted estimation error energy by $\mathcal{T}_K$.[128] Because of that, the weighting matrix L and the upper bound γ are additionally needed in $\mathcal{H}^\infty$ estimation in comparison to Kalman filtering.

By applying both parameters L and γ, the state estimation error covariance matrix P is artificially increased.[121] Thus, one trusts the given information $\mathcal{I} = P^{-1}$ less than before. A direct application of this approach will be given in section 5.1.6, especially equation (5.107).

THE CHOICE OF WEIGHTING MATRIX is, besides the upper bound γ, an additional design parameter for the $\mathcal{H}^\infty$ estimator design. Central advantage of using L is the ability to put emphasis on selected states.[128]

Although a weighting matrix L may be used in Kalman filtering to determine a desired signal $\hat{s}$ in equation (5.38), it has no influence on Riccati recursion (5.33), and thus on state estimation. Hence, the Kalman filter always leads to an optimal linear least

squares solution, not depending on the choice of L.[128] In opposite to that, parameter L must be defined in $\mathcal{H}^\infty$ theory and it actually does alter the estimation result. While Hassibi et al. excessively discuss $\mathcal{H}^\infty$ estimator applications and the following choices for L,[78] the case of L = C, which is referred to as filtering signals in additive noise, will be described in section 5.3.

Besides the game theory approach of Banavar,[129] further $\mathcal{H}^\infty$ theories can be applied, for example Lagrange multiplier,[121,128] J-spectral factorization[130] and so on. Here, methods of research areas like interpolation theory, operator theory, game theory, circuit theory and system theory may be applied.[78] Besides these different approaches, a rather direct theory based on generalized Kalman filters in so-called Krein spaces is shown in the following, because it directly builds upon the commonly known Kalman filtering approach.

5.1.4 TIME-VARIANT KREIN SPACE KALMAN FILTER

The core concept of Krein space based $\mathcal{H}^\infty$ theory is the generalization of the Kalman filter for an application in indefinite metric spaces. The basic approach for that is (i) to rewrite the central $\mathcal{H}^\infty$ criterion (5.57) as an indefinite-quadratic form, (ii) solve it with the help of a stationary point and (iii) numerically solve it with an innovation approach of a so-called Krein space Kalman filter, which requires the projection of a vector in Krein space.[78] The very basics of the scalar quadratic form has been explained in section 5.1.1.

AN INDEFINITE-QUADRATIC FORM   emerges, as the central criterion of $\mathcal{H}^\infty$ estimation, the bounding of maximum energy gain of equation (5.57), is reordered. For that, consider unknown discrete-time processes $[w_l, v_l]_{l=0}^k$:

$$\sup_{w,v} \frac{\sum\limits_{l=0}^{k} \tilde{s}_{l|l}^* \tilde{s}_{l|l}}{x_0^* \Pi_0^{-1} x_0 + \sum\limits_{l=0}^{k} w_l^* Q_l^{-1} w_l + \sum\limits_{l=0}^{k} v_l^* v_l} < \gamma^2 . \tag{5.58}$$

Therein, the initial state x_0 has been taken into account with the help of the Gramian matrix $\Pi_0 = \langle x_0, x_0 \rangle$. As mentioned above, this problem shall be rearranged in an indefinite-quadratic form. Thus, the weighted estimation error for filtered estimates $\tilde{s}_{k|k} = L_k x_k - \check{s}_{k|k}$ and the measurement noise $v_k = y_k - C_k x_k$ are introduced to the above equation:

$$\sup_{w,v} \frac{\sum\limits_{l=0}^{k} (\check{s}_{l|l} - L_l x_l)^* (\check{s}_{l|l} - L_l x_l)}{x_0^* \Pi_0^{-1} x_0 + \sum\limits_{l=0}^{k} w_l^* Q_l^{-1} w_l + \sum\limits_{l=0}^{k} (y_l - C_l x_l)^* (y_l - C_l x_l)} < \gamma^2 . \tag{5.59}$$

Here, the filtered estimate š of the desired signal s has been used.[78] This process is introduced for theoretical purposes only, and should not be confused with the actual output of estimator, denoted by $\hat{s}$.

To determine an optimal estimator, the criterion in equation (5.59) is reordered according to usual quadratic forms:

$$J_k\left(x_0, [w_l, y_l]_{l=0}^k\right) = x_0^* \Pi_0^{-1} x_0 + \sum_{l=0}^k \left(w_l^* Q_l^{-1} w_l + v_l^* v_l\right) - \gamma^{-2} \sum_{l=0}^k \tilde{s}_{l|l}^* \tilde{s}_{l|l} \quad > 0 \quad (5.60a)$$

$$= x_0^* \Pi_0^{-1} x_0 + \sum_{l=0}^k \begin{bmatrix} w_l \\ \bar{v}_l \end{bmatrix}^* \bar{M}_l^{-1} \begin{bmatrix} w_l \\ \bar{v}_l \end{bmatrix} \quad > 0 \,. \, (5.60b)$$

An indefinite-quadratic form emerges. Its central Gramian matrix $\bar{M}$ is indefinite, because of the introduced extended disturbance process

$$\bar{v}_k = \begin{bmatrix} v_k \\ \tilde{s}_{k|k} \end{bmatrix} = \begin{bmatrix} y_k \\ \check{s}_{k|k} \end{bmatrix} - \begin{bmatrix} C_k \\ L_k \end{bmatrix} x_k \quad \text{with} \quad \hat{R}_{v,k} = \langle \bar{v}_k, \bar{v}_l \rangle_{\mathcal{K}} = \begin{bmatrix} I & 0 \\ 0 & -\gamma^2 I \end{bmatrix} \delta_{kl} \,. \quad (5.61)$$

Note the difference between v and its extended form $\bar{v}$. It is important, because the lower block of $\bar{v}$ is an auxiliary process, which takes bound γ into account. Input Gramian matrix $\bar{M}$ of equation (5.60) follows:

$$\left\langle \begin{bmatrix} w_k \\ \bar{v}_k \end{bmatrix}, \begin{bmatrix} w_l \\ \bar{v}_l \end{bmatrix} \right\rangle_{\mathcal{K}} = \begin{bmatrix} Q_k & 0 \\ 0 & \begin{bmatrix} I & 0 \\ 0 & -\gamma^2 I \end{bmatrix} \end{bmatrix} \delta_{kl} = \begin{bmatrix} Q_k & \hat{S}_k \\ \hat{S}_k^* & \hat{R}_{v,k} \end{bmatrix} \delta_{kl} = \bar{M}_k \delta_{kl} \,. \quad (5.62)$$

Here, an important problem emerges: A negative Gramian matrix indicates negative power. In Hilbert space $\mathcal{H}$ the inner product is defined. Considering $x, y \in \mathcal{H}$, the inner product is defined

  (i) for swapped vectors by the conjugate transpose $\langle x, y \rangle = \langle y, x \rangle^*$,

 (ii) by a linear product with $a, b \in \mathbb{C}$ as $\langle ax_1 + bx_2, y \rangle = a \langle x_1, y \rangle + b \langle x_2, y \rangle$ and

(iii) as positive definite for scalar-products of itself $\langle x, x \rangle \geqslant 0$.

Thus, $\bar{v}$ is undefinable in a Hilbert space $\mathcal{H}$. Therefore, the more general Krein space $\mathcal{K}$ must be used instead, because it allows indefinite Gramian matrices $\langle x, x \rangle_{\mathcal{K}}$. This leads to the introduction of an important state space system:

A KREIN SPACE STATE SPACE SYSTEM   arises as the concept of quadratic forms is used to derive $\mathcal{H}^\infty$ estimators. It follows equation (5.61), and is a key element to find the stationary point, which itself leads the way to suboptimal $\mathcal{H}^\infty$ estimators:

$$x_{k+1} = A_k x_k + w_k \quad (5.63a)$$

$$\begin{bmatrix} y_k \\ \check{s}_{k|k} \end{bmatrix} = \begin{bmatrix} C_k \\ L_k \end{bmatrix} x_k + \bar{v}_k \,. \quad (5.63b)$$
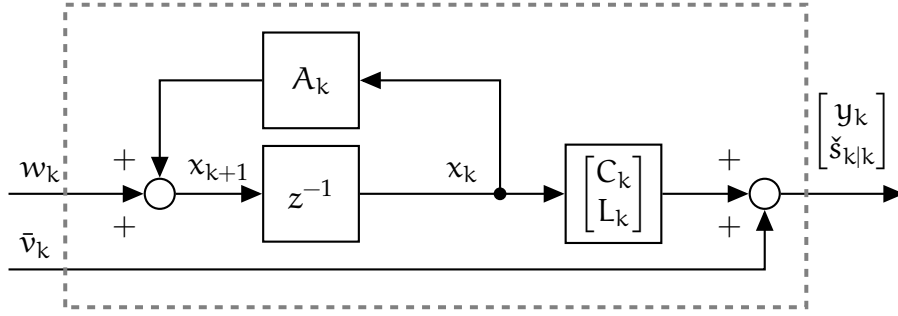
Figure 5.8: Krein Space State Space System

The Krein space state space system in equation (5.63) and figure 5.8 is quite similar to the standard system in equation (5.19). The straightforward idea is to use widespread Kalman filtering approaches on the basis of the Krein space state space system. But for that one must find a minimum of the indefinite-quadratic form in equation (5.60), which is determined in Krein space with the help of a stationary point.

THE STATIONARY POINT allows to minimize cost function J_k in equation (5.60). The stationary point is known for the deterministic case for a general variable z:[78]

$$\min J(z_0, y) = y^* R_y^{-1} y \quad \text{with} \quad z_0 = R_{sy} R_y^{-1} y, \quad R_z - R_{zy} R_y^{-1} R_{yz} > 0 . \tag{5.64}$$

This result follows the scalar quadratic form in equation (5.17), which is based on a positive definite joint Gramian matrix of z and y. While that demands the Hilbert space, equation (5.60) requires the Krein space. For that, the solution is partially equivalent: The stationary point follows with

$$\hat{z} = R_{zy} R_y^{-1} y \quad \text{with} \quad \langle \tilde{z}, \tilde{z} \rangle = R_z - R_{zy} R_y^{-1} R_{yz}, \quad \tilde{z} = z - \hat{z} , \tag{5.65}$$

but different existence conditions arise: Essentially, the inertia $\mathcal{I}$ (number of negative and positive eigenvalues) must be preserved after minimization:

$$\text{Existence Condition:} \quad \mathcal{I}(R_y) = \mathcal{I}(R_z - R_{zy} R_y^{-1} R_{yz}) . \tag{5.66}$$

Again, the problem can be seen as a projection result of z_k onto $\mathcal{Y}_k = \text{span}\left([y_l]_{l=0}^k\right)$ with $\hat{z}_k \in \mathcal{Y}_k$. However, as estimators usually work recursively, the fundamental estimation approach by using innovations in equation (5.25) is reconsidered:

$$\hat{z}_k = \sum_{l=0}^k \langle z, e_l \rangle \langle e_l, e_l \rangle^{-1} e_l \quad \text{and} \quad \min J_k(\hat{z}_k, y) = \sum_{l=0}^k e_l^* R_{e,l}^{-1} e_l . \tag{5.67}$$

Here, a minimum has been found for the general variable z by using the innovations approach of equation (5.67). To apply that approach to equation (5.60),

$$z \longrightarrow \begin{bmatrix} y_k \\ \check{s}_{k|k} \end{bmatrix} \quad \text{and} \quad \hat{e}_k = \begin{bmatrix} y_k \\ \check{s}_{k|k} \end{bmatrix} - \begin{bmatrix} \hat{y}_k \\ \hat{s}_{k|k} \end{bmatrix}, \quad \hat{R}_{e,k} = \langle \hat{e}_k, \hat{e}_k \rangle \tag{5.68}$$

are used. This leads to the stationary point, the minimum of J_k, in the context of recursive estimation:

$$\min J_k = \sum_{l=0}^{k} \hat{e}_l^* \hat{R}_{e,l}^{-1} \hat{e}_l \quad > 0 . \tag{5.69}$$

A minimum of the indefinite-quadratic form is found, which leads to the determination of estimation error $\hat{e}_k$. Here, the Krein space projection result $\hat{s}$ (the actual output of the estimator) emerges, which is depicted in figure 5.9.
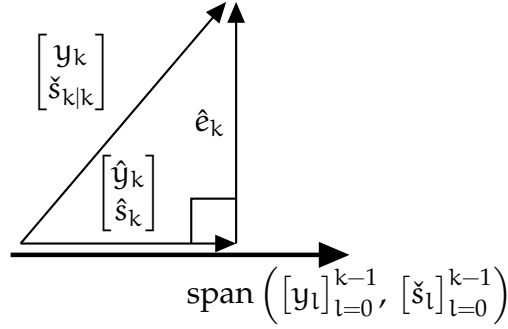
Figure 5.9: Projections in Krein Space

Very importantly, the existence condition of equation (5.66) may be rewritten here as[78]

$$\text{Existence Condition:} \quad \mathfrak{I}\left(\langle \bar{v}_k, \bar{v}_k \rangle \right) = \mathfrak{I}\left(\langle \hat{e}_k, \hat{e}_k \rangle \right) . \tag{5.70}$$

More details on that will be discussed later in equation (5.86).

THE KREIN SPACE KALMAN FILTER   is a natural consequence of the statements above, and is very similar to the standard Kalman filter, but with an extended innovation process

$$\hat{e}_k = \begin{bmatrix} e_{y,k} \\ e_{s,k} \end{bmatrix} = \begin{bmatrix} y_k \\ \check{s}_{k|k} \end{bmatrix} - \begin{bmatrix} \hat{y}_k \\ \hat{s}_k \end{bmatrix} = \begin{bmatrix} y_k \\ \check{s}_{k|k} \end{bmatrix} - \begin{bmatrix} C_k \\ L_k \end{bmatrix} \hat{x}_k . \tag{5.71}$$

Hence, consider the state estimation of equation (5.31)

$$\hat{x}_{k+1} = A_k \hat{x}_k + \hat{K}_{p,k} \hat{e}_k = A_{p,k} \hat{x}_k + \hat{K}_{p,k} y_k \quad \text{with} \quad A_{p,k} = A_k - \hat{K}_{p,k} \hat{C}_k \tag{5.72}$$

and estimation parameters $\hat{K}_p \in \mathbb{C}^{n \times (p+m)}$ and $\hat{R}_e \in \mathbb{R}^{(p+m) \times (p+m)}$. These parameters are analogue to the standard Kalman filtering solution of equation (5.30), but with extended matrices:

$$\hat{K}_{p,k} = \left(A_k P \hat{C}_k^* + \hat{S}_k \right) \hat{R}_{e,k}^{-1}, \qquad \hat{R}_{e,k} = \langle \hat{e}_k, \hat{e}_k \rangle = \hat{C}_k P_k \hat{C}_k^* + \hat{R}_{v,k} \tag{5.73}$$

$$\hat{C}_k = \begin{bmatrix} C_k \\ L_k \end{bmatrix}, \qquad \hat{R}_{v,k} = \begin{bmatrix} I & 0 \\ 0 & -\gamma^2 I \end{bmatrix}, \qquad \hat{S}_k = 0 . \tag{5.74}$$

Even the Riccati recursion (5.33) of Kalman filtering is carried on with extended matrices with

$$P_{k+1} = A_k P_k A_k^* - \hat{K}_{p,k} \hat{R}_{e,k} \hat{K}_{p,k}^* + Q_k \; . \tag{5.75}$$

Finally, an innovation form of the Krein space Kalman filter arises, which is analogue to the innovation model of equation (5.37). An estimation application of the standard and the Krein space Kalman filter is shown in both figures 5.6 and 5.10:

$$\hat{x}_{k+1} = A_k \hat{x}_k + \hat{K}_{p,k} \hat{e}_k \tag{5.76a}$$

$$\begin{bmatrix} y_k \\ \check{s}_{k|k} \end{bmatrix} = \begin{bmatrix} C_k \\ L_k \end{bmatrix} \hat{x}_k + \hat{e}_k \; . \tag{5.76b}$$
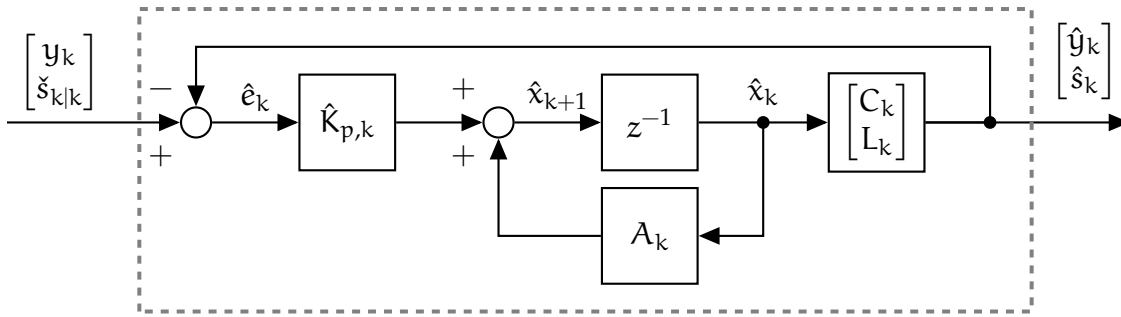
Figure 5.10: An Application of the Krein Space Kalman Filter

Both estimators of equations (5.37) and (5.76) are very similar and allow the estimation of $(\hat{x}, \hat{y}, \hat{s})$. Nevertheless, two major differences occur:

   (i) the Riccati recursion for P is different and

   (ii) the Krein space Kalman filter considers the additional input $\check{s}$.

Process $\check{s}$ is unmeasurable, thus a solution for numerical-practical estimation must be found. Therefore, the idea is to make the correlated innovation processes e_y and e_s of equation (5.71) with $\langle e_{y,k}, e_{s,k} \rangle \neq 0$ independent and then to reasonably define a presumption on the remaining estimation error.

THE LDU-FACTORIZATION   is advantageous to make e_y and e_s of equation (5.71) independent. Thus, the Gramian of $\hat{e}$ according to equation (5.73) is factorized by

$$\hat{R}_{e,k} = \begin{bmatrix} C_k \\ L_k \end{bmatrix} P \begin{bmatrix} C_k \\ L_k \end{bmatrix}^* + \begin{bmatrix} I & 0 \\ 0 & -\gamma^2 I \end{bmatrix} = \begin{bmatrix} C_k P_k C_k^* + I & C_k P_k L_k^* \\ L_k P_k C_k^* & L_k P_k L_k^* - \gamma^2 I \end{bmatrix} \tag{5.77a}$$

$$= \bar{L}_k D_k \bar{U}_k, \qquad \bar{L}_k = \bar{U}_k^* = \begin{bmatrix} I & 0 \\ L_k P_k C_k^* \hat{R}_{ey,k}^{-1} & I \end{bmatrix} \; . \tag{5.77b}$$

The indefinite structure is preserved by D:

$$D_k = \langle \tilde{e}_k, \tilde{e}_k \rangle_{\mathcal{K}} = \begin{bmatrix} R_{ey,k} & 0 \\ 0 & R_{es,k} \end{bmatrix} = \begin{bmatrix} I + C_k P_k C_k^* & 0 \\ 0 & \gamma^2 I - L_k \left(P_k^{-1} + C_k^* C_k \right)^{-1} L_k^* \end{bmatrix}.$$

(5.78)

Now, process $\tilde{e}_k \in \mathcal{K}$ is defined. This altered estimation error process

$$\tilde{e}_k = \bar{L}_k^{-1} \hat{e}_k = \begin{bmatrix} I & 0 \\ -L_k P_k C_k^* \hat{R}_{ey,k}^{-1} & I \end{bmatrix} \begin{bmatrix} e_{y,k} \\ e_{s,k} \end{bmatrix} = \begin{bmatrix} e_{y,k} \\ \tilde{e}_{s,k} \end{bmatrix}$$

(5.79)

has the important property $\langle e_{y,k}, \tilde{e}_{s,k} \rangle = 0$ following

$$\tilde{e}_{s,k} = -L_k P_k C_k^* R_{ey,k}^{-1} e_{y,k} + (\check{s}_{k|k} - \hat{s}_k)$$

(5.80a)

$$= \check{s}_{k|k} - (L_k P_k C_k^* R_{ey,k}^{-1} e_{y,k} + \hat{s}_k) = \check{s}_{k|k} - \hat{s}_{k|k},$$

(5.80b)

which is profoundly different from the original Gramian matrix $\langle e_{y,k}, e_{s,k} \rangle \neq 0$. The altered estimation error $\tilde{e}_s$ is a projection result, which is shown in figure 5.11.
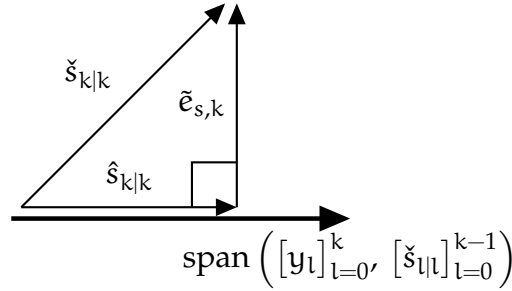
Figure 5.11: Projections in Krein Space: Altered Estimation Error

This allows an advantageous state estimate

$$\hat{x}_{k+1} = A_k \hat{x}_k + \hat{K}_{p,k} \bar{L}_k \check{e}_k = A_k \hat{x}_k + \begin{bmatrix} K_{py,k} & K_{ps,k} \end{bmatrix} \begin{bmatrix} e_{y,k} \\ \tilde{e}_{s,k} \end{bmatrix}$$

(5.81)

by determining the gain matrix subelements

$$\begin{bmatrix} K_{py,k} & K_{ps,k} \end{bmatrix} = \hat{K}_{p,k} \bar{L}_k = AP \begin{bmatrix} C_k^* & L_k^* \end{bmatrix} \begin{bmatrix} I & -R_{ey,k}^{-*} C_k P_k L_k^* \\ 0 & I \end{bmatrix} \begin{bmatrix} R_{ey,k}^{-1} & 0 \\ 0 & R_{es,k}^{-1} \end{bmatrix}$$

(5.82)

with

$$K_{py,k} = A_k P_k C_k^* R_{ey,k}^{-1} \quad \text{and} \quad K_{ps,k} = A_k P_k \left(L_k^* - C_k^* R_{ey,k}^{-*} C_k P_k L_k^* \right) R_{es,k}^{-1}.$$

(5.83)

More importantly, the inertia of Gramian matrix D, and thus (R_{ey}, R_{es}), define whether a Krein space Kalman filter may exist or not: D and $\hat{R}_v$ have the same inertia, if they have the same number of positive and negative eigenvalues.

EXISTENCE CONDITIONS must be recursively checked for every k, which follows equation (5.70). Essentially, the existence test evaluates, whether the indefinite structure of $\hat{R}_v$ in $\hat{R}_e$ still persists after numerical computations. Thus, the altered estimation error is introduced to the indefinite-quadratic form by

$$\min J_k\left(x_0, [w_l, y_l]_{l=0}^k\right) = \sum_{l=0}^k \hat{e}_l^* \bar{U}_l^{-1} D_l^{-1} \bar{L}_l^{-1} \hat{e}_l = \sum_{l=0}^k \tilde{e}_l^* \begin{bmatrix} R_{ey,l}^{-1} & 0 \\ 0 & R_{es,l}^{-1} \end{bmatrix} \tilde{e}_l \quad > 0 . \quad (5.84)$$

This operation is based on the inverse

$$\hat{R}_{e,k}^{-1} = \bar{U}_k^{-1} D_k^{-1} \bar{L}_k^{-1} \quad \text{with} \quad \bar{L}_k^{-1} = \bar{U}_k^{-*} = \begin{bmatrix} I & 0 \\ -L_k P_k C_k^* \hat{R}_{ey,k}^{-1} & I \end{bmatrix} . \quad (5.85)$$

The indefinite structure can be checked in $D_k = \langle \tilde{e}_k, \tilde{e}_k \rangle$ for every k following equation (5.84): Both matrices R_{ey} and R_{es} must be positive and negative definite, respectively:

$$\text{Existence Condition:} \quad R_{ey,k} \overset{!}{>} 0 \quad \text{and} \quad R_{es,k} \overset{!}{<} 0 . \quad (5.86)$$

This test is equivalent to

$$\text{Existence Condition:} \quad P_k^{-1} + C_k^* C_k - \gamma^{-2} L_k^* L_k \overset{!}{>} 0 , \quad (5.87)$$

which is observable by rewriting Riccati recursion (5.75):[131]

$$P_{k+1} = A_k \left(\underbrace{P_k^{-1} + C_k^* C_k - \gamma^{-2} L_k^* L_k}_{\text{Condition: } >0} \right)^{-1} A_k^* + Q_k . \quad (5.88)$$

The existence tests are advantageous, because they can directly be applied in square-root form.

5.1.5 A Special Case of A Posteriori $\mathcal{H}^\infty$ Estimators

Process $\check{s}_{k|k}$ must still be known to compute an a posteriori estimate

$$\hat{s}_{k|k} = \check{s}_{k|k} - \tilde{e}_{s,k} = \hat{s}_k + L_k P_k C_k^* R_{ey,k}^{-1} e_{y,k} \, . \tag{5.89}$$

Here, a closed solution for every possible a posteriori estimate $\check{s}_{k|k}$ is elaborate and difficult for numerical-practical applications.[78] Rather it is reasonable here to give an applicable solution based on a plausible choice on $\check{s}_{k|k}$, which is shown in the following:

In view of equation (5.69), the important idea is to guarantee that

$$\hat{e}_k^* \hat{R}_{e,k}^{-1} \hat{e}_k > 0 \quad \text{because} \quad \min J_k = \hat{e}_k^* \hat{R}_{e,k}^{-1} \hat{e}_k + \sum_{l=0}^{k-1} \hat{e}_l^* \hat{R}_{e,l}^{-1} \hat{e}_l \quad > 0 \, . \tag{5.90}$$

By applying the LDU factorization of equation (5.84), this can be rewritten to

$$\hat{e}_k^* \hat{R}_{e,k}^{-1} \hat{e}_k = \begin{bmatrix} e_{y,k}^* & \tilde{e}_{s,k}^* \end{bmatrix} \begin{bmatrix} R_{ey,k}^{-1} & 0 \\ 0 & R_{es,k}^{-1} \end{bmatrix} \begin{bmatrix} e_{y,k} \\ \tilde{e}_{s,k} \end{bmatrix} \stackrel{!}{>} 0 \quad \text{with} \quad R_{ey,k} > 0, \quad R_{es,k} < 0 \, . \tag{5.91}$$

Based on that, it is straightforward to define $\tilde{e}_{s,k} \rightarrow 0$ (or equivalently $\check{s}_{k|k} = \hat{s}_{k|k}$), which guarantees criterion (5.69).[131] Nevertheless, the existence criteria (5.86) must still be checked.

Now, by applying this presumption to the state estimation equation (5.81) with extended matrices

$$\hat{x}_{k+1} = A_k \hat{x}_k + \begin{bmatrix} K_{py,k} & K_{ps,k} \end{bmatrix} \begin{bmatrix} e_{y,k} \\ 0 \end{bmatrix} = A_k \hat{x}_k + K_{py,k} e_{y,k} \, , \tag{5.92}$$

the predicted form of the a posteriori $\mathcal{H}^\infty$ estimator follows:

$$\hat{x}_{k+1} = A_k \hat{x}_k + K_{py,k} e_{y,k} \tag{5.93a}$$
$$\hat{s}_{k|k} = L_k \hat{x}_k + L_k P_k C_k^* R_{ey,k}^{-1} e_{y,k} \, . \tag{5.93b}$$

Based on that, the extended matrices $(\hat{K}_p, \hat{R}_e)$ are reduced in size to

$$\hat{K}_p \rightarrow K_{py,k} = A_k P_k C_k^* R_{ey,k}^{-1} \quad \text{and} \quad \hat{R}_e \rightarrow R_{ey,k} = \langle e_{y,k}, e_{y,k} \rangle = I + C_k P_k C_k^* \, . \tag{5.94}$$

The predicted form above can be rearranged on the basis of filtered state estimates $\hat{s}_{k|k} = L_k \hat{x}_{k|k}$. By applying the filtered state estimate

$$\hat{x}_{k|k} = \hat{x}_k + P_k C_k R_{ey,k}^{-1} e_{y,k} \quad \text{with} \quad e_{y,k} = y_k - C_k A_k \hat{x}_{k|k} \, , \tag{5.95}$$

the filtered form of the a posteriori $\mathcal{H}^\infty$ estimator may be given by[80]

$$\hat{x}_{k+1|k+1} = A_k\hat{x}_{k|k} + P_kC_k^*R_{ey,k}^{-1}e_{y,k} \tag{5.96a}$$

$$\hat{s}_{k|k} = L_k\hat{x}_{k|k} . \tag{5.96b}$$

Nevertheless, the result $\hat{s}_{k|k}$ is identical for both, the a posteriori $\mathcal{H}^\infty$ estimator in predicted and filtered form. Furthermore, equation (5.92) can be rearranged to

$$\hat{x}_{k+1} = \left(A_k - K_{py,k}C_k\right)\hat{x}_k + K_{py,k}y_k = A_{p,k}\hat{x}_k + K_{py,k}y_k \tag{5.97a}$$

$$e_{y,k} = -C_k\hat{x}_k + y_k . \tag{5.97b}$$

Finally, the a posteriori $\mathcal{H}^\infty$ estimator $\mathcal{K}$, which maps y to $\hat{s}$, emerges by reordering

$$\hat{x}_{k+1} = \left(A_k - K_{py,k}C_k\right)\hat{x}_k + K_{py,k}y_k \tag{5.98a}$$

$$\hat{s}_{k|k} = L_k\left(I - P_kC_k^*R_{ey,k}^{-1}C_k\right)\hat{x}_k + L_kP_kC_k^*R_{ey,k}^{-1}y_k . \tag{5.98b}$$

Both, the estimation of $(\hat{s}, \hat{y})$ by the Kalman filter and the a posteriori $\mathcal{H}^\infty$ estimator is nearly identical and are depicted in the figures 5.6 and 5.12.
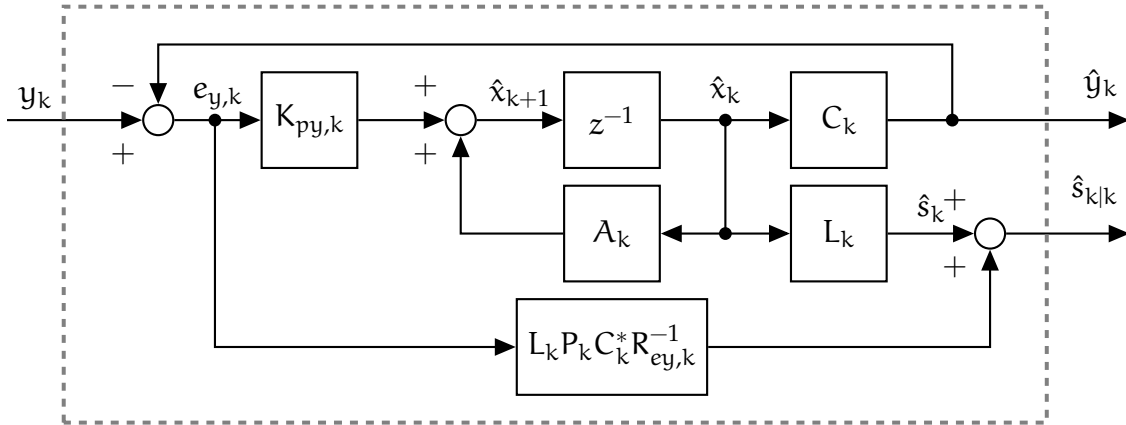
Figure 5.12: A Special Case of the A Posteriori $\mathcal{H}^\infty$ Estimator

The estimation parameters (K_y, R_e) and (K_{py}, R_{ey}) are similar, but have been derived on the basis of different Riccati recursions (5.33) and (5.75). Both recursions are connected, as is discussed below.

THE SPECIAL CASE OF KALMAN FILTERING can be derived from the given a posteriori $\mathcal{H}^\infty$ estimator. Here, it is interesting to see the connection between Kalman filtering and its generalization. As has been described in section 5.1.3, key element of $\mathcal{H}^\infty$ theory is the upper bound γ. By defining $\gamma \to \infty$, a Kalman filter can be deduced as a special case of $\mathcal{H}^\infty$ estimation.[78] To see that, parameter $R_{se,k}$ of equation (5.86) is analysed as

$$\gamma \to \infty : \qquad R_{se,k}^{-1} = \left(\gamma^2I - L_k\left(P_k^{-1} + C_k^*C_k\right)^{-1}L_k^*\right)^{-1} \longrightarrow 0 . \tag{5.99}$$

Thus, the second estimation error process $\tilde{e}_s$, which demands the Krein space, is irrelevant for $\gamma \to \infty$ in the quadratic form of equation (5.84). This simplifies parameter $\hat{R}_e$ of equation (5.77)

$$\hat{R}_{e,k}^{-1} = \bar{U}_k^{-1} D_k^{-1} \bar{L}_k^{-1} = \begin{bmatrix} I & \times \\ 0 & \times \end{bmatrix} \begin{bmatrix} R_{ey,k}^{-1} & 0 \\ 0 & 0 \end{bmatrix} \begin{bmatrix} I & 0 \\ \times & \times \end{bmatrix} = \begin{bmatrix} R_{ey,k}^{-1} & 0 \\ 0 & 0 \end{bmatrix} \tag{5.100}$$

and leads to $K_{ps,k} = 0$ for all k as can be seen by equation (5.73) with

$$\hat{K}_{p,k} = \begin{bmatrix} K_{py,k} & K_{ps,k} \end{bmatrix} = A_k P_k \begin{bmatrix} C_k^* & L_k^* \end{bmatrix} \begin{bmatrix} R_{ey,k}^{-1} & 0 \\ 0 & 0 \end{bmatrix} = \begin{bmatrix} A_k P_k C_k^* R_{ey,k}^{-1} & 0 \end{bmatrix} . \tag{5.101}$$

By applying that, Riccati recursions (5.33) and (5.75) are identical for $R_{v,k} = I$ and $S_k = 0$. Hence, the $\mathcal{H}^\infty$ norm of a Kalman filter surely is quite large, which indicates low robustness.[78] This brings us to the starting point, in which robustness of Kalman filtering and its approach have been debated in section 5.1.3.

5.1.6 A Brief Summary of A Priori $\mathcal{H}^\infty$ Estimation

In this dissertation a posteriori $\mathcal{H}^\infty$ estimators are primarily used. However, a priori $\mathcal{H}^\infty$ estimators can be derived too and allow a very illustrative demonstration of robustness implementation. Hence, a brief overview of a priori $\mathcal{H}^\infty$ estimation is subsequently given.

When altering the central filtering criterion of equation (5.58), the idea is to change the amount of known data, which leads to smoothing or prediction approaches. A priori estimates essentially are one-step predictions, thus the criterion is altered appropriately:

$$\sup_{w,v} \frac{\sum_{l=0}^{k} (\check{s}_l - L_l x_l)^* (\check{l}_k - L_l x_l)}{x_0^* \Pi_0^{-1} x_0 + \sum_{l=0}^{k-1} w_l^* w_l + \sum_{l=0}^{k-1} (y_l - C_l x_l)^* (y_l - C_l x_l)} < \gamma^2 . \tag{5.102}$$

Here, $\check{s}_k$ is an a priori estimate of s and the estimation error $\tilde{s}_k = L_k x_k - \check{s}_k$ has been used. It is important to note the different amount of data by $[\check{s}_l]_{l=0}^{k}$ and $[y_l, w_l]_{l=0}^{k-1}$. In the following, the cost function is rearranged analogously to the a posteriori theory by

$$J_k \left(x_0, [w_l, y_l]_{l=0}^{k-1} \right) = x_0^* \Pi_0^{-1} x_0 + \sum_{l=0}^{k-1} \begin{bmatrix} w_l \\ v_l \end{bmatrix}^* \bar{M}_l^{-1} \begin{bmatrix} w_l \\ v_l \end{bmatrix} - \gamma^{-2} \tilde{s}_k^* \tilde{s}_k \quad > 0 . \tag{5.103}$$

The derivation of the a priori $\mathcal{H}^\infty$ estimator is quite similar to the a posteriori case. Thus, a Krein space Kalman filter based on an innovation approach with

$$\bar{e}_k = \begin{bmatrix} e_{y,k} \\ \bar{e}_{s,k} \end{bmatrix} = \begin{bmatrix} y_k \\ \check{s}_k \end{bmatrix} - \begin{bmatrix} \hat{y}_k \\ \hat{s}_k \end{bmatrix} = \begin{bmatrix} y_k \\ \check{s}_k \end{bmatrix} - \begin{bmatrix} C_k \\ L_k \end{bmatrix} \hat{x}_k \tag{5.104}$$

is applied to the above indefinite-quadratic form J. Both, the innovation process and the stationary point, are comparable to the a posteriori case. Nevertheless, the minimum

$$\min J_k \left(x_0, \left[w_l, y_l \right]_{l=0}^{k-1} \right) = \sum_{l=0}^{k-1} \bar{e}_k^* R_{e,l}^{-1} \bar{e}_k + \bar{e}_{s,k}^* \left(-\gamma^2 I + L_k P_k L_k^* \right)^{-1} \bar{e}_{s,k} \quad > 0 \quad (5.105)$$

is more elaborate in contrast to the a posteriori solution in equation (5.69). Again, several conditions arise, which determine whether an estimator may exist or not.

EXISTENCE CONDITIONS must be recursively checked for all k, which is comparable to the a posteriori conditions of equation (5.86). Following the central cost function J of equation (5.105) the inertia of

$$-\gamma^2 I + L_k P_k L_k^* \overset{!}{<} 0 \quad \text{and} \quad I + C_k \tilde{P}_k C_k^* \overset{!}{>} 0 \tag{5.106}$$

must be maintained.[78] Thus, the number of positive and negative eigenvalues of $\hat{R}_e$ and $\hat{R}_v$ are the same. Fortunately, the given two existence conditions can be simplified to one condition

$$\tilde{P}_k = P_k \left(I - \gamma^{-2} L_k^* L_k P_k \right)^{-1} = \left(P_k^{-1} - \gamma^{-2} L_k^* L_k \right)^{-1} \overset{!}{>} 0 \,. \tag{5.107}$$

Basically, parameter P is artificially increased to get $\tilde{P}$, which leads to a more conservative estimation result. This makes the estimator robust because it presumes that at time instant k we have less information available than P_k^{-1}.[128] This recaptures the core of $\mathcal{H}^\infty$ theory.

A direct comparison of the a posteriori and the a priori condition of equations (5.87) and (5.107) reveals an important insight: The existence condition of the a priori estimator is more elaborate than the a posteriori one. Hence, the secondly named approach allows lower bounds γ, which indicate a higher robustness to noise uncertainties. Because of that, a posteriori $\mathcal{H}^\infty$ estimators are primarily used in this thesis.

A PRIORI $\mathcal{H}^\infty$ ESTIMATORS may be determined with the help of Riccati recursion (5.75) of the a posteriori case in connection with $\tilde{P}$ of equation (5.107). Alternatively, Riccati recursion

$$P_{k+1} = A_k \tilde{P}_k A_k^* - A_k \tilde{P}_k C_k^* (I + C_k \tilde{P}_k C_k^*)^{-1} C_k \tilde{P}_k A_k^* + Q_k \tag{5.108}$$

may be applied too. Either way, the central existence condition must be fulfilled, which allows the determination of a useful gain

$$K_{p,k} = A_k \tilde{P}_k C_k^* \left(I + C_k \tilde{P}_k C_k^* \right)^{-1} \,. \tag{5.109}$$

Finally, the a priori $\mathcal{H}^\infty$ estimator

$$\hat{x}_{k+1} = A_k \hat{x}_k + K_{p,k} \left(y_k - C_k \hat{x}_k \right) \tag{5.110a}$$

$$\hat{s}_k = L_k \hat{x}_k \tag{5.110b}$$

can be applied to recursively compute $(\hat{s}, \hat{y})$. Though different theories have been applied, similar estimator equations are given by Mangoubi (following Lagrange Multiplier),[128] Hassibi et al. (so-called strictly causal estimator)[78] and Shaked and Theodor.[80]

AGAIN, THE KALMAN FILTER can be seen as a special case of the a priori $\mathcal{H}^{\infty}$ estimator. As was shown for the a posteriori case, an important parameter is the choice of upper bound γ. There is a lowest possible value γ_{opt} at one side and on the other side $\gamma \to \infty$, which essentially is Kalman filtering. Of course, as γ decreases, a more conservative result emerges. The lowest possible value γ_{opt} is that point, where $\tilde{P}_k$ becomes singular and one cannot subtract more information than is available.[128]

An illustrative example is given by Takaba:[130] Here the dependency of eigenvalues of P according to the upper bound γ is analysed. At the lowest possible bound γ_{opt} eigenvalues of P tend to infinity. By increasing γ, the eigenvalues converge to the value of Kalman filtering solution. To show the reconstitution of Kalman filters, consider parameter $\tilde{P}$ of equation (5.107) as γ tends to ∞:

$$\gamma \to \infty: \qquad \tilde{P}_k = P_k \left(I - \gamma^{-2} L_k^* L_k P_k \right)^{-1} \longrightarrow P_k \,. \qquad (5.111)$$

Following that, the gain K_p of equations (5.30) and (5.109) are the same, and furthermore the Riccati recursions (5.75) and (5.33) are identical for $R_{\nu,k} = I$ and $S_k = 0$. Thus, parameter L no longer has an influence on the Riccati recursion and the Kalman filter of equation (5.37) is reconstituted.

5.2 Infinite Horizon: Popov Function Factorization

5.2.1 Wiener-Kalman Filter

The theory described before has been based on finite processes y, s and so forth. In opposite to that, infinite processes with $k \in [-\infty, \infty]$ and time-invariant model parameters are considered here, thus the following problem is referred to as the (doubly) infinite horizon.

In this section $\mathcal{H}^\infty$ estimators are derived in infinite horizon. The theory of Wiener-Kalman filtering is presented first, because its central canonical spectral factorization approach is essential for $\mathcal{H}^\infty$ theory too. A comprehensive summary of discussed theories for the infinite horizon is given in table 5.2.

	Wiener-Kalman Filter	**$\mathcal{H}^\infty$ Estimator**
1.	Least-Mean-Squares (eq. (5.149))	Worst-Case Analysis (eq. (5.157))
	$\|\mathcal{T}_K\|^2_{\mathcal{H}^2} = \frac{1}{2\pi}\int\limits_0^{2\pi}\left\|T_K(e^{j\theta})T_K^*(e^{j\theta})\right\|_F d\theta$	$\|\mathcal{T}_K\|^2_{\mathcal{H}^\infty} = \sup_\theta \sigma_{max}\left(T_K(e^{j\theta})T_K^*(e^{j\theta})\right)$
		$\|\mathcal{T}_K\|^2_{\mathcal{H}^\infty} < \gamma^2$
2.	Spectral Factorization (eq. (5.125))	Popov Function (5.164)
	$S_y(z) = H(z)MH^*(z^{-*})$	$\Sigma_f(z) = \bar{H}(z)\bar{M}\bar{H}^*(z^{-*})$
	Special Case of Popov Function	Extended: $\hat{C} = \begin{bmatrix} C \\ L \end{bmatrix}$, $\hat{R}_v = \begin{bmatrix} I & 0 \\ 0 & -\gamma^2 I \end{bmatrix}$
	$H(z) = \begin{bmatrix} C(zI - A)^{-1} & I \end{bmatrix}$	$\bar{H}(z) = \begin{bmatrix} \hat{C}(zI - A)^{-1} & I \end{bmatrix}$
	$M = E\left\{\begin{bmatrix} w_k \\ v_k \end{bmatrix}\begin{bmatrix} w_k \\ v_k \end{bmatrix}^*\right\} = \begin{bmatrix} Q & S \\ S^* & R_v \end{bmatrix}$	$\bar{M} = \left\langle \begin{bmatrix} w_k \\ \bar{v}_k \end{bmatrix}, \begin{bmatrix} w_k \\ \bar{v}_k \end{bmatrix} \right\rangle_{\mathcal{K}} = \begin{bmatrix} Q & 0 \\ 0 & \hat{R}_v \end{bmatrix}$
3.	Innovation Approach (eq. (5.131)) $S_y(z) = \Pi(z)R_e\Pi^*(z^{-*})$	Innovation Approach (eq. (5.171)) $\Sigma_f(z) = \hat{\Pi}(z)R_{\hat{e}}\hat{\Pi}^*(z^{-*})$
	$\Pi(z) = C(zI - A)^{-1}K_p + I$	$\hat{\Pi}(z) = \hat{C}(zI - A)^{-1}\hat{K}_p + I$
	$P = \text{Ric. Eq.}(A, C, Q, R, S)$ (5.126) $K_p = (APC^* + S)R_e^{-1}$ $R_e = E\{e_k e_k^T\} = CPC^* + R_v$	$P = \text{Ric. Eq.}(A, C, L, Q, \gamma)$ (5.166) $\hat{K}_p = \begin{bmatrix} K_{py} & \times \end{bmatrix} = AP\hat{C}^*R_{\hat{e}}^{-1}$ $R_{\hat{e}} = \langle \hat{e}_k, \hat{e}_k \rangle = \begin{bmatrix} R_{ye} & \times \\ \times & \times \end{bmatrix} = \hat{C}P\hat{C}^* + \hat{R}_v$
		Central Solution eq. (5.207): (K_{py}, R_{ye})

Table 5.2: Summary of Discussed Theories in Infinite Horizon

At first, central estimation concepts in infinite horizon are discussed. The presumption of $k \in [-\infty, \infty]$ and time-invariant parameters allows more advantageous estimator derivations. For example, the measurement process y and the innovation model Π are defined by

$$y = \left[y_k\right]_{k=-\infty}^{\infty} \quad \text{and} \quad \Pi = \left[\Pi_k\right]_{k=-\infty}^{\infty} \quad \text{with} \quad \Pi_{k-l} = \Pi_{kl} \, . \qquad (5.112)$$

Here, systems (e.g. Π_k) are not described by two indexes k and l anymore, but by a single one, k, only.

It is advantageous to treat estimation problems in the z-domain, which is conducted by the so-called bilateral z-transform, for instance

$$y(z) = \Pi(z)e(z) \quad \text{with} \quad y(z) = \sum_{k=-\infty}^{\infty} y_k z^{-k} \quad \text{and} \quad \Pi(z) = \sum_{k=-\infty}^{\infty} \Pi_k z^{-k} \, . \qquad (5.113)$$

Based on that, the analysis of causality and stability of a system, which was introduced in section 5.1.1, still is important. A system Π is causal and stable (or bounded), if the transfer matrix function $\Pi(z)$ is analytic on (and outside) the unit circle.[78] On the other side, it is anti-causal and stable (or bounded), if it is analytic on (and inside) the unit circle.

A typical example are real mechanical structures. The transfer matrix function of a mechanical system, for instance a bridge, can be identified with the help of the innovation model.[17] Matrix function $\Pi(e^{j\theta})$ may follow with $z = e^{j\theta}$, which is a special case of the z-transform, the so-called Fourier transform. This function clearly is analysed on the unit circle with $|z| = 1$ and is referred to as analytic if it is differentiable for $\theta \in [-\pi, \pi]$. Real mechanical structures must be in accordance with that. In contrary, the transfer function of a simulated, undamped mechanical model may be infinite at some points (resonance catastrophe), and thus are non-differentiable, which indicates a non-stable system.

Besides causality and stability, invertibility is an important property. In infinite horizon the inverse of a system is noted by $\Pi^{-1}(z)$, which is a matrix inverse. Generally, the matrix inverse $\Pi^{-1}(z)$ is non-unique, except for bounded inverse systems Π^{-1}.[78] If both systems $\Pi(z)$ and $\Pi^{-1}(z)$ are causal and stable (analytic on and outside the unit circle), then they are referred to as minimum phase.

WIENER FILTERING has been an important milestone of model based estimation on the basis of stochastic processes.[123] This technique was developed based on single-channel processes $y \in \mathbb{R}^p$ and $s \in \mathbb{R}^q$ with $p = q = 1$ in the frequency-domain ($z = e^{j\theta}$).

As will be shown below, the Wiener filtering approach[123] with $p = 1$ was further developed afterwards by Kalman for multi-variable processes ($p > 1$) on the basis of state space systems.[124] Then Kailath developed a straightforward estimation method by introducing a so-called innovation process.[125, 126] Central element of these estimation theories is a spectral factorization of measured spectra. These parametrized

spectra can be seen as special Popov functions. Finally, the Popov function approach allows to derive a $\mathcal{H}^\infty$ estimation technique on the basis of widespread Kalman filtering.[78]

An important element of Wiener filtering is the derivation of an estimator $\mathcal{K}$, depicted in figure 5.13, following stochastic presumptions.
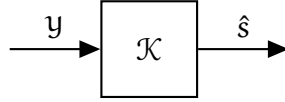
Figure 5.13: Estimator $\mathcal{K}$

It is important to note that state space systems are not applied yet to describe transfer matrix functions.

A Wiener smoothing solution

$$K(z) = \sum_{k=-\infty}^{\infty} K_k z^{-k} = S_{sy}(z)S_y^{-1}(z) \quad \text{with} \quad \mathcal{K} = \left[K_k\right]_{k=-\infty}^{\infty} \tag{5.114}$$

can be given by applying spectra

$$S_y(z) = \sum_{l=-\infty}^{\infty} R_y(l)z^{-k} \quad \text{and} \quad S_{sy}(z) = \sum_{l=-\infty}^{\infty} R_{sy}(l)z^{-k} \, . \tag{5.115}$$

The approach of Wiener[123] presupposes stationary random processes y and s with known 2nd order statistical parameters

$$R_y(l) = E\{y_k y_{k+l}^T\} \quad \text{and} \quad R_{sy}(l) = E\{s_k y_{k+l}^T\} \, . \tag{5.116}$$

The numerical accuracy of $K(z)$ in equation (5.114) is a demanding problem due to the inverse $S_y^{-1}(z)$. Besides that problem, a recursive filtering solution

$$R_{sy}(k) = \sum_{l=0}^{\infty} K_l R_y(k-l), \qquad \hat{s}_k = \sum_{l=-\infty}^{k} K_{k-l} y_l \quad \text{with} \quad K_{k-l} = 0 \quad \text{for } k < l \tag{5.117}$$

is more advantageous, which presupposes causality. A powerful approach for that has been the introduction of innovations.[125,126] Based on innovations e, a causal Wiener filter

$$\hat{s}_{k|k} = \sum_{l=-\infty}^{k} G_{k-l} e_l \quad \text{with} \quad G_{k-l} = 0 \quad \text{for } k < l \tag{5.118}$$

can be derived. As was shown for the time-variant Kalman filter in section 5.1.2, the innovation process e is by definition orthogonal to the past data space with $e_k \perp \mathcal{Y}_{k-1}$. Without presuming a state space model, this innovation process can be directly computed by the Gram-Schmidt procedure.[20] Now, by applying innovations, a causal filtering solution can be given by deriving a straightforward solution to the inverse S_y^{-1}.

THE CANONICAL SPECTRAL FACTORIZATION   is an approach to solve the above filtering problem. For that, a unique rational canonical spectral factor $\Pi(z) \in \mathbb{C}^{p \times p}$ and a positive-definite matrix $R_e \in \mathbb{R}^{p \times p}$ are introduced by

$$S_y(z) = \Pi(z) R_e \Pi^*(z^{-*}) . \tag{5.119}$$

This measurement spectrum factorization is always possible, if spectrum $S_y(z)$ has full rank and is positive definite on the unit circle, namely $z = e^{j\theta}$ for $\theta \in [-\pi, \pi]$. A positive definite spectrum $S_y(e^{j\theta})$ is in accordance with physical presumptions, but inaccuracies can disturb this property. If the canonical spectral factorization is computable, then

(i) $\Pi(z)$ and $\Pi^{-1}(z)$ are rational matrix functions, which are analytic on and outside the unit circle with $|z| \geqslant 1$ on the basis of

(ii) $\Pi(\infty) = I$ and a positive definite matrix R_e.

This gives an elegant solution to the inverse

$$S_y^{-1}(z) = \Pi^{-*}(z^{-*}) R_e^{-1} \Pi^{-1}(z) , \tag{5.120}$$

which is applied in equation (5.114) to get the Wiener-Hopf filtering solution

$$K(z) = \left\{ S_{sy}(z) \Pi^{-*}(z^{-*}) \right\}_+ R_e^{-1} \Pi^{-1}(z) . \tag{5.121}$$

Therein, the operation $\{\times\}_+$ refers to the causal part of $\times$.[20]

The original approach presumed scalar valued processes $p = 1$ and the Fourier transform with $z = e^{j\theta}$. Based on that, several methods to compute the canonical spectral factorization of S_y may be applied, like Bauer's method, the Levinson-Durbin algorithm or the Schur algorithm.[20]

In opposite to that, the canonical spectral factorization of vector processes with $p > 1$ (multi-variable processes) is more elaborate. Here, the Wiener-Kalman filter approach allows a solution, which is discussed below.

Most interestingly, the canonical spectral factorization is the key element in Wiener filtering, Wiener-Kalman filtering and Krein space based $\mathcal{H}^\infty$ estimation. Hence, this central idea is repeatedly applied in the following, which allows an illustrative derivation of $\mathcal{H}^\infty$ estimators.

THE WIENER-KALMAN FILTER   arose a decade after the definition of the Wiener filter in 1960 through the introduction of state space models.[124] The derived Kalman filter received enormous attention in the following decades by researchers, engineers and so forth. Subsequently, the canonical factorization approach of equation (5.119) is elaborated by applying state space parameters in spectrum S_y. These advancements are then the basis for $\mathcal{H}^\infty$ estimation derivations.

To parametrize spectrum S_y, the time-invariant pendant of state space model H in equation (5.19) is introduced by

$$x_{k+1} = Ax_k + \begin{bmatrix} I & 0 \end{bmatrix} \begin{bmatrix} w_k \\ v_k \end{bmatrix} = Ax_k + w_k \tag{5.122a}$$

$$y_k = Cx_k + \begin{bmatrix} 0 & I \end{bmatrix} \begin{bmatrix} w_k \\ v_k \end{bmatrix} = Cx_k + v_k \, . \tag{5.122b}$$

This is a restatement of equation (4.40), namely the model presumption for stochastic subspace identification. Therein, time-invariant state space parameters $A \in \mathbb{C}^{n \times n}$ and $C \in \mathbb{C}^{p \times n}$ are presupposed. Furthermore, both disturbance processes w and v are presumed by zero-mean, stationary vector random variables with known second order statistical parameters

$$\left\langle \begin{bmatrix} w_k \\ v_k \end{bmatrix}, \begin{bmatrix} w_l \\ v_l \end{bmatrix} \right\rangle = E \left\{ \begin{bmatrix} w_k \\ v_k \end{bmatrix} \begin{bmatrix} w_l \\ v_l \end{bmatrix}^* \right\} = \begin{bmatrix} Q & S \\ S^* & R_v \end{bmatrix} \delta_{kl} = M \delta_{kl} \, . \tag{5.123}$$

To provide a general approach, the Gramian matrix $\langle \times \rangle$ has been used here, which allows to treat both deterministic and stochastic disturbance processes at once.

Because w and v are the excitation of system H, parameter M is a so-called input Gramian matrix. By applying these presumptions, the z-transform of model H in equation (5.122)

$$y(z) = H(z) \begin{bmatrix} w(z) \\ v(z) \end{bmatrix} \quad \text{with} \quad H(z) = \begin{bmatrix} H_w(z) & I \end{bmatrix} = \begin{bmatrix} C(zI - A)^{-1} & I \end{bmatrix} \tag{5.124}$$

is advantageously applied to parametrize spectrum S_y with

$$S_y(z) = \begin{bmatrix} C(zI - A)^{-1} & I \end{bmatrix} \begin{bmatrix} Q & S \\ S^* & R_v \end{bmatrix} \begin{bmatrix} C(zI - A)^{-1} & I \end{bmatrix}^* = H(z)MH^*(z^{-*}) \, . \tag{5.125}$$

Based on that, the central idea is apparent: While in Wiener filtering spectrum S_y was directly applied, here it is parametrized with the help of a state space model. The parametrized form of S_y in equation (5.125) is a special case of so-called Popov functions. These functions arise in the Kalman-Yakubovich-Popov (KYP) Lemma,[132] whose results are needed below. Most notably, the Popov function of equation (5.125) is based here on

(i) a possibly indefinite input Gramian matrix M and

(ii) a system matrix A without unit circle eigenvalues, which indicates stability.

An indefinite input Gramian matrix is non-physical, because negative process power is impossible for real-life measurements. Nevertheless, this presumption allows a more general derivation, which leads to an $\mathcal{H}^\infty$ estimation approach. But at first, Wiener-Kalman filtering is explained in view of the KYP lemma. According to this lemma, the following statements are equivalent:

(i) Spectrum $S_y(z)$ is positive-definite for $z = e^{j\theta}$ with $\theta \in [-\pi, \pi]$.

(ii) The discrete-time algebraic Riccati equation (DARE)

$$P = A_p P A_p^* + \begin{bmatrix} I & -K_p \end{bmatrix} \begin{bmatrix} Q & S \\ S^* & R_v \end{bmatrix} \begin{bmatrix} I \\ -K_p^* \end{bmatrix} \tag{5.126a}$$

$$= APA^* - (APC^* + S)(CPC^* + R_v)^{-1}(APC^* + S)^* + Q \tag{5.126b}$$

$$= APA^* - K_p R_e K_p^* + Q \tag{5.126c}$$

with $A_p = A - K_p C$ has a unique hermitian solution P. If this is true, the closed-loop matrix A_p is stable and matrix R_e is positive definite.

(iii) The input Gramian M can be equivalently replaced by

$$M = \begin{bmatrix} Q & S \\ S^* & R_v \end{bmatrix} \longrightarrow \begin{bmatrix} Q - P + APA^* & S + APC^* \\ S^* + CPA^* & R_v + CPC^* \end{bmatrix} = \begin{bmatrix} K_p \\ I \end{bmatrix} R_e \begin{bmatrix} K_p^* & I \end{bmatrix} . \tag{5.127}$$

In equation (5.127) the equivalence class for input Gramians[20] has been applied. By applying this theory, spectrum S_y persists while Gramian M can be altered advantageously.

The introduction of innovations by R_e can be geometrically interpreted as an orthogonal projection, which was explained in section 5.1.2. Also note that the Riccati recursion (5.33) should converge for $k \to \infty$ with time-invariant state space parameters and a (Schur) stable matrix A to the above named hermitian solution P. Following that, important estimation parameters

$$K_p = (APC^* + S)R_e^{-1} \quad \text{with} \quad R_e = CPC^* + R_v \tag{5.128}$$

can be determined. In accordance with the innovation model in equation (5.37), the time-invariant system

$$y(z) = \Pi(z)e(z) \quad \text{with} \quad \Pi(z) = C(zI - A)^{-1}K_p + I \tag{5.129}$$

is introduced. Its inverse allows the determination of innovations by

$$e(z) = \Pi^{-1}(z)y(z) \quad \text{with} \quad \Pi^{-1}(z) = -C(zI - A_p)^{-1}K_p + I . \tag{5.130}$$

These systems are minimum phase and lead to an advantageous canonical spectral factorization of the Popov function with

$$S_y(z) = H(z)MH^*(z^{-*}) = \Pi(z)R_e\Pi^*(z^{-*}) , \tag{5.131}$$

which is a further development of the factorization in equation (5.119) due to the application of state space systems.

COVARIANCE-BASED KALMAN FILTERING is an alternative approach to the above derivations. It especially is useful in connection with stochastic subspace identification techniques. Here, the central idea is to apply known or rather identified covariance matrices in a parametrized form

$$R_y(l) = \langle y_k, y_{k+l} \rangle = \begin{cases} CA^{l-1}N, & l > 0 \\ R_y(0), & l = 0 \\ R_y^T(-l), & l < 0 \end{cases} . \tag{5.132}$$

Techniques to determine parametrized covariance matrices R_y based on measurements y has been covered in the subspace identification chapter 4, especially section 4.3.

By applying parametrized R_y, an alternative to the KYP-lemma factorization of S_y in equation (5.125) can be found. Therefore, consider the z-transform of R_y by

$$S_y(z) = \sum_{l=-\infty}^{\infty} R_y(l)z^{-l} = R_y(0) + \sum_{l=1}^{\infty} CA^{l-1}Nz^{-l} + \sum_{-\infty}^{l=-1} N^*(A^*)^{-l-1}C^*z^{-l} \quad (5.133a)$$

$$= R_y(0) + H_w(z)N + N^*H_w^*(z^{-*}) = H(z) \underbrace{\begin{bmatrix} 0 & N \\ N^* & R_y(0) \end{bmatrix}}_{M} H^*(z^{-*}) . \quad (5.133b)$$

Here, another input Gramian M, in comparison to the KYP lemma with equation (5.125), has been used. Depending on the average process power of states x, an infinite number of Gramians M are possible to derive the identical spectrum S_y. By defining the Lyapunov equation for the time-invariant system H by

$$\Pi = \langle x_k, x_k \rangle = A\Pi A^* + Q \quad \text{with } \Pi \geqslant 0 , \quad (5.134)$$

all possible matrices $M(\Pi)$ can be given:

$$M(\Pi) = \left\langle \begin{bmatrix} w_k \\ v_k \end{bmatrix}, \begin{bmatrix} w_k \\ v_k \end{bmatrix} \right\rangle = \begin{bmatrix} Q & S \\ S^* & R_v \end{bmatrix} = \begin{bmatrix} \Pi - A\Pi A^* & N - A\Pi C^* \\ N^* - C\Pi A^* & R_y(0) - C\Pi C^* \end{bmatrix} . \quad (5.135)$$

Due to the special case of $\Pi = 0$,[19] Gramian M in equation (5.133) may be positive semi-definite. Based on this parametrized form of S_y, the KYP lemma can also be applied to derive a canonical spectral factorization, which allows an innovation model determination. For that, consider the state estimation error of equation (5.22)

$$\tilde{x}_k = x_k - \hat{x}_k \quad \text{with} \quad P = \langle \tilde{x}_k, \tilde{x}_k \rangle = \langle x_k, x_k \rangle - \langle \hat{x}_k, \hat{x}_k \rangle = \Pi - \Sigma , \quad (5.136)$$

which allows the derivation of an alternative discrete-time algebraic Riccati equation

$$\Sigma = \Pi - P = \left(A\Pi A^* + Q \right) - \left(APA^* - K_p R_e K_p^* + Q \right) \quad (5.137a)$$

$$= A\Sigma A^* + K_p R_e K_p^* \quad (5.137b)$$

$$= A\Sigma A^* + \left(N - A\Sigma C^* \right) \left(R_y(0) - C\Sigma C^* \right)^{-1} \left(N - A\Sigma C^* \right)^* . \quad (5.137c)$$

Here, the estimator parameters of equation (5.128)

$$K_p = \left(APC^* + S \right) R_e^{-1} \quad = \left((A\Pi C^* + S) - A\Sigma C^* \right) R_e^{-1} \quad = \left(N - A\Sigma C^* \right) R_e^{-1} , \quad (5.138a)$$

$$R_e = R_v + CPC^* \quad = (R_v + C\Pi C^*) - C\Sigma C^* \quad = R_y(0) - C\Sigma C^* \quad (5.138b)$$

have been altered and applied. This method gives the opportunity to apply model $H(A, C)$ in connection with parameters $\left(N, R_y(0) \right)$ instead of (Q, R_v, S) to determine an innovation model, which is formerly useful for stochastic system identification techniques.

THE NUMERICAL SOLUTION to the algebraic Riccati equations (5.126) and (5.137) is again problematic. One can use the Doubling algorithm of equation (5.35), but in view of convergence and numerical accuracy this is not preferable. Instead solution P is found by an eigendecomposition of $\bar{G}$ following

$$P = V_2 V_1^{-1} \quad \text{with} \quad \begin{bmatrix} \tilde{A}^{-*} & \tilde{A}^{-*} C^* R_v^{-1} C \\ \tilde{Q} \tilde{A}^{-*} & \tilde{A} + \tilde{Q} \tilde{A}^{-*} C^* R_v^{-1} C \end{bmatrix} \begin{bmatrix} V_1 \\ V_2 \end{bmatrix} = \begin{bmatrix} V_1 \\ V_2 \end{bmatrix} \Lambda . \tag{5.139}$$

Because the infinite horizon is used here, the index k of $\bar{G}$ in equation (5.35) has been dropped above. Very importantly, matrix $\bar{G}$ is symplectic, hence

$$\bar{G}^{-1} = \begin{bmatrix} \bar{G}_{22}^* & -\bar{G}_{12}^* \\ -\bar{G}_{21}^* & \bar{G}_{11}^* \end{bmatrix} = J^{-1} \bar{G}^* J \quad \text{with} \quad J^{-1} = J^* = -J, \quad J = \begin{bmatrix} 0 & I \\ -I & 0 \end{bmatrix} . \tag{5.140}$$

To allow a singular system matrix $\tilde{A}$, the eigendecomposition is generalized to

$$\begin{bmatrix} I & C^* R_v^{-1} C \\ 0 & \tilde{A} \end{bmatrix} \begin{bmatrix} V_1 \\ V_2 \end{bmatrix} = \begin{bmatrix} \tilde{A}^* & 0 \\ -\tilde{Q} & I \end{bmatrix} \begin{bmatrix} V_1 \\ V_2 \end{bmatrix} \Lambda \quad \text{with} \quad \bar{G} = \begin{bmatrix} \tilde{A}^* & 0 \\ -\tilde{Q} & I \end{bmatrix}^{-1} \begin{bmatrix} I & C^* R_v^{-1} C \\ 0 & \tilde{A} \end{bmatrix} . \tag{5.141}$$

This is called a symplectic pencil.[34] Finally, the eigendecomposition is advanced for the case of a singular matrix R_v:[78]

$$P = V_2 V_1^{-1} \quad \text{with} \quad \begin{bmatrix} I & 0 & 0 \\ 0 & \tilde{A} & 0 \\ 0 & -C & 0 \end{bmatrix} \begin{bmatrix} V_1 \\ V_2 \\ V_3 \end{bmatrix} = \begin{bmatrix} \tilde{A}^* & 0 & C^* \\ -\tilde{Q} & I & 0 \\ 0 & 0 & R_v \end{bmatrix} \begin{bmatrix} V_1 \\ V_2 \\ V_3 \end{bmatrix} \Lambda . \tag{5.142}$$

Because an additional block row and column has been introduced, this is called an extended symplectic pencil, which follows the matrix product

$$\begin{bmatrix} \begin{bmatrix} \bar{G}_{11} & \bar{G}_{12} \\ \bar{G}_{21} & \bar{G}_{22} \end{bmatrix} & \begin{bmatrix} 0 \\ 0 \end{bmatrix} \\ \begin{bmatrix} 0 & -R_v^{-1} C \end{bmatrix} & 0 \end{bmatrix} = \begin{bmatrix} \begin{bmatrix} \tilde{A}^* & 0 \\ -\tilde{Q} & I \end{bmatrix} & \begin{bmatrix} C^* \\ 0 \end{bmatrix} \\ \begin{bmatrix} 0 & 0 \end{bmatrix} & R_v \end{bmatrix}^{-1} \begin{bmatrix} \begin{bmatrix} I & 0 \\ 0 & \tilde{A} \end{bmatrix} & \begin{bmatrix} 0 \\ 0 \end{bmatrix} \\ \begin{bmatrix} 0 & -C \end{bmatrix} & 0 \end{bmatrix} . \tag{5.143}$$

The eigenvalue determination of both shown symplectic pencils can be conducted by the QZ-algorithm as Patell[133] suggests. This may lead to useless results, as was elaborated by Mari.[36] Especially the requirement for a positive definite spectrum $S_y(e^{j\theta})$ is a problem. To overcome this problem, stabilization techniques have been defined, which are out of the scope of this thesis. Nevertheless, a brief overview of stabilization following Vaccaro and Vukina[35] will be exemplified in section 7.3.

5.2.2 GENERALIZATION TO INFINITE HORIZON $\mathcal{H}^\infty$ ESTIMATION

Wiener-Kalman filters, a special case of time-invariant Kalman filters, are susceptible to noise uncertainties, as was pointed out in section 5.1.3. Here, the generalization

to $\mathcal{H}^\infty$ theory shall be given in infinite horizon. In the following, stochastic and deterministic problems are treated at once, thus Gramian matrices $\langle \times \rangle$ are applied. Furthermore, the finite weighted estimation error of equation (5.47) is considered here too, in operator notation by

$$\tilde{s} = s - \hat{s} . \tag{5.144}$$

Now, a system, which maps disturbances w and v to the generalized estimation error $\tilde{s}$, shall be analysed. Therefore, operator descriptions are introduced with

$$s = \mathcal{L}w, \qquad \hat{s} = \mathcal{K}y \quad \text{and} \quad y = \mathcal{H}_w w + v . \tag{5.145}$$

Those operators are represented in infinite horizon by transfer matrices $L(z)$, $K(z)$ and $H_w(z)$, which leads to

$$s(z) = L(z)w(z), \qquad \hat{s}(z) = K(z)y(z) \quad \text{and} \quad y(z) = H_w(z)w(z) + v(z) . \tag{5.146}$$

The objective of estimation theory is the design of an estimator $\mathcal{K}$ for certain criteria. At the moment state space models are unnecessary, until the Popov function in section 5.2.3 is introduced.

To analyse the weighted estimation error, operator $\mathcal{T}_K$ of equation (5.49) is used again, which maps w and v to $\tilde{s}$. Its structure

$$\tilde{s} = \mathcal{L}w - \mathcal{K}(\mathcal{H}_w w + v) = \begin{bmatrix} \mathcal{L} - \mathcal{K}\mathcal{H}_w & -\mathcal{K} \end{bmatrix} \begin{bmatrix} w \\ v \end{bmatrix} = \mathcal{T}_K \begin{bmatrix} w \\ v \end{bmatrix} \tag{5.147}$$

directly follows the operator notation in equation (5.145). In comparison to a special case based on state space representations in figure 5.7, it is depicted in figure 5.14.
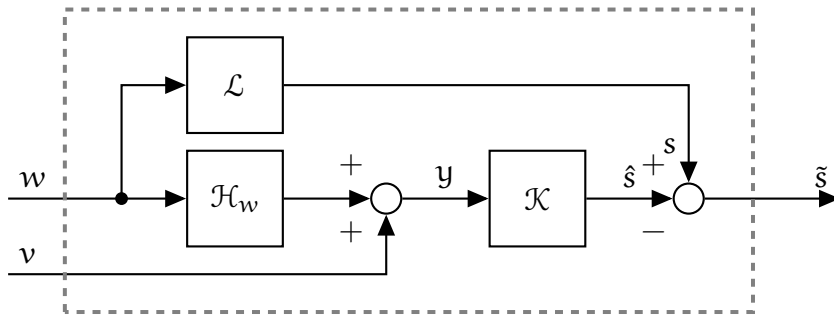
Figure 5.14: Operator $\mathcal{T}_K$

Because infinite processes and time-invariant systems are presumed, a transfer matrix function

$$T_K(z) = \begin{bmatrix} L(z) - K(z)H_w(z) & -K(z) \end{bmatrix} \tag{5.148}$$

can be given. Comparable to section 5.1.3, estimation theory focuses on the operator norm minimization of $\mathcal{T}_K$. Because infinite horizon problems are treated here, the transfer matrix function $T_K(z)$ of equation (5.148) is applied for that.

$\mathcal{H}^2$ **ESTIMATION** is a common approach, which is based on the operator $\mathcal{H}^2$ norm. A special case of this theory is Wiener-Kalman filtering. If jointly Gaussian processes w and v are presumed, Kalman filtering is also referred to as a least mean squares estimator.[78] As an illustration one may consider the stochastic example of equation (5.52).

However, the $\mathcal{H}^2$ norm was already applied in equation (5.50) for finite processes. In infinite horizon the Frobenius norm is applied by

$$\|\mathcal{T}_K\|_{\mathcal{H}^2}^2 = \operatorname{trace}\left(\mathcal{T}_K \mathcal{T}_K^*\right) = \frac{1}{2\pi} \int_0^{2\pi} \left\| \mathsf{T}_K(e^{j\theta}) \mathsf{T}_K^*(e^{j\theta}) \right\|_F d\theta \quad \text{with} \quad z = e^{j\theta}. \qquad (5.149)$$

Here, the trace of an operator has been used, which is generally defined in infinite horizon by

$$\operatorname{trace}(\mathcal{A}) = \frac{1}{2\pi} \int_0^{2\pi} \operatorname{trace}\left[\mathsf{A}(e^{j\theta})\right] d\theta. \qquad (5.150)$$

Because it is needed for further analyses, an optimal $\mathcal{H}^2$ smoothing solution shall be given subsequently. Non-causal $\mathcal{H}^2$ estimators should be more precisely than comparable causal filters, because infinite time series, and thus all available information, are used at once.[78] Hence, derived causal filters can only be as good as (non-causal) smoother $\mathcal{K}_s$.

To derive optimal $\mathcal{H}^2$ smoother, central element $\mathcal{T}_K \mathcal{T}_K^*$ of equation (5.149) is analysed:

$$\mathcal{T}_{Ks} \mathcal{T}_{Ks}^* = \left(\mathcal{L} - \mathcal{K}_s \mathcal{H}_w\right)\left(\mathcal{L} - \mathcal{K}_s \mathcal{H}_w\right)^* + \mathcal{K}_s \mathcal{K}_s^* \qquad (5.151a)$$

$$= \begin{bmatrix} \mathcal{K}_s & -I \end{bmatrix} \begin{bmatrix} I + \mathcal{H}_w \mathcal{H}_w^* & \mathcal{H}_w \mathcal{L}^* \\ \mathcal{L} \mathcal{H}_w^* & \mathcal{L} \mathcal{L}^* \end{bmatrix} \begin{bmatrix} \mathcal{K}_s^* \\ -I \end{bmatrix} = \begin{bmatrix} \mathcal{K}_s & -I \end{bmatrix} \Sigma_s \begin{bmatrix} \mathcal{K}_s^* \\ -I \end{bmatrix}. \qquad (5.151b)$$

The important advantage of the above rearranged equation is the separation of smoother $\mathcal{K}_s$ from Σ_s, which depends on $\mathcal{H}_w$ and $\mathcal{L}$. Operator Σ_s is the key element for the smoother derivation. For further analysis, a LDU decomposition is applied here

$$\Sigma_s = \begin{bmatrix} I & 0 \\ \Phi & I \end{bmatrix} \begin{bmatrix} \mathcal{E} & 0 \\ 0 & \mathcal{L} \mathcal{E}^{-1} \mathcal{L}^* \end{bmatrix} \begin{bmatrix} I & \Phi^* \\ 0 & I \end{bmatrix} \quad \text{with} \quad \Phi = \mathcal{L} \mathcal{H}_w^* \mathcal{E}^{-1}, \ \mathcal{E} = I + \mathcal{H}_w \mathcal{H}_w^*. \qquad (5.152)$$

This allows a deeper inside in $\mathcal{T}_{Ks} \mathcal{T}_{Ks}^*$, which leads to the searched non-causal estimator. By reconsidering the criterion of equation (5.151), the estimation error $\mathcal{T}_{Ks} \mathcal{T}_{Ks}^*$ can be split in two parts

$$\mathcal{T}_{Ks} \mathcal{T}_{Ks}^* = \left(\mathcal{K}_s - \Phi\right) \mathcal{E} \left(\mathcal{K}_s - \Phi\right)^* + \mathcal{L} \mathcal{E}^{-1} \mathcal{L}^*, \qquad (5.153)$$

which must be positive-definite in each case. In consequence, the smallest possible value of estimation error in equation (5.153) is found by eliminating the first term. This leads to a smoothing solution $\mathcal{K}_s = \Phi$ in z-domain

$$\mathsf{K}_s(z) = \Phi(z) = \mathsf{L}(z) \mathsf{H}_w^*(z^{-*}) \left(I + \mathsf{H}_w(z) \mathsf{H}_w^*(z^{-*})\right)^{-1}. \qquad (5.154)$$

Although the smoothing solution is optimal, an estimation error

$$T_{Ks}(z)T_{Ks}^*(z^{-*}) = L(z)\left(I + H_w(z)H_w^*(z^{-*})\right)^{-1}L^*(z^{-*}) \tag{5.155}$$

is unavoidable.

$\mathcal{H}^\infty$ **THEORY** allows the derivation of estimators, which are less susceptible to noise uncertainties, as was discussed in section 5.1.3. Its name has been derived in infinite horizon from the $\mathcal{H}^\infty$ norm, which is defined by the maximum singular value of a transfer matrix function.[78,121] Thus, the maximum singular value of $T_K(z)$ with $z = e^{j\theta}$ and $\theta \in [-\pi, \pi]$ leads to the central $\mathcal{H}^\infty$ criterion

$$\|\mathcal{T}_K\|_{\mathcal{H}^\infty}^2 = \sup_\theta \sigma_{max}\left(T_K(e^{j\theta})T_K^*(e^{j\theta})\right). \tag{5.156}$$

Note that the finite horizon case also is referenced to the $\mathcal{H}^\infty$ norm, which is a common inaccuracy: The finite horizon criterion in equation (5.54) is actually applied with the help of the induced 2-norm.

Again, the optimal solution to $\mathcal{H}^\infty$ estimation is possible for special cases only, and thus a suboptimal one

$$\|\mathcal{T}_K\|_{\mathcal{H}^\infty}^2 < \gamma^2 \tag{5.157}$$

is analysed instead. As was described for the $\mathcal{H}^2$ case, the non-causal solution should be the best possible estimation solution. Hence, it is reasonable to find the optimal upper bound γ_{opt} by examining the smoothing solution.

Most interestingly, the non-causal $\mathcal{H}^2$ estimation solution in equation (5.154) minimizes the estimation error for all possible disturbances (w, v), which includes the worst case. Hence, the smoother of equation (5.154) covers the $\mathcal{H}^\infty$ case too.[78] This leads to an optimal upper bound

$$\gamma_{opt}^2 = \|\mathcal{T}_{Ks}\|_{\mathcal{H}^\infty}^2 = \sup_\theta \sigma_{max}\left(T_{Ks}(e^{j\theta})T_{Ks}^*(e^{j\theta})\right). \tag{5.158}$$

Based on the non-causal solution, a causal one with $\gamma_{opt} \leqslant \gamma \leqslant \infty$ shall be subsequently derived. Therefore, the suboptimal criterion in equation (5.157) is rewritten in operator notation to

$$\mathcal{T}_K\mathcal{T}_K^* < \gamma^2 I \tag{5.159a}$$

$$\left(\mathcal{L} - \mathcal{K}\mathcal{H}_w\right)\left(\mathcal{L} - \mathcal{K}\mathcal{H}_w\right)^* + \mathcal{K}\mathcal{K}^* - \gamma^2 I < 0 \tag{5.159b}$$

$$\begin{bmatrix} \mathcal{K} & -I \end{bmatrix} \begin{bmatrix} I + \mathcal{H}_w\mathcal{H}_w^* & \mathcal{H}_w\mathcal{L}^* \\ \mathcal{L}\mathcal{H}_w^* & \mathcal{L}\mathcal{L}^* - \gamma^2 I \end{bmatrix} \begin{bmatrix} \mathcal{K}^* \\ -I \end{bmatrix} = \begin{bmatrix} \mathcal{K} & -I \end{bmatrix} \Sigma_f \begin{bmatrix} \mathcal{K}^* \\ -I \end{bmatrix} < 0. \tag{5.159c}$$

The identity operators I maps inputs to itself. Here, it is important to note the difference between the $\mathcal{H}^2$ and the $\mathcal{H}^\infty$ case, respectively equations (5.151) and (5.159).

In both cases, the central operator (Σ_s and Σ_f) is essential for estimator derivations, because here $\mathcal{K}$ has been separated from $\mathcal{H}_w$ and $\mathcal{L}$. But only in the $\mathcal{H}^\infty$ case $\gamma^2 I$ is applied due to the suboptimal approach.

In the following, the operator Σ_f shall be used in z-domain by

$$\Sigma_f(z) = \begin{bmatrix} I + H_w(z)H_w^*(z^{-*}) & H_w(z)L^*(z^{-*}) \\ L(z)H_w^*(z^{-*}) & L(z)L^*(z^{-*}) - \gamma^2 I \end{bmatrix} \tag{5.160}$$

to derive causal $\mathcal{H}^\infty$ estimators. As it was applied for the Wiener-Kalman filter, the canonical factorization of a certain Popov function is the key element here.

5.2.3 CANONICAL FACTORIZATION OF A POPOV FUNCTION IN KREIN SPACE

To derive a causal $\mathcal{H}^\infty$ estimator, the idea is to apply the KYP lemma, which was already used in section 5.2.1. For that, a Popov function must be set up. Reasonably, the central criterion of $\mathcal{H}^\infty$ estimation, namely the derived transfer matrix function $\Sigma_f(z)$ in equation (5.160) is used. Thus, state space representations

$$H_w(z) = C(zI - A)^{-1} \quad \text{and} \quad L(z) = L(zI - A)^{-1} \tag{5.161}$$

are introduced. These systems are reordered to reconstitute the Krein space state space model of equation (5.63) (and figure 5.8) with time-invariant parameters in z-domain by

$$\begin{bmatrix} y(z) \\ \check{s}(z) \end{bmatrix} = \begin{bmatrix} H_w(z) \\ L(z) \end{bmatrix} w(z) + \bar{v}(z) = \left[\begin{bmatrix} C \\ L \end{bmatrix} (zI - A)^{-1} \quad I \right] \begin{bmatrix} w(z) \\ \bar{v}(z) \end{bmatrix} . \tag{5.162}$$

Both noise processes w and $\bar{v}$ are still described by equation (5.62), but with $\bar{M}_k \to \bar{M}$:

$$\left\langle \begin{bmatrix} w_k \\ \bar{v}_k \end{bmatrix}, \begin{bmatrix} w_l \\ \bar{v}_l \end{bmatrix} \right\rangle_{\mathcal{K}} = \begin{bmatrix} Q & 0 \\ 0 & \begin{bmatrix} I & 0 \\ 0 & -\gamma^2 I \end{bmatrix} \end{bmatrix} \delta_{kl} = \begin{bmatrix} Q & \hat{S} \\ \hat{S}^* & \hat{R}_v \end{bmatrix} \delta_{kl} = \bar{M}\delta_{kl} . \tag{5.163}$$

Again, it is important to note that the Gramian matrix of the lower element of $\bar{v}$ is negative-definite. Hence, the Gramian matrix must be defined in Krein space $\mathcal{K}$, which was explained by describing the Krein space Kalman filter in section 5.1.4. The negative definite Gramian represents an auxiliary process, which is included to cover the upper bound γ.

By applying the Krein space state space model to Σ_f in equation (5.160), a Popov function

$$\Sigma_f(z) = \left[\begin{bmatrix} C \\ L \end{bmatrix} (zI - A)^{-1} \quad I \right] \begin{bmatrix} Q & 0 \\ 0 & \begin{bmatrix} I & 0 \\ 0 & -\gamma^2 I \end{bmatrix} \end{bmatrix} \begin{bmatrix} (zI - A^*)^{-1} \begin{bmatrix} C^* & L^* \end{bmatrix} \\ I \end{bmatrix} \tag{5.164}$$

arises. The above Popov function $\Sigma_f(z)$ is the $\mathcal{H}^\infty$ pendant to $S_y(z)$ in the Wiener-Kalman filtering case. Based on the parametrized matrix function $\Sigma_f(z)$, the KYP lemma can be applied to determine an $\mathcal{H}^\infty$ estimator.

THE EQUIVALENCE CLASS OF INPUT GRAMIANS   in equation (5.127) allowed the determination of Kalman filter parameters based on a positive definite Popov function S_y and the unique hermitian solution P. In the following, an equivalent approach is taken for the Popov function $\Sigma_f(z)$ in equation (5.164). By defining extended matrices

$$\hat{C} = \begin{bmatrix} C \\ L \end{bmatrix}, \qquad \hat{R}_v = \begin{bmatrix} I & 0 \\ 0 & -\gamma^2 I \end{bmatrix} \quad \text{and} \quad \hat{S} = 0\,, \tag{5.165}$$

the application of the KYP lemma is very similar: If a unique, hermitian, positive semi-definite solution P in accordance with the discrete-time algebraic Riccati equation

$$P = APA^* - \left(AP\hat{C}^* + \hat{S}\right)\left(\hat{C}P\hat{C}^* + \hat{R}_v\right)^{-1}\left(AP\hat{C}^* + \hat{S}\right)^* + Q \tag{5.166}$$

exists, then the input Gramian $\bar{M}$ can be replaced. Both Wiener-Kalman elements, the defined Riccati equation (5.126) and the equivalence class of input Gramians in equation (5.127), are comparable to the $\mathcal{H}^\infty$ case. Thus, an altered input Gramian

$$\bar{M} = \begin{bmatrix} Q & \hat{S} \\ \hat{S}^* & \hat{R}_v \end{bmatrix} \quad \longrightarrow \quad \begin{bmatrix} Q - P + APA^* & \hat{S} + AP\hat{C}^* \\ \hat{S}^* + \hat{C}PA^* & \hat{R}_v + \hat{C}P\hat{C}^* \end{bmatrix} = \begin{bmatrix} \hat{K}_p \\ I \end{bmatrix} \hat{R}_e \begin{bmatrix} \hat{K}_p^* & I \end{bmatrix} \tag{5.167}$$

follows. Because extended matrices have been used, estimator parameters have altered sizes $\hat{K}_p \in \mathbb{C}^{n \times (p+m)}$ and $\hat{R}_e \in \mathbb{R}^{(p+m) \times (p+m)}$) according to

$$\hat{K}_p = \left(AP\hat{C}^* + \hat{S}\right)\hat{R}_e^{-1} \quad \text{and} \quad \hat{R}_e = \hat{C}P\hat{C}^* + \hat{R}_v = \begin{bmatrix} CPC^* + I & CPL^* \\ LPC^* & LPL^* - \gamma^2 I \end{bmatrix}. \tag{5.168}$$

This operation is possible only, when

(i) the Riccati solution P is hermitian and positive semi-definite,

(ii) the closed-loop matrix $\hat{A}_p = A - \hat{K}_p\hat{C}$ is stable and

(iii) both matrices $(\hat{R}_v, \hat{R}_e)$ have the same inertia (number of positive and negative eigenvalues).

Especially in $(\hat{R}_v, \hat{R}_e)$ the indefinite structure, which requires the Krein space, is apparent. Based on that, a Krein space innovation model

$$\hat{\Pi}(z) = \hat{C}(zI - A)^{-1}\hat{K}_p + I \quad \text{with} \quad \Sigma_f(z) = \hat{\Pi}(z)\hat{R}_e\hat{\Pi}^*(z^{-*}) \tag{5.169}$$

can be determined, which is analogue to system $\Pi(z)$ in equation (5.129). Furthermore, a comparison of the Popov function factorizations of equations (5.131) and (5.169) shows a resemblance. In addition to that, innovation model $\hat{\Pi}$ is the time-invariant pendant to the finite horizon Krein space Kalman filter in equation (5.76). In the following, it is used in z-domain by

$$\begin{bmatrix} y(z) \\ \check{s}(z) \end{bmatrix} = \left(\begin{bmatrix} C \\ L \end{bmatrix}(zI - A)^{-1}\hat{K}_p + I\right)\begin{bmatrix} e_y(z) \\ e_s(z) \end{bmatrix} = \hat{\Pi}(z)\hat{e}(z)\,. \tag{5.170}$$

Here, the estimation error process of equation (5.71) is reused in z-domain. Hence, orthogonal projections in Krein space, shown in figure 5.9, are still used. However, the Krein space Kalman filter now is applied to the Popov function of equation (5.164):

$$\Sigma_f(z) = \left(\hat{C} \left(zI - A \right)^{-1} \hat{K}_p + I \right) \hat{R}_e \left(\hat{K}_p^* \left(z^{-*}I - A^* \right)^{-1} \hat{C}^* + I \right). \tag{5.171}$$

Unfortunately, the Krein space Kalman filter in finite and infinite horizon, respectively equations (5.76) and (5.170), is not applicable for estimation, because process š is unknown. Thus, the extended innovation process ê is not determinable. While in finite horizon a solution was found with the help of a LDU factorization in equation (5.77), here a step further is taken by applying the J-spectral factorization. This allows to derive a causal $\mathcal{H}^\infty$ estimator.

THE J-SPECTRAL FACTORIZATION is a commonly used technique in $\mathcal{H}^\infty$ theory.[130,134] It is introduced here, because it allows comprehensive estimator derivations.[78] Following the so-called J-spectral factor $W \in \mathbb{C}^{(p+m)\times(p+m)}$, this theory allows to determine a factorization

$$\Sigma_f(z) = W(z)JW^*(z^{-*}) \quad \text{with} \quad J = \begin{bmatrix} I & 0 \\ 0 & -I \end{bmatrix}. \tag{5.172}$$

Here, the central idea is to separate the indefinite property and to describe it with signature matrix J. In view of Popov function (5.171), matrix $\hat{R}_e$ is factorized and a spectral factor

$$W(z) = \left(\hat{C} \left(zI - A \right)^{-1} \hat{K}_p + I \right) \hat{R}_e^{1/2} \quad \text{with} \quad \hat{R}_e = \hat{R}_e^{1/2} J \hat{R}_e^{*/2} \tag{5.173}$$

is defined. Most interestingly, the inertia of R_e are clearly visible by analysing signature matrix J.

To determine the J-factorization of $\hat{R}_e$, the LDU-factorization of equation (5.77) is applied again by $\hat{R}_e = \bar{L}D\bar{L}^*$, but here with time-invariant parameters

$$\bar{L} = \begin{bmatrix} I & 0 \\ LPC^*R_{ey}^{-1} & I \end{bmatrix}, \qquad D = \begin{bmatrix} R_{ey} & 0 \\ 0 & R_{es} \end{bmatrix} \quad \text{and} \quad \bar{L}^{-1} = \begin{bmatrix} I & 0 \\ -LPC^*R_{ey}^{-1} & I \end{bmatrix}. \tag{5.174}$$

It now is reasonable to introduce $D = D^{1/2}JD^{*/2}$, thus matrices R_{ey} and R_{es} are factorized in accordance with J:

$$R_{ey} = R_{ey}^{1/2}R_{ey}^{*/2} = I + CPC^*, \quad R_{es} = -R_{es}^{1/2}R_{es}^{*/2} = \gamma^2 I - L\left(P^{-1} + C^*C \right)^{-1} L^*. \tag{5.175}$$

Following that $\hat{R}_e^{1/2} = \bar{L}D^{1/2}$ and its inverse $\hat{R}_e^{-1/2} = D^{-1/2}\bar{L}^{-1}$ are determinable following

$$\hat{R}_e^{1/2} = \begin{bmatrix} R_{ey}^{1/2} & 0 \\ LPC^*R_{ey}^{-*/2} & R_{es}^{1/2} \end{bmatrix} \quad \text{and} \quad \hat{R}_e^{-1/2} = \begin{bmatrix} R_{ey}^{-1/2} & 0 \\ -R_{es}^{-1/2}LPC^*R_{ey}^{-1} & R_{es}^{-1/2} \end{bmatrix}, \tag{5.176}$$

which leads to the introduction of process $\check{e}$ by

$$\check{e}_k = R_e^{-1/2}\hat{e}_k \quad \text{with} \quad \langle \hat{e}_k, \hat{e}_k \rangle = R_e \quad \text{and} \quad \langle \check{e}_k, \check{e}_k \rangle = J \, . \tag{5.177}$$

The rescaled innovation process $\check{e}$ is very important, because it is not influenced by the choice of systems $(\mathcal{H}, \mathcal{L})$ or noise parameters $(Q, \hat{R}_v, \hat{S})$, which covers the upper bound γ too. Hence, all information are covered by the spectral factor W. This is now applied to give an alternative representation of the Krein space Kalman filter in equation (5.170):

$$\begin{bmatrix} y(z) \\ \check{s}(z) \end{bmatrix} = \hat{\Pi}(z) \begin{bmatrix} e_y(z) \\ e_s(z) \end{bmatrix} = W(z) \begin{bmatrix} \check{e}_1(z) \\ \check{e}_2(z) \end{bmatrix} \, . \tag{5.178}$$

SUBOPTIMAL $\mathcal{H}^\infty$ ESTIMATORS are now derivable: A causal and bounded estimator $K(z)$ with $\mathcal{H}^\infty$ constraint, namely the criterion of equation (5.157), exists, if the canonical spectral factorization of Popov function (5.160)

$$\Sigma_f = W\mathcal{J}W^* = \begin{bmatrix} \mathcal{L}_{11} & \mathcal{L}_{12} \\ \mathcal{L}_{21} & \mathcal{L}_{22} \end{bmatrix} \begin{bmatrix} I & 0 \\ 0 & -I \end{bmatrix} \begin{bmatrix} \mathcal{L}_{11}^* & \mathcal{L}_{21}^* \\ \mathcal{L}_{12}^* & \mathcal{L}_{22}^* \end{bmatrix} \tag{5.179}$$

can be determined.[78] Furthermore, this is possible only, when

(i) the spectral factor W is causal,

(ii) the inverse operators $(W^{-1}, \mathcal{L}_{11}^{-1})$ are causal and bounded and

(iii) system $\mathcal{L}_{12}$ is strictly causal.

If this is true, then a central estimator $\mathcal{K}_{cen}$ and its generalization $\mathcal{K}_{gen}$ can be derived on the basis of spectral factor W. It hence is useful to give a parametrization of this operator first, which is possible due to introduced state space models $H_w(z)$ and $L(z)$ in equation (5.161). By comparison to equation (5.162), the spectral factor in z-domain

$$W(z) = \left(\begin{bmatrix} H_w(z) \\ L(z) \end{bmatrix} \hat{K}_p + I \right) \hat{R}_e^{1/2} = \left(\begin{bmatrix} H_w(z) \\ L(z) \end{bmatrix} \hat{K}_p \bar{L} + \bar{L} \right) D^{1/2} \quad \text{with} \quad \hat{R}_e^{1/2} = \bar{L}D^{1/2} \tag{5.180}$$

follows. Gain matrix $\hat{K}_p$ is rather complex and is hard to parametrize. In opposite to that, $\hat{K}_p L_f$ can be advantageously parametrized. This gives a solution, which is comparable to the finite horizon case in equation (5.82) with

$$\begin{bmatrix} K_{py} & K_{ps} \end{bmatrix} = \hat{K}_p \bar{L} = AP \begin{bmatrix} C^* & L^* \end{bmatrix} \begin{bmatrix} I & -R_{ey}^{-*}CPL^* \\ 0 & I \end{bmatrix} \begin{bmatrix} R_{ey}^{-1} & 0 \\ 0 & R_{es}^{-1} \end{bmatrix} \tag{5.181}$$

and gain matrices

$$K_{py} = APC^*R_{ey}^{-1} \quad \text{and} \quad K_{ps} = AP\left(L^* - C^*R_{ey}^{-*}CPL^* \right) R_{es}^{-1} \, . \tag{5.182}$$

Both gain matrices K_{py} and K_{ps} are applied in connection with uncorrelated processes e_y and $\tilde{e}_s$ analogue to equation (5.81). This allows the parametrization of the spectral factor

$$\begin{bmatrix} L_{11}(z) & L_{12}(z) \\ L_{21}(z) & L_{22}(z) \end{bmatrix} = \left(\begin{bmatrix} H_w(z) \\ L(z) \end{bmatrix} \begin{bmatrix} K_{py} & K_{ps} \end{bmatrix} + \begin{bmatrix} I & 0 \\ LPC^*R_{ey}^{-1} & I \end{bmatrix} \right) \begin{bmatrix} R_{ey}^{1/2} & 0 \\ 0 & R_{es}^{1/2} \end{bmatrix} \qquad (5.183a)$$

with subelements

$$\begin{bmatrix} L_{11}(z) \\ L_{21}(z) \end{bmatrix} = \begin{bmatrix} H_w(z)K_{py} + I \\ L(z)K_{py} + LPC^*R_{ey}^{-1} \end{bmatrix} R_{ey}^{1/2} \quad \text{and} \quad \begin{bmatrix} L_{12}(z) \\ L_{22}(z) \end{bmatrix} = \begin{bmatrix} H_w(z)K_{ps} \\ L(z)K_{ps} + I \end{bmatrix} R_{es}^{1/2} . \qquad (5.184)$$

Based on that, central and general $\mathcal{H}^\infty$ estimators are derived in the following.

5.2.4 Central and General $\mathcal{H}^\infty$ Estimators

While the derivations above have been devoted to analyse Popov function $\Sigma(z)$ by canonical factorization, here these results are applied to determine causal $\mathcal{H}^\infty$ Estimator. Therefore, reconsider the central criterion of equation (5.159) in connection with the derived Popov function (5.179):

$$\mathcal{T}_K \mathcal{T}_K^* - \gamma^2 I = \begin{bmatrix} \mathcal{K} & -I \end{bmatrix} \begin{bmatrix} \mathcal{L}_{11} & \mathcal{L}_{12} \\ \mathcal{L}_{21} & \mathcal{L}_{22} \end{bmatrix} \begin{bmatrix} I & 0 \\ 0 & -I \end{bmatrix} \begin{bmatrix} \mathcal{L}_{11}^* & \mathcal{L}_{21}^* \\ \mathcal{L}_{12}^* & \mathcal{L}_{22}^* \end{bmatrix} \begin{bmatrix} \mathcal{K}^* \\ -I \end{bmatrix} < 0 . \qquad (5.185)$$

This is the central criterion, which is used to determine an estimator $\mathcal{K}$ based on spectral factor $\mathcal{W}$. By introducing two operators

$$\mathcal{X} = \mathcal{K}\mathcal{L}_{11} - \mathcal{L}_{21} \quad \text{and} \quad \mathcal{Y} = \mathcal{K}\mathcal{L}_{12} - \mathcal{L}_{22} , \qquad (5.186)$$

the central criterion in equation (5.185) is rearranged to

$$\mathcal{T}_K \mathcal{T}_K^* - \gamma^2 I = \begin{bmatrix} \mathcal{X} & \mathcal{Y} \end{bmatrix} \mathcal{J} \begin{bmatrix} \mathcal{X}^* \\ \mathcal{Y}^* \end{bmatrix} = \mathcal{X}\mathcal{X}^* - \mathcal{Y}\mathcal{Y}^* < 0 . \qquad (5.187)$$

In the following, an $\mathcal{H}^\infty$ estimation approach is derived, in which the estimation error of equation (5.187) is minimized. This leads to the central estimator, which is depicted in figure 5.15:

$$\mathcal{K}_{\text{cen}} = \mathcal{L}_{21}\mathcal{L}_{11}^{-1} . \qquad (5.188)$$

This approach minimizes the estimation error in equation (5.187) with

$$\mathcal{X} = \left(\mathcal{L}_{21}\mathcal{L}_{11}^{-1} \right)\mathcal{L}_{11} - \mathcal{L}_{21} = 0 \quad \text{and} \quad \mathcal{Y} = \left(\mathcal{L}_{21}\mathcal{L}_{11}^{-1} \right)\mathcal{L}_{12} - \mathcal{L}_{22} . \qquad (5.189)$$
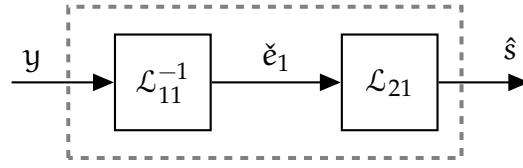
Figure 5.15: Central Estimator $\mathcal{K}_{cen}$

CENTRAL $\mathcal{H}^\infty$ ESTIMATORS can be parametrized following operator $\mathcal{K}_{cen}$ in equation (5.188). Because infinite horizon estimators are analysed, transfer system matrices $L_{21}(z)$ and $L_{11}^{-1}(z)$ must be determined. A state space representation of $\mathcal{L}_{11}$ and $\mathcal{L}_{21}$ have already been derived in equation (5.184):

$$L_{11}(z) = \left(C(zI - A)^{-1} K_{py} + I \right) R_{ey}^{1/2} \tag{5.190}$$

$$L_{21}(z) = \left(L(zI - A)^{-1} K_{py} + LPC^* R_{ey}^{-1} \right) R_{ey}^{1/2} . \tag{5.191}$$

Here, one notices the similarities to the Wiener-Kalman filter $\Pi(z)$ and $L_{11}(z)$ in equations (5.129) and (5.190). If certain assumptions are made ($R_v = I$, $S = 0$ and $\gamma \to \infty$), both systems are nearly identical. Thus, the inverse

$$L_{11}^{-1}(z) = R_{ey}^{-1/2} \left(- C(zI - A_p)^{-1} K_{py} + I \right) \quad \text{with} \quad A_p = A - K_{py} C \tag{5.192}$$

can be determined easily following equation (5.97). Furthermore, system $\mathcal{L}_{21}$ is comparable to the $\mathcal{H}^\infty$ estimator of equation (5.93), but with time-invariant parameters. This leads to a parametrized central estimator state space system in z-domain with

$$K_{cen}(z) = LPC^* R_{ey}^{-1} + L \left(I - PC^* R_{ey}^{-1} C \right) (zI - A_p)^{-1} K_{py} . \tag{5.193}$$

A comparison to the finite horizon $\mathcal{H}^\infty$ estimator in equation (5.98) shows a resemblance: An a posteriori $\mathcal{H}^\infty$ estimator was derived by eliminating the second estimation error process by $\tilde{e}_s = 0$. In infinite horizon an analogue approach has been taken by neglecting estimation error $\check{e}_2 = R_{es}^{-1/2} \tilde{e}_s$, thus operator $(\mathcal{L}_{12}, \mathcal{L}_{22})$ are unused.

In result the finite and the infinite horizon $\mathcal{H}^\infty$ estimators of equations (5.98) and (5.193) are the same, if time-invariant parameters are assumed and $\bar{M}_k \to \bar{M}$. However, the central estimator $\mathcal{K}_{cen} = \mathcal{L}_{21} \mathcal{L}_{11}^{-1}$ is a special (and reasonable) choice to minimize the criterion in equation (5.187). A generalization of that is shown below.

GENERAL $\mathcal{H}^\infty$ ESTIMATORS take both estimation error processes $\check{e}_1$ and $\check{e}_2$ into account. Because š is still unknown, process $\check{e}_2$ is non-determinable. Thus, a causal strictly contractive transfer operator $\mathcal{S}$ is introduced to define a relation of estimation error $\check{e}_2 = -\mathcal{S}\check{e}_1$.[78] This alters the Krein space Kalman filter to

$$\begin{bmatrix} y \\ š \end{bmatrix} = \begin{bmatrix} \mathcal{L}_{11} & \mathcal{L}_{12} \\ \mathcal{L}_{21} & \mathcal{L}_{22} \end{bmatrix} \begin{bmatrix} \check{e}_1 \\ -\mathcal{S}\check{e}_1 \end{bmatrix} = \begin{bmatrix} \mathcal{L}_{11} - \mathcal{L}_{12}\mathcal{S} \\ \mathcal{L}_{21} - \mathcal{L}_{22}\mathcal{S} \end{bmatrix} \check{e}_1 = \begin{bmatrix} \mathcal{L}_y \\ \mathcal{L}_s \end{bmatrix} \check{e}_1 . \tag{5.194}$$

Analogue to the relation of estimation error, operators $(\mathcal{X}, \mathcal{Y})$ of equation (5.187) are concatenated by

$$\mathcal{X} = \mathcal{Y}\mathcal{S} \quad \text{with} \quad \mathcal{T}_K \mathcal{T}_K^* - \gamma^2 I = \mathcal{Y}(\mathcal{S}\mathcal{S}^* - I)\mathcal{Y}^* < 0 \quad \text{and} \quad 0 \leqslant \mathcal{S}\mathcal{S}^* < I . \tag{5.195}$$

It is important to note the increase of estimation error $\mathcal{T}_K \mathcal{T}_K^*$ in equation (5.195) by choosing $\mathcal{S} > 0$. To derive a general $\mathcal{H}^\infty$ estimator, the relation $\mathcal{X} = \mathcal{Y}\mathcal{S}$, namely

$$\left(\mathcal{K}_{\text{gen}}\mathcal{L}_{11} - \mathcal{L}_{21}\right) = \left(\mathcal{K}_{\text{gen}}\mathcal{L}_{12} - \mathcal{L}_{22}\right)\mathcal{S} , \tag{5.196}$$

simply is rearranged to

$$\mathcal{K}_{\text{gen}} = \left(\mathcal{L}_{21} - \mathcal{L}_{22}\mathcal{S}\right)\left(\mathcal{L}_{11} - \mathcal{L}_{12}\mathcal{S}\right)^{-1} = \mathcal{L}_s \mathcal{L}_y^{-1} . \tag{5.197}$$

Here, the operators $(\mathcal{L}_y, \mathcal{L}_s)$ of equation (5.194) were used to define the general estimator $\mathcal{K}_{\text{gen}}$, which has been depicted in figure 5.16.
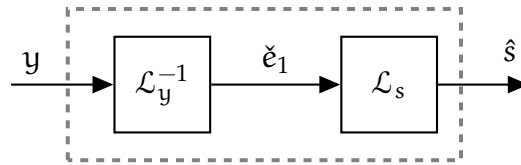
Figure 5.16: General Estimator $\mathcal{K}_{\text{gen}}$

Most notably, the case $\mathcal{S} = 0$ refers to the central estimation criterion with $\mathcal{X} = 0$ and $\mathcal{K}_{\text{cen}} = \mathcal{L}_{21}\mathcal{L}_{11}^{-1}$ in equation (5.189).

Again, a z-domain representation

$$K_{\text{gen}}(z) = \left(L_{21}(z) - L_{22}(z)S(z)\right)\left(L_{11}(z) - L_{12}(z)S(z)\right)^{-1} = L_s(z)L_y^{-1}(z) \tag{5.198}$$

is given due to the infinite horizon. Unfortunately, the numerical-practical design of $\mathcal{K}_{\text{gen}}$ is elaborate, because the inversion of $\mathcal{L}_y$ is non-trivial. However, general $\mathcal{H}^\infty$ estimators are sparsely applied only. For example, Hassibi et al.[78] primarily focus on the central solution with $\mathcal{S} = 0$. Nevertheless, Takaba[130] gives an algorithmic determination of an appropriate $S(z)$.

5.3 SUMMARY FOR FILTERING SIGNALS IN ADDITIVE NOISE

The theories presented so far describe a general solution to $\mathcal{H}^\infty$ estimation. To numerically compute $\mathcal{H}^\infty$ estimators, operator $\mathcal{L}$ must be defined, which represents the application of the computed filter. There are various approaches possible to define $\mathcal{L}$. In the frame of this thesis the approach of 'filtering signals in additive noise' is

relevant, and thus is presented below. Its core concept is $\mathcal{L} = \mathcal{H}_w$, which redefines the operator of weighted estimation error $\mathcal{T}_K$ in equation (5.147) to

$$\tilde{s} = \begin{bmatrix} \mathcal{H}_w - \mathcal{K}\mathcal{H}_w & -\mathcal{K} \end{bmatrix} \begin{bmatrix} w \\ v \end{bmatrix} = \mathcal{T}_K \begin{bmatrix} w \\ v \end{bmatrix} . \tag{5.199}$$

This operator is shown in figure 5.17.

Figure 5.17: Operator $\mathcal{T}_k$ for Filtering Signals in Additive Noise

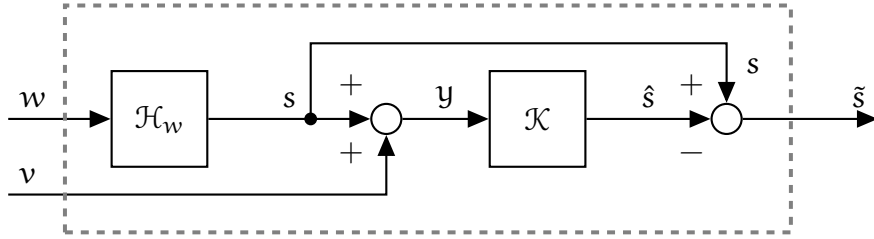Besides the operator $\mathcal{L}$, the upper bound γ must be defined to determine an $\mathcal{H}^\infty$ estimator. The best possible solution is the non-causal estimator in z-domain

$$T_{Ks}(z)T_{Ks}^*(z^{-*}) = H_w(z)\left(I + H_w(z)H_w^*(z^{-*})\right)^{-1} H_w^*(z^{-*}) , \tag{5.200}$$

whose estimation error has been discussed in section 5.2.2. Following that, the optimal upper bound is defined by the smoothing solution in equation (5.158) with

$$\gamma_{\text{opt}}^2 = \|\mathcal{T}_K\|_{\mathcal{H}^\infty}^2 = \max_\theta \sigma_{\max}\left(T_{Ks}(e^{j\theta})T_{Ks}^*(e^{j\theta})\right) . \tag{5.201}$$

A poorly working estimator is $\mathcal{K} = I$, because it would not filter the signal at all. It leads to a confident estimation error level

$$\gamma_{\text{conf}} = \|\mathcal{T}_K\|_{\mathcal{H}^\infty} = \left\| \begin{bmatrix} \mathcal{H}_w - \mathcal{H}_w & -I \end{bmatrix} \right\|_{\mathcal{H}^\infty} = \left\| \begin{bmatrix} 0 & -I \end{bmatrix} \right\|_{\mathcal{H}^\infty} = 1 , \tag{5.202}$$

which is always possible, if a hermitian, positive-definite solution P of Riccati equation (5.166) exists. The expedient choice of the upper bound for $\mathcal{H}^\infty$ estimation is in between $\gamma_{\text{opt}} \leqslant \gamma \leqslant \gamma_{\text{conf}}$ and must be determined recursively. Nevertheless, the definition $\gamma = \gamma_{\text{conf}} = 1$ always is feasible.[78]

TO FILTER SIGNALS IN ADDITIVE NOISE, the derivations of both the finite and infinite horizon can be advantageously used, which lead to similar results. Here, consider time-invariant state space parameters and a constant input Gramian matrix $\bar{M}$. Then the hermitian solution P of discrete-time Riccati equation (5.166) can be used to determine estimator parameters (K_{py}, R_{ey}) of equations (5.175) and (5.182), which leads to the central estimator

$$K_{\text{cen}}(z) = CPC^*R_{ey}^{-1} + C\left(I - PC^*R_{ey}^{-1}C\right)\left(zI - A_p\right)^{-1}K_{py} . \tag{5.203}$$

As was shown before, the central estimator $K_{cen}(z)$ of equation (5.193) is a z-domain equivalent to the a posteriori $\mathcal{H}^\infty$ estimator with time-invariant parameters. Thus, consider the a posteriori $\mathcal{H}^\infty$ estimator of equations (5.93) and (5.98)

$$\hat{x}_{k+1} = A\hat{x}_k + K_{py}e_k \qquad = A_p\hat{x}_k + K_{py}y_k \tag{5.204a}$$

$$\hat{y}_{k|k} = C\hat{x}_k + CPC^*R_{ey}^{-1}e_k \qquad = C(I - PC^*R_{ey}^{-1}C)\hat{x}_k + CPC^*R_{ey}^{-1}y_k \tag{5.204b}$$

with the filtered estimate $\hat{s}_{k|k} = \hat{y}_{k|k}$. The state space representation of an estimator $\mathcal{K}$ is additionally depicted in figure 5.18.
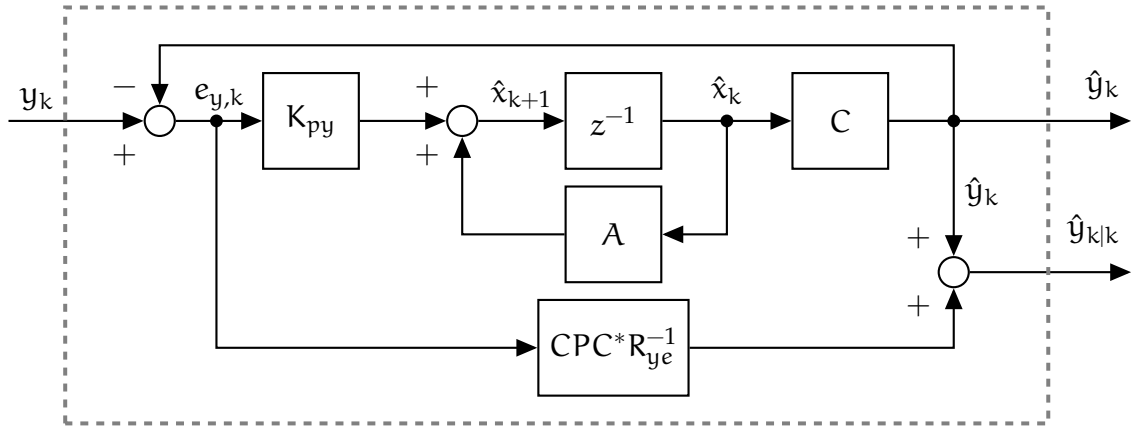
Figure 5.18: $\mathcal{H}^\infty$ Estimator for Filtering Signals in Additive Noise

System $L_{11}(z)$ of equation (5.190) is important, because it leads to

$$S_y(z) = L_{11}(z)L_{11}^*(z^{-*}) = \bar{\Pi}(z)R_{ye}\bar{\Pi}^*(z^{-*}) \quad \text{with} \quad \bar{\Pi}(z) = C(zI - A)^{-1}K_{py} + I . \tag{5.205}$$

For that, operator $\mathcal{L}_{12}$ is neglected, which follows the central estimation approach. System $\bar{\Pi}$ essentially is the $\mathcal{H}^\infty$ pendant for the Wiener-Kalman Popov function factorization S_y of equation (5.131). Very importantly for $\gamma \to \infty$, both equations (5.131) and (5.205) are identical, because in this case

$$\gamma \longrightarrow \infty : \quad \bar{\Pi} = \Pi \quad \text{and} \quad R_{ye} = R_e . \tag{5.206}$$

For details on this matter see section 5.1.5. Finally, system $\bar{\Pi}(A, K_{py}, C)$

$$\hat{x}_{k+1} = A\hat{x}_k + K_{py}e_{y,k} \tag{5.207a}$$

$$y_k = C\hat{x}_k + e_{y,k} \tag{5.207b}$$

and its inverse $\bar{\Pi}^{-1}(A_p, K_{py}, C)$

$$\hat{x}_{k+1} = A_p\hat{x}_k + K_{py}y_k \tag{5.208a}$$

$$e_{y,k} = -C\hat{x}_k + y_k \tag{5.208b}$$

are defined in time-domain, because they are reused for damage identification in chapter 6. Both systems $\bar{\Pi}$ and $\bar{\Pi}^{-1}$ are minimum phase.

5.4 Mechanical System Example

5.4.1 Filtering Displacement Measurements in Additional Noise

In this section the core of $\mathcal{H}^\infty$ estimation is demonstrated at the mechanical system example of chapter 3, especially section 3.3.1: A cantilever arm is modelled as a single degree of freedom system with time-invariant mechanical parameters

$$m = 7.25 \times 10^{-3} \frac{\text{Ns}^2}{\text{mm}}, \quad k \approx 8.1 \frac{\text{N}}{\text{mm}}, \quad d = 10^{-2} \frac{\text{Ns}}{\text{mm}} \quad \text{and} \quad \zeta = \frac{d}{d_{\text{crit}}} \approx 2\% \quad (5.209)$$

following equation (3.41). As was shown in equation (3.43), continuous-time state space parameters

$$A_c = \begin{bmatrix} 0 & 1 \\ -m^{-1}k & -m^{-1}d \end{bmatrix}, \quad B_c = \begin{bmatrix} 0 \\ m^{-1} \end{bmatrix} \quad \text{and} \quad C_c = \begin{bmatrix} 1 & 0 \end{bmatrix} \quad (5.210)$$

can be directly determined. For the numerical computation $\Delta t = 1/20\text{s}$ has been chosen with $t = k\Delta t$. Thus, the zero-order-hold method of equation (3.15) is applied to compute discrete-time state space parameters (A, B, C). Here, displacements y are measured. Because stationary processes are presumed, a time-invariant state space model $H(A, C)$ in z-domain

$$H_w(z) = C(zI - A)^{-1} \quad \text{with} \quad y(z) = H_w(z)w(z) + v(z) \quad (5.211)$$

is defined. The process noise w follows a force excitation

$$w(z) = Bf(z), \quad (5.212)$$

which is typical for mechanical systems. In this analysis, structural displacements are measured in a noise-disturbed environment, which is considered by v. This is a usual set-up for large-scale structures, for instance bridges, wind energy plants and so forth.

The research issue is to analyse the 'filtering signals in additive noise' approach following different estimation techniques for the above described mechanical system example. Most importantly, noise uncertainties are considered, while the true model of equations (5.211) is known. The mechanical system $\mathcal{H}$ is excited by ergodic, white, noise processes w and v with Gramian matrices

$$Q_{\text{true}} = B \langle f_k, f_k \rangle B^* \quad \text{with} \quad \langle f_k, f_k \rangle = E\{f_k f_k^\mathsf{T}\} = 5N^2, \quad (5.213a)$$

$$R_{\text{true}} = \langle v_k, v_k \rangle = E\{v_k v_k^\mathsf{T}\} = 3\text{mm}^2 \quad \text{and} \quad S_{\text{true}} = \langle f_k, v_k \rangle = 0. \quad (5.213b)$$

It thus is a stochastic problem and covariance matrices must be used to determine disturbance parameters. However, the true Gramian matrices are unknown to the estimator designer. Thus, simple estimator design parameters

$$Q_{\text{design}} = \begin{bmatrix} 1\text{mm}^2 & 0 \\ 0 & 1\frac{\text{mm}^2}{\text{s}^2} \end{bmatrix}, \quad R_{\text{design}} = 1\text{mm}^2 \quad \text{and} \quad S_{\text{design}} = 0 \quad (5.214)$$

are chosen instead. To give an impression of the set-up, the power spectra of x and y due to

$$S_y(e^{j\theta}) = H_w(e^{j\theta})Q_{true}H_w^*(e^{j\theta}) + R_{true} = S_x(e^{j\theta}) + R_{true} \tag{5.215}$$

are shown in figure 5.19. Furthermore, exemplary time series of x and y are shown, to illustrate the influence of measurement noise.
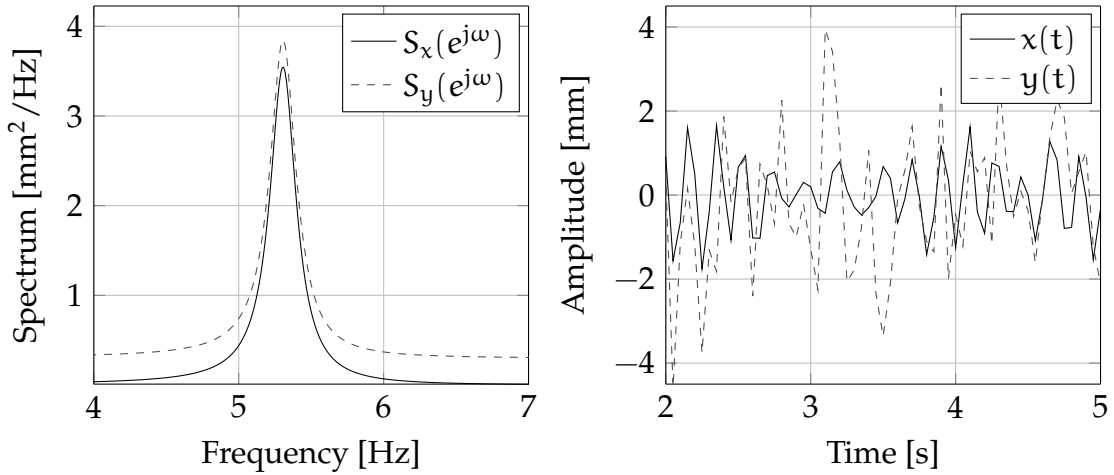
Figure 5.19: Theoretical Spectra and Exemplary Time-Series

5.4.2 ESTIMATOR DESIGN FOR FILTERING SIGNALS IN ADDITIVE NOISE

In the following, four different estimators are designed following the discussed estimation theories of this chapter:

(i) A non-causal $\mathcal{H}^2$ estimator,

(ii) Two causal, central $\mathcal{H}^\infty$ estimators with different upper bounds γ and

(iii) A causal $\mathcal{H}^2$ estimator (Wiener-Kalman-filter, $\gamma \to \infty$).

THE NON-CAUSAL $\mathcal{H}^2$ ESTIMATOR should be the best approach, because available time series are used at once. In accordance with the described theory of section 5.2.2, a non-causal $\mathcal{H}^2$ estimator

$$K_s(z) = H_w(z)H_w^*(z^{-*})\left(1 + H_w(z)H_w^*(z^{-*})\right)^{-1} \tag{5.216}$$

is determined first by applying equation (5.154). This leads to an estimation error

$$T_{Ks}(e^{j\theta})T_{Ks}^*(e^{j\theta}) = H_w(e^{j\theta})\left(1 + H_w(e^{j\theta})H_w^*(e^{j\theta})\right)^{-1}H_w^*(e^{j\theta}) \tag{5.217}$$

according to equation (5.200). In accordance with equation (5.201), this leads to the optimal bound

$$\gamma_{opt}^2 = \|\mathcal{T}_{Ks}\|_{\mathcal{H}^\infty}^2 \approx 0.9956 \text{mm}^2 \,. \tag{5.218}$$

Most interestingly, a lower optimal value γ_{opt} could be found, if a larger damping ζ would be chosen.

TWO CENTRAL $\mathcal{H}^\infty$ ESTIMATORS are designed next. The first one is applied with $\gamma^2 = \gamma_{opt}^2 = 0.9956$. Usually, an iterative process must be conducted to determine the lowest possible value γ for Riccati equation (5.166). However, in this case the optimal value γ_{opt} has been directly applicable, which led to the following estimator parameters:

$$P_{\infty,1} \approx \begin{bmatrix} 15\text{mm}^2 & -8\frac{\text{mm}^2}{\text{s}} \\ -8\frac{\text{mm}^2}{\text{s}} & 16,400\frac{\text{mm}^2}{\text{s}^2} \end{bmatrix}, \quad R_{ey,1} \approx 15.8\text{mm}^2, \quad K_{py,1} \approx \begin{bmatrix} -0.08 \\ -30.01/\text{s} \end{bmatrix} . \tag{5.219}$$

To allow a comparison to the first $\mathcal{H}^\infty$ estimator, a second one is designed with an arbitrary choice for the upper bound $\gamma^2 = 1.5$:

$$P_{\infty,2} \approx \begin{bmatrix} 2.1\text{mm}^2 & -0.8\frac{\text{mm}^2}{\text{s}} \\ -0.8\frac{\text{mm}^2}{\text{s}} & 1,273.4\frac{\text{mm}^2}{\text{s}^2} \end{bmatrix}, \quad R_{ey,2} \approx 3.1\text{mm}^2, \quad K_{py,2} \approx \begin{bmatrix} -0.06 \\ -21.59/\text{s} \end{bmatrix} . \tag{5.220}$$

Based on the computed estimator parameters, two central $\mathcal{H}^\infty$ with

$$K_\infty(z) = CPC^*R_{ey}^{-1} + C\left(I - PC^*R_{ey}^{-1}C\right)\left(zI - A_p\right)^{-1}K_{py} \tag{5.221}$$

have been determined following equation (5.203).

FINALLY, A WIENER-KALMAN FILTER, which is an optimal $\mathcal{H}^2$ estimator, is designed by applying the theory of section 5.2.1. As was shown in section 5.1.5, it can be referred to as a special case of $\mathcal{H}^\infty$ estimation with $\gamma \to \infty$. To design the estimator, Riccati equation (5.126) is solved and applied to determine parameters R_e and K_p:

$$P_2 \approx \begin{bmatrix} 1.5\text{mm}^2 & -0.5\frac{\text{mm}^2}{\text{s}} \\ -0.5\frac{\text{mm}^2}{\text{s}} & 629.8\frac{\text{mm}^2}{\text{s}^2} \end{bmatrix}, \quad R_e \approx 2.5\text{mm}^2, \quad K_p \approx \begin{bmatrix} -0.05 \\ -19.37/\text{s} \end{bmatrix} . \tag{5.222}$$

To be comparable to the formerly described central $\mathcal{H}^\infty$ estimators, equation (5.203)

$$K_2(z) = CPC^*R_e^{-1} + C\left(I - PC^*R_e^{-1}C\right)\left(zI - A_p\right)^{-1}K_p \tag{5.223}$$

has been used again to construct the estimator.

5.4.3 ESTIMATION RESULTS AND CONCLUSIONS

A comparison of estimator design parameters shows the core concept of $\mathcal{H}^\infty$ estimation: By introducing an upper bound γ, a more conservative estimator is designed. Thus, by lowering γ, estimator parameters (P, R_e, K_p) rise, which is in accordance with the elaborations of section 5.1.3. In the following, all four estimators are used to estimate the noise-free output (displacements) of the mechanical system. Then estimation error are compared.

Because stochastic processes (w, v) have been used, computed time-series $(y, \hat{s})$ can be analysed directly. For instance the averaged periodogramm[119] is an appropriate tool for raw spectrum estimation. Although this method is very useful, theoretical spectra (following state space representations) are much smoother. Nevertheless, all raw and theoretical spectra and Gramian matrices have been compared and are transparently related.
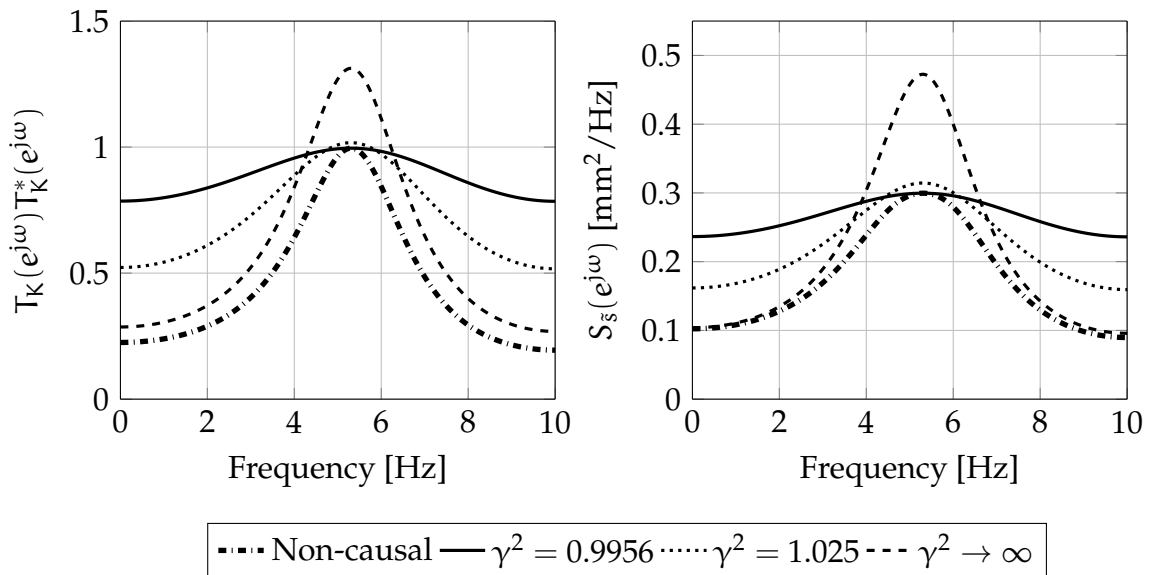
Figure 5.20: Estimation Error

On the left of figure 5.20 the theoretical estimation error $T_K(e^{j\theta})T_K^*(e^{j\theta})$ of equation (5.148) is shown for all four estimation cases. As was expected, the non-causal estimator outperforms the other ones. Furthermore, the Wiener-Kalman filter ($\gamma \to \infty$) clearly is a least-mean-squares estimator, because it has a very low area below $T_K(e^{j\theta})T_K^*(e^{j\theta})$.

Especially the first central $\mathcal{H}^\infty$ estimator has an increased total area. Nevertheless, the estimation error peak (nearby the natural frequency of the mechanical system) is bounded for both central $\mathcal{H}^\infty$ estimators. This estimation error bounding is the core

functionality of $\mathcal{H}^\infty$ theory. Based on these theoretical estimation errors, the real one is interesting. For that, the estimation error spectrum

$$S_{\tilde{s}}(e^{j\theta}) = T_K(e^{j\theta}) \left\langle \begin{bmatrix} w_k \\ v_k \end{bmatrix}, \begin{bmatrix} w_k \\ v_k \end{bmatrix} \right\rangle T_K^*(e^{j\theta}) = T_K(e^{j\theta}) \begin{bmatrix} Q_{\text{true}} & S_{\text{true}} \\ S_{\text{true}}^* & R_{\text{true}} \end{bmatrix} T_K^*(e^{j\theta}) \qquad (5.224)$$

is additionally computed and depicted in figure 5.20. These spectra are in general non-determinable by the estimator designer, because true Gramians $(Q_{\text{true}}, R_{\text{true}}, S_{\text{true}})$ are still unknown. However, the knowledge of the real estimation error spectra seems to be unnecessary, because its principal form is very similar to $T_K(e^{j\theta})T_K^*(e^{j\theta})$.

Finally, a comparison of the average process power of estimation error $\tilde{s}$ is analysed with the help of Gramian $R_{\tilde{s}}(0) = \langle \tilde{s}_k, \tilde{s}_k \rangle$. To determine theoretical Gramians, a basic (but effective) inverse Fourier transform

$$R_{\tilde{s}}(0) = \begin{cases} 2.66\text{mm}^2 : & \gamma^2 = \gamma_{\text{opt}}^2 \\ 2.25\text{mm}^2 : & \gamma^2 = 1.025 \\ 2.18\text{mm}^2 : & \gamma^2 \to \infty \end{cases} \quad \text{with} \quad R_{\tilde{s}}(0) = \frac{1}{2\pi} \int_0^{2\pi} S_{\tilde{s}}(e^{j\theta}) \, d\theta \qquad (5.225)$$

is used. These results can be seen in comparison to $R_y = \langle y_k, y_k \rangle = 4.22\text{mm}^2$. As is apparent here, the first central $\mathcal{H}^\infty$ estimator has the largest average process power of the estimation error due to the large area below $S_{\tilde{s}}(e^{j\theta})$ in figure 5.20. On the other hand, the second central $\mathcal{H}^\infty$ estimator and the Wiener-Kalman filter have similar but lower estimation error variances.

DAMAGE LOCALIZATION BY STATE PROJECTION ESTIMATION ERROR

CHAPTER OUTLINE

In this chapter the new damage localization technique state projection estimation error (SP2E) is proposed. This chapter is in part pre-published by the author.[Art1,Art2] Each article gives another viewpoint on SP2E. Furthermore, method SP2E was broadly discussed at conferences.[Proc1,Proc2]
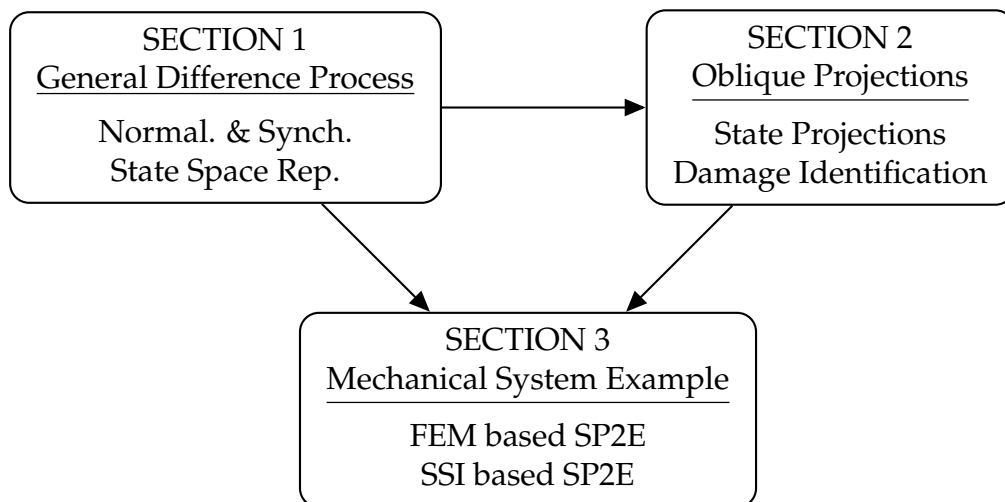
Figure 6.1: Chapter Outline

In principal, SP2E is based on a difference process d, which is introduced in the first section. For that, $\mathcal{H}^\infty$ estimators, a generalization of Kalman filters, are suitable, because both deterministic and stochastic signals can be treated at once. Furthermore, the structural excitation can be unknown. The difference process may then be analysed for damage identification by its average process power $\bar{P}_d$. Most importantly, a difference process normalization and synchronization is discussed. Finally, a state space representation is found for advantageous average process power determination.

Afterwards, section 2 covers state projection techniques. These methods enhance the formerly described results, which leads to the average process power $\bar{P}_{d,V}$. In the end section 3 is devoted to a mechanical system example. Here, fundamentally different approaches based on first principles (e.g. finite element models, white box) and

system identification (e.g. stochastic subspace identification) are used to show the method's capability.

6.1 THE DIFFERENCE PROCESS

6.1.1 GENERAL DIFFERENCE PROCESS

According to the fundamental axioms in structural health monitoring,[53] damage identification is based on a comparison of two system states. This has already been applied on the basis of corresponding mechanical parameters in section 4.4. Therein the differences of integral quantities of mechanical systems, especially corresponding parameters rather than modal data, have been analysed. This was suitable for damage identification based on deterministic system identification. However, a difference of Markov parameters on the basis of stochastic identification is not useful. Instead the central idea is to analyse a difference process

$$d = s_j - s_i \, . \tag{6.1}$$

Here, s_i and s_j are determinable processes of a mechanical structure in two different structural states i and j. Various approaches are possible to describe s, respectively the state of a mechanical system. At this point a fundamental classification distinguishes between processes computed by white box models (e.g. finite element models, multi-body simulations) and black box models (identified state space models, ARMA models, etc.).

THE AVERAGE PROCESS POWER is an excellent approach to analyse the difference process d. Hence, Gramian matrix $R_d \in \mathbb{R}^{p \times p}$ and spectrum $S_d \in \mathbb{C}^{p \times p}$ are introduced by

$$S_d(z) = \sum_{l=-\infty}^{\infty} R_d(l) z^{-l} \quad \text{and} \quad R_d(l) = \left\langle d_{k+l}, d_k \right\rangle \, . \tag{6.2}$$

In practice a finite sequence $d = [d_k]_{k=0}^N$ must be used. The average process power can then be estimated by $R_d(0)$. According to Parseval's theorem, $R_d(0)$ may be equivalently derived in time and frequency domain with $k \in \mathbb{N}$ and $\theta \in [-\pi, \pi]$:

$$R_d(0) = \left\langle d_k, d_k \right\rangle = \frac{1}{N+1} \sum_{k=0}^{N} d_k d_k^T = \frac{1}{2\pi} \int_0^{2\pi} S_d(z) \, d\theta \quad \text{with} \quad z = e^{j\theta} \, . \tag{6.3}$$

6.1.2 PARAMETRIZATION OF A MECHANICAL STRUCTURE

There are several approaches to parametrize a mechanical structure, which then leads to the required process s. At one hand, first principle based models, for example equation (3.7) of chapter 3, can be used. On the other hand, system identification techniques lead to numerically identified systems, for instance equation (4.40).

To allow a possible real-time structural damage identification technique, an approach based on stochastic subspace identification is advantageous, because generally valid models (state space models) with low complexity (and thus low model order) may be automatically determined based on measurements only. Furthermore, elaborate test loads can be omitted. Although a finite element based approach can also be used to parametrize H, the identification approach is undertaken below. For that, state space equation (4.40) is presupposed, which is briefly depicted in figure 6.2:

$$x_{k+1} = Ax_k + \begin{bmatrix} I & 0 \end{bmatrix} \begin{bmatrix} w_k \\ v_k \end{bmatrix} = Ax_k + w_k \tag{6.4a}$$

$$y_k = Cx_k + \begin{bmatrix} 0 & I \end{bmatrix} \begin{bmatrix} w_k \\ v_k \end{bmatrix} = Cx_k + v_k \; . \tag{6.4b}$$
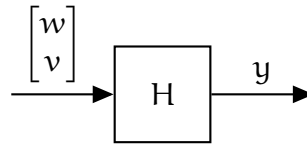
Figure 6.2: Model of Mechanical Structure

STOCHASTIC SUBSPACE IDENTIFICATION   has been elaborated in chapter 4. In the following, a short recap is given: Based on measurements y only (e.g. accelerations at bridges, towers, etc.) stochastic subspace identification can be derived covariance based and data driven. Especially the covariance based approach presupposes an ergodic, stationary process y. Thus, covariance matrix function $R_y \in \mathbb{R}^{p \times p}$ and spectrum $S_y \in \mathbb{C}^{p \times p}$ arise with

$$S_y(z) = \sum_{l=-\infty}^{\infty} R_y(l) z^{-l} \quad \text{and} \quad R_y(l) = \langle y_{k+l}, y_k \rangle \; . \tag{6.5}$$

These measurements are parametrized with the help of state space system $H(A, C)$. This model is determined by system identification techniques. Its parameters are $A \in \mathbb{C}^{n \times n}$ and $C \in \mathbb{C}^{p \times n}$. Here, n is the number of states and p the number of measured signals, thus $x \in \mathbb{C}^n$ and $y \in \mathbb{R}^p$. Modelled by process noise $w \in \mathbb{C}^n$, the mechanical system is excited by wind, traffic, waves and so forth. Nevertheless,

measurement noise $v \in \mathbb{R}^p$ (e.g. static noise, quantizing noise) must be considered and both noise disturbances w and v are presumed as white noise processes.[19, 20] Because a state space form has been used, the z-domain equivalent can easily be given by rearranging the central system parameters A and C to

$$y(z) = \sum_{k=-\infty}^{\infty} y_k z^{-k} = H(z) \begin{bmatrix} w(z) \\ v(z) \end{bmatrix}, \quad H(z) = \begin{bmatrix} H_w(z) & I \end{bmatrix} = \begin{bmatrix} C(zI - A)^{-1} & I \end{bmatrix}. \quad (6.6)$$

Following the covariance based approach the identification of A and C essentially follows the parametrization of spectrum S_y and covariance function R_y by analysing a spectral factorization

$$S_y(z) = H(z)MH^*(z^{-*}) \quad \text{with} \quad M = \left\langle \begin{bmatrix} w_k \\ v_k \end{bmatrix}, \begin{bmatrix} w_k \\ v_k \end{bmatrix} \right\rangle = \begin{bmatrix} Q & S \\ S^* & R_v \end{bmatrix}. \quad (6.7)$$

In large-scale experiments noise processes w and v are unknown. Following that, the equivalence class of input Gramians[20]

$$M(\Pi_x) = \begin{bmatrix} Q & S \\ S^* & R_v \end{bmatrix} = \begin{bmatrix} \Pi_x - A\Pi_x A^* & N - A\Pi_x C^* \\ N^* - C\Pi_x A^* & R_y(0) - C\Pi_x C^* \end{bmatrix} \quad (6.8)$$

defines an infinite number of possible states x, which all lead to the identical spectrum S_y. Thus, states x may have no physical meaning in the frame of stochastic subspace identification. Nevertheless, Gramian matrices Q and $\Pi_x \in \mathbb{C}^{n \times n}$ are related by a Lyapunov equation

$$\Pi_x = \langle x_k, x_k \rangle = A\Pi_x A^* + Q. \quad (6.9)$$

Unfortunately, the identified system H is incapable of determining a process s, which is needed for equation (6.1). However, estimation theory allows an approach for that.

ESTIMATION THEORY   is, among others, devoted to the determination of a general signal s under certain constraints, which was excessively discussed in chapter 5. Generally, a weighting matrix L is introduced to define a theoretical signal $s_k = Lx_k$. By estimating this signal, for instance by $\hat{s}_k = L\hat{x}_k$, the central criterion of $\mathcal{H}^\infty$ estimation is defined by applying the general estimation error $\tilde{s}_k = s_k - \hat{s}_k$:[121]

$$\|T_K\|_{\mathcal{H}^\infty} = \sup_\theta \sigma_{max}\left(T_K(e^{j\theta})\right) < \gamma, \quad \lim_{N \to \infty} \frac{\sum_{k=0}^{N-1} \|\tilde{s}_k\|_2^2}{\sum_{k=0}^{N-1} \left(\|w_k\|_2^2 + \|v_k\|_2^2\right)} < \gamma^2. \quad (6.10)$$

In this equation the origin of name is apparent by the infinity $\mathcal{H}^\infty$ norm, which can be computed by the greatest singular value of transfer matrices $T_K(e^{j\theta})$ with $\theta \in [-\pi, \pi]$. Therein, T_K is a system, which maps w and v to $\tilde{s}$. The right side of equation (6.10) is a time domain equivalent, which describes the relation between w and v to $\tilde{s}$. Here,

the initial state is zero. Bounded by a user defined upper value γ, both criteria take noise uncertainties into account.[78] This is very advantageous, because real world noise processes w and v are still unknown.

It is very important to note that the case of $\gamma \to \infty$ leads to the classical Kalman filter, which in result is a least-mean-squares estimator. For that, it is common to solve Riccati equation (5.137). Unfortunately, the named Riccati equation often is not solvable, because of inaccuracies in the measurement and identification process of real large-scale structures. To be solvable, several criteria (stability, observability, controllability and positivity) must be maintained.[36] Although stabilization methods have been defined,[36,37] a useful solution may be questionable for a physical interpretation. Besides the described numerical issues, uncertainties must be considered for estimator derivations, which is not possible by Kalman filtering, but an $\mathcal{H}^\infty$ approach.

To solve the $\mathcal{H}^\infty$ estimation problem, the indefinite quadratic estimation theory[78] can be used. Following this theory, all signals are treated uniformly. Thus, deterministic and stochastic approaches are unified, which is (among others) applied by dealing with Gramian matrices. It proposes a solution, which is equivalent to the classical Kalman-Yakubovich-Popov (KYP) lemma, in z-domain

$$S_y(z) = \Pi(z)R_e\Pi^*(z^{-*}) \quad \text{with} \quad \Pi(z) = C(zI - A)^{-1}K_p + I, \quad R_e = \langle e_k, e_k \rangle . \quad (6.11)$$

System Π is an important element of estimation theory. Again, a time-domain equivalent can easily be given by

$$\hat{x}_{k+1} = A\hat{x}_k + K_p e_k \quad (6.12a)$$

$$y_k = C\hat{x}_k + e_k = \hat{y}_k + e_k . \quad (6.12b)$$

This general case $\Pi(A, K_p, C)$ usually is found with the special case of central solution (5.193) for which the Riccati solution P of equation (5.166) is relevant. The named Riccati equation can be solved differently, but most commonly a generalized Schur form of a generalized symplectic pencil is applied.[34] Then gain $K_p \to K_{py}$ can be computed following equation (5.182), which leads to system Π in figure 6.3.

Figure 6.3: System Π

It is advantageous because its inverse in time-domain

$$\hat{x}_{k+1} = A_p\hat{x}_k + K_p y_k \quad (6.13a)$$

$$e_k = -C\hat{x}_k + y_k = -\hat{y}_k + y_k \quad (6.13b)$$

and its z-domain equivalent are directly determinable:

$$e(z) = \Pi^{-1}(z)y(z), \quad \text{with} \quad \Pi^{-1}(z) = -C(zI - A_p)^{-1}K_p + I . \quad (6.14)$$

To be computable, weighting matrix L must be defined, which is non-relevant in the Kalman filtering case.[121] For mechanical structures the 'filtering signals in additive noise' approach of section 5.3 is important, which applies $L = C$. Hence, $\hat{s}_k = \hat{y}_k = C\hat{x}_k$ follows and a uniform upper bound $\gamma = 1$ can be applied according to equation (5.202). In the following, an approach is chosen for which the estimate $\hat{s}$ is chosen for equation (6.1):

$$\hat{s}_k = \hat{y}_k = C\hat{x}_k \quad \text{with} \quad \hat{x}_{k+1} = A_p\hat{x}_k + K_p y_k. \tag{6.15}$$

6.1.3 SYNCHRONIZATION AND NORMALIZATION

The section above covered the parametrization of Π based on measurements y, which led to an estimate $\hat{s}$ for equation (6.1). Now, consider the successive identification of Π_i over days, weeks and so on (denoted by i), which is depicted in figure 6.4. Here, the $\mathcal{H}^2$ norm has been used as a measure of identified Π_i, which may be defined differently.
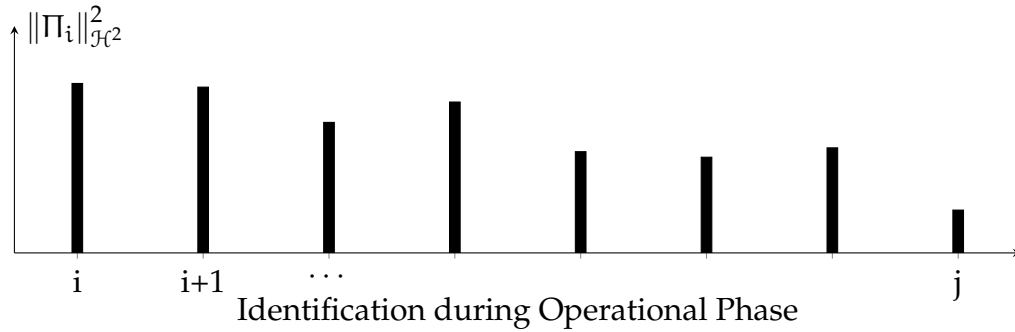
Figure 6.4: Schematical Identification of Estimators Π during the Lifetime of a Mechanical Structure

Structural health monitoring systems must be able to distinguish between an undamaged and a damaged structural state. Thus, index i and j are defined: Index 1) reference and index 2) potentially damaged structural state. Consequentially, in reference state (calibration of monitoring system) measurement y_1 has been measured to identify H_1 and determine an $\mathcal{H}^\infty$ estimator Π_1. In opposite to that, H_2 and Π_2 are determined in a potentially damaged structural state of the mechanical system. Finally, the estimate $\hat{s}_1$ follows Π_1 and $\hat{s}_2$ is in accordance with Π_2.

To analyse the difference process d, index 3) 'theoretical analysis state' is introduced. It refers to a general input signal y_3, which is applied to Π_1^{-1} and Π_2^{-1} to determine $\hat{s}_1$ and $\hat{s}_2$ respectively:

$$d_k = -\hat{s}_{1,k} + \hat{s}_{2,k} = -\hat{y}_{1,k} + \hat{y}_{2,k}. \tag{6.16}$$

By using process y_3, synchronization and normalization of both processes $\hat{s}_1$ and $\hat{s}_2$ is achieved, which will be subsequently explained. Because the estimate $\hat{s} = \hat{y}$ has been used following the 'filtering signals in additive noise' approach, the former equation is equivalent to a difference of estimation error because

$$d_k = -\hat{y}_{1,k} + \hat{y}_{2,k} = \left(y_{3,k} - \hat{y}_{1,k}\right) - \left(y_{3,k} - \hat{y}_{2,k}\right) = e_{1,k} - e_{2,k} \,. \qquad (6.17)$$

Here, a z-domain equivalent can directly be given with

$$d(z) = \sum_{k=-\infty}^{\infty} d_k z^{-k} = e_1(z) - e_2(z) \,. \qquad (6.18)$$

Because a general input process y_3 has been used, $\mathcal{H}^\infty$ estimators are advantageous here: (i) Noise processes w and v are unknown, for example at bridges, offshore wind energy plants, airplanes, and so forth. (ii) Input y_3 is, so far, undefined (an approach for that is given in section 6.2.1). In summary, both arguments emphasize the consideration of noise and model uncertainties. Hence, $\mathcal{H}^\infty$ estimators are an appropriate choice.

Yan et al.[77] proposed a damage detection technique based on the Kalman filter and a novelty index of estimation error. Essentially, the novelty index is a weighted 2-norm of the estimation error. It is interesting to note that this technique can be derived from equation (6.17) with $\gamma \to \infty$, $y_3 = y_2$ and $e_2 = 0$. Following Yan et al. the novelty index, respectively the weighted 2-norm of estimation error e_1, rises if a damage occurs.

In the following, the general difference process d is analysed to define an applicable damage localization technique.

6.1.4 ADVANTAGEOUS DETERMINATION OF AVERAGE PROCESS POWER

The former statements proposed a new process d on the basis of two $\mathcal{H}^\infty$ estimators Π_1 and Π_2, which may be analysed on the basis of the average process power $R_d(0)$. Although the former definitions can directly be applied, a numerically advantageous approach is given below. Furthermore, this allows to introduce state projection techniques.

As was shown before, process d can be seen as a difference of estimates, which constitutes an observer equation

$$d_k = -\hat{y}_{1,k} + \hat{y}_{2,k} = -C_1 \hat{x}_{1,k} + C_2 \hat{x}_{2,k} = \begin{bmatrix} -C_1 & C_2 \end{bmatrix} \begin{bmatrix} \hat{x}_{1,k} \\ \hat{x}_{2,k} \end{bmatrix} \,. \qquad (6.19)$$

THUS, STATE SPACE SYSTEM Δ follows, which maps y_3 to d. This system $\Delta(A_\Delta, B_\Delta, C_\Delta)$ is shown in figure 6.5b and can be defined by

$$x_{\Delta,k+1} = \begin{bmatrix} \hat{x}_{1,k+1} \\ \hat{x}_{2,k+1} \end{bmatrix} = \begin{bmatrix} A_{p,1} & 0 \\ 0 & A_{p,2} \end{bmatrix} \begin{bmatrix} \hat{x}_{1,k} \\ \hat{x}_{2,k} \end{bmatrix} + \begin{bmatrix} K_{p,1} \\ K_{p,2} \end{bmatrix} y_{3,k} \quad = A_\Delta x_{\Delta,k} + B_\Delta y_{3,k} \quad (6.20a)$$

$$d_k = \begin{bmatrix} -C_1 & C_2 \end{bmatrix} \begin{bmatrix} \hat{x}_{1,k} \\ \hat{x}_{2,k} \end{bmatrix} \qquad\qquad = C_\Delta x_{\Delta,k}. \qquad (6.20b)$$

(a) System Ω (b) System Δ
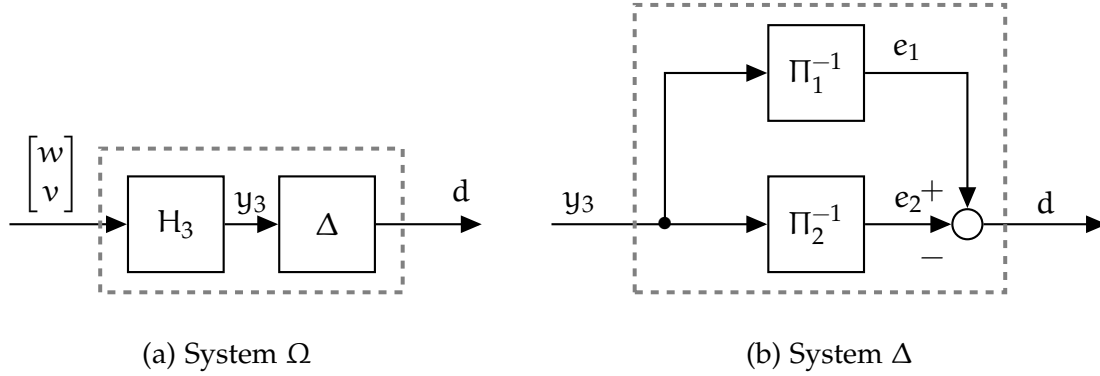
Figure 6.5: State Space Systems Ω and Δ

Essentially, model Δ can be seen as a difference of inverse estimators $\Pi_1^{-1}(A_{p,1}, K_{p,1}, C_1)$ and $\Pi_2^{-1}(A_{p,2}, K_{p,2}, C_2)$, in z-domain with

$$d(z) = \Delta(z)y_3(z) \quad \text{and} \quad \Delta(z) = \Pi_1^{-1}(z) - \Pi_2^{-1}(z) = C_\Delta (zI - A_\Delta)^{-1} B_\Delta. \qquad (6.21)$$

At this point an important element is apparent: Because input y_3 is applied to both inverse estimators uniformly, the two estimation error processes e_1 and e_2 are synchronized and normalized. Hence, they are comparable.

Spectrum $S_d(z)$ of equation (6.2) is applicable for damage identification, because it rises as $\Delta(z)$ increases. Based on state space system Δ, spectrum S_d can be determined following

$$S_d(z) = \Delta(z)S_{y3}(z)\Delta^*(z^{-*}) \quad \text{with} \quad S_{y3}(z) = H_3(z)M_3H_3^*(z^{-*}). \qquad (6.22)$$

In this equation the parametrized spectrum $S_{y3}(z)$ in accordance with equation (6.7) has been used with

$$H_3(z) = \begin{bmatrix} C_3 (zI - A_3)^{-1} & I \end{bmatrix}, \qquad M_3 = \begin{bmatrix} \Pi_{33} - A_3\Pi_{33}A_3^* & N_3 - A_3\Pi_{33}C_3^* \\ N_3^* - C_3\Pi_{33}A_3^* & R_{y3}(0) - C_3\Pi_{33}C_3^* \end{bmatrix}. \qquad (6.23)$$

The central idea is to use a smooth, identified spectrum S_{y3}, instead of a raw measured one. Thus, numerical accuracy (in the sense of damage identification) can be improved. By continuing this thought, a new state space model emerges for advantageous damage analysis.

STATE SPACE SYSTEM Ω maps standard inputs w and v, for example white noise processes, to the difference process d: If w and v are standard input processes and d shows inherent structural damage information, then structural damage can be identified more easily by analysing Ω. To derive a state space model Ω, the general input process y_3 is described here with system $H_3(A_3, C_3)$ in accordance with equation (6.22), which is depicted in figure 6.5a. By applying model $H_3(A_3, C_3)$, a state space model form for $\Omega(A_\Omega, B_\Omega, C_\Omega)$ is chosen with

$$
\begin{bmatrix} \hat{x}_{1,k+1} \\ \hat{x}_{2,k+1} \\ x_{3,k+1} \end{bmatrix} = \begin{bmatrix} A_{p,1} & 0 & K_{p,1}C_3 \\ 0 & A_{p,2} & K_{p,2}C_3 \\ 0 & 0 & A_3 \end{bmatrix} \begin{bmatrix} \hat{x}_{1,k} \\ \hat{x}_{2,k} \\ x_{3,k} \end{bmatrix} + \begin{bmatrix} 0 & K_{p,1} \\ 0 & K_{p,2} \\ I & 0 \end{bmatrix} \begin{bmatrix} w_k \\ v_k \end{bmatrix} \quad = A_\Omega x_{\Omega,k} + B_\Omega \begin{bmatrix} w_k \\ v_k \end{bmatrix}
$$

(6.24a)

$$
d_k = \begin{bmatrix} -C_1 & C_2 & 0 \end{bmatrix} \begin{bmatrix} \hat{x}_{1,k} \\ \hat{x}_{2,k} \\ x_{3,k} \end{bmatrix} \quad = C_\Omega x_{\Omega,k} .
$$

(6.24b)

Full rank of A_Ω is supposed. Furthermore, a detailed depiction of system Ω is given in figure 6.6 at the end of section 6.1. Therein projection constraints of section 6.2 are already given. Based on model Ω, spectrum S_d of equations (6.2) and (6.22) can be advanced to

$$
S_d(z) = \Omega(z)M_3\Omega^*(z^{-*}) \quad \text{with} \quad \Omega(z) = \Delta(z)H_3(z) = C_\Omega \left(zI - A_\Omega\right)^{-1} B_\Omega .
$$

(6.25)

At this point a central advantage of the approach in equation (6.17) in comparison to the method of Yan et al.[77] gets apparent: Because $d_k = e_1 - e_2$ is used instead of e_1, measurement noise v is eliminated:

$$
e_{1,k} = C_3 x_{3,k} + v_k - \hat{y}_{1,k}, \qquad e_{2,k} = C_3 x_{3,k} + v_k - \hat{y}_{2,k}
$$

(6.26a)

$$
d_k = \left(C_3 x_{3,k} + v_k - \hat{y}_{1,k}\right) - \left(C_3 x_{3,k} + v_k - \hat{y}_{2,k}\right) = -\hat{y}_{1,k} + \hat{y}_{2,k} .
$$

(6.26b)

THE AVERAGE PROCESS POWER   can efficiently be determined with the help of the former statements. As was pointed out in section 6.1.1, structural damage shall be analysed by determining the average process power $R_d(0)$. Because unknown noise disturbances w and v are presupposed as standard inputs, for example white noise processes, and state space model Ω maps those to d, system parameters $(A_\Omega, B_\Omega, C_\Omega)$ may be advantageously applied to compute $R_d(0)$ by solving a Lyapunov equation

$$
\Pi_d = \left\langle x_{\Omega,k}, x_{\Omega,k} \right\rangle = A_\Omega \Pi_d A_\Omega^* + B_\Omega M_3 B_\Omega^* .
$$

(6.27)

Therein M_3 has been used, which is a presumed Gramian matrix of disturbance processes according to equation (6.22). This leads to the required solution

$$
R_d(0) = \left\langle d_k, d_k \right\rangle = C_\Omega \Pi_d C_\Omega^* = \begin{bmatrix} -C_1 & C_2 & 0 \end{bmatrix} \begin{bmatrix} \Pi_{11} & \Pi_{12} & \Pi_{13} \\ \Pi_{21} & \Pi_{22} & \Pi_{23} \\ \Pi_{31} & \Pi_{32} & \Pi_{33} \end{bmatrix} \begin{bmatrix} -C_1^* \\ C_2^* \\ 0 \end{bmatrix}
$$

(6.28a)

$$
= \begin{bmatrix} -C_1 & C_2 \end{bmatrix} \begin{bmatrix} \Pi_{11} & \Pi_{12} \\ \Pi_{21} & \Pi_{22} \end{bmatrix} \begin{bmatrix} -C_1^* \\ C_2^* \end{bmatrix} .
$$

(6.28b)

Although one may work in the z-domain, the numerical integration of S_d can be omitted.

Matrix Π_{33} must be chosen here to define M_3. Nevertheless, its choice has no influence on $(\Pi_{11}, \Pi_{12}, \Pi_{21}, \Pi_{22})$ and thus on $R_d(0)$. Therefore, $\Pi_{33} = 0$ is a reasonable choice in agreement with stochastic subspace identification.

Finally, the principal diagonal of $R_d(0)$ is referred to as $\bar{P}_d \in \mathbb{R}^p$, whose elements are the average process power of d at each measurement position. The vector $\bar{P}_d$ can be applied for damage identification, which is elaborated below.

6.1.5 Damage Localization

The connection between structural damage and the difference process d in general is evident, as it is an indirect comparison of two identified systems, which represent the measurement at a mechanical structure in its reference and potentially altered state. To show the capability of d for damage localization, two fundamental different lines of arguments are subsequently discussed: At first a system-theoretic, and thus very general, approach is given. Afterwards, the second order differential equation (3.2) based argument leads to a mechanical understanding, but with the cost of simplifying presumptions. Because both arguments have advantages and disadvantages, none of both is preferable.

THE SYSTEM-THEORETIC APPROACH   begins with a very important presumption: According to de Boe and Golinval,[135] a small structural alteration of a mechanical system (monitored by a sensor array) is primarily observable at those sensors, which are in the vicinity of the damaged structural element. Based on that, de Boe and Golinval used the sensor validation technique of Friswell and Inman[136] to determine the subset of virtually damaged sensors, respectively the damaged substructure.

This technique is interesting, because more recent research by Kulla[137] showed a method to distinguish between identified faults from environmental and operational conditions (e.g. temperature), sensor faults and actual structural damage.

The named sensor validation technique for structural health monitoring systems usually is based on measurements only.[138] Because it is based on applied projections of those measurements, the method is numerically stable, but may be imprecise. More accurate results are computable by using model-based techniques. Here, the conducted research on fault identification and isolation (FDI) offers several possible approaches, for example Kalman filter and $\mathcal{H}^\infty$ estimator based fault isolation.[139, 140] A comprehensive overview of FDI can be found in Hwang et al.[141]

Both fault detection and isolation approaches, the data-based and the model-based, define a residual

$$e_1 = y_2 - \hat{y}_1, \tag{6.29}$$

following a measurement of the potentially altered state y_2 and an estimate based on it. This estimate follows determined properties of the reference state, thus it is denoted by $\hat{y}_1$. Here, the introduced notation of section 6.1.3 has been continued. Nevertheless, $y_3 \to y_2$ is presumed for simplicity.

In general, there are methods to allow fault isolation, and thus damage localization, based on e_1, for example by applying Beard's method[142] or others. Nevertheless, the derived null-space based fault detection[77,90,143,144] leads to damage localization only, if mechanical parameters are introduced. This may follow the definition of e_1 in equation (5.24):

$$e_{1,k} = (C_2 x_{2,k} + v_k) - C_1 \hat{x}_{1,k} = -C_1 \bar{x}_{1,k} + C_\Delta x_{2,k} + v_k \qquad (6.30a)$$

$$\text{with} \quad \bar{x}_{1,k} = \hat{x}_{1,k} - x_{2,k} \quad \text{and} \quad C_\Delta = C_2 - C_1 \quad \text{for} \quad n_1 = n_2 . \qquad (6.30b)$$

Of course, a measure of e_1 leads to nowhere, as it mainly consists of measurement noise v, if a small structural alteration is present. Thus, it is very reasonable to replace $y_2 \to \hat{y}_2$, which leads to difference process d in equation (6.16).

Secondly, residuum e_1 is typically determined by a Kalman filtering approach, which is not able to cope with noise and model uncertainties. Because system alterations are the important property to be found, this can lead to estimation errors. Here, the application of $\mathcal{H}^\infty$ estimation leads to appropriate results,[141] as was already pointed out in section 6.1.3.

In summary, the difference process d, following two $\mathcal{H}^\infty$ estimators, is a vastly improvement of residuum e_1. An analysis of its average process power indicates structural damage.

THE MECHANICAL PARAMETER BASED ARGUMENT is a fundamental different approach than was shown before, and it follows the second order differential equation (3.2). Here, the basic idea is to analyse the result by using (K_1, M_1, D_1) and (K_2, M_2, D_2) on the cost of vast presumptions. Afterwards, the special case of mechanical parameter based systems is generalized.

For a moment consider two linear, continuous-time state space systems $G_1(K_1, M_1, D_1)$ and $G_2(K_2, M_2, D_2)$ of equations (3.7a) and (3.9) with a uniform system order $n_1 = n_2 = 2N$. Both continuous-time systems are restructured as discrete-time ones by zero order hold, and are used to determine $\mathcal{H}^\infty$ estimators Π_1 and Π_2. This then leads to a difference process

$$d_k = -\hat{y}_{1,k} + \hat{y}_{2,k} = -C_1 \hat{x}_{1,k} + C_2 \hat{x}_{2,k} = \left(-C_1 \bar{x}_{1,k} + C_2 \bar{x}_{2,k} \right) + C_\Delta x_{3,k} \qquad (6.31a)$$

$$\text{with} \quad \bar{x}_{1,k} = \hat{x}_{1,k} - x_{3,k}, \quad \bar{x}_{2,k} = \hat{x}_{2,k} - x_{3,k} \quad \text{and} \quad C_\Delta = C_2 - C_1 . \qquad (6.31b)$$

Essentially d is the sum of processes $(-C_1\bar{x}_1, C_2\bar{x}_2)$ and $C_\Delta x_3$. Especially the later one is important and is analysed in more detail below. In view of zero order hold of equation (3.15), both discrete-time observer matrices are defined by

$$C_1 = -M_1^{-1} \begin{bmatrix} K_1 & D_1 \end{bmatrix} \quad \text{and} \quad C_2 = -M_2^{-1} \begin{bmatrix} K_2 & D_2 \end{bmatrix} . \qquad (6.32)$$

This allows to define C_Δ. For that matter, the cases of mass and stiffness alterations are considered:

- MASS ALTERATION with $\tilde{M} = M_1^{-1} - M_2^{-1} > 0$ and $K_\Delta = K_1 - K_2 = 0$:

$$C_\Delta = M_1^{-1} \begin{bmatrix} K & D \end{bmatrix} - M_2^{-1} \begin{bmatrix} K & D \end{bmatrix} \qquad = \tilde{M} \begin{bmatrix} K & D \end{bmatrix} . \qquad (6.33)$$

- STIFFNESS ALTERATION with $\tilde{M} = M_1^{-1} - M_2^{-1} = 0$ and $K_\Delta = K_1 - K_2 \neq 0$:

$$C_\Delta = M^{-1} \begin{bmatrix} K_1 & D \end{bmatrix} - M^{-1} \begin{bmatrix} K_2 & D \end{bmatrix} \qquad = M^{-1} \begin{bmatrix} K_\Delta & 0 \end{bmatrix} . \qquad (6.34)$$

As can clearly be seen, an alteration of mass M or stiffness K leads to an increase of C_Δ, while a damping variation is considered to be negligible. Hence, an alteration of element (i, i) in M or K leads to an increase of row vector i in C_Δ, and thus increases element i in the average process power $\bar{P}_d$.

The above discussion is based on the special case of mechanical parameter based systems, which for instance are determined by finite element models (FEM). For an automated structural health monitoring system the usage of finite element models is elaborated, as was pointed out in the introduction in section 1.2. On the other side, identification techniques lead to general system descriptions with possible non-physical system states. Furthermore, stochastic identification techniques are unable to determine a physical gain matrix. Thus, mechanical parameters (K, M, D) are non-determinable on the basis of measurements y only.

Three issues follow from the above discussion:

(i) Difference process d should be reduced to its damage identification core, namely $C_\Delta x_3$,

(ii) The usage of a general system descriptions is desirable and

(iii) The presumption of model orders $n_1 = n_2$ must be relaxed.

Therefore, state projections are subsequently applied, as those are an ideal approach for named the issues above.
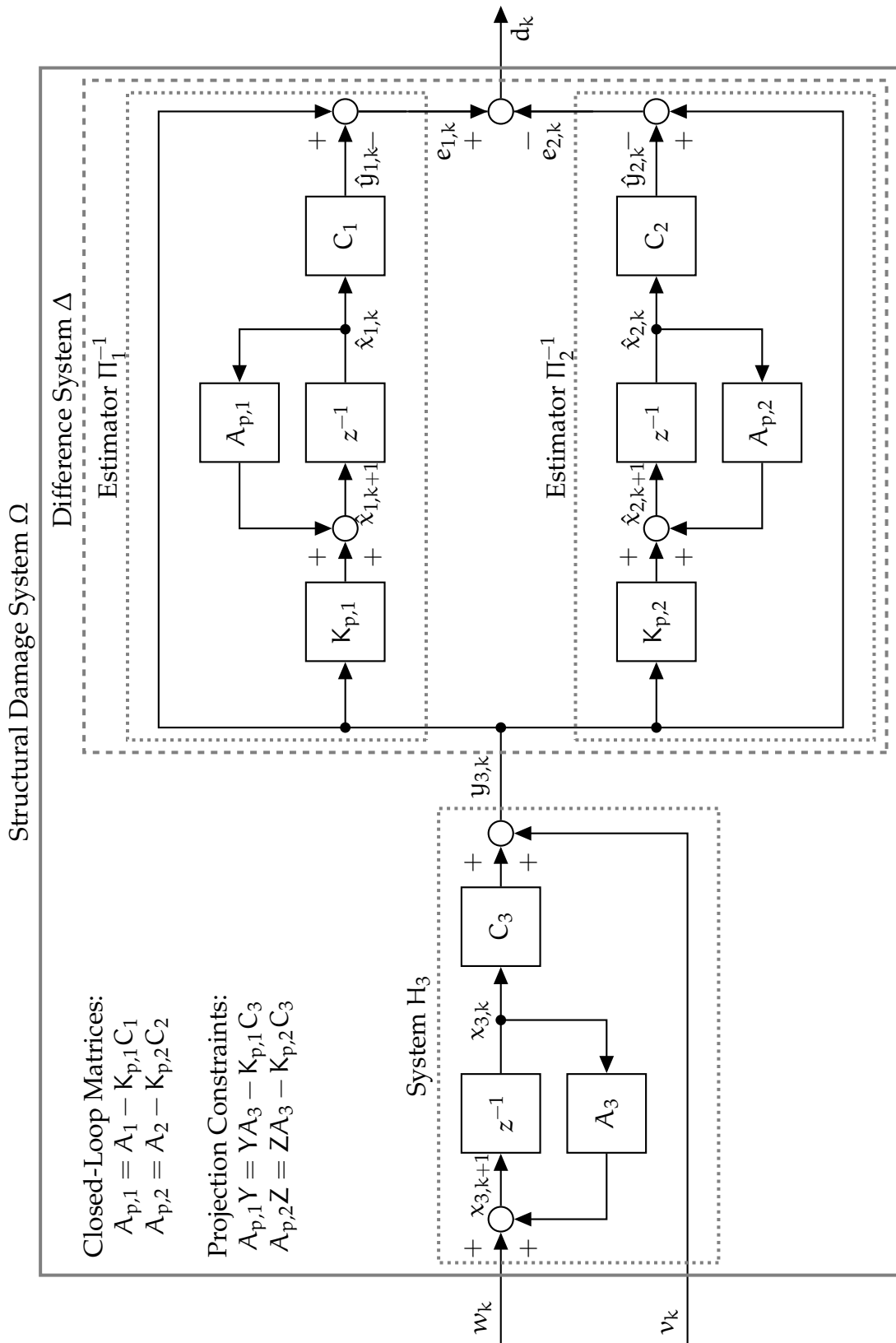
Figure 6.6: Structural Error System Ω

6.2 STATE PROJECTION ESTIMATION ERROR (SP2E) FOR DAMAGE LOCALIZATION

6.2.1 COMPLEMENTARY SUBSPACES AND OBLIQUE PROJECTIONS

While the average process power $R_d(0)$ of equation (6.28) can be applied to identify structural damage, it is enhanced in this section by projection techniques to suppress numerical noise.

Basically, y_3 is a test signal which is applied to Δ in equation (6.20). Hence, it can be understood as an approach for synchronization and normalization. Its response d must be in accordance with its input y_3. In the following, a projection approach is described, which takes advantage of this fact.

SUBSPACES OF A_Ω reveal essential parts of x_Ω. Because process d follows the product of observer matrix C_Ω and states x_Ω in equation (6.24), the subspaces of these states are studied below. Hence, an eigenvalue decomposition

$$A_\Omega = X\Lambda X^{-1} = \sum_{i=1}^{3} X_i \Lambda_i \bar{X}_i \quad \text{with} \quad X = \begin{bmatrix} X_1 & X_2 & X_3 \end{bmatrix} = \begin{bmatrix} X_{11} & 0 & X_{13} \\ 0 & X_{22} & X_{23} \\ 0 & 0 & X_{33} \end{bmatrix} \quad (6.35)$$

is applied. At this point a reasonable form of matrix X has been chosen, which is explained in the following: A_Ω is an upper block diagonal matrix, which is important to note. At first eigenvectors and eigenvalues of the principal block diagonal are constituted to be known and are denoted by

$$A_{p,1}X_{11} = X_{11}\Lambda_1, \quad A_{p,2}X_{22} = X_{22}\Lambda_2 \quad \text{and} \quad A_3 X_{33} = X_{33}\Lambda_3 . \quad (6.36)$$

Here, all three matrices $A_{p,1}$, $A_{p,2}$ and A_3 have full rank. If diagonal matrices Λ_1 and Λ_2 are eigenvalues of $A_{p,1}$ and $A_{p,2}$ respectively, then they must be eigenvalues of the whole matrix A_Ω. For that, corresponding eigenvectors are augmented with zeros:

$$\begin{bmatrix} A_{p,1} & 0 & K_{p,1}C_3 \\ 0 & A_{p,2} & K_{p,2}C_3 \\ 0 & 0 & A_3 \end{bmatrix} \begin{bmatrix} X_{11} \\ 0 \\ 0 \end{bmatrix} = \begin{bmatrix} A_{p,1}X_{11} \\ 0 \\ 0 \end{bmatrix} = \begin{bmatrix} X_{11} \\ 0 \\ 0 \end{bmatrix} \Lambda_1 \quad (6.37a)$$

$$\begin{bmatrix} A_{p,1} & 0 & K_{p,1}C_3 \\ 0 & A_{p,2} & K_{p,2}C_3 \\ 0 & 0 & A_3 \end{bmatrix} \begin{bmatrix} 0 \\ X_{22} \\ 0 \end{bmatrix} = \begin{bmatrix} 0 \\ A_{p,2}X_{22} \\ 0 \end{bmatrix} = \begin{bmatrix} 0 \\ X_{22} \\ 0 \end{bmatrix} \Lambda_2 . \quad (6.37b)$$

Furthermore, diagonal matrix Λ_3 gives eigenvalues of A_3 with eigenvectors X_{33}. Because A_Ω is not a block diagonal matrix, the above argument can not be repeated here in view of

$$\begin{bmatrix} A_{p,1} & 0 & K_{p,1}C_3 \\ 0 & A_{p,2} & K_{p,2}C_3 \\ 0 & 0 & A_3 \end{bmatrix} \begin{bmatrix} X_{13} \\ X_{23} \\ X_{33} \end{bmatrix} = \begin{bmatrix} A_{p,1}X_{13} + K_{p,1}C_3 X_{33} \\ A_{p,2}X_{23} + K_{p,2}C_3 X_{33} \\ A_3 X_{33} \end{bmatrix} = \begin{bmatrix} X_{13} \\ X_{23} \\ X_{33} \end{bmatrix} \Lambda_3 . \quad (6.38)$$

If X_{13} and X_{23} are zero matrices, eigenvectors in X_{33} are zero too, which is a trivial but useless case. Thus, X_{13} and X_{23} must be introduced.

However, the lower block row gives the searched argument in the above equation: If the principal diagonal of Λ_3 are eigenvalues of A_3, then those are also eigenvalues of A_Ω. Nevertheless, additional constraints must be fulfilled, which will subsequently be explained. In summary, sub blocks of eigenvectors in X have been determined.

THE INVERSION of eigenvector block matrix X directly follows the Schur complement. By defining a positive definite matrix

$$M = \begin{bmatrix} A & B \\ C & D \end{bmatrix} = X = \begin{bmatrix} \begin{bmatrix} X_{11} & 0 \\ 0 & X_{22} \end{bmatrix} & \begin{bmatrix} X_{13} \\ X_{23} \end{bmatrix} \\ \begin{bmatrix} 0 & 0 \end{bmatrix} & \begin{bmatrix} X_{33} \end{bmatrix} \end{bmatrix} \quad \text{with} \quad MM^{-1} = I, \qquad (6.39)$$

the general 3×3 block inverse can directly be given with

$$M^{-1} = \begin{bmatrix} (A - BD^{-1}C)^{-1} & -(A - BD^{-1}C)^{-1}BD^{-1} \\ -D^{-1}C(A - BD^{-1}C)^{-1} & D^{-1} + D^{-1}C(A - BD^{-1}C)^{-1}BD^{-1} \end{bmatrix}. \qquad (6.40)$$

This leads to the inverse

$$X^{-1} = \begin{bmatrix} \bar{X}_1 \\ \bar{X}_2 \\ \bar{X}_3 \end{bmatrix} = \begin{bmatrix} X_{11}^{-1} & 0 & -X_{11}^{-1}Y \\ 0 & X_{22}^{-1} & -X_{22}^{-1}Z \\ 0 & 0 & X_{33}^{-1} \end{bmatrix} \quad \text{with} \quad Y = X_{13}X_{33}^{-1}, \quad Z = X_{23}X_{33}^{-1}. \qquad (6.41)$$

By multiplying both first block rows of equation (6.38) with X_{33}^{-1} from right, projection constraints

$$YA_3 = A_{p,1}Y + K_{p,1}C_3 \quad \text{and} \quad ZA_3 = A_{p,2}Z + K_{p,2}C_3 \qquad (6.42)$$

arise. In view of the closed-loop system matrix definitions

$$A_1 = A_{p,1} + K_{p,1}C_1 \quad \text{and} \quad A_2 = A_{p,2} + K_{p,2}C_2, \qquad (6.43)$$

one may then conclude the following:

$$H_3(A_3, C_3) = \begin{cases} H_1(A_1, C_1) \longrightarrow Y = I \\ H_2(A_2, C_2) \longrightarrow Z = I \end{cases}. \qquad (6.44)$$

In summary, parameters Y and Z are easy determinable for special cases of $H_3(A_3, C_3)$. Thus, an appropriate choice for H_3 is the potentially damaged state H_2, because signals y_2 are measurable at the moment of analysis. These signals can be applied in equation (6.20), which can allow a real-time damage identification. However, real-time applications are beyond the scope of this thesis.

COMPLEMENTARY SUBSPACES are a central element of subsequently applied projection techniques. They are denoted by $\mathcal{U} \cap \mathcal{V} = 0$ and refer to the direct sum $\mathcal{W} = \mathcal{U} \oplus \mathcal{V}$.[104] This is applied to analyse the column space of A_Ω, which is noted by $\mathcal{W}$. Then complementary subspaces $\mathcal{U}$ and $\mathcal{V}$ are defined by

$$\mathcal{W} = \mathcal{U}_1 \oplus \mathcal{U}_2 \oplus \mathcal{V} \quad \text{and} \quad \mathcal{U}_1 = \text{span}(X_1), \ \mathcal{U}_2 = \text{span}(X_2), \ \mathcal{V} = \text{span}(X_3) . \tag{6.45}$$

In general, oblique projectors are determined by U and V, whose columns are a basis for $\mathcal{U}$ and $\mathcal{V}$ respectively:[104]

$$P_U = \begin{bmatrix} U \,|\, 0 \end{bmatrix} \begin{bmatrix} U & V \end{bmatrix}^{-1}, \qquad P_V = I - P_U = \begin{bmatrix} 0 \,|\, V \end{bmatrix} \begin{bmatrix} U & V \end{bmatrix}^{-1} . \tag{6.46}$$

Here, P_U is a projector onto $\mathcal{U}$ along $\mathcal{V}$, while the complementary one P_V projects onto $\mathcal{V}$ along $\mathcal{U}$. Now, by applying subspaces of A_Ω with

$$\begin{bmatrix} U \,|\, V \end{bmatrix} = X = \begin{bmatrix} X_1 & X_2 \,|\, X_3 \end{bmatrix} \quad \text{and} \quad \begin{bmatrix} U & V \end{bmatrix}^{-1} = X^{-1} , \tag{6.47}$$

projectors are derived following equation (6.46). These projectors must be idempotent and $P_U + P_V = I$.[104]

By applying the results for X and its inverse of equations (6.35) and (6.41), spectral projectors P arise. Now, projectors are derived following equation (6.46):

$$P_U = X_1 \bar{X}_1 + X_2 \bar{X}_2 = \begin{bmatrix} X_{11} & 0 \\ 0 & X_{22} \\ 0 & 0 \end{bmatrix} \begin{bmatrix} X_{11}^{-1} & 0 & -X_{11}^{-1}Y \\ 0 & X_{22}^{-1} & -X_{22}^{-1}Z \end{bmatrix} = \begin{bmatrix} I & 0 & -Y \\ 0 & I & -Z \\ 0 & 0 & 0 \end{bmatrix} \tag{6.48a}$$

$$P_V = X_3 \bar{X}_3 = \begin{bmatrix} X_{13} \\ X_{23} \\ X_{33} \end{bmatrix} \begin{bmatrix} 0 & 0 & X_{33}^{-1} \end{bmatrix} = \begin{bmatrix} 0 & 0 & Y \\ 0 & 0 & Z \\ 0 & 0 & I \end{bmatrix} . \tag{6.48b}$$

These projectors allow system matrix projections

$$P_U A_\Omega = \sum_{i=1}^{2} X_i \Lambda_i \bar{X}_i = \begin{bmatrix} A_{p,1} & 0 & -A_{p,1}Y \\ 0 & A_{p,2} & -A_{p,2}Z \\ 0 & 0 & 0 \end{bmatrix}, \quad P_V A_\Omega = X_3 \Lambda_3 \bar{X}_3 = \begin{bmatrix} 0 & 0 & YA_3 \\ 0 & 0 & ZA_3 \\ 0 & 0 & A_3 \end{bmatrix} . \tag{6.49}$$

At this point the projection constraints of equation (6.42) can be seen because $A_\Omega = P_U A_\Omega + P_V A_\Omega$.

6.2.2 STATE PROJECTIONS

The idea is to determine the damage relevant part in d, which follows x_Ω. Hence, the determined projectors P_U and P_V are applied to study essential elements of the state vector. A graphical representation of these elements is given in figure 6.7:

$$x_{U,k} = P_U x_{\Omega,k} = \begin{bmatrix} I & 0 & -Y \\ 0 & I & -Z \\ 0 & 0 & 0 \end{bmatrix} \begin{bmatrix} \hat{x}_{1,k} \\ \hat{x}_{2,k} \\ x_{3,k} \end{bmatrix} = \begin{bmatrix} \hat{x}_{1,k} - Y x_{3,k} \\ \hat{x}_{2,k} - Z x_{3,k} \\ 0 \end{bmatrix} = \begin{bmatrix} \tilde{x}_{1,k} \\ \tilde{x}_{2,k} \\ 0 \end{bmatrix} \tag{6.50a}$$

$$x_{V,k} = P_V x_{\Omega,k} = \begin{bmatrix} 0 & 0 & Y \\ 0 & 0 & Z \\ 0 & 0 & I \end{bmatrix} \begin{bmatrix} \hat{x}_{1,k} \\ \hat{x}_{2,k} \\ x_{3,k} \end{bmatrix} = \begin{bmatrix} Y \\ Z \\ I \end{bmatrix} x_{3,k} . \tag{6.50b}$$
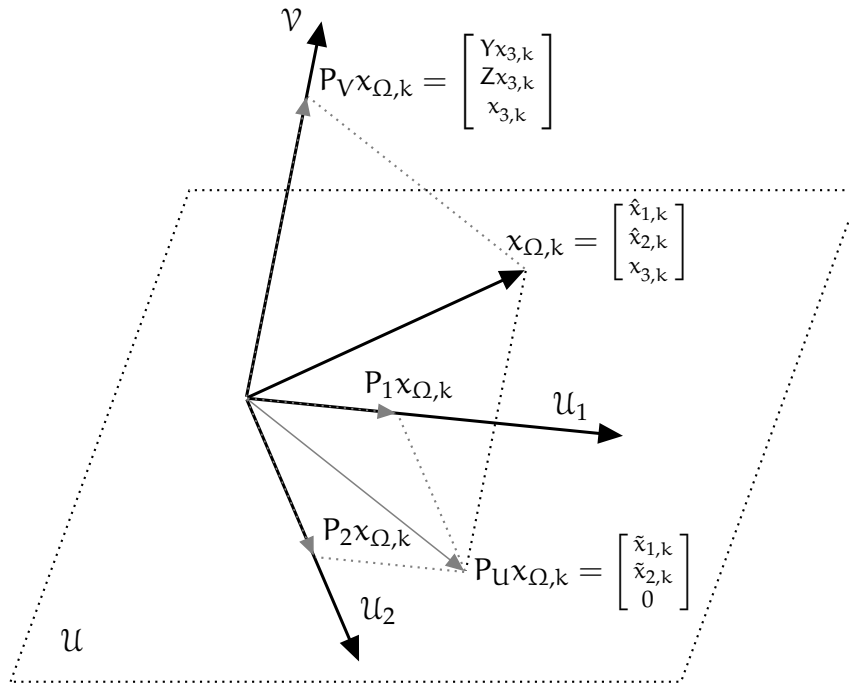
Figure 6.7: Projection of the State Vector

Because H_1, H_2 and H_3 may have different model orders, parameters Y and Z are fundamental to determine state differences $\tilde{x}_1$ and $\tilde{x}_2$. In comparison to $\bar{x}_1$ and $\bar{x}_2$ in equation (6.31), a clear improvement is observable here. Very importantly, the state differences $\tilde{x}_1$ and $\tilde{x}_2$ essentially are numerical noise, which is especially plausible for $Y = I$ or $Z = I$ according to equation (6.44).

Both processes x_U and x_V are central elements of x_Ω and are computable by applying projectors to the control equation (6.24a) of model Ω:

$$P_U x_{\Omega,k+1} = \begin{bmatrix} \tilde{x}_{1,k+1} \\ \tilde{x}_{2,k+1} \\ 0 \end{bmatrix} = \begin{bmatrix} A_{p,1} & 0 & -A_{p,1}Y \\ 0 & A_{p,2} & -A_{p,2}Z \\ 0 & 0 & 0 \end{bmatrix} \begin{bmatrix} \hat{x}_{1,k} \\ \hat{x}_{2,k} \\ x_{3,k} \end{bmatrix} + \begin{bmatrix} -Y & K_{p,1} \\ -Z & K_{p,2} \\ 0 & 0 \end{bmatrix} \begin{bmatrix} w_k \\ v_k \end{bmatrix} \quad (6.51a)$$

$$P_V x_{\Omega,k+1} = \begin{bmatrix} Y x_{3,k+1} \\ Z x_{3,k+1} \\ x_{3,k+1} \end{bmatrix} = \begin{bmatrix} 0 & 0 & YA_3 \\ 0 & 0 & ZA_3 \\ 0 & 0 & A_3 \end{bmatrix} \begin{bmatrix} \hat{x}_{1,k} \\ \hat{x}_{2,k} \\ x_{3,k} \end{bmatrix} + \begin{bmatrix} Y & 0 \\ Z & 0 \\ I & 0 \end{bmatrix} \begin{bmatrix} w_k \\ v_k \end{bmatrix} . \quad (6.51b)$$

THE ESSENTIAL PARTS OF d follow state projections of x_Ω. It thus is reasonable to deal with $d_k = d_{U,k} + d_{V,k}$ following

$$d_{U,k} = C_\Omega x_{U,k} = \begin{bmatrix} -C_1 & C_2 & 0 \end{bmatrix} \begin{bmatrix} \tilde{x}_{1,k} \\ \tilde{x}_{2,k} \\ 0 \end{bmatrix} = -C_1 \tilde{x}_{1,k} + C_2 \tilde{x}_{2,k} \quad \text{and} \quad (6.52a)$$

$$d_{V,k} = C_\Omega x_{V,k} = \begin{bmatrix} -C_1 & C_2 & 0 \end{bmatrix} \begin{bmatrix} Y \\ Z \\ I \end{bmatrix} x_{3,k} = \left(-C_1 Y + C_2 Z \right) x_{3,k} = C_T x_{3,k} . \quad (6.52b)$$

Process d_U can be interpreted as numerical noise, because it follows x_U. On the other side d_V describes structural damage and is determined by the observer matrix C_T and states x_3. Parameter C_T is a core projection result. It is dedicated to the output by considering observer matrices C_1 and C_2. This reveals an important relation: If the difference between $\Pi_1(A_1, K_{p,1}, C_1)$ and $\Pi_1(A_2, K_{p,2}, C_2)$ increases, then C_T ascends too.

Then the z-domain equivalent shows the projection spectral results

$$S_{d,U} = \Omega_U(z) M_3 \Omega_U^*(z^{-*}), \quad S_{d,V} = \Omega_V(z) M_3 \Omega_V^*(z^{-*}) \quad \text{with} \quad \Omega(z) = \Omega_U(z) + \Omega_V(z) . \quad (6.53)$$

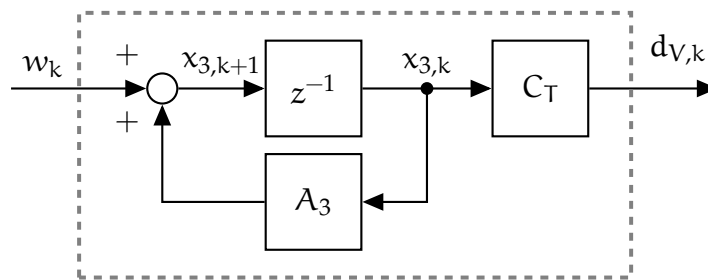Figure 6.8: System Ω_V

Here, projected systems

$$\Omega_U(z) = C_\Omega \left(zI - P_U A_\Omega \right)^{-1} P_U B_\Omega \quad \text{and} \quad \Omega_V(z) = \begin{bmatrix} C_T \left(zI - A_3 \right)^{-1} & 0 \end{bmatrix} \quad (6.54)$$

have been used. System Ω_V has been depicted in figure 6.8. It gives a representation of d_V in equation (6.52b). Systems Ω and Ω_V can be compared with the help of figures 6.6 and 6.8.

It is important to note the difference between C_Δ in equations (6.33) and (6.34) and the formerly introduced C_T, which reveals some important key aspects of SP2E:

(i) The output is described by a difference of observer matrices C_1 and C_2 with regard to model order differences and appropriate column spaces, which is taken into account with Y and Z.

(ii) The difference process d is the response to a test signal y_3, which itself is described by x_3.

(iii) Introduced states x_3 might be physical and non-physical.

It therefore is reasonable to use matrix C_T and states x_3 only to determine structural damage.

6.2.3 Enhanced Average Process Power

The identification of structural damage is conducted by analysing the average process power $R_d(0)$. Although this Gramian can be used for damage identification purposes, it is advantageous to apply the state projection estimation error (SP2E) technique for an enhancement, which led to process d_V in equation (6.52b). The original average process power of equation (6.28)

$$R_d(0) = \langle d_k, d_k \rangle = \frac{1}{2\pi} \int_0^{2\pi} S_d(e^{j\theta})\, d\theta = C_\Omega (P_U + P_V)\Pi_d (P_U^* + P_V^*) C_\Omega^* \tag{6.55a}$$

$$= R_{d,U}(0) + R_{d,V}(0) + \left(R_{d,UV}(0) + R_{d,VU}(0) \right) \tag{6.55b}$$

can arguably be described by four parts. The first one is

$$R_{d,U}(0) = \frac{1}{2\pi} \int_0^{2\pi} S_{d,U}(e^{j\theta})\, d\theta = \begin{bmatrix} -C_1 & C_2 \end{bmatrix} \left\langle \begin{bmatrix} \tilde{x}_{1,k} \\ \tilde{x}_{2,k} \end{bmatrix}, \begin{bmatrix} \tilde{x}_{1,k} \\ \tilde{x}_{2,k} \end{bmatrix} \right\rangle \begin{bmatrix} -C_1^* \\ C_2^* \end{bmatrix}. \tag{6.56}$$

is numerical noise, because it follows the Gramian of state differences $\tilde{x}_1$ and $\tilde{x}_2$. On the other hand,

$$R_{d,V}(0) = \frac{1}{2\pi} \int_0^{2\pi} S_{d,V}(e^{j\theta})\, d\theta = C_T \Pi_{33} C_T^* \quad \text{with} \quad \Pi_{33} = A_3 \Pi_{33} A_3^* + Q_3 \tag{6.57}$$

refers to the important part of $R_d(0)$. Besides that the cross Gramian matrices $R_{d,UV}(0)$ and $R_{d,VU}(0)$ are considered as irrelevant.

By comparing equations (6.28) and (6.57), central differences are apparent: In opposite to the determination of $R_d(0)$, the choice of matrix Π_{33} is relevant here. Because noise disturbances w and v are unknown, Gramian matrix Π_{33} is not unique. Hence, the input Gramian M_3 of equation (6.7) follows an infinite number of possible Π_{33}. An approach for that is given in the following.

A DAMAGE IDENTIFICATION APPROACH   is proposed here on the basis of a reasonable choice: There are various possibilities to describe input y_3, for example by state space system H_3.

As was described in section 6.2.1, the choice $H_3 = H_2$ is advantageous, for instance for real-time damage identification, and is thus used here. According to equations (6.44) and (6.50a), this leads to $Z = I$ and $\tilde{x}_{2,k} = x_{2,k} - \hat{x}_{2,k}$. Now, $x_{2,k} \to \hat{x}_{2,k}$ is set, as structural damage should not be observable in noise. Therefore, the Gramian matrix $\Pi_{33} \to \Pi_{22}$ follows, which shows the central difference to the approach of Yan et al.[77] in equation (6.26): $d_k \longrightarrow (e_{1,k} - v_k)$. This allows an approach

$$R_{d,V}(0) = C_T \Pi_{22} C_T^* \quad \text{with} \quad H_3 = H_2 \quad \text{and} \quad \Pi_{33} \longrightarrow \Pi_{22}\,. \tag{6.58}$$

Here, the principal diagonal, denoted by $\bar{P}_{d,V}$, must be analysed to identify structural damage. Most importantly, elaborate numerical integration can be omitted. Furthermore, Gramian matrix Π_{22} is independent of the choice of M_3. A comprehensive flowchart of SP2E is given in figure 6.9.
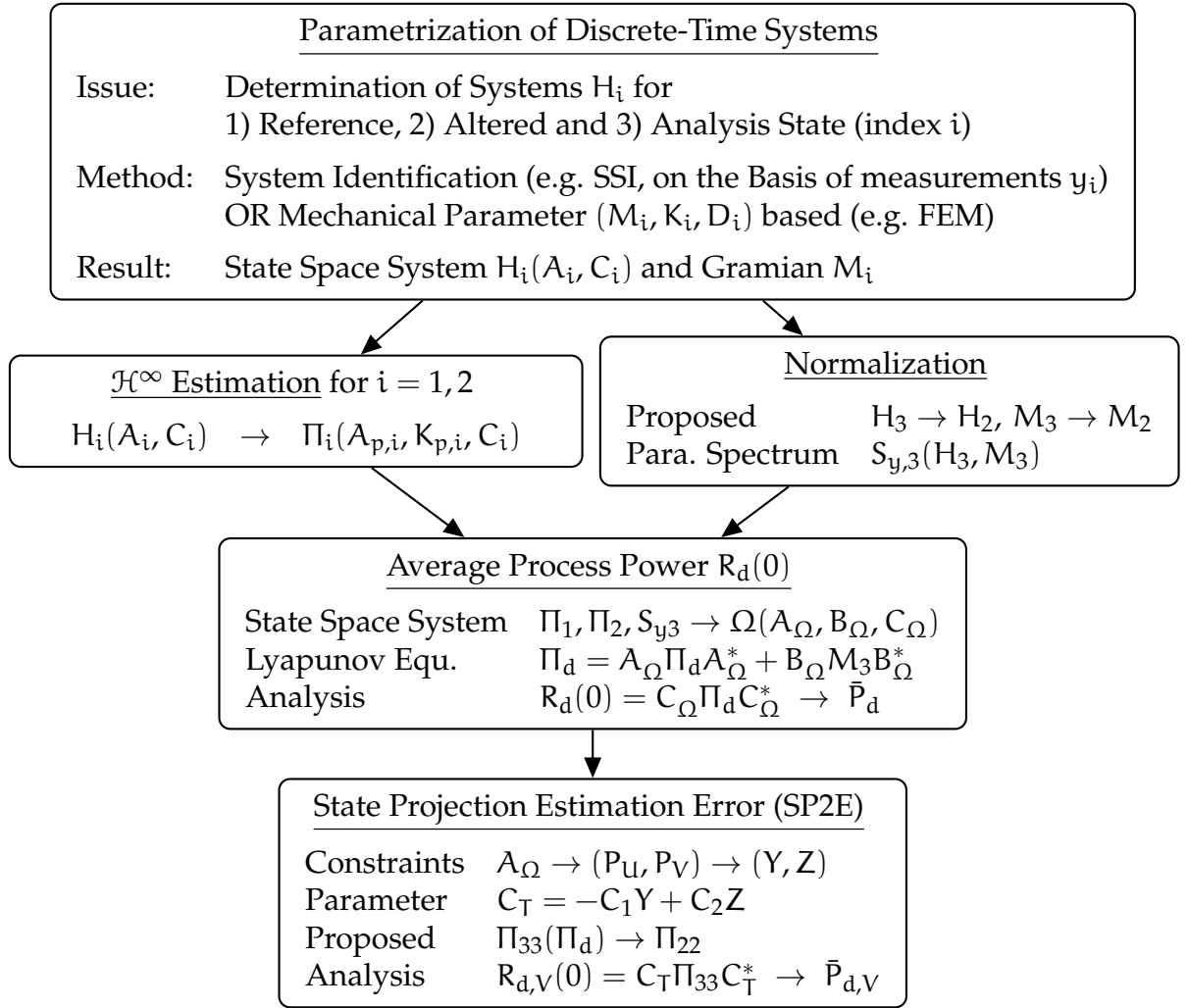

Parametrization of Discrete-Time Systems

Issue: Determination of Systems H_i for
1) Reference, 2) Altered and 3) Analysis State (index i)

Method: System Identification (e.g. SSI, on the Basis of measurements y_i)
OR Mechanical Parameter (M_i, K_i, D_i) based (e.g. FEM)

Result: State Space System $H_i(A_i, C_i)$ and Gramian M_i

$\mathcal{H}^\infty$ Estimation for $i = 1, 2$

$H_i(A_i, C_i) \quad \rightarrow \quad \Pi_i(A_{p,i}, K_{p,i}, C_i)$

Normalization

Proposed $\quad H_3 \rightarrow H_2, M_3 \rightarrow M_2$
Para. Spectrum $\quad S_{y,3}(H_3, M_3)$

Average Process Power $R_d(0)$

State Space System $\quad \Pi_1, \Pi_2, S_{y3} \rightarrow \Omega(A_\Omega, B_\Omega, C_\Omega)$
Lyapunov Equ. $\quad \Pi_d = A_\Omega \Pi_d A_\Omega^* + B_\Omega M_3 B_\Omega^*$
Analysis $\quad R_d(0) = C_\Omega \Pi_d C_\Omega^* \quad \rightarrow \quad \bar{P}_d$

State Projection Estimation Error (SP2E)

Constraints $\quad A_\Omega \rightarrow (P_U, P_V) \rightarrow (Y, Z)$
Parameter $\quad C_T = -C_1 Y + C_2 Z$
Proposed $\quad \Pi_{33}(\Pi_d) \rightarrow \Pi_{22}$
Analysis $\quad R_{d,V}(0) = C_T \Pi_{33} C_T^* \quad \rightarrow \quad \bar{P}_{d,V}$

Figure 6.9: Flowchart SP2E

6.2.4 SUMMARY OF METHOD SP2E

A summary of SP2E is given below on the basis of former statements:

(i) Identify (H_1, Π_1) and (H_2, Π_2) based on mechanical parameters (M, K, D) or measurements y (see section 6.1.2).

(ii) Define the test input y_3, for example $H_3 = H_2$, and reorder estimator parameters $(A_1, K_{p,1}, C_1)$ and $(A_2, K_{p,2}, C_2)$ according to equation (6.24).

(iii) Compute parameters (Y, Z) according to defined projectors of equation (6.48).

(iv) Solve Lyapunov equation (6.27) based on a first presumption $\Pi_{33} = 0$.

(v) Analyse the average process power $\bar{P}_{d,V}$ following equation (6.58).

6.3 Mechanical System Example

6.3.1 Mechanical Parameter Based SP2E

The simulated example of section 3.3.2, chapter 3, has been repeatedly analysed in this dissertation. Here, this example is finished by analysing structural damage with SP2E. This then is the basis for real laboratory experiments in part III. Because the actual method verification follows therein, central concepts shall be shown only below. Therefore, the principal function of SP2E on the basis of first principle based (white box) and identification based (black box) models is discussed. To begin with, the case of known mechanical parameters (white box) is applied.

Consider two continuous-time systems G_1 and G_2 with $n = 2N_1 = 2N_2$, which map forces f to accelerations $\ddot{x}$, according to equations (3.7) and (3.9). Thus, mechanical parameters $M_1, K_1, D_1 \in \mathbb{R}^{N_1 \times N_1}$, $M_2, K_2, D_2 \in \mathbb{R}^{N_2 \times N_2}$ are known. Based on that continuous-time state space systems $G_1(\bar{A}_1, \bar{B}_1, \bar{C}_{a,1}, \bar{D}_{a,1})$, $G_2(\bar{A}_2, \bar{B}_2, \bar{C}_{a,2}, \bar{D}_{a,2})$ are derived. This example is, of course, a simplification, which allows to demonstrate the application of $R_{d,V}(0)$ in equation (6.57).

Following the concepts of the summary in section 6.2.4, $H_3 = H_2$ is chosen. Thus, Π_{33} is the Gramian matrix of z_2 (state vector of altered structural system). Hence, the principal diagonal of Π_{33} can be seen as the average process power of all known displacement and velocity measurements in z_2.

Numerical results shall now be analysed and elaborated, hence a numerical practical example is analysed. For that, the zero-order-hold method of equation (3.15) is applied with $\Delta t = 2 \cdot 10^{-4}$s. Here, system G was used in modal form. While A and C have been applied to equation (6.4), the input Gramian matrix of equation (6.7) was defined by

$$M = \left\langle \begin{bmatrix} w_k \\ v_k \end{bmatrix}, \begin{bmatrix} w_k \\ v_k \end{bmatrix} \right\rangle = \begin{bmatrix} Q & S \\ S^* & R_v \end{bmatrix} = \begin{bmatrix} B \\ D \end{bmatrix} \begin{bmatrix} B^* & D^* \end{bmatrix} . \qquad (6.59)$$

This have been done for three times, respectively for three structural states:

(i) Reference state,

(ii) Mass increase of ≈ 1.25kg at M_3 and

(iii) Stiffness degradation between M_5 and M_6 (lowering the second moment of area about 16.7%).

In the following, the reference state (index 1) is compared to the altered states each (index 2). Thus, two damage scenarios shall be analysed by SP2E. The results for that are shown in figures 6.10a and 6.10b.

As can be seen, the mass and the stiffness alteration have been detected and localized correctly by SP2E. Furthermore, the projection techniques essentially have no influ-
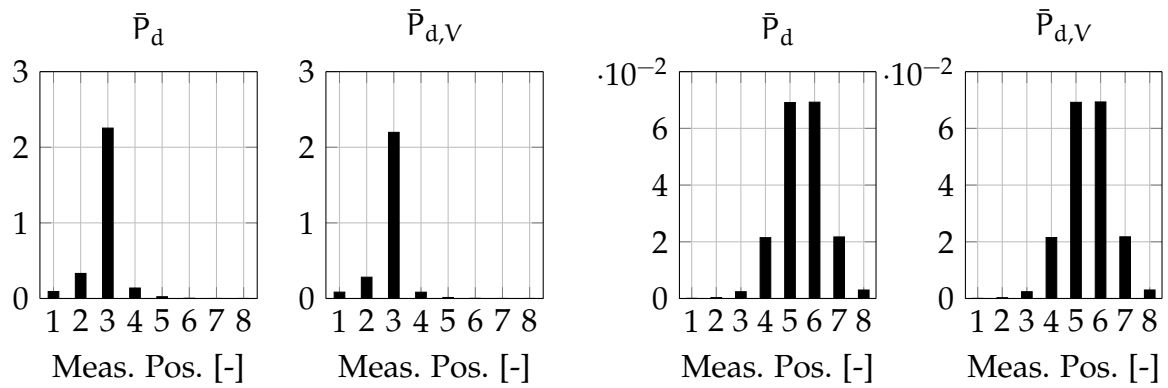
(a) Mass Alteration at M_3 (b) Stiffness Alteration between M_5 and M_6

Figure 6.10: Mechanical Parameter based SP2E, Results in $\left[(m/s^2)^2\right]$

ence. This is plausible, because potential numerical disturbances are not present. In a next step numerically identified mechanical systems are used.

6.3.2 SSI BASED SP2E

SSI based SP2E essentially uses the canonical correlation based stochastic subspace identification of section 4.3.3, which has been applied in section 4.5. The identified system in modal form has been applied commonly with equations (6.7) and (6.8). This then was the basis for SSI based SP2E.
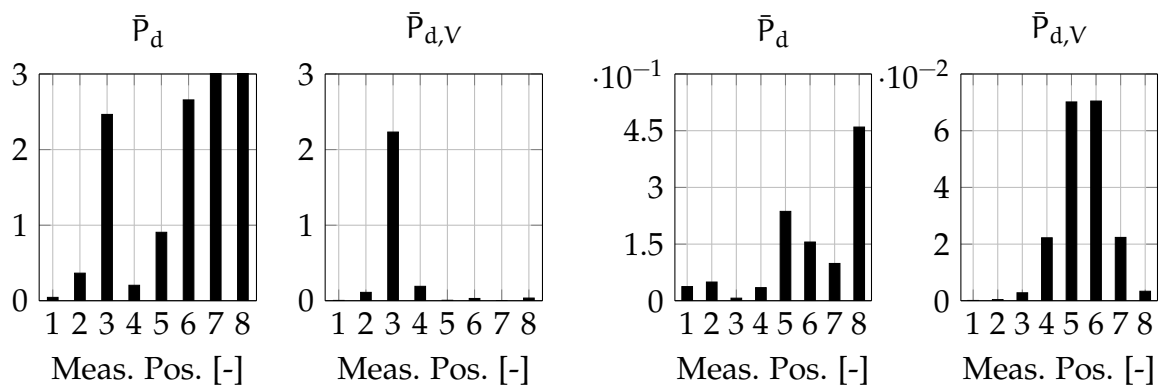
(a) Mass Alteration at M_3 (b) Stiffness Alteration between M_5 and M_6

Figure 6.11: SSI Based SP2E, Results in $\left[(m/s^2)^2\right]$

Figures 6.11a and 6.11b show the damage identification results for the SSI based SP2E. By comparing $\bar{P}_d$ to $\bar{P}_{d,V}$, one can see that projection techniques are necessary to localize structural alterations. The difference clearly follows numerical inaccuracies in the

identification process. Nevertheless, the results of $\bar{P}_{d,V}$ for the mechanical parameter and the SSI based approach nearly are identical.

The shown SP2E results are a small part of the whole analysis. In this chapter the fundamental functionality has been shown and discussed only. Based on that part III of this thesis, especially chapter 8, is devoted to analyse damage identification results for a laboratory structure.

Part III

VERIFICATION OF THE STATE PROJECTION ESTIMATION ERROR METHOD IN LABORATORY EXPERIMENTS

SUBSPACE IDENTIFICATION OF A LABORATORY STRUCTURE

Chapter Outline

The theories of former chapters have repeatedly been applied at the simulated mechanical system example of section 3.3.2 in chapter 3. Henceforth, the discussed theories are exemplified with laboratory data. Thus, in the present chapter the laboratory set-up is discussed first in section 1. Here, the used measurement instrumentation is important because it determines subsequent results, for example the estimation of spectra. Based on that, the covariance based stochastic subspace identification of the laboratory structure is explained. In the end exemplary results of $\mathcal{H}^\infty$ estimation are elaborated.

$$
\boxed{\begin{array}{c} \text{SECTION 1} \\ \underline{\text{Laboratory Set-Up}} \\[4pt] \text{Measurement Instrum.} \\ \text{Spectrum Estimation} \end{array}} \longrightarrow \boxed{\begin{array}{c} \text{SECTION 2} \\ \underline{\text{Stochastic Subspace Id.}} \\[4pt] \text{Covariance Model Id.} \\ \text{Operational Modal An.} \end{array}}
$$

$$
\boxed{\begin{array}{c} \text{SECTION 3} \\ \underline{\text{Kalman Filt. \& } \mathcal{H}^\infty \text{ Estim.}} \\[4pt] \text{The Positivity Problem} \\ \text{Filt. Sig. in Add. Noise} \end{array}}
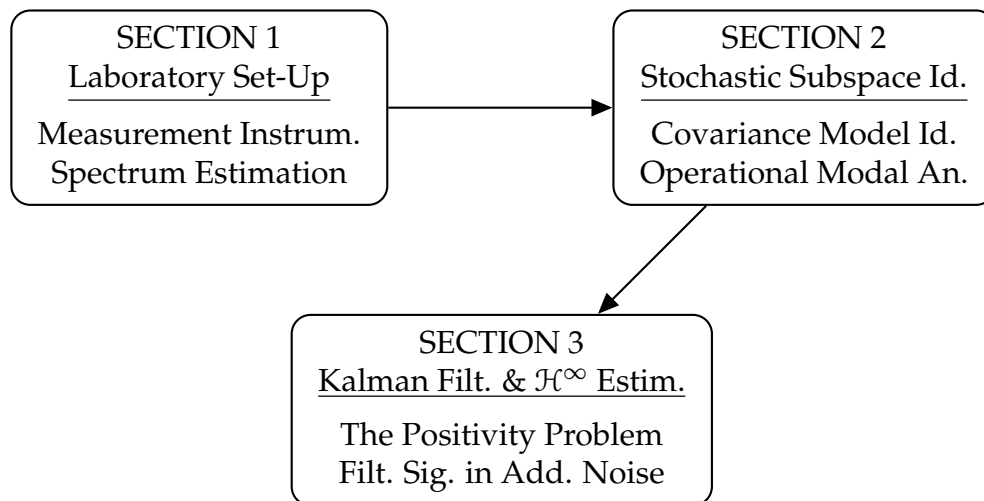$$

Figure 7.1: Chapter Outline

All numerical process steps have been analysed and conducted by self-developed programs. However, this chapter serves as a basis for the subsequent one. While here the structural reference state is discussed only, the application and identification of structural alterations is carried out in chapter 8.
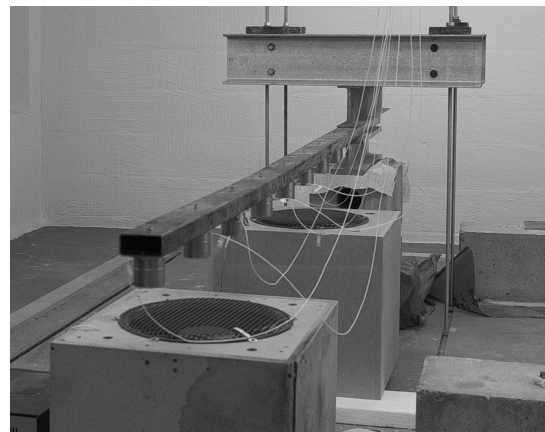
7.1 Laboratory Set-Up

7.1.1 Description of Laboratory Experiments

The laboratory experiments have been conducted at Leipzig University of Applied Sciences. In these experiments a cantilever arm (bending beam) with a length of 2.45m has been used, which is shown in figure 7.2: A steel rectangular hollow section $80 \times 40 \times 2.9$mm. The whole construction was built upon a block type machine foundation.
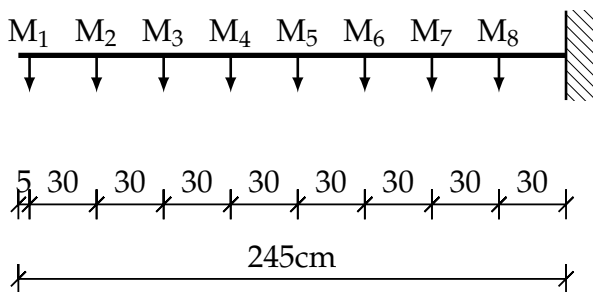
(a) Mechanical System: Cantilever Arm

(b) Laboratory Structure

Figure 7.2: Laboratory Set-Up

In figure 7.2 the measurement positions $M_1 \ldots M_8$ are apparent (equally spaced 30cm), thus the total number of measurement positions $p = 8$. By adding the masses of beam and sensors, a total mass of approximately 19.4kg follows. Because of former experiments, the beam already was pre-damaged: In former experiments a saw cut (≈ 2.5cm depth) between M_4 and M_5 has been applied and closed afterwards.

AMBIENT EXCITATIONS have been used because automated structural health monitoring shall generally be possible. These stochastic excitations were simulated by two self-built loudspeakers, hence acoustic noise. To build those, wooden boxes $50 \times 54 \times 50$cm have been equipped with speaker CPA $15 - 1000$ (15" diameter, nominal power 1000W; company SpeaKa), which have their optimal frequency response between $20 \ldots 2.500$Hz. While both loudspeaker enclosures were built as bass reflex systems, the maximal standard sound pressure level of the CPA $15 - 1000$ is 98dB. The orientation of both loudspeakers can be seen in figure 7.2.

Very importantly, the ambient excitation is not white noise. Although a white noise process has been simulated in Matlab (company MathWorks) and used as the loudspeaker's input, the frequency response of both sound systems clearly is not flat. In accordance with the discussed $\mathcal{H}^\infty$ estimation theories, the structural excitation sim-

ply is unknown. Besides that actual real world excitations, for instance vehicle traffic at bridges, are unknown too. Nevertheless, the laboratory excitation has demonstrably been ergodic.

THE MEASUREMENT CHAIN is depicted in figure 7.3: Eight uni-axial accelerometers PCB 393C of company PCB Piezotronics have been used. Their sensitivity is $101.9 \text{mV}/(\text{m/s}^2)$. Furthermore, the optimal frequency range ($\pm 5\%$) is between $0.0025 \ldots 800 \text{Hz}$.
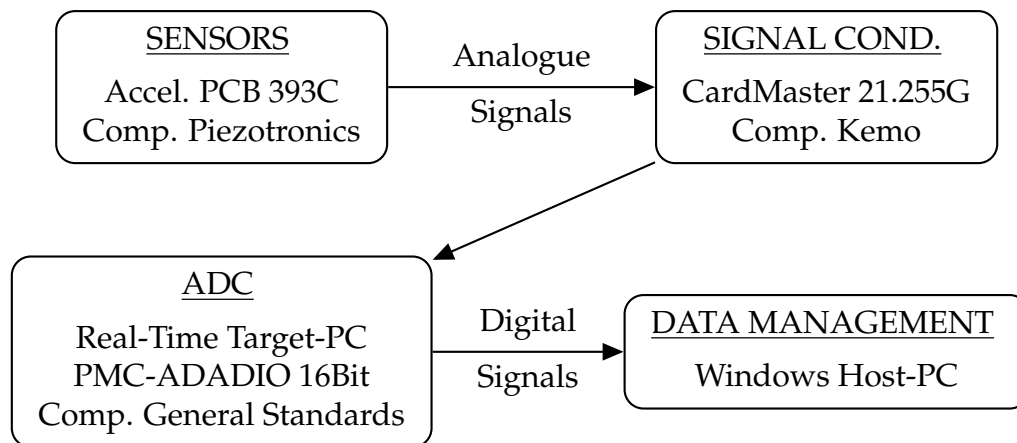

Figure 7.3: Measurement Chain

Based on analogue sensor voltage signals, measurement data must be digitized. For that, signal condition is necessary to prevent aliasing and to reduce quantization noise. Thus, the CardMaster 21.255G (input ± 10V, company Kemo) was utilized. Its linear phase response low pass was used with appropriate amplifications. Because a constant sampling frequency of $f_s = 1.250 \text{Hz}$ has been used, the filter cut off frequency $f_c = 400 \text{Hz}$ was applied in accordance with the Nyquist-Shannon sampling theorem ($f_s \geqslant 2 f_c$). Here, the cut-off frequency $f_c = 400 \text{Hz}$ had been chosen to measure the first sixth vertical bending modes.

The analogue-digital-conversion (ADC) has been realized by a real-time target machine (xPC Target, Company MathWorks). Therefore, a standard personal computer (PC) was equipped with PMC-ADADIO (input ± 10V, ADC 16Bit, company General Standards) and has been booted with a real-time operating system. Here, the central advantage is the exact synchronous data sampling without interrupts.

Afterwards the discrete-time measurement data was processed on a host-PC (standard Windows machine with Matlab), for instance conversion from voltage to acceleration. Because of the following data management, the sampling frequency $f_s = 1.250 \text{Hz}$ was chosen on purpose. At this point a trade-off between resolution and numerical calculation possibilities had to be considered. For example the singular value decomposition is bounded by the number of matrix row and columns, thus the number

of data samples k in $t = k\Delta t$. By increasing the sampling frequency (lowering Δt), shorter data length (time t) can be processed at once.

7.1.2 POWER SPECTRAL DENSITY ESTIMATION

There are various methods to estimate the power spectral density of a signal y. Because of its common usage, Welch's method[119] is used below, and thus shall be explained briefly. While the original work in 1967 was based on single channel signals, multivariate analyses are presupposed here.

Broadly speaking, the central idea of Welch's method is an averaging of modified periodograms to reduce the variance of spectral results. This is necessary, because the spectral variance cannot be reduced by using larger data sets. Periodograms essentially are the Fourier transform of autocorrelation estimates. Because the fast Fourier transform is common for that, a data length of the power of two should be taken to prevent zero padding or cutting data.

The modification of periodograms reveals an important element of this spectral estimation approach: The measured data is split in data segments. Those shortened signals typically have an overlap to previous segments by 50%, which increases the number of averaging.

Every data segment is scaled by a chosen window function, which is an approach to reduce leakage. This modifies the resulting periodogram. Spectral leakage is a phenomenon that describes additional peaks in a Fourier spectrum following no physical, but numerical origins. One major leakage source is created by using finite discrete-time signals.

There are plenty window functions possible to reduce spectral leakage. Very importantly, the choice of window function is a trade-off between high resolution and high dynamic range. Typical high resolution windows are the rectangular and the Kaiser window. These kind of windows are capable to give precise frequency estimates of comparable magnitudes, but fail if frequency contents are vastly different. On the other side windows, which provide a high dynamic, allow appropriate estimates of altering peak heights. An example is the Blackman-Harris window. If one needs both characteristics, a window in between these extremes may be chosen, like the Hamming or the Hann window.

7.1.3 SPECTRAL RESULTS

In result of the described laboratory set-up, discrete-time acceleration signals of eight measurement positions with units m/s^2 have been gathered. While these signals are the basis of the following analyses, structural assumptions (like stiffness, mass, etc.) are explicitly not proposed or used. Furthermore, the excitation is unknown.

To identify the mechanical system, the covariance based stochastic subspace identification of section 4.3 in chapter 4 shall be applied. For that, a covariance matrix function $R_y(l)$ must be determined. As was already explained for the numerical example in section 4.5, the inverse Fourier transform of an averaged periodogram following Welch[119] is applied because this technique allows advantageous data averaging.

The averaged periodogramm is based on a fast Fourier transform, which is optimized for data length with the power of two. Hence, a spectral resolution with $N = 2^{15}$ was chosen. Here, a study of $N = 2^{\mathcal{N}}$ with $\mathcal{N} \in \mathbb{N}, \mathcal{N} = 11, \ldots, 18$ confirmed an appropriate trade-off between the spectral resolution and necessary averaging. By analysing spectrum variations due to different data amounts, a measurement length of 1h was proven to be applicable. This implies 270 spectral averages with a 50% data overlap. Here, different measurement durations (up to 4 days) have been analysed. Because of ergodicity, these very long durations are unnecessary.

The resulting measured power spectral density (PSD) S_y has the unit $(m/s^2)^2/Hz$. Because it is a matrix function, this spectrum may be difficult to analyse. Thus, the largest singular value of $S_y(e^{j\theta})$ is plotted in figure 7.4. As was discussed before, the inverse Fourier transform of S_y leads to the covariance matrix function $R_y(l)$, which again is hard to analyse. Nevertheless, to get an impression, figure 7.4 also shows the auto-covariance function at M_1.
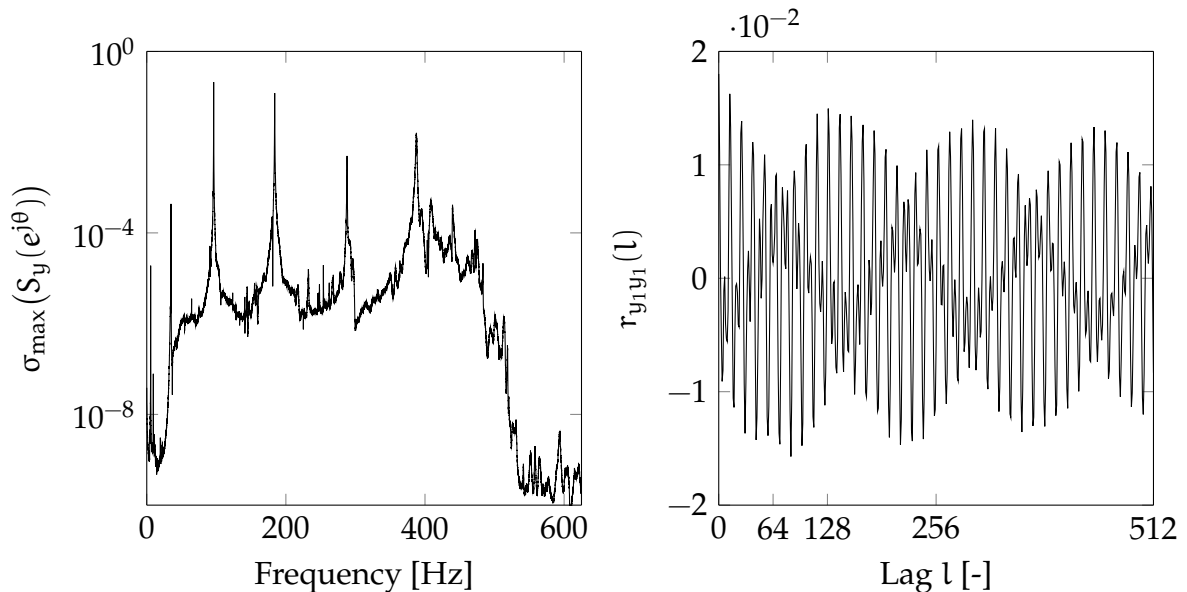

Figure 7.4: Measured Reference Spectrum S_y and Auto-Covariance Function at M_1

A central element of the averaged periodogram is the application of window functions. Only if a rectangular window is used, result $R_y(l)$ is identical to those of time-domain methods, for example $R_y(l) = 1/(N+1) \sum_{k=0}^{N} y_k y_{k+l}$. However, the covariance matrix function $R_y(l)$ is an estimate due to finite measurements. Because window functions clearly improve spectral results, the Hann window has been used

nonetheless. Again this is a trade-off, which followed a study of different window applications (e.g. Hann window, Hamming window, Chebyshev window). It is beyond the scope of this thesis to discuss spectral estimation approaches in more detail.

THE SPECTRAL ANALYSIS is very important, because its results determine all upcoming procedures. While the given covariance function shows remarkable periodicity, sixth vertical bending modes clearly are apparent in spectrum S_y. Besides that, measurement noise processes are present too. For instance natural frequencies of the clamping construction have been tracked, which was verified in separate measurements. More details on measured natural frequencies of the actual test structure will be given in the operational modal analysis section 7.2.2.

The spectral estimate obviously is a raw spectrum, which is determined by the ambient excitation. As can be seen, frequencies beyond the cut-off frequency $f_c = 400Hz$ are filtered. On the other side the low frequency range (up to 30Hz) is limited too, which follows the frequency response of the loudspeakers. Hence, the first vertical bending mode at $\approx 5.6Hz$ is poorly excited. Although the height of most peaks can be computed appropriately by averaging, the estimate of the first natural frequency remains uncertain. Based on spectral data, the loudspeaker's input could be adjusted to overcome the above problems. But in view of possible unknown excitations in $\mathcal{H}^\infty$ estimation this was omitted.

Finally, a comparison of simulated and measured spectra in figures 3.6 and 7.4 reveals imprecise simulation presumptions. Especially the applied and closed saw cut (pre-damage) is not considered in simulations. Nevertheless, the simulation example serves as a method demonstration only and (possibly updated) mechanical parameters, like stiffness, mass and damping, are explicitly not used for damage identification.

7.2 STOCHASTIC SUBSPACE IDENTIFICATION

7.2.1 COVARIANCE MODEL IDENTIFICATION

One the basis of former statements a system $H(A, C)$ of the laboratory structure shall be parametrized. Here, the elaborations of the subspace identification chapter 4 are important. Following the concept of averaged spectra, or equivalently covariance functions, the covariance based stochastic subspace identification is an appropriate technique.

To identify the structure, the singular value decomposition of equation (4.51) must be conducted, which directly applies the determined covariance matrix function $R_y(l)$. At this point the number of block rows and columns m is a central element to be defined. The more data is processed at once, the longer the numerical computation takes, but more precise results can also be expected. In view of advantageous

analysability by FFT, m has been chosen to the power of two. Based on a short comparison study, $m = 2^9 = 512$ was finally chosen.

It is important to note the consequences of choice m. First of all, figure 7.4 gives an impression of the used amount of relevant data and the effect of using less. Secondly, the Fourier transform of that shortened covariance function again is a spectrum, but with a lower resolution in comparison to the primal one in figure 7.4. Synthezising above, the reduced amount of spectral, or covariance, data in SSI may have tremendous impacts on identification results, as was observed by the author.

The singular values of equation (4.51) are very important to determine an appropriate model order n. While in simulated scenarios like figure 4.9, the model order n can easily be seen by a gap in $\sigma_n \gg \sigma_{n+1}$, real-life data usually is non-analysable by that method. This will be discussed below in connection with figure 7.5. Although the CCA technique of section 4.3.3 was very successful in simulation experiments, it allowed poor model order determination in real-life experiments only. Thus, the extension to the central CCA equation (4.80) is not an option to improve the algorithm.

THE STABILIZATION DIAGRAM   is a common tool for model order determination in modern system identification techniques. Following Peeters,[44] it is practically useful to over-specify the model order and to eliminate numerical fragments afterwards. For that matter, the stabilization diagram is a practical approach to compare modal results for several possible model orders, which leads to an engineering oriented rank decision.

Figure 7.5 on page 154 gives a stabilization diagram example. While the left side shows the actual stabilization digram, the right one gives related singular values. As it was mentioned before, a clear gap in the singular values is not present here.

The given stabilization diagram has the measured raw spectrum in its background. While the vertical axis gives exemplary model orders, modal results are marked by grey dots. Here, the operational modal analysis follows equation (4.54). Furthermore, the model reduction technique in accordance with section 3.2.3 is applied and its results are presented by black crosses and text, which gives the damping. To truncate modes, criteria of relevant eigenvalues have been defined:

i) Eigenvalues λ_i and $\lambda_{i,i+1}$ must emerge complex conjugated.

ii) The modal damping must be plausible, thus $0 < \zeta < 3\%$.

iii) Identified frequencies have to be near by spectral peaks.

iv) Frequency positions and modal dampings must be stable according to an increasing model order, which is the origin of method name.

v) Computed unscaled mode shapes ϕ_i and $\phi_{i,i+1}$ have to be complex conjugated. In principal ϕ_i is a vector of p complex values. Only if these values are inphase, a mode shape is present. An example is given in figure 7.6 on page 155.

vi) The model following complex conjugated eigenvalues λ_i and $\lambda_{i,i+1}$ should lead to the description of a single spectral peak, which is illustrated in figure 7.6. Therein the complete model with $n = 36$ is reduced to a single mode pair, which perfectly describes the third vertical bending mode.

If a single named criterion is violated, the analysed eigenvalue is truncated. Here, black crosses (with damping texts) mark complex conjugated eigenvalues in figure 7.5, which fulfil all named criteria.
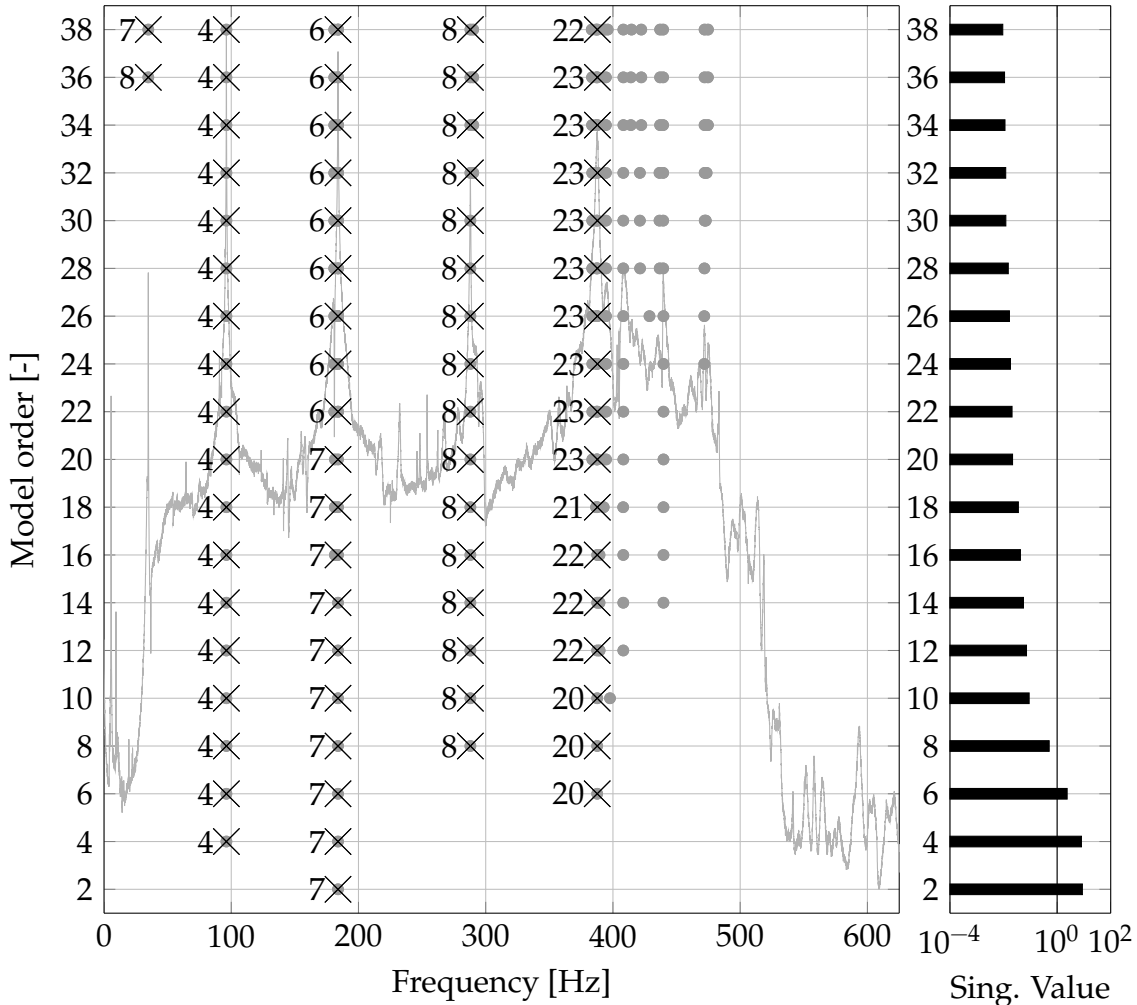

Figure 7.5: Stabilization Diagram: Left) Identified Frequencies (Grey Dot), Model Reduction (Black Cross) and Modal Dampings (Text in 10^{-4}) in front of the Measured Spectrum; Right) Singular Values

THE IDENTIFICATION RESULT   now can be given by carefully analysing the stabilization diagram of figure 7.5. Firstly, the shown model order results are chosen exemplarily to clarify general aspects. Secondly, there are various method variations possible because of its practical approach. Nevertheless, stabilization diagram ap-
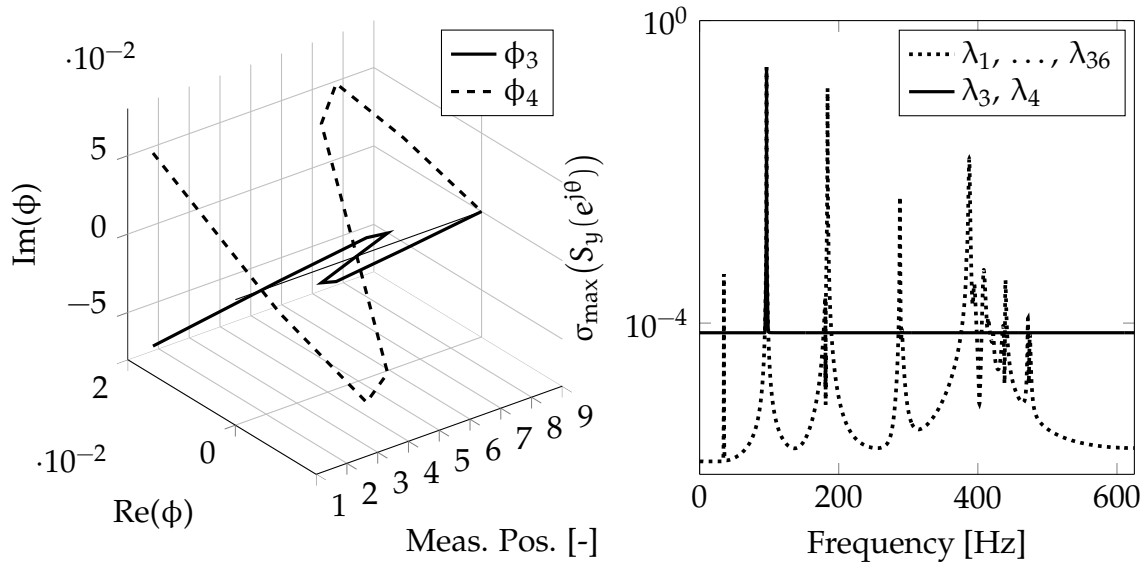
Figure 7.6: Mode Pair for $f = 96.2\text{Hz}$; Linear Interpolation for ϕ

proaches are not the primary focus of this thesis, and the author refers to Goursat et al.[145]

As can be seen in figure 7.5 the relevant frequencies and modal dampings are stable due to increasing model orders. Very interestingly, rank $n = 8$ could be a reasonable choice following the singular values, which leads to a model with the 3rd to the 6th vertical bending mode. Because five natural frequencies shall be identified, model order $n = 36$ has been chosen here. Unfortunately, $n \geqslant 204$ with $\sigma_{204} \approx 3 \cdot 10^{-4}$ would be necessary to identify the first natural frequency too. Due to very disadvantageous numerical inaccuracies, model order $n = 36$ was chosen to be sufficient.

The spectral identification results are presented in figure 7.7. While the left side shows the identified spectrum following $n = 36$, the right one gives the model reduction result. As can be seen on left several frequencies have additionally been identified. Most importantly, the unscaled mode shapes of these additional frequencies clearly indicate noise processes. Because the defined selection criteria are violated, model reduction truncates this information. The named situation is equivalent to the grey dots and black crosses in figure 7.5 at $n = 36$.

Both spectra $S_y(e^{j\theta})$, the primary identified and the truncated one, are indefinite at some θ. This is especially apparent for the right spectrum in figure 7.7: Because of an indefinite spectrum beyond the sixth natural frequency, the first singular value is suddenly increased. An indefinite spectrum clearly is non-physical and it follows numerical inaccuracies. This has a tremendous impact on possible estimator derivations in section 7.3.

In result of the identification process a system $H(A, C)$ with additional parameters N and $R_y(0)$ is determined, which leads to the discussed spectrum of figure 7.7. Here,
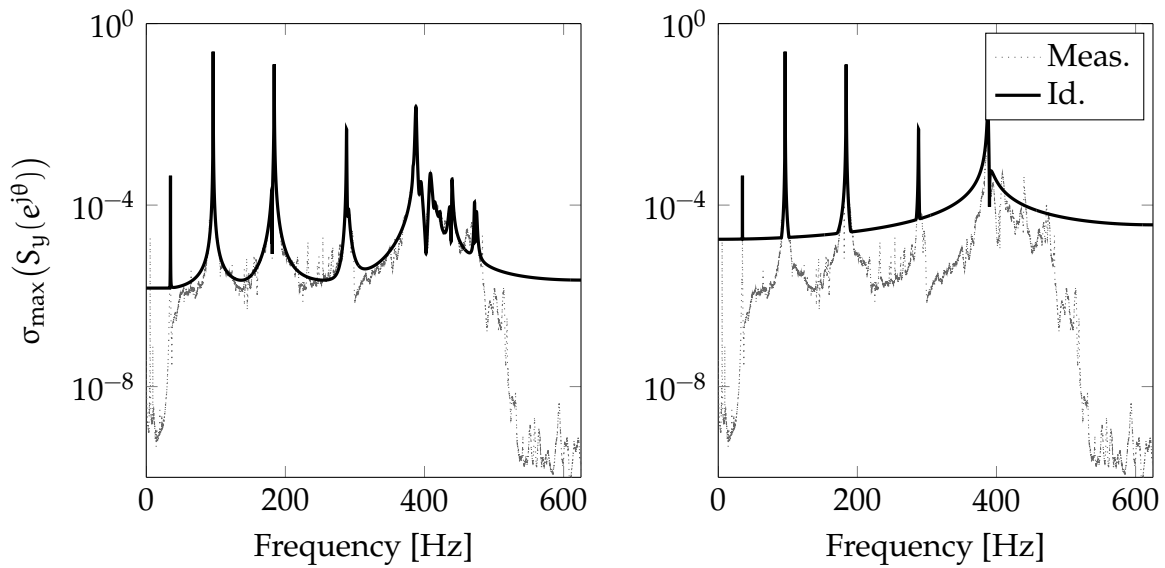
Figure 7.7: Measured and Identified Spectra: Identification with $n = 36$ (left) and Model Reduction to $n = 10$ (right)

the central advantage can be seen: The huge amount of data (1h) is reduced to four relatively small matrices, which are capable to describe the most relevant structural-dynamical properties. Furthermore, a smooth spectrum can be analysed instead of the measured raw spectrum, which is especially useful for damage identification, as will be seen in chapter 8.

7.2.2 Operational Modal Analysis

The primary result of covariance based stochastic subspace identification is system $H(A, C)$ in connection with additional parameters $(N, R_y(0))$. Based on $H(A, C)$ modal characteristics (f, ζ, ϕ) can be determined. Although most authors devoted to structural health monitoring would understand modal parameters as intended results for damage identification, this is explicitly not undertaken in this thesis. Instead system $H(A, C)$ is applied to identify an estimator $\Pi(A_p, K_p, C)$ in section 7.3, which is needed for SP2E in chapter 8.

Having these circumstances in mind, identified modal parameters are useful for engineering oriented plausibility. Modal results are depicted in figure 7.8. The modal identification again follows equation (4.54). Here, the unscaled mode shapes ϕ show a resemblance to the simulated case in figure 3.5. Besides that, the actual natural frequency positions are lower in comparison to the simulated case, because of the pre-damage. Furthermore, less vertical bending modes were identified due to measurement instrumentation.
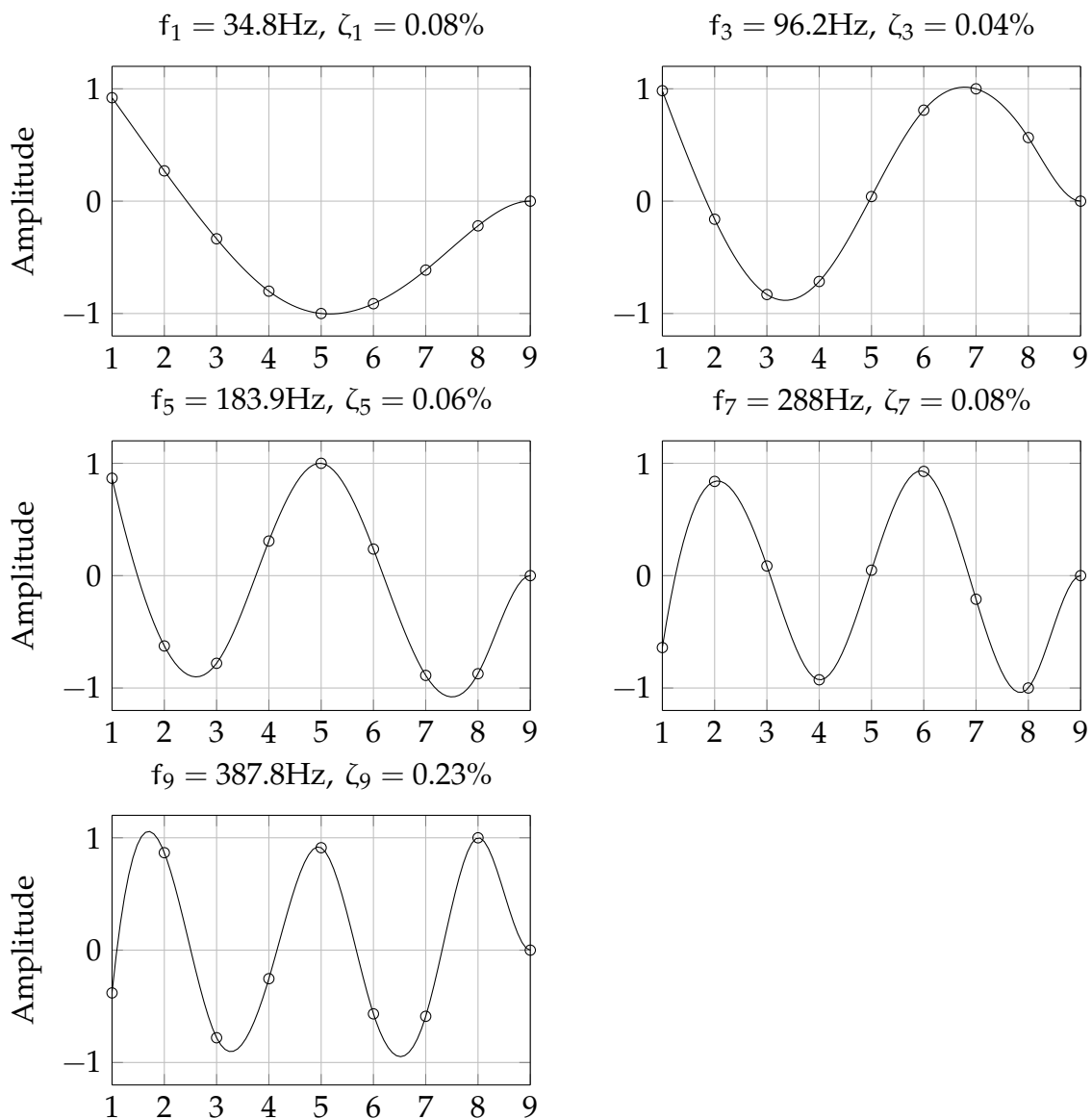
Figure 7.8: Operational Modal Analysis: Normalized Mode Shapes (Circles) and Cubic Spline Interpolation (Continuous Line)

Operational damping estimation is a known weakness, see for example Rainieri et al.[56] This problem can be seen here too: An estimated modal damping of about 0.04% to 0.23% is questionable. Nevertheless, damping estimation is not the primary focus here and possible inaccuracies are seen as a minor influence for subsequent results.

7.3 KALMAN FILTERING AND $\mathcal{H}^\infty$ ESTIMATION

Because system $H(A, C)$ is unusable for recursive signal determination, estimation theory is subsequently applied. Here, chapter 5 serves as a basis. From a classical viewpoint, it is common to determine a covariance based Kalman filter.[17] To do so, the spectral representation of equation (5.133) can be applied in accordance with the Kalman-Yakubovich-Popov (KYP) lemma. Thus, the parametrized spectrum of figure 7.7 must be used to determine an estimator for the laboratory structure. By applying the KYP lemma, the canonical factorization of S_y following equation (5.131) is conducted and an $\mathcal{H}^2$ optimal estimator Π can be determined. This estimator then can be the basis for following damage identification techniques.

Crucial element of the KYP lemma is the change of input Gramian matrix $M \to R_e$, which may be interpreted geometrically as orthogonal projections. Therefore, gain K_p must be determined, which can follow Riccati equation (5.137). Various criteria must be fulfilled for Riccati equations to be solvable in the context of the KYP lemma, as has already been pointed out in section 5.2.1.

Following Vaccaro and Vukina[35] three main criteria must be accomplished for the named Riccati equation to be solvable: i) Observability, ii) Controllability and iii) Positivity. Nevertheless, both of the first two criteria are already fulfilled by the applied singular value decomposition in covariance based stochastic subspace identification, as Vaccaro and Vukina[35] point out.

Thus, the positivity problem is the crucial one, which demands a positive definite spectrum $S_y(e^{j\theta})$ for $\theta \in [-\pi, \pi]$. According to Mari[36] spectrum S_y may be indefinite because system matrix A is not (Schur) stable. For further information on that matter see Akçay.[37] Considering the present laboratory example, all eigenvalues of A lie inside the unit circle, which indicates stability. Here, the necessity of model reduction techniques is emphasized (see figure 7.7), because identified noise terms may have dampings $\zeta \leqslant 0$.

In summary, the positivity problem can hardly be avoided for real-life measurements. Hence, correction methods may be applied. In the following, the method of Vaccaro and Vukina[35] is exemplified. For that, consider $S_y(e^{j\theta}) = \{S_y(e^{j\theta})\}_- + \{S_y(e^{j\theta})\}_+$. At this point $\{S_y\}_-$ represents the negative semidefinite part of spectrum S_y, thus $\{S_y\}_- \leqslant 0$. One could say this is what causes the whole trouble. The named positivity problem already had been apparent in figure 7.7.

Now, the central idea is to overcome the positivity problem by adding a white noise process $\{R_y(0)\}_{New} = R_y(0) + \Delta$, such that $S_y(e^{j\theta}) > 0$ for $\theta \in [-\pi, \pi]$. Here, matrix $\Delta \in \mathbb{R}^{p \times p}$ follows an eigendecomposition of $S_y(e^{j\theta})$. Furthermore, the spectral alteration by $\{R_y(0)\}_{New} = R_y(0) + \Delta$ may be disadvantageous, thus Vaccaro and Vukina also give an algorithm to alter N instead of $R_y(0)$. However, this leads to an identical spectrum and is thus omitted here.
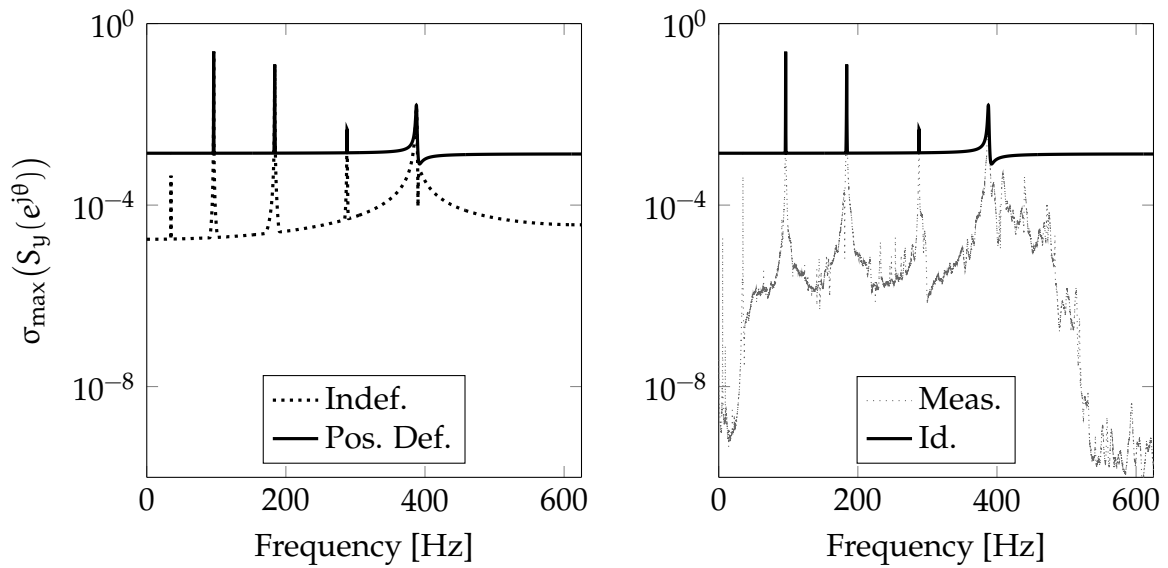
Figure 7.9: Positivity Problem: Left) Comparison of Identified (Indefinite and 'Corrected') Spectra S_y; Right) Measurement and Identified Positive Definite Spectrum

The above statements lead to a positive definite spectral result, which is shown in figure 7.9. Unfortunately, the corrected spectrum S_y is disadvantageously altered. Because a noise process with large magnitude is necessary, the second vertical bending mode is completely lost. Furthermore, the height of the other peaks is significantly increased. It is even worse, because the added noise process is determined numerically only, hence it is non-physical. Summarizing above, the resulting positive definite spectrum clearly is not applicable for damage identification purposes.

To overcome the above problems, the usage of a positive definite Gramian matrix M instead in equation (5.133) can be useful. In connection with an observable and stable system $H(A, C)$, which model reduction ensures, a Kalman filter must be determinable. As good as this sounds, chosen imprecise noise parameters are disadvantageous for classical $\mathcal{H}^2$ estimation methods, because noise uncertainties should be taken into account.

$\mathcal{H}^\infty$ ESTIMATION is capable of taking noise uncertainties into account, as has been pointed out several times before. In the following, the 'filtering signals in additive noise' approach of section 5.3 is presupposed. Because of the applied model reduction technique, system H is stable and observable. Thus, Riccati equation (5.166) can definitely be solved, which is necessary to determine the $\mathcal{H}^\infty$ estimator Π of equation (5.205). The solution P follows the defined upper bound γ. While the case $\gamma = 1$ leads to $\|P\|_2 \approx 3.580$, Kalman filtering ($\gamma \to \infty$) is much more confident by $\|P\|_2 \approx 210$. Because of noise uncertainties, the $\mathcal{H}^\infty$ case with $\gamma = 1$ is used subsequently.
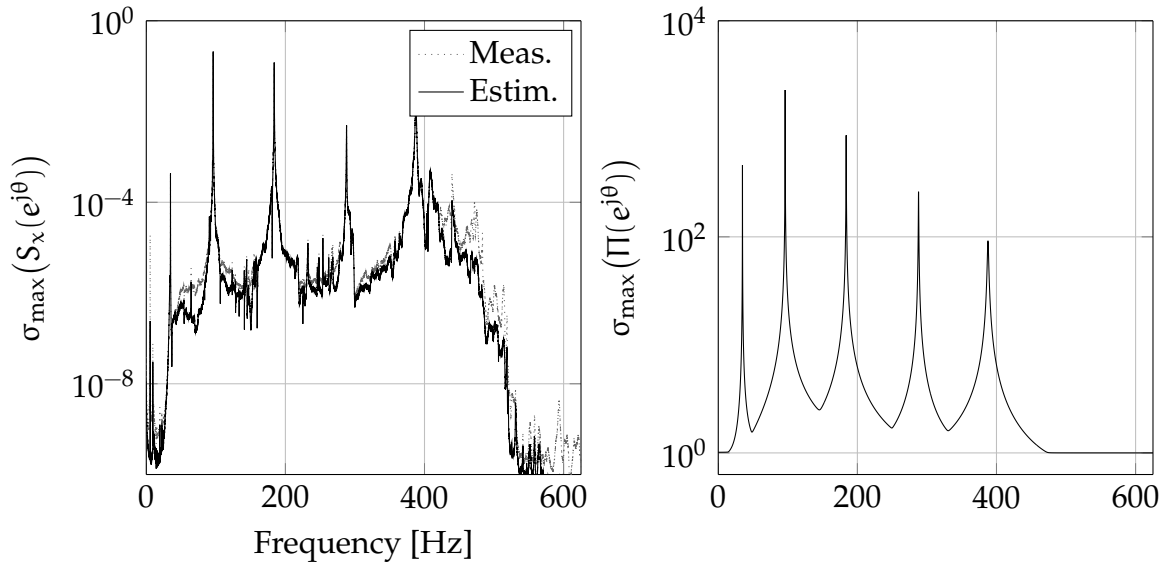
Figure 7.10: $\mathcal{H}^\infty$ Estimation (Left) and Frequency Response of $\mathcal{H}^\infty$ Estimator Π (Right))

By applying the central estimator K_{cen} of equation (5.203), an estimated spectrum $S_{\hat{s}}(e^{j\theta}) = K_{cen}(e^{j\theta})S_y(e^{j\theta})K_{cen}^*(e^{j\theta})$ can be computed, which is shown in figure 7.10.

Because of the chosen value $\gamma = 1$, the transfer function of estimator $\sigma_{max}\left(K_{cen}(e^{j\theta})\right) \leqslant 1$ for $\theta \in [-\pi, \pi]$. As can be seen in the named figure, the measurement noise is partially reduced. Besides that the second to the sixth bending mode peaks are not affected. Because the first natural frequency was not identified, it is filtered out.

In result of the estimator determination, system $\Pi(A, K_p, C)$ can be used for damage identification purposes. Its frequency response is also shown in figure 7.10. This result is the condensed information of the laboratory structure. The inverse $\Pi^{-1}(e^{j\theta})$ is even more interesting, as it maps measured structural responses (accelerations) to the estimation error e, which can be applied for damage identification.

8

EXPERIMENTAL DAMAGE LOCALIZATION BY SP2E

Chapter Outline

This chapter shows the central verification of SP2E by laboratory experiments. The conducted sensitivity studies are based on laboratory measurements only. Neither simulations nor updated mechanical parameters have been used. While the former chapter 7 discussed the identification of the structural reference state, the parametrization of several structural states by SSI and $\mathcal{H}^\infty$ estimation is presupposed here. As it is typical for structural health monitoring, damage identification is conducted via a comparison of a reference and a (potentially) damaged state. Some of the subsequent results have been pre-published by the author.[Art1, Art2]
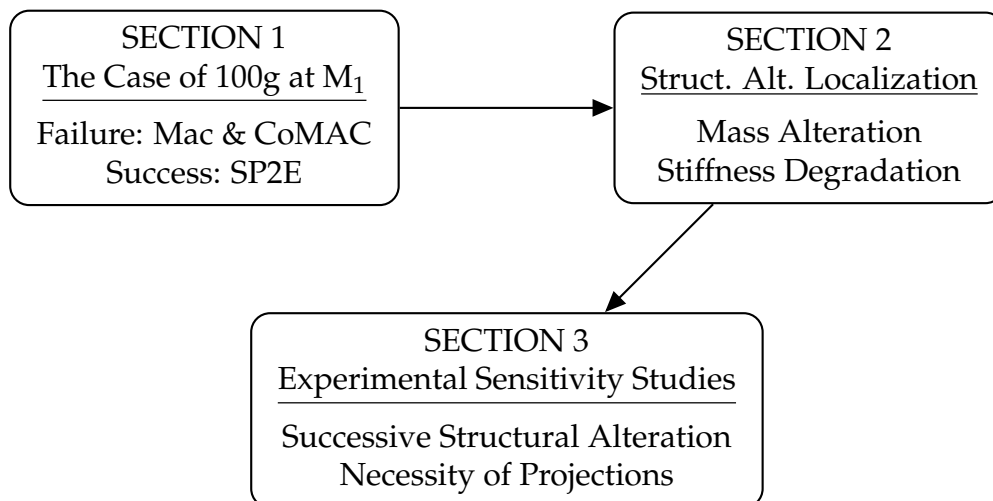

Figure 8.1: Chapter Outline

The conducted and analysed laboratory experiments comprise mass alterations and stiffness degradations. At first four series of measurements, corresponding to four positions of mass alterations, have been conducted. Here, the positions M_1, M_3, M_5 and M_7 were chosen. In each measurement series over 18 experiments have been carried out, in which additional mass configurations 100g, 200g, 400g, 600g, 1000g and 1600g were studied. An exemplary configuration of 1kg at M_1 is shown in figure 8.2a.

The additional masses were realized by magnets. This modification has been chosen, because these reversible experiments were repeated several times for verification. Al-

ternative additional mass configurations were analysed too. By applying those, the influence of magnetic field was proven to be negligible.
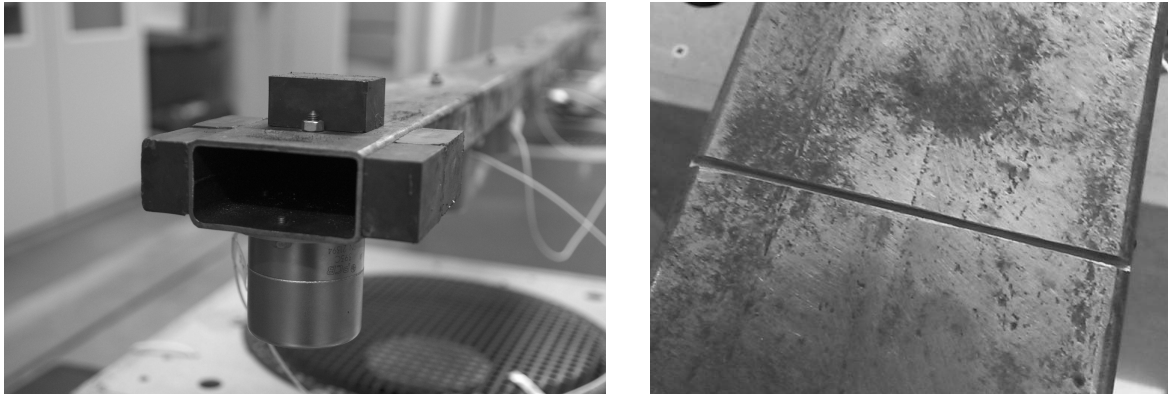
(a) Mass Alteration of 1kg at M_1

(b) Stiffness Degradation by 2.5mm Saw Cut (Material Thickness 2.9mm)

Figure 8.2: Two Examples of Applied Structural Alterations

Besides that mass alterations in between measurement positions were also analysed. Finally, stiffness degradations by successive deepened saw cuts complement the whole experimental analysis. An example can be found in figure 8.2b. Each named experiment was repeated to proof reproducibility.

To give a comprehensive overview of the conducted experiments, the discussion follows a successive generalization. Hence, section 1 begins with results of a detailed case study, especially the additional mass of 100g at M_1. In addition to that, a comparison to simple damage identification techniques shows the necessity for SP2E. Based on that, section 2 is devoted to several case studies of mass alterations and stiffness degradations. In the end section 3 gives several experimental sensitivity studies, which provide an excellent overview of the capability of SP2E in a laboratory environment.

## 8.1 A Detailed Case Study: 100g at M_1

8.1.1 Classical Methods: MAC & CoMAC

To demonstrate the advantages of SP2E, the damage case of 100g additional mass at M_1 is elaborated below. Considering a total weight of 19.4kg (bending beam and sensors), the mass is increased about 0.5%.

In the following, a technique is necessary in the frame of structural health monitoring, which is able to detect and localize the structural alteration. Thus, the spectra of both measurements are compared first in figure 8.3a. As can be seen here both measured spectra, reference and altered, are very similar: While noise terms remain

nearly unchanged, the natural frequencies of the cantilever arm slightly decrease. Very importantly, the relative frequency shift, depicted in figure 8.3b, is below 6‰.
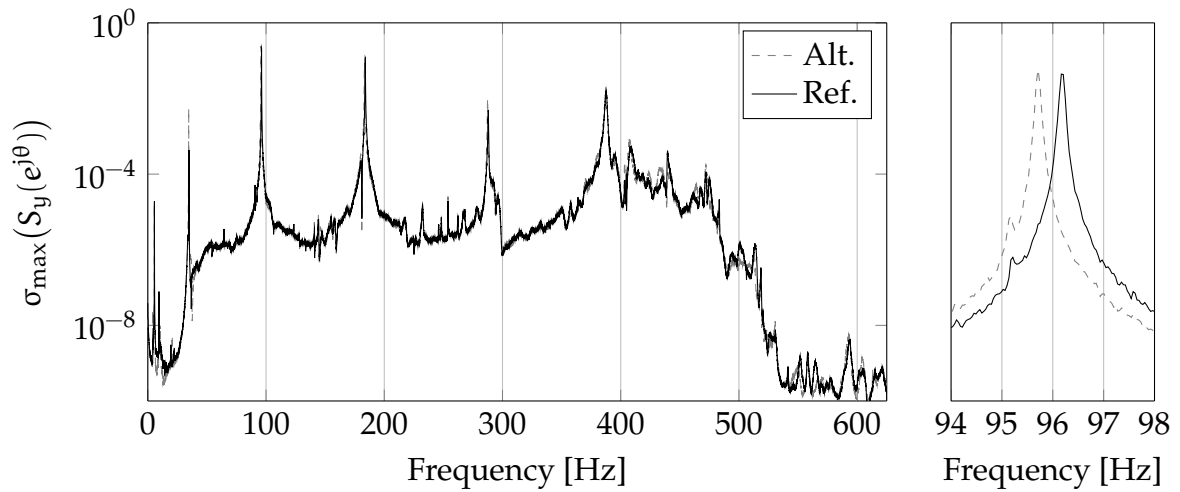
(a) Comparison of Measured Spectra (Left) and Zoom at 3rd Natural Frequency (Right)
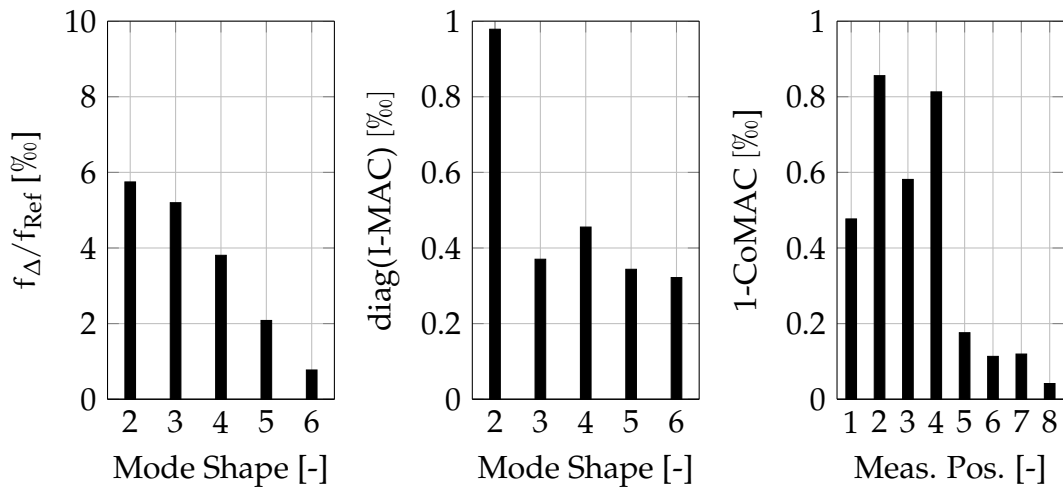
(b) Modal Alteration

Figure 8.3: Spectral Influence Study of 100g at M_1

Both measurements are processed nearly identical: By applying the covariance based stochastic subspace identification of section 7.2, two state space systems $H_1(A_1, C_1)$ and $H_2(A_2, C_2)$ are parametrized. Based on them unscaled mode shapes ϕ_1 and ϕ_2 have been determined, which shall serve for damage identification. Because identified modal dampings may be questionable,[56] they are not called in for that.

One of the most applied techniques to analyse mode shape alterations surely is the modal assurance criterion (MAC). An overview of it and method variations, like the coordinate MAC (CoMAC), can be found in Allemang.[55] By applying ϕ_1 and ϕ_2, the MAC matrix shows similarities between both sets of mode shapes. Hence, in

our case a 5×5 matrix emerges, which nearly is an identity matrix. This can be proven by analysing the Frobenius norm of its difference by $\|MAC - I\|_F \approx 0.01$. To get an impression, the principal diagonal of this difference matrix is also depicted in figure 8.3b: Here, a MAC value above 99.9% indicates a remarkable resemblance. A deviation below 1‰ is very low and may result from numerical inaccuracies. In summary, both sets of unscaled mode shapes ϕ_1 and ϕ_2 nearly are identical.

Secondly, the CoMAC is determined. This value indicates measurement positions, which lead to the mode shape alterations. Obviously, this value is above 99.9% for every position, because it is interconnected with the MAC values.

Based on the above discussion more recent damage identification techniques, like curvatures and modal strain energy, can be applied. Nevertheless, the fundamental problem shall be addressed here only: Damage detection and localization based on modal data only is at least a challenge. Because it is beyond the scope of this thesis, a comprehensive comparison to contemporary damage identification results is omitted.

8.1.2 State Projection Estimation Error

The application of technique state projection estimation error (SP2E) follows chapter 6, especially the summary of section 6.2.4. While the former methods have been based on modal data only, here identified systems $H_1(A_1, C_1)$ and $H_2(A_2, C_2)$ are used to determine $\mathcal{H}^\infty$ estimators. This leads to systems $\Pi_1(A_1, K_{p1}, C_1)$ and $\Pi_2(A_2, K_{p2}, C_2)$. Their inverse can be used to recursively compute estimation error processes e_1 and e_2, whose difference $d = e_1 - e_2$ is important for damage identification.

Because it is more illustrative from an engineering oriented viewpoint, a spectral approach (frequency domain) is subsequently focussed. For that, some additional notations are necessary:

$$S_{e1}(z) = \Pi_1^{-1}(z)S_{y2}(z)\Pi_1^{-*}(z^{-*}), \quad S_{e2}(z) = \Pi_2^{-1}(z)S_{y2}(z)\Pi_2^{-*}(z^{-*}) \tag{8.1a}$$

$$\text{with} \quad S_{y2}(z) = H_2(z)M_2H_2^*(z^{-*}) \quad \text{and} \quad z = e^{j\theta} . \tag{8.1b}$$

These spectral results are depicted in figure 8.4. As can be seen there, both spectra S_{e1} and S_{e2} nearly are white noise, thus are very similar. However, S_{e1} has additional spectral peaks following the input S_{y2} due to slight system alterations. It is important to remark that estimator Π_1 was designed on the basis of S_{y1}, not S_{y2}. Finally, the central advantage of using the identified spectrum S_{y2} following H_2 and M_2, in opposite to the originally measured raw one, is apparent: Determined spectra are smooth, and hence are advantageous to analyse.

As have been pointed out in chapter 6, a key idea of using d instead of e_1 is the reduction of measurement noise. This effect can clearly be seen in figure 8.4. Very interestingly, the difference process is mainly determined by the important frequency content of S_{y2}, which already was present in S_{e1}. This important spectral content
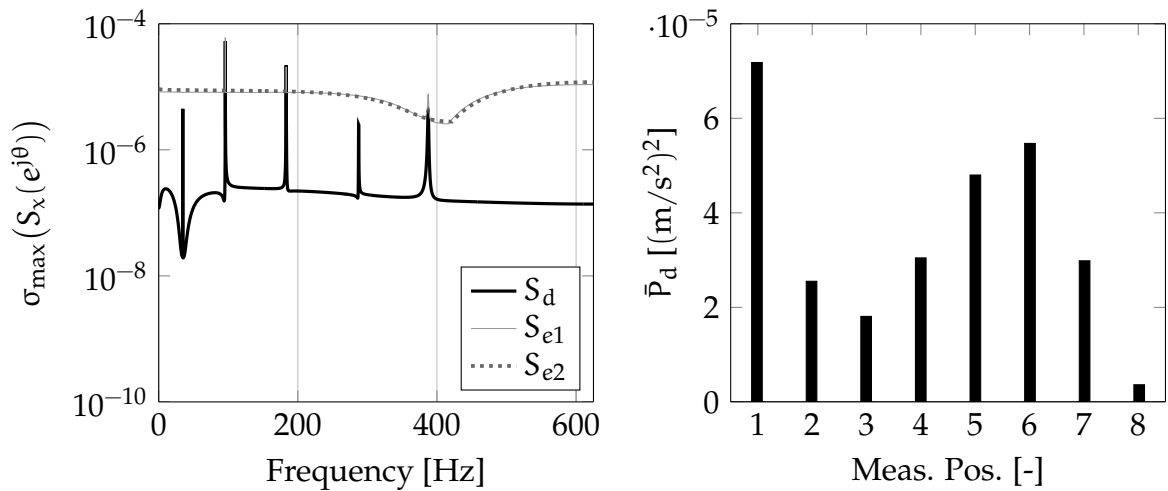
Figure 8.4: Damage Identification by $\bar{P}_d$ Following S_d

follows the inherent modal properties of the altered system (state 2). In an online structural health monitoring concept this refers to the current (possibly altered) structural state.

Finally, the average process power $\bar{P}_d$ is computed by equation (6.28). It roughly gives an indication on the first measurement position as the damage location. It now is reasonable to concentrate on the relevant frequency content in S_d to enhance the damage identification result. Therefore, projection techniques are applied.

STATE PROJECTIONS have been elaborated in section 6.2. Because of their introduction, a definition of states x_2 becomes necessary. Therefore, the choice $\Pi_{33} \to \Pi_{22}$ is
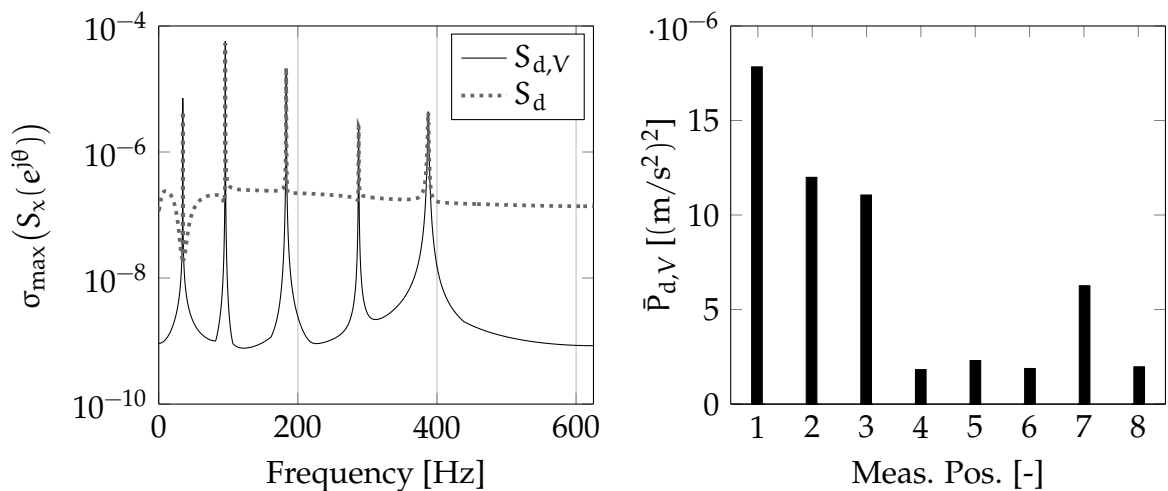

Figure 8.5: SP2E Results: Damage Identification by $\bar{P}_{d,V}$ Following $S_{d,V}$

applied following the summary of section 6.2.4. Essentially, this decision presupposes a nearly perfect state estimate in Π_2, which of course is more a practical assumption than a theoretical general one.

The projection results are given in figure 8.5. As was expected, the relevant frequency content in S_d now is more significant. While the peak heights and positions remain, the noise in between natural frequencies is reduced. This emphasizes the necessity of projection techniques.

For damage identification the result $\bar{P}_{d,V}$ is computed by equation (6.58). A comparison of $\bar{P}_d$ to $\bar{P}_{d,V}$ in figures 8.4 and 8.5 again emphasizes the need of projection methods: Now, the damage location is indicated correctly. Although result $\bar{P}_{d,V}$ may seem like it follows the first bending mode, natural frequency was not identified at all (see section 7.2).

By analysing figure 8.5, one can dig deeper by applying model reduction techniques. This allows to study the influence of each mode shape on the result $\bar{P}_{d,V}$. But in view of real-life monitoring situations this is not expedient, because one simply does not know which frequency part of S_d points on an occurred structural damage in the first place.

In summary, method SP2E properly indicates the position of experimentally added mass (approximately 0.5% of total structural mass). In the end the question emerges, which magnitude of $\bar{P}_{d,V}$ is relevant. To decide whether $\bar{P}_{d,V}$ of about $10^{-6}(\mathrm{m/s}^2)^2$ should be considered as an indication of damage, a reference value must be introduced. This is done in connection with further damage scenarios in the following.

8.2 Damage Localization and the Reference Value

8.2.1 Mass Alterations at and between Measurement Positions

The idea of introducing a reference value is a logical consequence of former statements: By using two different measurements of the same structural state, a SP2E result can be computed, which shows the possible numerical accuracy. For structural health monitoring concepts this is conducted during the baseline phase, which gives the basis for the actual inspection phase. This formal structure has been described in accordance with Fassois et al.[146] Thus, two measurements of the reference state should be used for that.

Following the above concept of reference value, its result is depicted in figure 8.6a. Hence, an average process power $\bar{P}_{d,V}$ of about $10^{-9}(\mathrm{m/s}^2)^2$ has been the lower numerical bound in the author's analyses. This value is plausible, because $R_{d,V}(0)$ should tend to be a zero matrix, if no damage occurred.

Besides that, two additional damage scenarios, 100g at M_5 and M_7, are also shown in the named figure. Both results are approximately $10^{-5}(\mathrm{m/s}^2)^2$, and thus are signifi-

cantly larger than the reference value. Furthermore, they correctly indicate the right position of experimentally added mass.
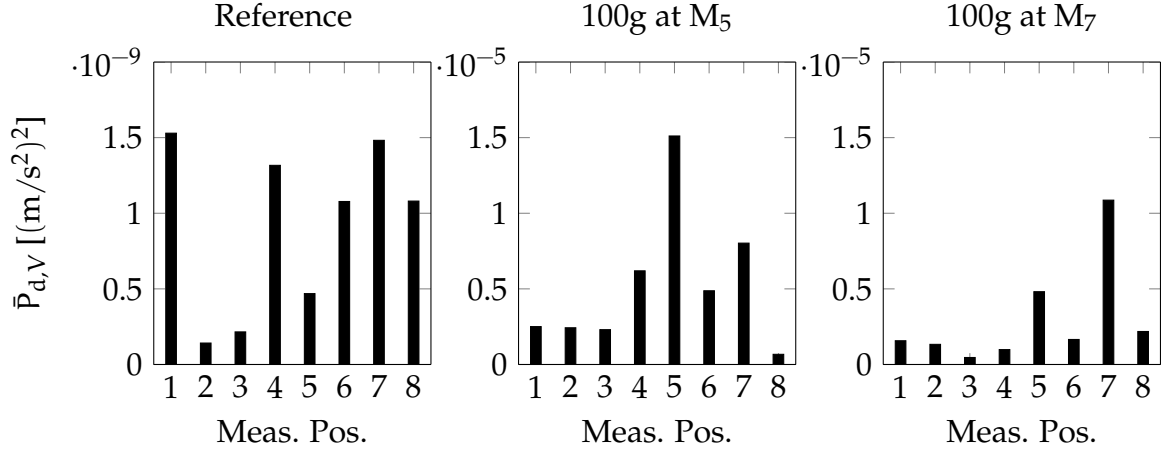
(a) Reference State (left), 100g at M_5 (Middle) and 100g at M_7 (right)
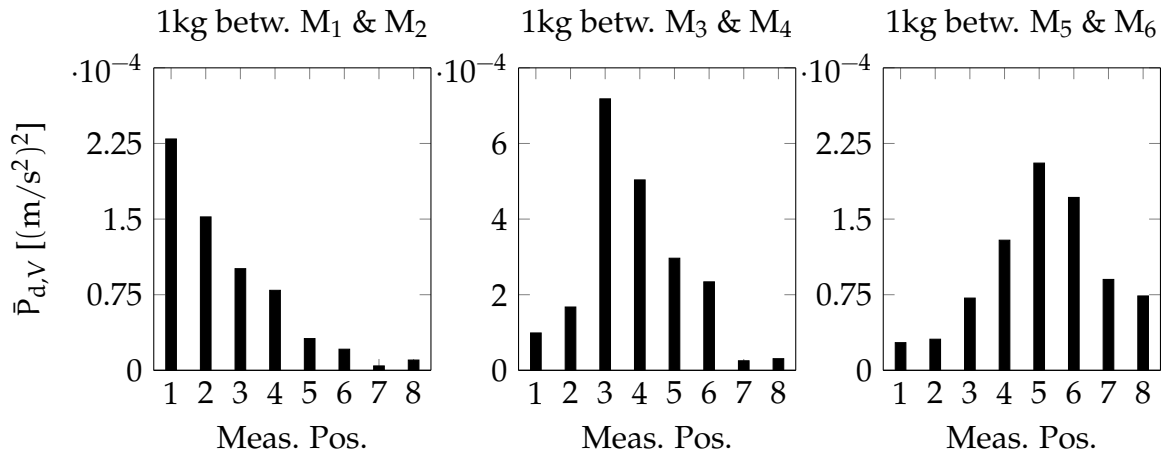
(b) Applied Mass between Measurement Positions

Figure 8.6: Average Process Power $\bar{P}_{d,V}$ for Mass Alterations

MASS ALTERATIONS BETWEEN MEASUREMENT POSITIONS have also been studied. The result for that is given in figure 8.6b. Here, 1kg has been successively applied between two accelerometers in three different test scenarios. Again the central damage identification result $\bar{P}_{d,V}$ is much larger than the determined reference value.

Always these two elements in $\bar{P}_{d,V}$ rise most, where experimentally added mass has been applied. Furthermore, the average process power of about $10^{-4}(m/s^2)^2$ is larger than the 100g scenarios, which is plausible. Hence, the localization of additional mass in between measurement points is experimentally verified.

8.2.2 STIFFNESS DEGRADATIONS

Rather than identifying mass alterations, structural health monitoring systems must be able to detect and localize stiffness degradations. Therefore, the stiffness of the laboratory structure has been reduced by successively deepening a saw cut between M_5 and M_6. By applying SP2E, the damage shall be localized. Following that, the results are shown in figure 8.7.
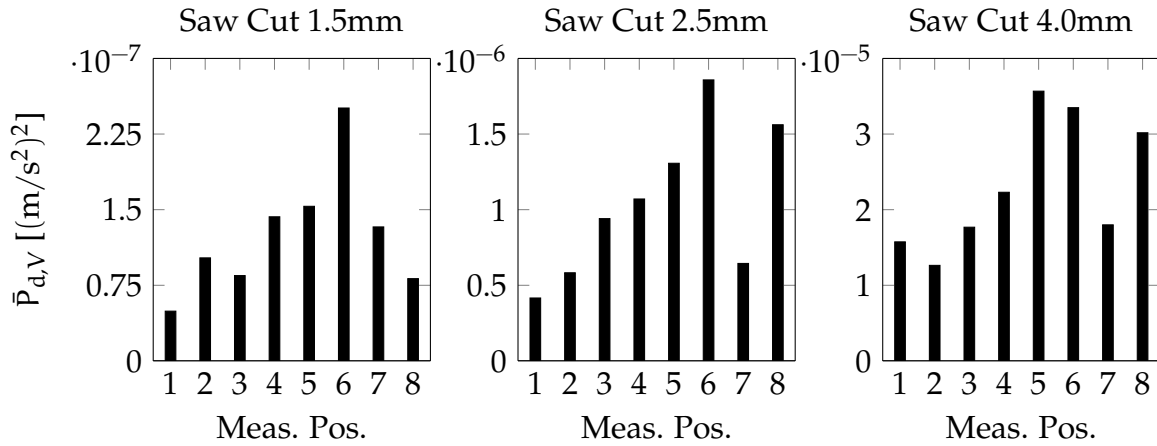

Figure 8.7: Average Process Power $\bar{P}_{d,V}$ for Stiffness Degradations between M_5 and M_6: Saw Cuts $1.5\ldots4.0$mm

Again a reference value was found first by comparing two measurements of the un-damaged structural state, which led to a plausible value $\bar{P}_{d,V}$ below $10^{-9}(m/s^2)^2$. Then a saw cut has been applied. By increasing the experimentally induced damage, the average process power $\bar{P}_{d,V}$ rises. Furthermore, high values at M_5 and M_6 indicate the right damage position. Hence, stiffness reductions are experimentally locatable by SP2E. Nevertheless, the damage localization results are less clear in comparison to the case of applied masses.

8.3 EXPERIMENTAL SENSITIVITY STUDIES

8.3.1 EXPERIMENTAL SUCCESSIVE MASS ALTERATION

In this section four experimental sensitivity studies are shown and discussed. In these studies additional structural mass was applied at the laboratory structure of figure 7.2 in separate configurations: Four series of measurements, corresponding to four positions of mass alterations, have been conducted. Here the positions M_1, M_3, M_5 and M_7 were chosen. In each measurement series over 18 experiments have been carried out, in which additional mass configurations 100g, 200g, 400g, 600g, 1000g and

1600g were studied. Each experiment was repeated to proof reproducibility. Thus, magnets have been applied.
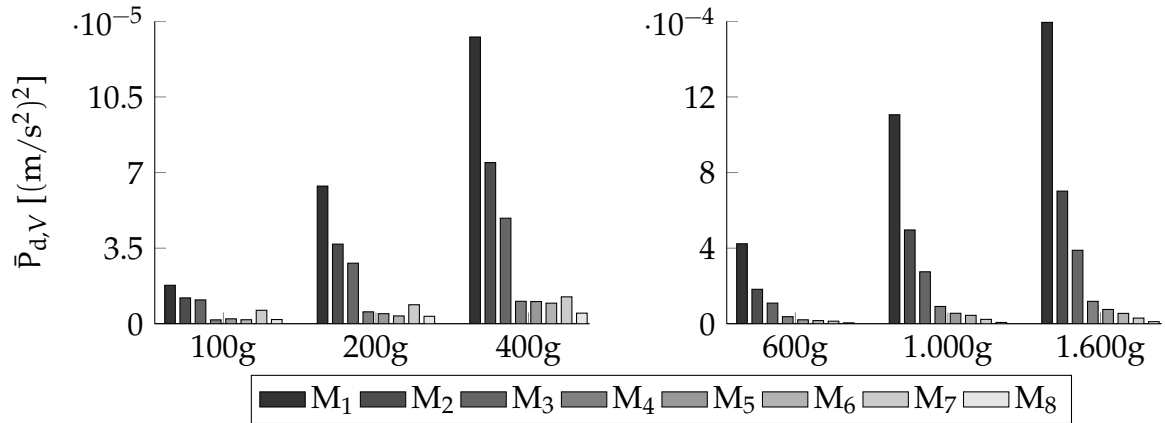
(a) Experimentally Applied Mass at M_1
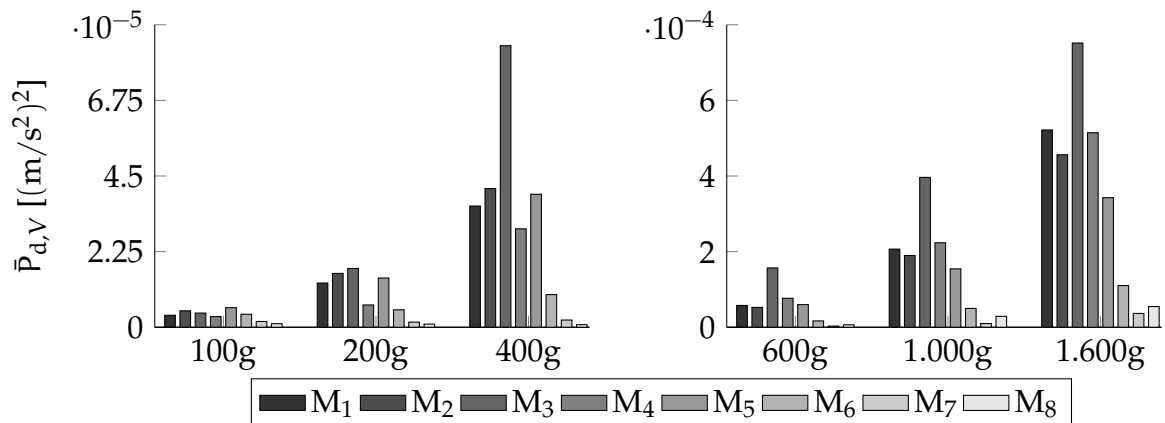
(b) Experimentally Applied Mass at M_3

Figure 8.8: Experimental Sensitivity Studies for M_1 and M_3

THE SUCCESSIVE MASS INCREASE at M_1 is considered first, which is depicted in figure 8.8a. Note here that the left diagram is scaled differently than the right one. While the first result have already been discussed in connection with figure 8.5, further experiments are also shown. As can be seen for every mass configuration, the first measurement position is correctly indicated by SP2E. Furthermore, $\bar{P}_{d,V}$ increases as heavier additional mass is applied. In connection with confirmed reproducibility these facts emphasize plausibility of method SP2E.

By looking at figure 8.8a, one may falsely assume to revisit the first bending mode. This is impossible, because the first natural frequency was omitted in the identification process, as was explained in section 7.2.

Based on the results for M_1, the experiments have been repeated for an mass alteration at M_3 in figure 8.8b. Here, the only result occurred (100g at M_3) where damage was detected, but not localized. Nevertheless, $\bar{P}_{d,V}$ indicates the right damage position for mass larger than 100g. Very interestingly, numerical inaccuracies are more present here.
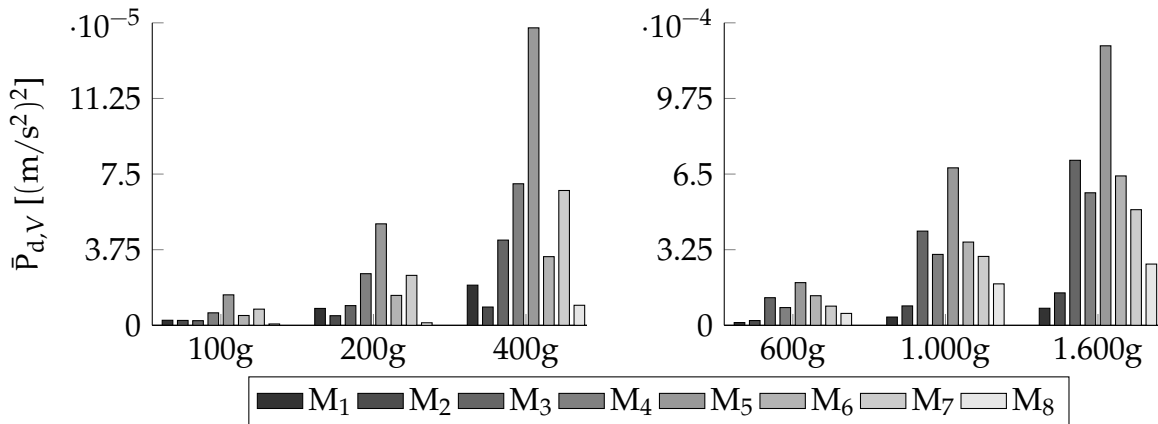
(a) Experimentally Applied Mass at M_5

(b) Experimentally Applied Mass at M_7

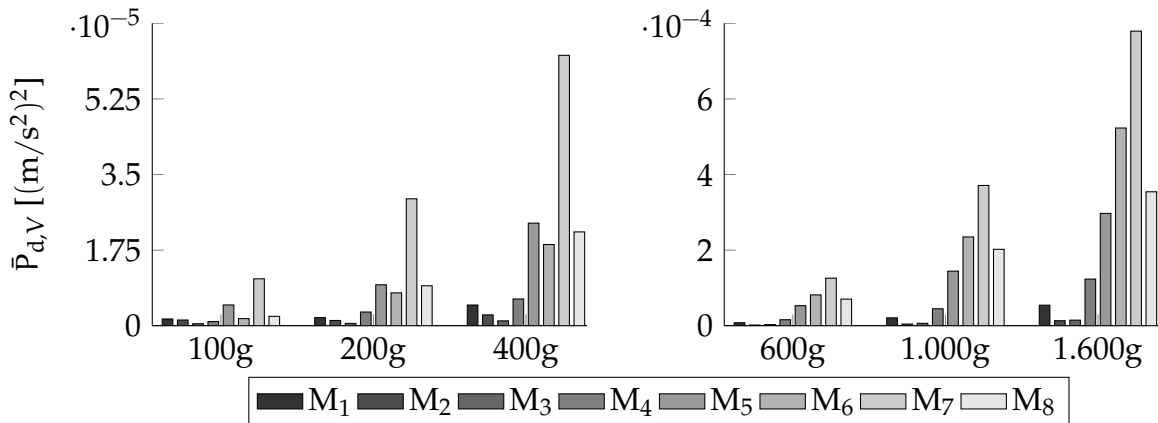Figure 8.9: Experimental Sensitivity Studies for M_5 and M_7

Finally, the measurement series for M_5 and M_7 are given in figures 8.9a and 8.9b. The recognized new insights are revisited here. Again, all damage identification results $\bar{P}_{d,V}$ indicate the right damage position.

By analysing the given sensitivity studies, the connection between increased values in the average power $\bar{P}_{d,V}$ and the point of mass alteration becomes evident. Hence, the localization of experimentally added structural mass was successful.

8.3.2 NECESSITY OF PROJECTIONS

Finally, the influence of projection techniques shall be discussed once more. While figure 8.5 already gave projection results for a single damage case, here its influence for a whole measurement series shall be analysed. To show the necessity of projection techniques, their influence is shown at the example of mass alterations at M_1 in the following. The results of sensitivity studies at M_3, M_5 and M_7 are omitted here, because redundant information is apparent there.
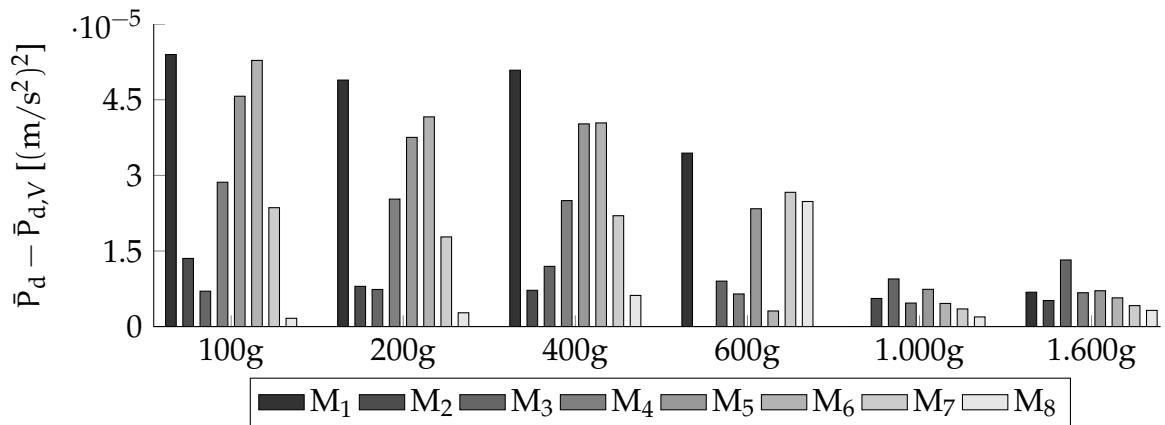
Figure 8.10: Influence of Projections

To analyse the influence of projections, the difference $\bar{P}_d - \bar{P}_{d,V}$ is depicted in figure 8.10. In every mass configuration this noise has a comparable magnitude, which is plausible because structural alterations should not decrease numerical accuracy. Furthermore, damage localization of small structural damage (100g and 200g) was possible only by applying projection techniques. In summary, projection techniques enhance the damage identification by SP2E and is necessary to allow the localization of small structural damage.

9

DISSERTATION SYNTHESIS

9.1 SUMMARY

A new damage identification method on the basis of state projection estimation error (SP2E) is proposed in this dissertation. It can allow online structural health monitoring (SHM) for automatic structural damage localization. To derive that, several theories have been demonstrated in this thesis. At the beginning first principle based mechanical systems and resulting structural response determination in time and frequency domain in accordance with force excitations have been discussed. To demonstrate the explained techniques, a simulated structural dynamics example then was pointed out.

This then led to the subspace identification of mechanical structures, which applies known excitations and responses to parametrize a general system accordingly. Here, a distinction between stochastic and deterministic methods is fundamental for method derivations. These techniques then entered an operational modal analysis example.

In view of the former methods, the application of corresponding mechanical parameters, like the experimental flexibility, seems plausible for damage localization. Nevertheless, an automated SHM technique requires ambient structural excitations, like wind, vehicle traffic and waves. Thus, stochastic subspace identification techniques are necessary, which in general are problematic for a gain determination. Here, the positivity problem to solve a Riccati equation for Kalman gain determinations can be named as an example. Unfortunately, this would be necessary to apply corresponding mechanical parameters. As a consequence, barely known and new methods have been introduced and explained afterwards.

A generalization of the Kalman filter is the so called $\mathcal{H}^\infty$ estimator. These generalized systems allow to cope with model and noise uncertainties, which is necessary in view of former statements. The indefinite quadratic estimation theory, which is based on projections in Krein spaces, has been elaborated, because this $\mathcal{H}^\infty$ theory can be seen as a direct application of the commonly known Kalman-Yakubovich-Popov (KYP) Lemma for extended systems.

To give a comprehensive estimator overview, the finite horizon, beginning with time-varying Kalman filter, and the infinite horizon, formerly known for the Wiener-Kalman filter, was explained. While the first named approach focuses on indefinite quadratic forms in time domain, the second approach is devoted to the canonical spectral factorization of a Popov function. Here, the Popov function's basic form, the power spectral density of measurements for the Kalman filter, needed to be extended.

This then led to the introduction of the central $\mathcal{H}^\infty$ estimator, an important result of estimation theory. Finally, the application case of 'filtering signals in additive noise' was discussed and applied at the formerly introduced structural dynamics example.

By considering all the former theories, the technique 'state projection estimation error' (SP2E) was finally introduced. In principle it is based on a defined difference process, applied by estimation errors following the Krein space based $\mathcal{H}^\infty$ theory. To analyse this damage process, the average process power was proposed. The difference process then was revisited by system theoretic viewpoints, which led to the advantageous numerical determination of average process power by a Lyapunov equation.

Although the theory of difference process implements inherent measurement noise reduction, numerical accuracy can be improved even further by projection techniques. Here, projection methods are applied to system states, whose results are discussed. In summary, a stable damage identification method was derived.

Very importantly, the newly proposed method SP2E was verified in laboratory experiments. To do so, the subspace identification of a laboratory structure at Leipzig University of Applied Sciences was elaborated first. Here, the identification was conducted by self-developed software. All chosen identification parameters are justified. Afterwards, the $\mathcal{H}^\infty$ estimation in context of 'filtering signals in additive noise' was discussed.

The experimental verification was proven by four experimental sensitivity studies. While the localization of experimental structural alterations have been discussed in detail first, an overview of about 100 measurements is given afterwards. These experiments comprise mass alterations and stiffness degradations. A major element of this are four measurement series, corresponding to four positions of experimental mass alterations. Additional masses have been separately applied at four different measurement positions. Additional mass configurations in six different scenarios were studied and in each measurement series over 18 experiments were carried out, considering a repetition to prove repeatability.

Sensitivity studies are conducted by experimental structural alterations in the laboratory, not simulations. In summary, the experiments proved the applicability of SP2E for damage localization. The experiment have been repeated and results are plausible.

9.2 CONCLUSIONS

Automated structural health monitoring requires ambient vibrations. Hence, stochastic identification methods must be utilized. While operational modal analysis allows the computation of natural frequencies and unscaled mode shapes, damage identification based on them may be a challenge. Unfortunately, the gain determination is problematic for stochastic methods, as would be necessary for the determination of corresponding mechanical parameters. In consequence, a damage identification

technique based on ambient vibrations, capable of dealing with structural excitation uncertainties is required.

To overcome the above problems, method SP2E has been proposed on the basis of output-only identification, $\mathcal{H}^\infty$ estimation and oblique projections. By combining these methods, several advantages arise:

i) Measured processes can be treated as stochastic and deterministic ones.

ii) Disturbance inputs w and v may be unknown due to $\mathcal{H}^\infty$ estimation.

iii) White (e.g. FEM) and black-box approaches (e.g. SSI) can be used. Furthermore, these different model-types can be combined.

iv) Systems with inconsistent model orders can be used, because of developed projection constraint parameters (Y, Z).

v) State space systems have been used. Hence, time and z-domain problems can be treated equivalently.

vi) The synchronization and normalization of process d has been introduced on the basis of a general input y_3. This circumvents the gain determination problem.

vii) The usage of a parametrized input S_{y3} leads to smooth damage identification results.

viii) Because estimation theory has been applied, a real-time damage identification technique is in principle possible.

The proposed method SP2E has comprehensively been evaluated in laboratory experiments. These experiments comprise test scenarios with altered mass and stiffness configurations. Furthermore, four experimental sensitivity studies were analysed. Here, structural alteration have been applied experimentally, not in simulations. The repeated, objective experimental results are very promising. Finally, the requirement for projection techniques was shown experimentally.

9.3 PROSPECTIVE RESEARCH

While plenty research has already been done on SP2E, from development to verification, open scientific questions remain. The author recognizes three main research areas, which are necessary for SP2E to become industrial standard:

i) SP2E algorithm optimization, especially in view of real-time capability.

ii) Theoretical and practical compensation of environmental and operational conditions (EOC).

iii) Application in large-scale experiments.

The first argument is self-explanatory: Further studies on the SP2E algorithm may improve numerical accuracy and damage identification results. Here, the path of

system theoretic methods should be followed further on. Furthermore, a comparison to modern damage identification techniques, like modal strain energy, might show advantages and disadvantages for large-scale applications.

Secondly, the method urgently needs an approach to compensate environmental and operational conditions (EOC). It is well known that these conditions, especially temperature, may have tremendous effects on damage identification results. Usually natural frequencies are normalized only, but here whole systems need adjustments. Finally, the experimental work must be continued. Because an application at large structures, like wind energy plants and bridges, is intended, pilot projects need to be started first.

Finally, the author recognizes numerous more possible theoretical developments. In view of the experimental results so far, a remarkable potential of SP2E for future applications truly is given.

BIBLIOGRAPHY

[1] A. Lenzen and D. Hartmann. Stochastic structural analysis and lifetime oriented optimization. *Optimization*, 47(3-4):369–381, 2000.

[2] L.F Cabeza, L. Rincón, V. Vilariño, G. Pérez, and A. Castell. Life cycle assessment (LCA) and life cycle energy analysis (LCEA) of buildings and the building sector: A review. *Renewable and Sustainable Energy Reviews*, 29:394–416, 2014.

[3] H. Islam, M. Jollands, and S. Setunge. Life cycle assessment and life cycle cost implication of residential buildings – a review. *Renewable and Sustainable Energy Reviews*, 42:129–140, 2015.

[4] H. Waller and R. Schmidt. *Schwingungslehre für Ingenieure: Theorie, Simulation und Anwendung*. Springer Berlin Heidelberg, 1989.

[5] M. Link. *Modal Analysis and Testing*, chapter Updating of analytical models - Basic procedures and extensions, pages 281–304. Kluwer Academic Publishers, 1999.

[6] A. Deraemaeker and K. Worden. *New Trends in Vibration Based Structural Health Monitoring*. CISM International Centre for Mechanical Sciences. Springer, 2012.

[7] W. Ostachowicz and A. Güemes. *New Trends in Structural Health Monitoring*. CISM International Centre for Mechanical Sciences. Springer, 2013.

[8] L. Gaul, H. Albrecht, and J. Wirnitzer. Semi-active friction damping of large space truss structures. *Shock and Vibration*, 11(3-4):173–186, 2004.

[9] A. Lenzen and H. Waller. From black to white box models in structural mechanics. *2nd International Conference Lifetime Oriented Design Concepts (ICLODC)*, 2004.

[10] J. Mottershead, M. Broggi, H.M. Gomes, Y. Govers, H. Haddad Khodaparast, M. Link, E. Patelli, and T.A.N. Silva. Perspectives on model updating. *ICEDyn 2015 - International Conference on Structural Engineering Dynamics*, 2015.

[11] C. Xia and G. De Roeck. Modal analysis of the jalon viaduct using FE updating. *Proceedings of the 9th International Conference on Structural Dynamics, EURODYN 2014*, 2014.

[12] J.E. Mottershead, M. Link, and M. Friswell. The sensitivity method in finite element model updating: a tutorial. *Mechanical systems and signal processing*, 25(7):2275–2296, 2011.

[13] M. Link and M. Weiland. Extending a deterministic computational model updating technique to estimating the parameter variability caused by non-deterministic test data-a tool for structural health monitoring. *Proceedings of ISMA2014 including USD2014*, 2014.

[14] Y. Govers, H.H. Khodaparast, M. Link, and J.E. Mottershead. A comparison of two stochastic model updating methods using the DLR AIRMOD test structure. *Mechanical Systems and Signal Processing*, 52:105–114, 2015.

[15] A. Cunha, E. Caetano, F. Magalhães, and C. Moutinho. Recent perspectives in dynamic testing and monitoring of bridges. *Structural Control and Health Monitoring*, 20(6):853–877, 2013.

[16] H. Sohn, C.R. Farrar, F.M. Hemez, D.D. Shunk, D.W. Stinemates, B.R. Nadler, and J.J. Czarnecki. A review of structural health monitoring literature: 1996–2001. *Los Alamos National Laboratory*, 2003.

[17] P. Van Overschee and B. De Moor. *Subspace Identification for Linear Systems: Theory, Implementation, Applications*. Kluwer Academic Publishers, 1996.

[18] L. Ljung. *System Identification: Theory for the User, PTR Prentice Hall Information and System Sciences Series*. Prentice Hall, New Jersey, 1999.

[19] T. Katayama. *Subspace Methods for System Identification*. Communications and Control Engineering. Springer, 2005.

[20] T. Kailath, A.H. Sayed, and B. Hassibi. *Linear Estimation*. Prentice Hall, 2000.

[21] B.L. Ho and R.E. Kalman. Effective construction of linear state-variable models from input/output functions. *Automatisierungstechnik*, 14(1–12):545–548, 1966.

[22] P. Van Overschee and B. De Moor. N4SID: Subspace algorithms for the identification of combined deterministic-stochastic systems. *Automatica*, 30(1, Special Issue on Statistical Signal Processing and Control):75–93, 1994.

[23] M. Verhaegen and P. Dewilde. Subspace model identification part 1. the output-error state-space model identification class of algorithms. *International journal of control*, 56(5):1187–1210, 1992.

[24] M. Verhaegen and P. Dewilde. Subspace model identification part 2. analysis of the elementary output-error state-space model identification algorithm. *International journal of control*, 56(5):1211–1241, 1992.

[25] C. Ebert. *Systemidentifikation zur Modellierung mechanischer Strukturen: Markovparameter zur experimentellen Schadenserfassung*. Dissertation, Universität Siegen, 2013.

[26] P.L. Faurre. Stochastic realization algorithms. *System Identification: Advances and Case Studies*, 126:1–25, 1976.

[27] W.E. Larimore. Canonical variate analysis in identification, filtering and adaptive control. *Proc. 29th IEEE Conference on Decision and Control*, pages 596–604, 1990.

[28] H. Akaike and Hirotugu Akaike. Markovian representation of stochastic processes by canonical variables. *SIAM Journal on Control*, 13(1):162–173, 1975.

[29] T. Katayama. Realization of stochastic systems with exogenous inputs and subspace identification methods. *Automatica*, 35(10):1635–1652, 1999.

[30] M. Verhaegen. Identification of the deterministic part of MIMO state space models given in innovations form from input-output data. *Automatica*, 30(1):61–74, 1994.

[31] G. van der Veen, J.W. Wingerden, M. Bergamasco, M. Lovera, and M. Verhaegen. Closed-loop subspace identification methods: an overview. *IET Control Theory & Applications*, 7(10):1339–1358, 2013.

[32] T. Katayama, H. Kawauchi, and G. Picci. Subspace identification of closed loop systems by the orthogonal decomposition method. *Automatica*, 41(5):863–872, 2005.

[33] V. Sima. *Algorithms for Linear-Quadratic Optimization*. Chapman & Hall/CRC Pure and Applied Mathematics. Taylor & Francis, 1996.

[34] V. Ionescu, C. Oară, and M. Weiss. *Generalized Riccati Theory and Robust Control: A Popov Function Approach*. Wiley, 1999.

[35] R.J. Vaccaro and T. Vukina. A solution to the positivity problem in the state-space approach to modeling vector-valued time series. *Journal of Economic Dynamics and Control*, 17(3):401 – 421, 1993.

[36] J. Mari. Modifications of rational transfer matrices to achieve positive realness. *Signal Processing*, 80(4):615–635, 2000.

[37] H. Akçay. Subspace-based spectrum estimation in frequency-domain by regularized nuclear norm minimization. *Signal Processing*, 99:69–85, 2014.

[38] P. Mellinger, M. Döhler, and L. Mevel. Variance estimation of modal parameters from output-only and input/output subspace-based system identification. *Journal of Sound and Vibration*, 379:1–27, 2016.

[39] N.M.M. Maia and J.M.M Silva. *Theoretical and experimental modal analysis*. Research Studies Press, 1997.

[40] R. Brincker, L. Zhang, and P. Andersen. Modal identification from ambient responses using frequency domain decomposition. *Proc. of the 18th International Modal Analysis Conference (IMAC), San Antonio, Texas*, 2000.

[41] R. Brincker, C. Ventura, and P. Andersen. Damping estimation by frequency domain decomposition. In *19th International Modal Analysis Conference*, pages 698–703, 2001.

[42] K. Fukuzono. *Investigation of multiple-reference Ibrahim time domain modal parameter estimation technique*. University of Cincinnati, 1986.

[43] B. Peeters and G. De Roeck. Reference-based stochastic subspace identification for output-only modal analysis. *Mechanical Systems and Signal Processing*, 13(6):855–878, 1999.

[44] B. Peeters. *System identification and damage detection in civil engineering*. PhD thesis, KU Leuven, 2000.

[45] E. Reynders, K. Maes, G. Lombaert, and G. De Roeck. Uncertainty quantification

in operational modal analysis with stochastic subspace identification: validation and applications. *Mechanical Systems and Signal Processing*, 66:13–30, 2016.

[46] P. Guillaume, P. Verboven, S. Vanlanduit, H. Van der Auweraer, and B. Peeters. A poly-reference implementation of the least-squares complex frequency-domain estimator. In *Proceedings of IMAC*, volume 21, pages 183–192, 2003.

[47] B. Cauberghe. *Applied frequency-domain system identification in the field of experimental and operational modal analysis*. PhD thesis, VUB, Brussel, 2004.

[48] B. Peeters, F. Vanhollebeke, and H. van der Auweraer. Operational polymax for estimating the dynamic properties of a stadium structure during a football game. *Proceedings of the IMAC*, 23, 2005.

[49] J. Helsen, C. Devriendt, W. Weijtjens, and P. Guillaume. Experimental dynamic identification of modeshape driving wind turbine grid loss event on nacelle testrig. *Renewable Energy*, 85:259–272, 2016.

[50] E. Reynders and G. De Roeck. Reference-based combined deterministic–stochastic subspace identification for experimental and operational modal analysis. *Mechanical Systems and Signal Processing*, 22(3):617–637, 2008.

[51] C.R. Farrar, S.W. Doebling, and D.A. Nix. Vibration–based structural damage identification. *Philosophical Transactions of the Royal Society of London A: Mathematical, Physical and Engineering Sciences*, 359(1778):131–149, 2001.

[52] A. Rytter. *Vibration based inspection of civil engineering structures*. PhD thesis, department of building technology and structural enginnering, Aalborg University, 1993.

[53] K. Worden, C.R. Farrar, G. Manson, and G. Park. The fundamental axioms of structural health monitoring. In *Proceedings of the Royal Society of London A: Mathematical, Physical and Engineering Sciences*, volume 463, pages 1639–1664. The Royal Society, 2007.

[54] H.G. Natke and C. Cempel. *Model-aided diagnosis of mechanical systems: Fundamentals, detection, localization, assessment*. Springer Science & Business Media, 2012.

[55] R.J. Allemang. The modal assurance criterion–twenty years of use and abuse. *Sound and vibration*, 37(8):14–23, 2003.

[56] C. Rainieri, G. Fabbrocino, and E. Cosenza. Some remarks on experimental estimation of damping for seismic design of civil constructions. *Shock and Vibration*, 17(4, 5):383–395, 2010.

[57] R.P. Bandara, T.H.T. Chan, and D.P. Thambiratnam. Frequency response function based damage identification using principal component analysis and pattern recognition technique. *Engineering Structures*, 66:116–128, 2014.

[58] V.H. Nguyen and J.C. Golinval. Localization and quantification of damage in beam-like structures using sensitivities of principal component analysis results. *Mechanical Systems and Signal Processing*, 24(6):1831–1843, 2010.

[59] J. Ciambella and F. Vestroni. The use of modal curvatures for damage localization in beam-type structures. *Journal of Sound and Vibration*, 340:126–137, 2015.

[60] D. Dessi and G. Camerlengo. Damage identification techniques via modal curvature analysis: overview and comparison. *Mechanical Systems and Signal Processing*, 52:181–205, 2015.

[61] W. Fan and P. Qiao. A strain energy-based damage severity correction factor method for damage identification in plate-type structures. *Mechanical Systems and Signal Processing*, 28:660–678, 2012.

[62] A. Lenzen and H. Waller. Identification using the algorithm of singular value decomposition – an application to the realisation of dynamic systems and to fault detection and localisation. *Mechanical systems and signal processing*, 11(3):441–457, 1997.

[63] E. Reynders and G. De Roeck. A local flexibility method for vibration-based damage localization and quantification. *Journal of sound and vibration*, 329(12):2367–2383, 2010.

[64] A.Z. Hosseinzadeh, A. Bagheri, G.G. Amiri, and K.Y. Koo. A flexibility-based method via the iterated improved reduction system and the cuckoo optimization algorithm for damage quantification with limited sensors. *Smart Materials and Structures*, 23(4), 2014.

[65] M.L. Fugate, H. Sohn, and C.R. Farrar. Vibration-based damage detection using statistical process control. *Mechanical Systems and Signal Processing*, 15(4):707–721, 2001.

[66] P.J. McGetrick and C.W Kim. A parametric study of a drive by bridge inspection system based on the Morlet wavelet. In *Key Engineering Materials*, volume 569, pages 262–269. Trans Tech Publ, 2013.

[67] A. Deraemaeker, E. Reynders, G. De Roeck, and J. Kullaa. Vibration-based structural health monitoring using output-only measurements under changing environment. *Mechanical systems and signal processing*, 22(1):34–56, 2008.

[68] H. Sohn and C.R. Farrar. Statistical process control and projection techniques for damage detection. In *Proceedings of European COST F3 Conference on System Identification and Structural Health Monitoring (pp. 105–114*. Citeseer, 2000.

[69] M. Zhang, R. Schmidt, and B. Markert. Structural damage detection methods based on the correlation functions. In *Proceedings of the 9th International Conference on Structural Dynamics*, 2014.

[70] C. Schaal, S. Bischoff, and L. Gaul. Energy-based models for guided ultrasonic wave propagation in multi-wire cables. *International Journal of Solids and Structures*, 64:22–29, 2015.

[71] F.J. Cara, J. Juan, E. Alarcón, E. Reynders, and G. De Roeck. Modal contribution and state space order selection in operational modal analysis. *Mechanical Systems and Signal Processing*, 38(2):276–298, 2013.

[72] F. Vicario, M.Q. Phan, R. Betti, and R.W. Longman. Output-only observer/Kalman filter identification (O3KID). *Structural Control and Health Monitoring*, 22(5):847–872, 2015.

[73] Y. Arici and K.M Mosalam. Modal identification of bridge systems using state-space methods. *Structural Control and Health Monitoring*, 12(3-4):381–404, 2005.

[74] M. Wu and A.W. Smyth. Application of the unscented Kalman filter for real-time nonlinear structural system identification. *Structural Control and Health Monitoring*, 14(7):971–990, 2007.

[75] X. Liu, Ponciano J. E.A., and N.A.J. Lieven. Extended Kalman filtering for the detection of damage in linear mechanical structures. *Journal of Sound and Vibration*, 325(4):1023–1046, 2009.

[76] S. Xing, M.W. Halling, and S. Pan. Application of substructural damage identification using adaptive Kalman filter. *Journal of Civil Structural Health Monitoring*, 4(1):27–42, 2014.

[77] A.M. Yan, P. De Boe, and J.C. Golinval. Structural damage diagnosis by Kalman model based on stochastic subspace identification. *Structural Health Monitoring*, 3(2):103–119, 2004.

[78] B. Hassibi, A.H. Sayed, and T. Kailath. *Indefinite-Quadratic Estimation and Control: A Unified Approach to H^2 and H^∞ Theories*. SIAM Studies in Applied Mathematics. Society for Industrial and Applied Mathematics, 1999.

[79] J.C. Doyle, K. Glover, P.P. Khargonekar, and B.A. Francis. State-space solutions to standard H_2 and H_∞ control problems. *IEEE Transactions on Automatic Control*, 34(8):831–847, 1989.

[80] U. Shaked and Y. Theodor. H_∞-optimal estimation: A tutorial. *Proceedings of the 31st IEEE Conference on Decision and Control*, 1992.

[81] K. Zhou, J.C. Doyle, and K. Glover. *Robust and optimal control*, volume 40. Prentice hall New Jersey, 1996.

[82] F. Yu, C. Lv, and Q. Dong. A novel robust H_∞ filter based on krein space theory in the sins/cns attitude reference system. *Sensors*, 16(3):396, 2016.

[83] J.S. Hwang, H. Kim, and J. Kim. Estimation of the modal mass of a structure with a tuned-mass damper using H-infinity optimal model reduction. *Engineering structures*, 28(1):34–42, 2006.

[84] T. Sato and K. Qi. Adaptive H_∞ filter: its application to structural identification. *Journal of Engineering Mechanics*, 124(11):1233–1240, 1998.

[85] B. Chen and S. Nagarajaiah. H_-/H_∞ structural damage detection filter design using an iterative linear matrix inequality approach. *Smart Materials and Structures*, 17(3), 2008.

[86] J.M. Ko and Y.Q. Ni. Technology developments in structural health monitoring of large-scale bridges. *Engineering structures*, 27(12):1715–1725, 2005.

[87] Y.Q. Ni, H.F. Zhou, K.C. Chan, and J.M. Ko. Modal flexibility analysis of cable-stayed Ting Kau Bridge for damage identification. *Computer-Aided Civil and Infrastructure Engineering*, 23(3):223–236, 2008.

[88] M. Fraser, A. Elgamal, X. He, and J.P. Conte. Sensor network for structural health monitoring of a highway bridge. *Journal of Computing in Civil Engineering*, 24(1):11–24, 2009.

[89] F.M.R.L. Magalhães. *Operational modal analysis for testing and monitoring of bridges and special structures*. PhD thesis, Faculty of Engineering of the University of Porto, 2012.

[90] P. Kraemer. *Schadensdiagnoseverfahren für die Zustandsüberwachung von Offshore-Windenergieanlagen*. Dissertation, Universität Siegen, 2011.

[91] C.C. Ciang, J.R. Lee, and H.J. Bang. Structural health monitoring for a wind turbine system: a review of damage detection methods. *Measurement Science and Technology*, 19(12):122001, 2008.

[92] B. Lu, Y. Li, X. Wu, and Z. Yang. A review of recent advances in wind turbine condition monitoring and fault diagnosis. In *Power Electronics and Machines in Wind Applications, 2009. PEMWA 2009. IEEE*, pages 1–7. IEEE, 2009.

[93] D. Adams, J. White, M. Rumsey, and C. Farrar. Structural health monitoring of wind turbines: method and application to a hawt. *Wind Energy*, 14(4):603–623, 2011.

[94] R.A. Swartz, J.P. Lynch, S. Zerbst, B. Sweetman, and R. Rolfes. Structural monitoring of wind turbines using wireless sensor networks. *Smart structures and systems*, 6(3):183–196, 2010.

[95] M. Benedetti, V. Fontanari, and D. Zonta. Structural health monitoring of wind towers: remote damage detection using strain sensors. *Smart Materials and Structures*, 20(5):055009, 2011.

[96] Y.Q. Ni, Y. Xia, W.Y. Liao, and J.M. Ko. Technology innovation in developing the structural health monitoring system for Guangzhou New TV Tower. *Structural Control and Health Monitoring*, 16(1):73–98, 2009.

[97] F. Ubertini, G. Comanducci, N. Cavalagli, A.L. Pisello, A.L. Materazzi, and F. Cotana. Environmental effects on natural frequencies of the san pietro bell tower in perugia, italy, and their removal for structural performance assessment. *Mechanical Systems and Signal Processing*, 82:307–322, 2017.

[98] M. De Angelis, H. Luş, R. Betti, and R.W. Longman. Extracting physical parameters of mechanical models from identified state-space representations. *Journal of Applied Mechanics*, 69(5):617–625, 2002.

[99] H. Luş, M. De Angelis, R. Betti, and R. Longman. Constructing second-order models of mechanical systems from identified state space realizations. part i: Theoretical discussions. *Journal of Engineering Mechanics*, 129(5):477–488, 2003.

[100] A. Lenzen. *Untersuchung von dynamischen Systemen mit der Singulärwertzerlegung: Erfassung von Strukturveränderungen*. Dissertation, Ruhr-Universität Bochum, Institut für Mechanik, 1994.

[101] P. Andersen. *Identification of civil engineering structures using vector ARMA models*. PhD thesis, Aalborg University, 1997.

[102] W. Gawronski. *Advanced Structural Dynamics and Active Control of Structures*. Mechanical Engineering Series. Springer New York, 2004.

[103] J. Wirnitzer. *Schwingungsreduktion flexibler Raumfahrtstrukturen mittels semiaktiver Reibverbindungen*. Dissertation, Universität Stuttgart, 2004.

[104] C.D. Meyer. *Matrix Analysis and Applied Linear Algebra*. Society for Industrial and Applied Mathematics (SIAM), 2000.

[105] K. De Cock. *Principal Angles In System Theory, Information Theory And Signal Processing*. PhD thesis, Katholieke Universiteit Leuven, 2002.

[106] M. Gevers. A personal view of the development of system identification: A 30-year journey through an exciting field. *IEEE Control Systems*, 26(6):93–105, 2006.

[107] H.P. Zeiger and A.J. McEwen. Approximate linear realizations of given dimension via Ho's algorithm. *IEEE Transactions on Automatic Control*, 19(2):153–153, 1974.

[108] B. Peeters and G. De Roeck. Stochastic system identification for operational modal analysis: a review. *Journal of Dynamic Systems, Measurement, and Control*, 123(4):659–667, 2001.

[109] Edwin Reynders. System identification methods for (operational) modal analysis: review and comparison. *Archives of Computational Methods in Engineering*, 19(1):51–124, 2012.

[110] F. Magalhães and A. Cunha. Explaining operational modal analysis with data from an arch bridge. *Mechanical systems and signal processing*, 25(5):1431–1450, 2011.

[111] M. Aoki. *State Space Modeling of Time Series*. Springer Berlin Heidelberg, 2013.

[112] F.R. Gantmacher, H. Boseck, K. Stengert, and D. Soyka. *Matrizentheorie*. Springer Berlin Heidelberg, 2013.

[113] R. Brincker and P. Andersen. Understanding stochastic subspace identification. *Proceedings of the 24th IMAC, St. Louis, Missouri*, pages 279–311, 2006.

[114] K.F. Alvin, L.D. Peterson, and K.C. Park. Method for determining minimum-order mass and stiffness matrices from modal test data. *AIAA Journal*, 33(1):128–135, 1995.

[115] D. Bernal and B. Gunes. Flexibility based approach for damage characterization: benchmark application. *Journal of Engineering Mechanics*, 130(1):61–70, 2004.

[116] A.M. Yan and J.C. Golinval. Structural damage localization by combining flexibility and stiffness methods. *Engineering Structures*, 27(12):1752–1761, 2005.

[117] A. Lenzen and C. Ebert. Experiments for damage detection by subspace identification on real mechanical structures. *2nd International Operational Modal Analysis Conference*, 2007. , Ed.: R. Brinker, N. Møller.

[118] A. Lenzen and C. Ebert. Experiments for damage detection by subspace identification on a tied arch bridge. *Bridge, Maintenance, Safety, Management and Life-Cycle Optimization: Proceedings of the Fifth International IABMAS Conference, 2010*, 2010.

[119] P.D. Welch. The use of fast fourier transform for the estimation of power spectra: A method based on time averaging over short, modified periodograms. *IEEE Transactions on Audio and Electroacoustics*, 15:70–73, 1967.

[120] A. Cunha and E. Caetano. Experimental modal analysis of civil engineering structures. *Sound and Vibration*, 40(6):12–20, 2006.

[121] D. Simon. *Optimal State Estimation: Kalman, H_∞, and Nonlinear Approaches*. Wiley, 2006.

[122] M. Papageorgiou. *Optimierung: Statische, Dynamische, Stochastische Verfahren*. Springer London, Limited, 2012.

[123] N. Wiener. *Extrapolation, interpolation, and smoothing of stationary time series*, volume 2. MIT press Cambridge, 1949.

[124] R.E. Kalman. A new approach to linear filtering and prediction problems. *Journal of Fluids Engineering*, 82(1):35–45, 1960.

[125] T. Kailath. An innovations approach to least-squares estimation–part i: Linear filtering in additive white noise. *IEEE transactions on automatic control*, 13(6):646–655, 1968.

[126] T. Kailath and P. Frost. An innovations approach to least-squares estimation–part ii: Linear smoothing in additive white noise. *IEEE Transactions on Automatic Control*, 13(6):655–660, 1968.

[127] B.D.O. Anderson and J.B. Moore. *Optimal Filtering*. Dover Books on Electrical Engineering Series. Dover Publications, Incorporated, 2005.

[128] R.S. Mangoubi. *Robust Estimation and Failure Detection: A Concise Treatment*. Advances in Industrial Control. Springer London, 2012.

[129] R.N. Banavar. *A game theoretic approach to linear dynamic estimation*. PhD thesis, Texas University, Austin, 1992.

[130] K. Takaba and T. Katayama. Discrete-time H_∞ algebraic riccati equation and parametrization of all H_∞ filters. *International Journal of Control*, 64(6):1129–1149, 1996.

[131] Ali H Sayed, Babak Hassibi, and Thomas Kailath. Inertia conditions for the minimization of quadratic forms in indefinite metric spaces. *Recent Developments in Operator Theory and Its Applications*, 87:309–347, 1996.

[132] F. Najson. On the Kalman–Yakubovich–Popov lemma for discrete-time positive linear systems: a novel simple proof and some related results. *International Journal*

of Control, 86(10):1813–1823, 2013.

[133] R.V. Patel. On computing the eigenvalues of a symplectic pencil. *Linear algebra and its applications*, 188:591–611, 1993.

[134] Q.C. Zhong. J-spectral factorization of regular para-hermitian transfer matrices. *Automatica*, 41(7):1289–1293, 2005.

[135] P. De Boe and J.-C. Golinval. Principal component analysis of a piezosensor array for damage localization. *Structural health monitoring*, 2(2):137–144, 2003.

[136] M.I. Friswell and D.J. Inman. Sensor validation for smart structures. *Journal of intelligent material systems and structures*, 10(12):973–982, 1999.

[137] J. Kullaa. Distinguishing between sensor fault, structural damage, and environmental or operational effects in structural health monitoring. *Mechanical Systems and Signal Processing*, 25(8):2976–2989, 2011.

[138] G. Kerschen, P. De Boe, J.-C. Golinval, and K. Worden. Sensor validation using principal component analysis. *Smart Materials and Structures*, 14(1):36, 2004.

[139] J. Chen, R.J. Patton, and H.-Y. Zhang. Design of unknown input observers and robust fault detection filters. *International Journal of control*, 63(1):85–105, 1996.

[140] J.-Y. Keller. Fault isolation filter design for linear stochastic systems. *Automatica*, 35(10):1701–1706, 1999.

[141] I. Hwang, S. Kim, Y. Kim, and C.E. Seah. A survey of fault detection, isolation, and reconfiguration methods. *IEEE Transactions on Control Systems Technology*, 18(3):636–653, 2010.

[142] R.V. Beard. *Failure accomodation in linear systems through self-reorganization.* PhD thesis, Massachusetts Institute of Technology, 1971.

[143] M. Basseville, L. Mevel, and M. Goursat. Statistical model-based damage detection and localization: subspace-based residuals and damage-to-noise sensitivity ratios. *Journal of Sound and Vibration*, 275(3-5):769 – 794, 2004.

[144] A.-M. Yan and J.-C. Golinval. Null subspace-based damage detection of structures using vibration measurements. *Mechanical Systems and Signal Processing*, 20(3):611–626, 2006.

[145] M. Goursat, M. Döhler, L. Mevel, and P. Andersen. Crystal clear SSI for operational modal analysis of aerospace vehicles. *Structural Dynamics*, 3:1421–1430, 2011.

[146] S.D. Fassois and J.S. Sakellariou. Statistical time series methods for SHM. *Encyclopedia of structural health monitoring*, 2009.

PUBLISHED WORK

List of Published Articles

[Art1] A. Lenzen and M. Vollmering. An output only damage identification method based on $\mathcal{H}_{\infty}$ theory and state projection estimation error (SP2E). *Structural Control and Health Monitoring*, 24(11), 2017.

[Art2] A. Lenzen and M. Vollmering. On experimental damage localization by SP2E: Application of $\mathcal{H}^{\infty}$ estimation and oblique projections. *Mechanical Systems and Signal Processing*, 104:648–662, 2018.

List of Presentations and Published Proceedings

[Proc1] A. Lenzen and M.Vollmering. A new technique for damage localisation using estimates in krein spaces. *6th International Operational Modal Analysis Conference*, Proceedings:239–248, 2015.

[Proc2] A. Lenzen and M.Vollmering. Eine neue Methodik zur schwingungsbasierten Schadensidentifikation. *5.VDI-Fachtagung Baudynamik 2015*, VDI-Berichte 2244:171–185, 2015.

[Proc3] A. Lenzen and M.Vollmering. Vergleich verschiedener Ansätze zur Identifikation instationärer Eigenfrequenzen. *4.VDI-Fachtagung Schwingungsanalyse & Identifikation 2016*, VDI-Berichte 2259:179–196, 2016.

CURRICULUM VITAE

Personal Data

Birth:	Leipzig, Germany | 15.December 1989
Address:	Ilmenauer Weg 16, 04205 Leipzig, Germany
Phone:	+49 341 3076-6657
email:	Max.Vollmering@htwk-leipzig.de

Work Experience

2013 - *Current* | **Scientific Employee at Leipzig University of Applied Sciences, Structural Dynamics (Prof. Armin Lenzen)**
Accomplished projects of the German Research Foundation (Deutsche Forschungsgemeinschaft; DFG) and Saxon State Ministry for Science and the Arts (Sächsisches Staatsministerium für Wissenschaft und Kunst; SMWK)

2010 - 2013 | **Research Assistant at Leipzig University of Applied Sciences, Structural Dynamics (Prof. Armin Lenzen)**
Assistance at a project of the German Research Foundation (Deutsche Forschungsgemeinschaft; DFG)

2008 - 2011 | **Various Internships for Several Months Each**
Worked at Alpin Bau und Service GmbH Leipzig, ICL Ingenieur Consult Leipzig and Wölfel Beratende Ingenieure

Academic Career

2011 - 2014 | **Study of Civil Engineering at Leipzig University of Applied Sciences**
Graduated as Master of Science; Specialized in Structural Engineering

2008 - 2011 | **Study of Civil Engineering at Leipzig University of Applied Sciences**
Graduated as Bachelor of Engineering

1996 - 2008 | **School Education, Abitur**

EHRENWÖRTLICHE ERKLÄRUNG

Ich erkläre hiermit ehrenwörtlich, dass ich die vorliegende Arbeit ohne unzulässige Hilfe Dritter und ohne Benutzung anderer als der angegebenen Hilfsmittel angefertigt habe. Die aus anderen Quellen direkt oder indirekt übernommenen Daten und Konzepte sind unter Angabe der Quelle gekennzeichnet.

Bei der Auswahl und Auswertung folgenden Materials haben mir die nachstehend aufgeführten Personen in der jeweils beschriebenen Weise entgeltlich/unentgeltlich geholfen: Keine.

Weitere Personen waren an der inhaltlich-materiellen Erstellung der vorliegenden Arbeit nicht beteiligt. Insbesondere habe ich hierfür nicht die entgeltliche Hilfe von Vermittlungs- bzw. Beratungsdiensten (Promotionsberater oder anderer Personen) in Anspruch genommen. Niemand hat von mir unmittelbar oder mittelbar geldwerte Leistungen für Arbeiten erhalten, die im Zusammenhang mit dem Inhalt der vorgelegten Dissertation stehen.

Die Arbeit wurde bisher weder im In- noch im Ausland in gleicher oder ähnlicher Form einer anderen Prüfungsbehörde vorgelegt.

Ich versichere ehrenwörtlich, dass ich nach bestem Wissen die reine Wahrheit gesagt und nichts verschwiegen habe.

Leipzig, 18. September 2017

_____
Ort, Datum

_____
Unterschrift